

UCSF

UC San Francisco Electronic Theses and Dissertations

Title

The cellular and circuit mechanisms of hyperkinetic movement disorders

Permalink

<https://escholarship.org/uc/item/5st0p75w>

Author

Girasole, Allison Elizabeth

Publication Date

2019

Supplemental Material

<https://escholarship.org/uc/item/5st0p75w#supplemental>

Peer reviewed|Thesis/dissertation

The cellular and circuit mechanisms of hyperkinetic movement disorders

by

Allison Elizabeth Girasole

DISSERTATION

Submitted in partial satisfaction of the requirements for degree of

DOCTOR OF PHILOSOPHY

in

Neuroscience

in the

GRADUATE DIVISION

of the

UNIVERSITY OF CALIFORNIA, SAN FRANCISCO

Approved:

DocuSigned by:

Anatol Kreitzer

Anatol Kreitzer

03F45B9A4CF445E...

Chair

DocuSigned by:

Alexandra Nelson

Alexandra Nelson

DocuSigned by:

Philip Starr

Philip Starr

DocuSigned by:

Kevin Bender

Kevin Bender

A996F2A5C1214BE...

Committee Members

Copyright 2019

By

Allison Elizabeth Girasole

Dedications

To my parents, Art & Mary Girasole, and my sister, Emily Girasole

For their love, support, and dedication to my success and well-being throughout my entire life.

To Dr. Jeffrey Michael Knowles

A life taken too soon that continues to inspire long after death. For your creativity, friendship, and adventurous spirit in both neuroscience and beyond.

Acknowledgments

Obtaining one's PhD is not done in solitude, it takes a village of support. I have immense gratitude to the community that helped me achieve my doctoral degree. First and foremost, I would like to thank my mentor, Dr. Alexandra B. Nelson. Not only is Alexandra an incredible scientist, she is a beloved professor, physician, colleague, leader, and friend within the UCSF community. She is also superwoman in disguise. There are few people I would willingly commit to starting a lab with and Alexandra was an obvious choice. The professional example she sets for her students is unparalleled, and I am incredibly proud to have been her first graduate student. From day one, the tone she set in establishing our laboratory—one of rigor, scientific detail, productivity, and a love for science—is something I'll always remember. As a dedicated mentor, she has challenged me both scientifically and intellectually, while providing support when needed. While Alexandra's talent in writing, collecting data, and public speaking is undeniable, her ability to teach and help her students develop these skills is even more impressive; Alexandra has always been committed to my scientific and personal development. It is impossible to put into words my respect for Alexandra and the gratitude I have for her kind actions over the years. Not only was I able to work on exactly what I wanted to in graduate school, I had so much fun while doing it. Thank you, ABN, for helping to instill within me the confidence I needed to move forward!

Not surprisingly, Alexandra has cultivated an incredible team to whom I owe much thanks. I am incredibly grateful to all of the current and past members of the Nelson laboratory. To Michael Ryan, Match McGregor, and Jonathan Schor, I would not be the scientist I am today without your never-ending support, constant witty chatter, insight, friendship, and expertise. Thank you for reading every manuscript draft, listening to all my presentations, and keeping me sane when no one else could. The bond shared in our laboratory is like a family; not many other labs run marathon relays, hold Sunday dinners, and religiously celebrate birthdays together. I am

especially grateful for the technical assistance provided by Matthew Lum, Chloe Jean Bair-Marshall, Rea Brakaj, Diane Nathaniel, and Xiao Tong. Thank you for keeping all our mice in a row and supplies in check. A special acknowledgement to Mike—my collaborator, dear friend, work husband, and confidant. Our project would not have been half of what it is without your participation. Thank you for the patience, support, and grace you showed while embarking on an unknown project with a crazy type-A lab mate (i.e. me). I have learned and continue to learn so much through the example you set and the leader you exemplify.

I'm deeply grateful to the broader UCSF neuroscience community who has supported me through the years, including the Neuroscience Graduate Program and our program administrators Pat Veitch and Lucita Nacionales. Your support has been immense. I would like to thank my thesis committee, Anatol Kreitzer, Kevin Bender, and Phil Starr with whom many fruitful scientific ideas and conversations originated with. Thank you, Anatol, for your support and allowing Alexandra and I to work in your laboratory while we were transitioning into our own space. Further, a huge thank you to Kevin for being my unofficial second mentor and a key part of my support system in graduate school. I give special thanks to Viktor Kharazia and Scott Wegner (Alcohol and Addiction Research Group) for patiently teaching me how to do histology and immunohistochemistry and DeLaine Larsen (UCSF Nikon Imaging Center) for her extensive help and expertise with microscopy on my FosTRAP project. Further, I'd like to acknowledge Massimo Scanziani, Loren Frank, and Felice Dunn for their excellent scientific advice and professional guidance throughout the years. Finally, while there are so many people who have assisted with the projects in this dissertation I'd like to thank Audrey Brumback, Arnaud Lalive, Chris Donahue, David Kastner, Guy Bouvier, Ken Burke, Max Liu, Perry Sprat, and Scott Owen specifically for their help, support, and inspiration.

I am immensely thankful to our collaborator at NIMH, Charles (Chip) Gerfen, for his assistance in our monosynaptic rabies tracing experiments. Chip's pipeline for sectioning, staining, and analyzing all of our brain tissue has provides an incredible data set that will be used

in the Nelson Laboratory for years to come. This fascinating part of our story would not have been possible without Chip's enthusiasm, expertise, and generosity of his time and resources.

I would like to acknowledge my classmates in the Neuroscience Program, in particular Margaret Cunniff, Rachel Care, Jiggy Athilingam, Alexandra Clemente, and Mari Sosa. This group of incredible, brilliant, and hard-working women motivate and inspire me every day to be a better scientist and person. I could not have gotten through graduate school without them.

I'd like to thank my wonderful family in San Francisco, including my Minty House roommates: Anna Gillespie, Tali Mazor, Rachel Care, Liza Dadiomov, and Sofia Lavrentyeva. Further, thank you to Lauren Stoxen, Jeff Goodwin, and Jeff Knowles for making my time in San Francisco so memorable. I'd like to highlight my best friend, Anna. Graduate school, UCSF, the Minty House, and life in San Francisco would have been nothing without you. Thank you for giving me a home and for being my mentor, colleague, leader, adventure-buddy, co-chef, and cycling partner. Your courage and fearlessness inspire me every single day.

I cannot overstate my gratitude for my partner, Clinton Hayes. My number one supporter, Clinton is always ready with a plan when I need a break from science. Clinton's been there to celebrate many milestones and has helped to support me through every setback. His ear is always open to listen and his patience with my busy schedule is admirable. Thank you, Clinton for helping me through this incredible journey. Jeff would be proud of us! I cannot forget to mention Luke, our favorite furry little man, who brings so much joy to my life.

I am most thankful, to my family—my sister, Emily Girasole, my parents, Art and Mary Girasole, and my Gramma, Elizabeth Girasole for their continued support my entire life. My parents are relentless in their love and care for their two daughters and have dedicated themselves fully to the success of Emily and myself. Thank you for everything, Mom and Dad.

Finally, the work described in this thesis was done with the support of the National Science Foundation Graduate Research Fellowships Program and the UCSF Discovery Fellows Program.

Author Contributions

Chapter 1 of this dissertation was written by Allison Girasole and figure 1 is modified with permission from:

Nelson, A.B. & Kreitzer, A.C. (2014). Reassessing models of basal ganglia function and dysfunction. *Annu. Rev. Neurosci.* 37, 117-135.

Chapter 2 of this dissertation was written by Alexandra Nelson and Allison Girasole. This manuscript is currently in revision. Contributions: A.B.N. and A.C.K. designed the experiments. A.B.N. performed and analyzed the *in vivo* physiology and chemogenetic experiments. A.B.N. and A.E.G. performed and analyzed the slice physiology experiments. M.O. and K.K. analyzed gene expression datasets from postmortem human tissue. H.S.Y. and L.P. generated and characterized the PNKD mouse model, and consulted regarding behavioral experiments. A.B.N. and A.C.K. wrote the manuscript with contributions from all authors.

Chapter 3 of this dissertation is reproduced in its entirety with permission from:

Girasole, A.E., Lum M.Y., Nathaniel, D., Bair-Marshall, C.J., Guenthner, C.J., Luo, L., Kreitzer, A.C., Nelson, A.B. (2018). A subpopulation of striatal neurons mediates levodopa-induced dyskinesia. *Neuron* 97(4): 787–795.e6.

Contributions: A.E.G., and A.B.N. designed the experiments. A.E.G., A.B.N., M.Y.L., D.N., and C.J.B.-M. performed experiments. C.J.G. and L.L. generated the FosTRAP mouse line and consulted on related protocols. A.E.G. and A.B.N. wrote the manuscript with contributions from all authors.

Chapter 4 of this dissertation was written by Allison Girasole. All research in this chapter is represents ongoing and unpublished research. This project was done in collaboration with Michael Ryan of the Nelson Lab and Charles Gerfen at the NIMH. Contributions: A.E.G., M.B.R., and A.B.N. designed the experiments. A.E.G., M.B.R., and A.B.N. performed all *in vivo* experiments. A.E.G., M.B.R., M.M.M., and A.B.N. performed slice physiology experiments. A.E.G., M.B.R., C.J.B-M., X.T., and R.J.B. performed surgical experiments. C.R.G. processed, analyzed, and consulted on all monosynaptic rabies injected brains. R.J.B. performed immunohistochemistry experiments.

Chapter 5 of this dissertation was written by Allison Girasole.

All chapters in this dissertation were edited and reviewed by Alexandra Nelson and members of the Nelson Laboratory.

The cellular and circuit mechanisms of hyperkinetic movement disorders

Allison Elizabeth Girasole

Abstract

The basal ganglia are a series of interconnected subcortical nuclei involved in movement, action selection, and decision making. These processes are dependent on the coordinated output of the striatal direct and indirect pathways, which is dysregulated in neurological conditions such as Parkinson's disease, Huntington's Disease, and forms of dystonia. However, the specific cells, circuits, and patterns of activity within the brain that contribute to disease manifestations, such as involuntary movements, or dyskinesias, are not well understood. To address this gap, we have used two mouse models of human dyskinesias, paroxysmal nonkinesigenic dyskinesia (PNKD) and levodopa-induced dyskinesia (LID), to investigate whether aberrant striatal activity is a root cause of dyskinesia. Using a variety of *in vivo* and *ex vivo* techniques to both record and manipulate neural activity, we found that abnormal patterns of activity in the striatum give rise to dyskinesia. Interestingly, in PNKD we see profound reductions in striatal indirect pathway activity during dyskinesia, whereas in LID there are decreases in indirect pathway activity, but also abnormally high direct pathway activity during dyskinesia. Further, we found that the decrease in indirect pathway activity is necessary and sufficient for drug-induced dyskinesia in PNKD, while an increase in activity in a subset of direct pathway neurons is necessary and sufficient for drug-induced dyskinesia in LID. In both models, we found evidence of aberrant striatal synaptic plasticity as a cellular correlate

of dyskinesia: depressed excitatory input onto indirect pathway neurons in the case of PNKD, and enhanced excitatory input onto direct pathway neurons in LID. While these results are largely in support of the classical model of basal ganglia function, we also found heterogeneity within the canonical direct pathway in LID, and identified a subclass of direct pathway neurons with exceptionally high levodopa-evoked firing that correlates strongly with dyskinesia. Importantly, these results may guide the development of new therapeutics for hyperkinetic disorders based on targeting specific subclasses of striatal neurons or their connections.

Table of Contents

Chapter 1: Introduction	1
1.1 Overview of Dissertation.....	1
1.2 Introduction.....	4
1.3 Figures.....	17
1.4 References	19
Chapter 2: Striatal indirect pathway dysfunction underlies motor deficits in a mouse model of human dyskinesia	28
2.1 Abstract	29
2.2 Introduction.....	30
2.3 Results.....	33
2.4 Discussion	49
2.5 Experimental Procedures	54
2.6 Author Contributions & Acknowledgements.....	73
2.7 Figures.....	74
2.8 Supplemental Figures.....	84
2.9 Supplemental Tables.....	89
2.10 References	91
Chapter 3: A subset of striatal neurons mediates levodopa-induced dyskinesia	101
3.1 Abstract	102
3.2 Introduction.....	103
3.3 Results	105
3.4 Discussion	115

3.5 Experimental Procedures	118
3.6 Author Contributions & Acknowledgements.....	132
3.7 Figures.....	116
3.8 Supplemental Figures.....	133
3.9 References	143
Chapter 4: Altered synaptic connectivity onto a distinct subset of striatal neurons in levodopa-induced dyskinesia	148
4.1 Abstract	149
4.2 Introduction.....	150
4.3 Results	153
4.4 Discussion	165
4.5 Experimental Procedures	170
4.6 Author Contributions & Acknowledgements.....	183
4.7 Figures.....	184
4.8 Tables.....	195
4.9 References	196
Chapter 5: Conclusion.....	202
5.1 Conclusion & Significance	202

List of Tables

Chapter 2

Table 1: Human CNS transcriptomes analyzed in this study.	89
Table. Dyskinesia Gene Set.....	90

Chapter 4

Table 1: <i>Ex vivo</i> excitability parameters for TRAPed dMSNs, unTRAPed dMSNs and iMSNs and before and after SKF 81297	195
--	-----

List of Figures

Chapter 1

Figure 1: The Basal Ganglia	17
Figure 2. Classical Model of Basal Ganglia Function.....	18

Chapter 2

Figure 1: Dyskinesia-associated genes are co-expressed with markers Of indirect pathway neurons in human striatum.....	74
Figure 2. Dyskinetic attacks in PNKD mice are accompanied by Decreased firing rates in striatal projection neurons.....	75
Figure 3. iMSNs are differentially suppressed during caffeine-triggered dyskinesia.....	76
Figure 4. Chemogenetic inhibition of iMSNs causes dyskinesia in PNKD mice.....	77
Figure 5. Chemogenetic activation of iMSNs blunts dyskinesia in PNKD mice.....	79
Figure 6. Excitatory transmission unchanged onto dMSNs in dyskinetic PNKD mice.....	80
Figure 7. Excitatory transmission is reduced onto iMSNs in dyskinetic PNKD mice.....	81
Figure 8. Cannabinoid CB1 antagonists block iMSN suppression and dyskinesia in PNKD mice	83
Supplemental Figure 1: Dyskinesia alters striatal firing rates in PNKD mice.....	84
Supplemental Figure 2: Recordings from optogenetically-identified dMSNs and iMSNs in wild-type and PNKD mice.....	85
Supplemental Figure 3: Chemogenetic activation of iMSNs blunts dyskinesia in PNKD mice	86

Supplemental Figure 4: Caffeine does not modulate intrinsic excitability in WT or PNKD dMSNs.....	87
--	----

Supplemental Figure 5: Caffeine does not modulate intrinsic excitability in WT or PNKD iMSNs.....	88
--	----

Chapter 3

Figure 1: FosTRAP captures levodopa-induced dyskinesia (LID)-associated striatal cells.....	133
--	-----

Figure 2. TRAPed cells are primarily direct pathway medium spiny neurons... ..	134
---	-----

Figure 3. Optogenetic reactivation of TRAPed striatal neurons, but not TRAPed S1 or M1 cortical neurons, causes dyskinesia in the absence of levodopa	135
--	-----

Figure 4. Optogenetic inhibition of TRAPed striatal neurons, but not all direct pathway neurons, ameliorates levodopa-induced dyskinesia.....	137
--	-----

Supplemental Figure 1: Levodopa-induced dyskinesia is associated with c-Fos expression.....	138
--	-----

Supplemental Figure 2: c-Fos activated neurons are primarily direct pathway cells.	140
--	-----

Supplemental Figure 3: Optogenetic reactivation of TRAPed striatal neurons, but not TRAPed S1 or M1 cortical neurons, causes dyskinesia in the absence of levodopa.....	141
--	-----

Supplemental Figure 4: Optogenetic inhibition of TRAPed striatal neurons, but not a random subset of direct pathway striatal neurons, ameliorates dyskinesia.	142
---	-----

Chapter 4

Figure 1: Levodopa evokes high firing rates in TRAPed neurons, which correlate with dyskinesia severity.....	184
---	-----

Figure 2. Experimental design for monosynaptic rabies tracing studies	186
--	-----

Figure 3. Summary of monosynaptic inputs onto direct and indirect pathway neurons in healthy and 6-OHDA/levodopa treated mice	188
Figure 4. Comparison of monosynaptic inputs onto striatal direct, indirect, and TRAPed neurons in parkinsonian mice treated with levodopa.....	189
Figure 5. TRAPed neurons show increased presynaptic input from Npas1+ GPe neurons.....	190
Figure 6. Summary of cortical inputs onto direct pathway, indirect pathway, and FosTRAP neurons in healthy and 6-OHDA/levodopa treated mice.....	191
Figure 7. Excitatory transmission is preferentially increased onto TRAPed neurons in 6-OHDA/levodopa treated mice.....	192
Figure 8. Intrinsic excitability is not altered in striatal medium spiny neurons in the presence of dopamine agonists in LID mice	194

CHAPTER 1

Introduction

1.1 Overview of Dissertation

The function of the basal ganglia has perplexed scientists and clinicians for decades. While the anatomy and connectivity are largely agreed upon, how these interconnected nuclei contribute to human behavior, including movement, motivation, and cognition, is still a source of significant debate. Much of our understanding of the basal ganglia comes from neurological conditions in which the function of the basal ganglia goes awry, such as Parkinson's disease and Huntington's Disease. From studying these disorders and associated animal models, a rich literature has emerged, which informed influential models and generated hypotheses that are still being tested today. Furthermore, technological developments, such as cell type-specific fluorophore lines, Cre recombinase mouse lines, and optogenetics, have permitted significant strides in our understanding of the basal ganglia. However, the precise cellular and circuit mechanisms underlying basal ganglia dysfunction in neurological conditions, such as hyperkinetic movement disorders, is unknown. More specifically, it is unclear how the primary input nucleus of the basal ganglia, the striatum, changes in a hyperkinetic state. To address these issues, we have implemented two mouse models of dyskinesia, a movement disorder in which patients develop abnormal involuntary movements. One model is based on the rare autosomal dominant human disorder, paroxysmal nonkinesigenic dyskinesia (PNKD), and the other on levodopa-induced dyskinesia (LID), a drug-induced movement disorder seen in patients with Parkinson's disease. Our goal was to find 1) the specific

brain regions and cell types involved in producing involuntary movements, and 2) to identify the patterns of activity underlying these movements. Interestingly, across the two phenotypically similar models, different patterns of striatal activity were associated with involuntary movement, but our findings suggest that an imbalance in activity between the direct and indirect pathways may be a shared feature. Further, our results suggest that targeting functional subclasses of neurons, within classically defined cell types, may be needed to optimally treat these conditions.

In Chapter 1, I will introduce the basal ganglia circuit, discuss the prevailing models of basal ganglia function and dysfunction, introduce several diseases of the basal ganglia, and outline theories regarding the origin of hyperkinetic movement disorders.

In Chapter 2, I will describe a study of striatal circuit dysfunction in a mouse model of a type of inherited human dyskinesia, paroxysmal nonkinesigenic dyskinesia (PNKD). This work is currently being revised for resubmission. In this study, we have incorporated unsupervised human genetics, *in vivo* and *in vitro* electrophysiology, chemogenetics, and behavior in a mouse model of PNKD to elucidate the role of striatal circuit dysfunction during dyskinesia. We discovered that dyskinesia in PNKD mice results from transient loss of striatal indirect pathway activity, likely driven by aberrant endocannabinoid-mediated synaptic depression. Together, our data indicate that targeting indirect pathway activity may be an effective strategy for treating some forms of dyskinesia.

In Chapter 3, we investigated the circuit basis of a phenotypically similar, but etiologically distinct movement disorder, levodopa-induced dyskinesia (LID), a medical complication of dopamine replacement therapy in Parkinson's disease. This work was published in *Neuron* in 2018 (Girasole et al., 2018). We used a novel activity-dependent

mouse line called FosTRAP, Targeted Recombination in Active Populations (Guenther et al., 2013) in conjunction with a well-validated mouse model of LID, to capture neurons brain-wide that are activated during LID, as a means to identify the specific brain regions and neuronal cell-types that are causally involved in dyskinesia. Using this approach, we were able to optogenetically reactivate or inhibit these same neurons, and found that LID-associated striatal neurons, but not motor cortical or sensory cortical neurons, bidirectionally control dyskinesia. Further, we found that TRAPed striatal neurons are primarily direct pathway neurons, and show robust increases in firing *rate in vivo* following administration of levodopa. This work suggests that targeting subsets of striatal direct pathway neurons could be a novel therapeutic target in LID.

In Chapter 4, we explored the cellular and synaptic mechanisms that distinguish TRAPed striatal neurons from other striatum neurons in the sensorimotor striatum. This work, a collaborative project with fellow graduate student Michael Ryan, is still in preparation for submission. We have used *in vivo* and *in vitro* electrophysiology, as well as Cre-dependent rabies tracing, to investigate the differences between TRAPed striatal neurons and direct pathway neurons more broadly. *In vivo*, we found that, as compared to direct pathway neurons in general, TRAPed cells show markedly elevated levodopa-evoked firing rates, which typically correlate on a moment-to-moment basis with dyskinesia severity. While we found changes in the monosynaptic inputs using modified rabies tracing to direct and indirect pathway neurons in parkinsonian/levodopa-treated versus healthy mice, we did not find a difference in the distribution of inputs to TRAPed versus other direct pathway neurons. However, we found evidence of functional differences in excitatory input onto TRAPed neurons, using *ex vivo* electrophysiology.

These experiments suggest a presynaptic mechanism may contribute to the distinct physiology of TRAPed neurons, and in turn to dyskinesia. Further experiments will be needed to fully elucidate this phenomenon.

Finally, in Chapter 5, I will provide brief conclusions, future areas of study, and discuss some of the important remaining questions regarding dyskinesia pathophysiology.

1.2 Introduction

Anatomy of the basal ganglia:

The basal ganglia are a group of interconnected subcortical nuclei. One of the most evolutionarily conserved brain circuits, the basic anatomy and connectivity of the basal ganglia is preserved from the lamprey to the human (Reiner et al., 1998; Stephenson-Jones et al., 2012). Individual nuclei of the basal ganglia can be subdivided into input, output, or intrinsic nuclei. The primary input nucleus of the basal ganglia is the caudate/putamen (in rodents a single contiguous structure, the striatum), integrating excitatory cortical and thalamic input with neuromodulatory inputs from the midbrain, to influence basal ganglia output (McGeorge and Faull, 1987). Striatal principal neurons, medium spiny neurons (MSNs), are its sole output, and can be subdivided further into the direct and indirect pathways, which will be discussed at length below. The internal segment of the globus pallidus (GPi; the entopeduncular nucleus is the rodent analog) and substantia nigra pars reticulata (SNr) serve as the primary output nuclei of the basal ganglia, sending inhibitory projections to thalamus (Parent and Parent, 2004) and brainstem motor centers. Finally, the intrinsic nuclei, acting as important connecting

points and relay centers between the input and output nuclei, consist of the globus pallidus pars externa (GPe) and the subthalamic nucleus (STN). Of note, the STN is the only excitatory nuclei in the basal ganglia and is also considered an input nucleus as it receives “hyperdirect” input from motor cortices (Kitai and Deniau, 1981; Monakow et al., 1978; Nambu et al., 1996). Further, the basal ganglia receive extensive dopaminergic inputs from spontaneously active neurons of the substantia nigra pars compacta (SNc) and the ventral tegmental area (VTA). SNc dopamine neurons primarily innervate the dorsal portion of the striatum, whereas VTA neurons project to the ventral striatum. Recent studies have also showed the midbrain dopamine neurons co-release glutamate or γ -aminobutyric acid (GABA) (Stuber et al., 2010; Tritsch et al., 2012), adding depth to how the activity of dopamine neurons might affect the basal ganglia. The role of co-release on behavior is currently unclear. In addition to these canonical synaptic connections, many interconnections exist between basal ganglia nuclei, the function of which is still unclear, but likely of importance (Lanciego et al., 2012). Together with their inputs and outputs, the basal ganglia form a functional network with both open- and closed-loop configurations

Diseases of the basal ganglia:

The study of movement disorders has been instrumental in shaping our understanding of basal ganglia function, and constitutes a major motivation for ongoing research. A basic understanding of these conditions (including Parkinson’s disease and levodopa-induced dyskinesia, Huntington’s Disease, and dystonia) informed the design and interpretation of the experiments in this dissertation.

Parkinson's disease & levodopa-induced dyskinesia:

Parkinson's disease (PD) is a complex multisystem neurodegenerative disorder, affecting approximately 1% of adults over the age of 60. This condition is characterized by cognitive, behavioral, and motor symptoms. Some disease symptoms are thought to arise directly from neurodegenerative cell loss in brainstem nuclei, SNc/VTA, and cerebral cortex in later states of the disease (Irwin et al., 2012). Other symptoms, however, are hypothesized to occur as an indirect result of neurodegeneration, driven by aberrant patterns of activity in surviving neurons that have lost neuromodulatory inputs (such as dopamine). The motor symptoms of PD, such as bradykinesia, rigidity, and tremor, are generally responsive to dopamine replacement therapy with levodopa and/or dopamine agonists, or basal ganglia deep brain stimulation (DBS). The fact that both levodopa and DBS can greatly reduce parkinsonism implies reversible circuit dysfunction as a major driver of motor symptoms, and was an inspiration for the studies in this thesis. While levodopa is the gold standard treatment for PD, and alleviates many motor symptoms, treatment complications can arise. After prolonged use, typically 5-10 years, levodopa treatment may be limited by the emergence of drug-induced abnormal involuntary movements, termed levodopa-induced dyskinesia (LID). LID is widely believed to result from hypersensitivity to dopamine treatment, and depends on both the degree of dopamine denervation and chronic pulsatile treatment with levodopa (Borgkvist et al., 2018). The striatum, and specifically the striatal direct pathway, is hypothesized to be a key player in the generation of LID (Berton et al., 2009; Buck and Ferger, 2010; Jenner, 2008; Liang et al., 2008; Perez et al., 2017; Ryan et al., 2018; Singh et al., 2015).

Huntington's Disease:

Huntington's Disease (HD) is an inherited neurodegenerative disease caused by expansion of the CAG trinucleotide repeat in the huntingtin (HTT) gene. The HTT gene is located on chromosome 4 and those with 40 or more CAG repeats in one HTT allele will develop this disease. Patients with HD have progressive neuropsychiatric, cognitive, and motor symptoms, and eventually the disease is lethal. Neurodegenerative changes, including cell loss, occur in both striatum and cortex, but early in the disease course may be selective for neurons of the striatal indirect pathway (Albin et al., 1990; Deng et al., 2004; Reiner et al., 1988). The reasons for selective vulnerability of striatal indirect pathway neurons are unclear, but their expression of dopamine type 2 (D2) receptors may be one explanation (Plotkin and Surmeier, 2015). Later in the disease, neurodegeneration and atrophy is also observed in the cortex, as evidenced by imaging in living patients, and from post-mortem studies (Halliday et al., 1998; Jernigan et al., 1991; Rosas et al., 2001). One of the most prominent and distinctive clinical features of HD is chorea, which are random, involuntary, often dance-like movements. Behavioral symptoms often predate motor symptoms, and include apathy, anxiety, irritability, depression, OCD, and psychosis (Craufurd et al., 2001). Cognitive disturbances also often arise before motor symptoms, and include impaired processing speed, emotion recognition, and executive function (Papoutsis et al., 2014; Stout et al., 2012). Though currently there are no disease-modifying treatments for HD, inhibitors of the vesicular monoamine transport type 2 (VMAT), such as tetrabenazine, or dopamine receptor antagonists (antipsychotics) are often used to manage chorea. These agents disrupt

dopaminergic neurotransmission, either from decreased packaging of dopamine into synaptic vesicles, or blocking of dopamine receptors themselves.

Dystonia:

Dystonia is characterized by involuntary, sustained muscle contractions, often resulting in repetitive twisting movements and abnormal postures. In the most common type of primary generalized dystonia, DYT1, a mutation in the *dyt1* gene leads to dysfunction of the protein torsinA (Ozelius et al., 1997). Since no neurodegeneration or gross changes in brain morphology are seen on brain imaging or at autopsy in patients with primary dystonias, aberrant circuit dysfunction is hypothesized as a causal mechanism. In fact, these observations constitute another major motivation for studying neural circuit activity in movement disorders. Comorbid non-motor features, such as sensory abnormalities and neuropsychiatric problems, may be seen in patients with isolated dystonia (Albanese et al., 2019). Anticholinergics have been a first-line pharmacological therapy for dystonia, though their precise mechanism of action is unknown and their side effects are often dose-limiting. DBS, particularly of the GPi, is a particularly effective intervention for treating many forms of primary dystonia, again pointing to neural activity as a reversible driver of movement disorder symptoms.

The classical model of basal ganglia function in health and disease:

In an attempt to resolve the complexity of the basal ganglia anatomy and connectivity, and to explain the pathophysiology of movement disorders, investigators have developed several influential models of basal ganglia function. These include, but

are not limited to, the parallel circuit model (Alexander et al., 1986), center-surround (action selection) model (Mink, 1996; Mink and Thach, 1993), striosome and matrix model (Brimblecombe and Cragg, 2017; Crittenden and Graybiel, 2011), and the classical model (Albin et al., 1989; Alexander and Crutcher, 1990; DeLong, 1990). For the purposes of this dissertation, I will primarily focus on the classical model.

The classical model, also called the rate or standard model, was developed in the late 1980s and early 1990s by DeLong, Albin, Penney, Young, and colleagues (Albin et al., 1989; Alexander and Crutcher, 1990; DeLong, 1990). This model has critically shaped our understanding of how the basal ganglia contribute to movement initiation and suppression. The model divides the basal ganglia into two pathways, the direct and indirect pathways. At the level of the striatum, GABAergic projection neurons, termed medium spiny neurons (MSNs), can be divided into direct and indirect pathway medium spiny neurons (dMSNs and iMSNs, respectively). These projection neurons comprise nearly 90% of the striatum in humans, and an even greater proportion in rodents (Chang et al., 1982; Graveland and DiFiglia, 1985; Penney and Young, 1983). The remaining <10% of striatal neurons are interneurons: GABAergic interneurons (Tepper et al., 2010) (including parvalbumin-, calretinin-, and neuropeptide Y-expressing subtypes) and cholinergic interneurons. Many striatal interneurons are intrinsically spontaneously active, including striatal cholinergic interneurons and NPY-expressing neurons are intrinsically active both *in vivo* and in *ex vivo* preparations (Inokawa et al., 2010; Kawaguchi, 1993; Kimura et al., 1984; Wilson et al., 1990), setting them apart from the mostly quiet MSNs, which are hyperpolarized in *ex vivo* preparations, and fire between 0-2 Hz under most conditions *in vivo*. According to the classical model, activation of the

direct pathway promotes movement by directly suppressing basal ganglia output, ultimately disinhibiting the thalamus (Albin et al., 1989; Alexander and Crutcher, 1990; DeLong, 1990). Indirect pathway activation, conversely, suppresses movement by increasing basal ganglia output via the GPe, STN, and SNr, finally inhibiting the thalamus (Albin et al., 1989; Alexander and Crutcher, 1990; DeLong, 1990). Optogenetic studies in freely moving mice support the idea that dMSNs and iMSNs have opposing roles in movement, and also in behavioral reinforcement (Kravitz et al., 2010; Kravitz et al., 2012). However, in rodent observational studies, both dMSNs and iMSNs increase activity at movement onset, with similar time courses (Cui et al., 2013; Klaus et al., 2017), diverging from the predictions of the classical model. While the classical model may be oversimplified, it has generated testable predictions regarding firing rate throughout the basal ganglia in health and disease, and has served as an important foundation for the aforementioned models of basal ganglia function.

In addition to their distinct projection targets, direct and indirect pathway neurons express distinct cellular markers. Direct pathway neurons express the excitatory G_s -coupled dopamine D1 receptors, whereas indirect pathway neurons express the inhibitory G_i -coupled dopamine D2 receptor (Gerfen et al., 1990). While direct proof from *in vivo* studies is currently lacking, based on *in vitro* studies, it is believed that dopamine excites direct pathway neurons and inhibits indirect pathway neurons, via the distinct signaling cascades associated with D1 and D2 receptors (Hernandez-Lopez et al., 1997; Hernandez-Lopez et al., 2000; Planert et al., 2013). In addition to their respective dopaminergic receptors, dMSNs express the $G_{i/o}$ coupled muscarinic receptor (M4) and iMSNs express G_s -coupled adenosine-2a (A2a) receptors. Thus, depending on the

animal's behavioral state or context, neuromodulators can exert bidirectional control over the two pathways (Lerner and Kreitzer, 2011). Neuromodulators are likely to influence activity in striatal direct and indirect pathway neurons via the unique complement of receptors found on each striatal cell type.

The classical model also predicts that dopamine loss, as occurs in Parkinson's disease (PD), will cause bidirectional changes in the activity of direct and indirect pathway neurons. The model predicts that the loss of dopamine will disinhibit iMSNs, resulting in increased firing rates, while loss of dopamine will reduce excitatory effects on dMSNs, resulting in decreased firing rates (Albin et al., 1989; DeLong, 1990). Pivotal studies have shown indirect support for the rate model via *in vivo* recordings of downstream basal ganglia nuclei in parkinsonian nonhuman primates and in patients undergoing surgical treatment of Parkinson's disease (Bergman et al., 1994; Fillion and Tremblay, 1991; Soares et al., 2004). More recently, additional support for this model comes from single-unit recordings in optogenetically labeled dMSNs and iMSNs in parkinsonian mice, which showed a persistent reduction in dMSN activity and increased iMSN activity during immobility (Ryan et al., 2018). Another recent study, using implanted GRIN lenses to image calcium signaling in awake-behaving animals, found similar changes in the activity of dMSNs and iMSNs in parkinsonian mice, and revealed changes in how these neurons encode the spatiotemporal dynamics of locomotion (Parker et al., 2018). However, there are limitations and inconsistencies within the rate model, to which we point readers to an excellent review (Ellens and Leventhal, 2013). Using a mouse model of human dyskinesia in Chapter 2, we will directly assess the predictions of the rate model in direct or indirect pathway neurons and related cellular mechanisms during involuntary movements.

As a corollary to this model for basal ganglia dysfunction in parkinsonism, it is hypothesized that hyperkinetic conditions may also be caused by an imbalance in the two pathways, including overactivation of the striatal direct pathway or suppression of the indirect pathway (Albin et al., 1989; DeLong, 1990). This hypothesis has been stated explicitly for conditions like LID; while dopamine replacement therapy with levodopa produces relief from akinesia, prolonged use and ongoing degeneration of dopaminergic neurons leads to vulnerability to LID. Several pieces of direct and indirect evidence from the striatum (Girasole et al., 2018; Liang et al., 2008; Parker et al., 2018; Ryan et al., 2018) and downstream basal ganglia nuclei (Boraud et al., 1998; Levy et al., 2001; Lozano et al., 2000; Papa et al., 1999), as well as studies of striatal gene expression (Heiman et al., 2014; Jenner, 2008) in patients and animal models, support this hypothesis. However, as we will demonstrate in Chapter 3 and 4, there is likely heterogeneity in the response of direct pathway neurons in mediating this behavior. In sum, the classical model has provided an excellent foundation, as well as a framework to generate testable hypotheses related to basal ganglia function in disease.

Cellular Mechanisms Underlying Levodopa-Induced Dyskinesia:

There are changes in cellular and circuit function throughout the basal ganglia in Parkinson's disease. How these changes might contribute to motor dysfunction is detailed in an excellent review on this topic (McGregor and Nelson, 2019). Levodopa-induced dyskinesia (LID) may arise through cellular and circuit vulnerabilities that result from chronic dopamine depletion (LID only occurs in patients with moderately advanced disease), but also through the effects of chronic levodopa treatment (in patients, LID

arises after years of treatment). These two drivers are difficult to disentangle in patients, who experience the progression of underlying disease and chronic treatment in parallel, but the fact that dyskinesia develops more quickly in patients who initiate treatment at a later stage of disease (Aquino and Fox, 2015), and the fact that some persons without PD who have been chronically (inadvertently) treated with levodopa did not develop dyskinesias (Huot, 2015), implies that chronic levodopa treatment alone does not explain LID. Though the causal mechanisms of levodopa-induced dyskinesia are as yet unclear, there are several strong hypotheses regarding cellular and circuit correlates, based upon studies in both human patients and animal models of LID.

A longstanding hypothesis in the field suggests that the chronic loss of dopamine, and/or dopamine replacement, leads to impaired striatal synaptic plasticity. Evidence for this hypothesis has been found in *ex vivo* recording studies in toxin-based rodent models of PD/LID, several of which are highlighted here (Bagetta et al., 2012; Fieblinger et al., 2014; Jenner, 2008; Picconi et al., 2003; Shen et al., 2015). In rodents of PD, striatal long term depression (LTD) is reduced (Bagetta et al., 2011; Calabresi et al., 1997; Kreitzer and Malenka, 2007; Shen et al., 2008), but treatments that restore LTD may also ameliorate motor symptoms (Kreitzer and Malenka, 2007). In rodent models of LID, investigators have found evidence of aberrant striatal long term potentiation (LTP), namely inability to depotentiate previously strengthened excitatory inputs in unidentified MSNs and dMSNs (Picconi et al., 2003; Shen et al., 2015). Again, pharmacological agents that restored depotentiation also ameliorated LID (Shen et al., 2015). Evidence of aberrant plasticity in LID includes altered AMPA/NMDA ratio (implying prior LTP and insertion of new postsynaptic AMPA receptors), which was observed by another group

(Bagetta et al., 2012). In hemiparkinsonian mice, motor sensitization to levodopa appears in part due to increased GABA release from dMSN projections to the SNr, facilitated by loss of normal GABA_B mediated inhibition (Borgkvist et al, 2015). This elegant study implied some forms of PD/LID-associated plasticity could occur outside of the striatum.

A related idea is that the number or distribution of synaptic inputs changes in PD/LID. Indeed, using various methods, investigators have found anatomical changes in presumed corticostriatal and thalamostriatal synapses in the brains of Parkinson's disease patients, such as reduction in the number of spines or changes in postsynaptic morphology in the caudate/putamen (McNeill et al., 1988; Villalba and Smith, 2018). Many similar observations have been made in animal models of disease (Day et al., 2006; Ingham et al., 1989; Smith and Villalba, 2008; Villalba et al., 2009; Villalba and Smith, 2018). In LID, several investigators have reported a reduction in spine density, but enlarged striatal spines (Nishijima et al., 2014), which might suggest a strengthening or reorganization of residual excitatory corticostriatal input. However, other studies have found a differential changes in direct and indirect pathway striatal spines in models of LID (Fieblinger et al., 2014; Suarez et al., 2014). The sensorimotor striatum receives excitatory synaptic input from all over the brain (Berendse and Groenewegen, 1990; Gerfen, 1992; Gerfen and Bolam, 2010; Hunnicutt et al., 2016; Smith et al., 2011), but these inputs might be re-weighted by chronic dopamine depletion and/or dopamine replacement therapy (Fieblinger and Cenci, 2015; Fieblinger et al., 2014; Nishijima et al., 2014; Suarez et al., 2014; Zhang et al., 2013). However, a comprehensive mapping of striatal inputs in dopamine-depleted or dopamine depleted and levodopa treated mice

has never been conducted. In Chapter 4, we will directly test whether LID is associated with pathway-specific changes in the distribution or function of striatal inputs.

Researchers have also hypothesized that changes in signaling, such as altered dopamine receptor expression or downstream signaling cascades may occur in parkinsonian animals with chronic levodopa treatment. Postsynaptic dopamine receptors have been an area of focus, as they are the direct target of dopamine projecting neurons from the midbrain. Indeed, many studies have focused on looking at expression of striatal D1-like (D1 and D5 receptors) and D2-like (D2, D3, and D4 receptors) in LID. Surprisingly, however, there is little agreement in the field from studies in postmortem human or animal tissue that dopamine receptor density changes in PD/LID (Hurley and Jenner, 2006). It is worth noting that several studies have seen an increase in the density of D1 receptors in the striatum of MPTP-treated primates. (Aubert et al., 2005; Guigoni et al., 2005; Guigoni et al., 2007). Additionally, changes in D2 receptor expression are variable (Hurley and Jenner, 2006). However, other investigators have focused on the intracellular effectors of these receptors. One of the downstream pathways of dopaminergic signaling that also contributes to receptor desensitization, the beta-arrestin pathway, has been implicated in LID (Urs et al., 2015). One of the common findings across many models and labs, however, is the increased expression of transcription factors like immediate early genes (IEGs) in the striatum of dyskinetic rodents and primates (Andersson et al., 1999; Andersson et al., 2003; Berton et al., 2009; Cao et al., 2010; Westin et al., 2001). These IEGs are believed to be surrogates of neuronal activity, and include c-Fos, FosB, and Δ FosB. Striatal expression of IEGs correlates with dyskinesia severity (Berton et al., 2009) and intrastriatal infusion of anti-sense oligonucleotides targeting FosB and Δ FosB

have been shown to decrease dyskinesia severity (Andersson et al., 1999), while overexpression of Δ FosB in the striatum reproduces dyskinesia (Cao et al., 2010), suggesting that changes in striatal activity and/or associated intracellular signaling may causally contribute to dyskinesia. Taken together, many molecular changes may play a role in the development and expression of levodopa-induced dyskinesia. In Chapter 3, we will take advantage of these IEGs in LID through the use of an activity-dependent mouse line to “capture” dyskinesia-associated neuron ensembles. Finally, in Chapter 4, we will investigate whether changes in dopamine receptor sensitivity are preferentially expressed in these dyskinesia-associated neurons.

Based on the foundational work across many neuroscience disciplines, we formulated the hypothesis the *striatum* was the causal locus within the basal ganglia that is capable of producing dyskinesia. During my thesis I explored this topic using a variety of experimental techniques, including *in vivo* and *ex vivo* electrophysiology, optogenetics, monosynaptic rabies tracings, immunohistochemistry and two mouse models of dyskinesia. The remaining chapters of this dissertation will expound on our discoveries highlighting the cells, circuits, and patterns of activity within the basal ganglia that are involved in the production of hyperkinetic movement disorders.

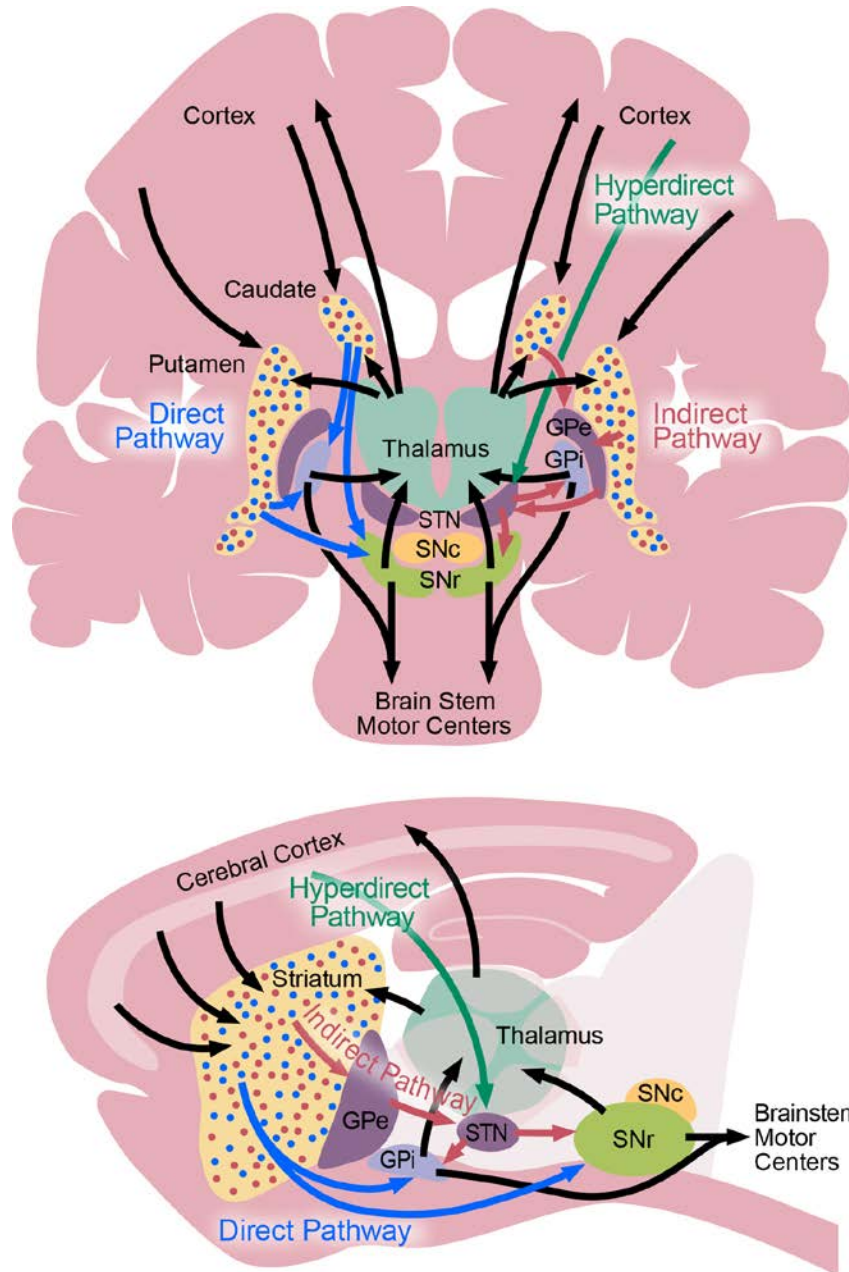


Figure 1. Simplified basal ganglia circuit diagram. Basal ganglia nuclei and their major connections in primates (top) in coronal view and in rodents (bottom) in sagittal view. Many additional connections between nuclei have been omitted for clarity. In both panels, the direct pathway is shown in blue, the indirect pathway is shown in red, and the hyperdirect pathway is in green. Black arrows represent connections shared by multiple pathways. Blue and red dots in primate caudate/putamen and rodent striatum represent direct pathway-forming and indirect pathway-forming medium spiny neurons, respectively. Abbreviations: GPe, globus pallidus, pars externa; GPi, globus pallidus, pars interna; SNc, substantia nigra, pars compacta; SNr, substantia nigra, pars reticulata; STN, subthalamic nucleus.

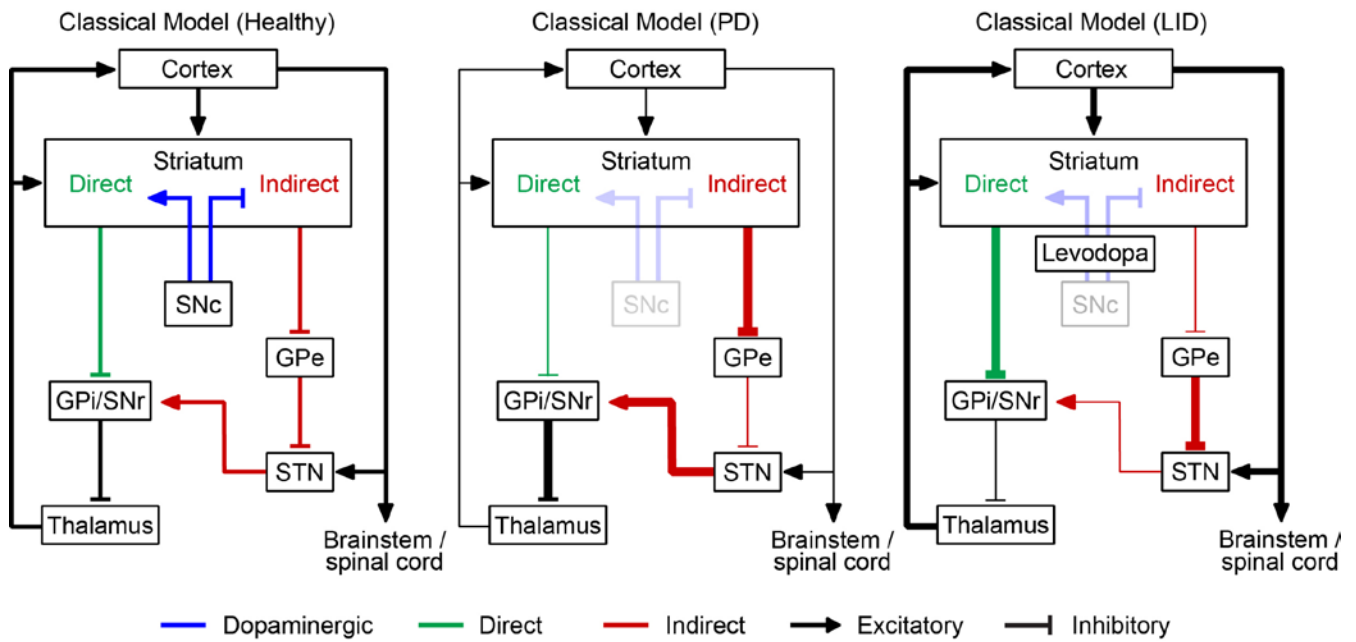


Figure 2. The classical model of the basal ganglia. The classical model in healthy (left), parkinsonian (center), and dyskinetic state (right). Adapted from DeLong, 1990.

1.4 References

- Albanese, A., Di Giovanni, M., and Lalli, S. (2019). Dystonia: diagnosis and management. *Eur J Neurol* 26, 5-17.
- Albin, R.L., Young, A.B., and Penney, J.B. (1989). The functional anatomy of basal ganglia disorders. *Trends Neurosci* 12, 366-375.
- Albin, R.L., Young, A.B., Penney, J.B., Handelin, B., Balfour, R., Anderson, K.D., Markel, D.S., Tourtellotte, W.W., and Reiner, A. (1990). Abnormalities of striatal projection neurons and N-methyl-D-aspartate receptors in presymptomatic Huntington's disease. *N Engl J Med* 322, 1293-1298.
- Alexander, G.E., and Crutcher, M.D. (1990). Functional architecture of basal ganglia circuits: neural substrates of parallel processing. *Trends Neurosci* 13, 266-271.
- Alexander, G.E., DeLong, M.R., and Strick, P.L. (1986). Parallel organization of functionally segregated circuits linking basal ganglia and cortex. *Annu Rev Neurosci* 9, 357-381.
- Andersson, M., Hilbertson, A., and Cenci, M.A. (1999). Striatal fosB expression is causally linked with L-DOPA-induced abnormal involuntary movements and the associated upregulation of striatal prodynorphin mRNA in a rat model of Parkinson's disease. *Neurobiol Dis* 6, 461-474.
- Andersson, M., Westin, J.E., and Cenci, M.A. (2003). Time course of striatal DeltaFosB-like immunoreactivity and prodynorphin mRNA levels after discontinuation of chronic dopaminomimetic treatment. *Eur J Neurosci* 17, 661-666.
- Aquino, C.C., and Fox, S.H. (2015). Clinical spectrum of levodopa-induced complications. *Mov Disord* 30, 80-89.
- Aubert, I., Guigoni, C., Hakansson, K., Li, Q., Dovero, S., Barthe, N., Bioulac, B.H., Gross, C.E., Fisone, G., Bloch, B., *et al.* (2005). Increased D1 dopamine receptor signaling in levodopa-induced dyskinesia. *Ann Neurol* 57, 17-26.
- Bagetta, V., Picconi, B., Marinucci, S., Sgobio, C., Pendolino, V., Ghiglieri, V., Fusco, F.R., Giampa, C., and Calabresi, P. (2011). Dopamine-Dependent Long-Term Depression Is Expressed in Striatal Spiny Neurons of Both Direct and Indirect Pathways: Implications for Parkinson's Disease. *Journal of Neuroscience* 31, 12513-12522.
- Bagetta, V., Sgobio, C., Pendolino, V., Del Papa, G., Tozzi, A., Ghiglieri, V., Giampa, C., Zianni, E., Gardoni, F., Calabresi, P., *et al.* (2012). Rebalance of striatal NMDA/AMPA receptor ratio underlies the reduced emergence of dyskinesia during D2-like dopamine agonist treatment in experimental Parkinson's disease. *J Neurosci* 32, 17921-17931.

- Berendse, H.W., and Groenewegen, H.J. (1990). Organization of the thalamostriatal projections in the rat, with special emphasis on the ventral striatum. *J Comp Neurol* 299, 187-228.
- Bergman, H., Wichmann, T., Karmon, B., and DeLong, M.R. (1994). The primate subthalamic nucleus. II. Neuronal activity in the MPTP model of parkinsonism. *J Neurophysiol* 72, 507-520.
- Berton, O., Guigoni, C., Li, Q., Bioulac, B.H., Aubert, I., Gross, C.E., Dileone, R.J., Nestler, E.J., and Bezard, E. (2009). Striatal overexpression of DeltaJunD resets L-DOPA-induced dyskinesia in a primate model of Parkinson disease. *Biol Psychiatry* 66, 554-561.
- Boraud, T., Bezard, E., Guehl, D., Bioulac, B., and Gross, C. (1998). Effects of L-DOPA on neuronal activity of the globus pallidus externalis (GPe) and globus pallidus internalis (GPi) in the MPTP-treated monkey. *Brain Res* 787, 157-160.
- Borgkvist, A., Lieberman, O.J., and Sulzer, D. (2018). Synaptic plasticity may underlie L-DOPA induced dyskinesia. *Current Opinion in Neurobiology* 48, 71-78.
- Brimblecombe, K.R., and Cragg, S.J. (2017). The Striosome and Matrix Compartments of the Striatum: A Path through the Labyrinth from Neurochemistry toward Function. *Acs Chem Neurosci* 8, 235-242.
- Buck, K., and Ferger, B. (2010). L-DOPA-induced dyskinesia in Parkinson's disease: a drug discovery perspective. *Drug Discov Today* 15, 867-875.
- Calabresi, P., Saiardi, A., Pisani, A., Baik, J.H., Centonze, D., Mercuri, N.B., Bernardi, G., and Borrelli, E. (1997). Abnormal synaptic plasticity in the striatum of mice lacking dopamine D2 receptors. *J Neurosci* 17, 4536-4544.
- Cao, X., Yasuda, T., Uthayathas, S., Watts, R.L., Mouradian, M.M., Mochizuki, H., and Papa, S.M. (2010). Striatal overexpression of DeltaFosB reproduces chronic levodopa-induced involuntary movements. *J Neurosci* 30, 7335-7343.
- Chang, H.T., Wilson, C.J., and Kitai, S.T. (1982). A Golgi study of rat neostriatal neurons: light microscopic analysis. *J Comp Neurol* 208, 107-126.
- Craufurd, D., Thompson, J.C., and Snowden, J.S. (2001). Behavioral changes in Huntington Disease. *Neuropsychiatry Neuropsychol Behav Neurol* 14, 219-226.
- Crittenden, J.R., and Graybiel, A.M. (2011). Basal Ganglia disorders associated with imbalances in the striatal striosome and matrix compartments. *Front Neuroanat* 5, 59.

- Cui, G., Jun, S.B., Jin, X., Pham, M.D., Vogel, S.S., Lovinger, D.M., and Costa, R.M. (2013). Concurrent activation of striatal direct and indirect pathways during action initiation. *Nature* 494, 238-242.
- Day, M., Wang, Z., Ding, J., An, X., Ingham, C.A., Shering, A.F., Wokosin, D., Ilijic, E., Sun, Z., Sampson, A.R., *et al.* (2006). Selective elimination of glutamatergic synapses on striatopallidal neurons in Parkinson disease models. *Nat Neurosci* 9, 251-259.
- DeLong, M.R. (1990). Primate models of movement disorders of basal ganglia origin. *Trends Neurosci* 13, 281-285.
- Deng, Y.P., Albin, R.L., Penney, J.B., Young, A.B., Anderson, K.D., and Reiner, A. (2004). Differential loss of striatal projection systems in Huntington's disease: a quantitative immunohistochemical study. *J Chem Neuroanat* 27, 143-164.
- Ellens, D.J., and Leventhal, D.K. (2013). Review: electrophysiology of basal ganglia and cortex in models of Parkinson disease. *J Parkinsons Dis* 3, 241-254.
- Fieblinger, T., and Cenci, M.A. (2015). Zooming in on the small: the plasticity of striatal dendritic spines in L-DOPA-induced dyskinesia. *Mov Disord* 30, 484-493.
- Fieblinger, T., Graves, S.M., Sebel, L.E., Alcacer, C., Plotkin, J.L., Gertler, T.S., Chan, C.S., Heiman, M., Greengard, P., Cenci, M.A., *et al.* (2014). Cell type-specific plasticity of striatal projection neurons in parkinsonism and L-DOPA-induced dyskinesia. *Nat Commun* 5, 5316.
- Filion, M., and Tremblay, L. (1991). Abnormal spontaneous activity of globus pallidus neurons in monkeys with MPTP-induced parkinsonism. *Brain Res* 547, 142-151.
- Gerfen, C.R. (1992). The Neostriatal Mosaic - Multiple Levels of Compartmental Organization in the Basal Ganglia. *Annual Review of Neuroscience* 15, 285-320.
- Gerfen, C.R., and Bolam, J.P. (2010). The Neuroanatomical Organization of the Basal Ganglia. *Hbk Behav Neurosci* 20, 3-28.
- Gerfen, C.R., Engber, T.M., Mahan, L.C., Susel, Z., Chase, T.N., Monsma, F.J., Jr., and Sibley, D.R. (1990). D1 and D2 dopamine receptor-regulated gene expression of striatonigral and striatopallidal neurons. *Science* 250, 1429-1432.
- Girasole, A.E., Lum, M.Y., Nathaniel, D., Bair-Marshall, C.J., Guenther, C.J., Luo, L., Kreitzer, A.C., and Nelson, A.B. (2018). A Subpopulation of Striatal Neurons Mediates Levodopa-Induced Dyskinesia. *Neuron* 97, 787-795 e786.
- Graveland, G.A., and DiFiglia, M. (1985). The frequency and distribution of medium-sized neurons with indented nuclei in the primate and rodent neostriatum. *Brain Res* 327, 307-311.

Guenther, C.J., Miyamichi, K., Yang, H.H., Heller, H.C., and Luo, L. (2013). Permanent genetic access to transiently active neurons via TRAP: targeted recombination in active populations. *Neuron* 78, 773-784.

Guigoni, C., Aubert, I., Li, Q., Gurevich, V.V., Benovic, J.L., Ferry, S., Mach, U., Stark, H., Leriche, L., Hakansson, K., *et al.* (2005). Pathogenesis of levodopa-induced dyskinesia: focus on D1 and D3 dopamine receptors. *Parkinsonism Relat Disord* 11 Suppl 1, S25-29.

Guigoni, C., Doudnikoff, E., Li, Q., Bloch, B., and Bezard, E. (2007). Altered D(1) dopamine receptor trafficking in parkinsonian and dyskinetic non-human primates. *Neurobiol Dis* 26, 452-463.

Halliday, G.M., McRitchie, D.A., Macdonald, V., Double, K.L., Trent, R.J., and McCusker, E. (1998). Regional specificity of brain atrophy in Huntington's disease. *Exp Neurol* 154, 663-672.

Heiman, M., Heilbut, A., Francardo, V., Kulicke, R., Fenster, R.J., Kolaczyk, E.D., Mesirov, J.P., Surmeier, D.J., Cenci, M.A., and Greengard, P. (2014). Molecular adaptations of striatal spiny projection neurons during levodopa-induced dyskinesia. *Proc Natl Acad Sci U S A* 111, 4578-4583.

Hernandez-Lopez, S., Bargas, J., Surmeier, D.J., Reyes, A., and Galarraga, E. (1997). D1 receptor activation enhances evoked discharge in neostriatal medium spiny neurons by modulating an L-type Ca²⁺ conductance. *J Neurosci* 17, 3334-3342.

Hernandez-Lopez, S., Tkatch, T., Perez-Garci, E., Galarraga, E., Bargas, J., Hamm, H., and Surmeier, D.J. (2000). D2 dopamine receptors in striatal medium spiny neurons reduce L-type Ca²⁺ currents and excitability via a novel PLC[β 1]-IP3-calcineurin-signaling cascade. *J Neurosci* 20, 8987-8995.

Hunnicutt, B.J., Jongbloets, B.C., Birdsong, W.T., Gertz, K.J., Zhong, H., and Mao, T. (2016). A comprehensive excitatory input map of the striatum reveals novel functional organization. *Elife* 5.

Huot, P. (2015). L-DOPA-induced dyskinesia, is striatal dopamine depletion a requisite? *J Neurol Sci* 351, 9-12.

Hurley, M.J., and Jenner, P. (2006). What has been learnt from study of dopamine receptors in Parkinson's disease? *Pharmacol Ther* 111, 715-728.

Ingham, C.A., Hood, S.H., and Arbuthnott, G.W. (1989). Spine density on neostriatal neurones changes with 6-hydroxydopamine lesions and with age. *Brain Res* 503, 334-338.

- Inokawa, H., Yamada, H., Matsumoto, N., Muranishi, M., and Kimura, M. (2010). Juxtacellular labeling of tonically active neurons and phasically active neurons in the rat striatum. *Neuroscience* 168, 395-404.
- Irwin, D.J., White, M.T., Toledo, J.B., Xie, S.X., Robinson, J.L., Van Deerlin, V., Lee, V.M., Leverenz, J.B., Montine, T.J., Duda, J.E., *et al.* (2012). Neuropathologic substrates of Parkinson disease dementia. *Ann Neurol* 72, 587-598.
- Jenner, P. (2008). Molecular mechanisms of L-DOPA-induced dyskinesia. *Nat Rev Neurosci* 9, 665-677.
- Jernigan, T.L., Salmon, D.P., Butters, N., and Hesselink, J.R. (1991). Cerebral structure on MRI, Part II: Specific changes in Alzheimer's and Huntington's diseases. *Biol Psychiatry* 29, 68-81.
- Kawaguchi, Y. (1993). Physiological, morphological, and histochemical characterization of three classes of interneurons in rat neostriatum. *J Neurosci* 13, 4908-4923.
- Kimura, M., Rajkowski, J., and Evarts, E. (1984). Tonically discharging putamen neurons exhibit set-dependent responses. *Proc Natl Acad Sci U S A* 81, 4998-5001.
- Kitai, S.T., and Deniau, J.M. (1981). Cortical inputs to the subthalamus: intracellular analysis. *Brain Res* 214, 411-415.
- Klaus, A., Martins, G.J., Paixao, V.B., Zhou, P., Paninski, L., and Costa, R.M. (2017). The Spatiotemporal Organization of the Striatum Encodes Action Space. *Neuron* 96, 949.
- Kravitz, A.V., Freeze, B.S., Parker, P.R., Kay, K., Thwin, M.T., Deisseroth, K., and Kreitzer, A.C. (2010). Regulation of parkinsonian motor behaviours by optogenetic control of basal ganglia circuitry. *Nature* 466, 622-626.
- Kravitz, A.V., Tye, L.D., and Kreitzer, A.C. (2012). Distinct roles for direct and indirect pathway striatal neurons in reinforcement. *Nat Neurosci* 15, 816-818.
- Kreitzer, A.C., and Malenka, R.C. (2007). Endocannabinoid-mediated rescue of striatal LTD and motor deficits in Parkinson's disease models. *Nature* 445, 643-647.
- Lanciego, J.L., Luquin, N., and Obeso, J.A. (2012). Functional neuroanatomy of the basal ganglia. *Cold Spring Harb Perspect Med* 2, a009621.
- Lerner, T.N., and Kreitzer, A.C. (2011). Neuromodulatory control of striatal plasticity and behavior. *Curr Opin Neurobiol* 21, 322-327.
- Levy, R., Dostrovsky, J.O., Lang, A.E., Sime, E., Hutchison, W.D., and Lozano, A.M. (2001). Effects of apomorphine on subthalamic nucleus and globus pallidus internus neurons in patients with Parkinson's disease. *J Neurophysiol* 86, 249-260.

- Liang, L., DeLong, M.R., and Papa, S.M. (2008). Inversion of dopamine responses in striatal medium spiny neurons and involuntary movements. *J Neurosci* 28, 7537-7547.
- Lozano, A.M., Lang, A.E., Levy, R., Hutchison, W., and Dostrovsky, J. (2000). Neuronal recordings in Parkinson's disease patients with dyskinesias induced by apomorphine. *Ann Neurol* 47, S141-146.
- McGeorge, A.J., and Faull, R.L. (1987). The organization and collateralization of corticostriate neurones in the motor and sensory cortex of the rat brain. *Brain Res* 423, 318-324.
- McGregor, M.M., and Nelson, A.B. (2019). Circuit Mechanisms of Parkinson's Disease. *Neuron* 101, 1042-1056.
- McNeill, T.H., Brown, S.A., Rafols, J.A., and Shoulson, I. (1988). Atrophy of medium spiny I striatal dendrites in advanced Parkinson's disease. *Brain Res* 455, 148-152.
- Mink, J.W. (1996). The basal ganglia: focused selection and inhibition of competing motor programs. *Prog Neurobiol* 50, 381-425.
- Mink, J.W., and Thach, W.T. (1993). Basal ganglia intrinsic circuits and their role in behavior. *Curr Opin Neurobiol* 3, 950-957.
- Monakow, K.H., Akert, K., and Kunzle, H. (1978). Projections of the precentral motor cortex and other cortical areas of the frontal lobe to the subthalamic nucleus in the monkey. *Exp Brain Res* 33, 395-403.
- Nambu, A., Takada, M., Inase, M., and Tokuno, H. (1996). Dual somatotopical representations in the primate subthalamic nucleus: evidence for ordered but reversed body-map transformations from the primary motor cortex and the supplementary motor area. *J Neurosci* 16, 2671-2683.
- Nishijima, H., Suzuki, S., Kon, T., Funamizu, Y., Ueno, T., Haga, R., Suzuki, C., Arai, A., Kimura, T., Suzuki, C., *et al.* (2014). Morphologic changes of dendritic spines of striatal neurons in the levodopa-induced dyskinesia model. *Mov Disord* 29, 336-343.
- Ozelius, L.J., Hewett, J.W., Page, C.E., Bressman, S.B., Kramer, P.L., Shalish, C., de Leon, D., Brin, M.F., Raymond, D., Corey, D.P., *et al.* (1997). The early-onset torsion dystonia gene (DYT1) encodes an ATP-binding protein. *Nat Genet* 17, 40-48.
- Papa, S.M., Desimone, R., Fiorani, M., and Oldfield, E.H. (1999). Internal globus pallidus discharge is nearly suppressed during levodopa-induced dyskinesias. *Ann Neurol* 46, 732-738.

- Papoutsis, M., Labuschagne, I., Tabrizi, S.J., and Stout, J.C. (2014). The cognitive burden in Huntington's disease: pathology, phenotype, and mechanisms of compensation. *Mov Disord* 29, 673-683.
- Parent, M., and Parent, A. (2004). The pallidofugal motor fiber system in primates. *Parkinsonism Relat Disord* 10, 203-211.
- Parker, J.G., Marshall, J.D., Ahanonu, B., Wu, Y.W., Kim, T.H., Grewe, B.F., Zhang, Y., Li, J.Z., Ding, J.B., Ehlers, M.D., *et al.* (2018). Diametric neural ensemble dynamics in parkinsonian and dyskinetic states. *Nature* 557, 177-182.
- Penney, J.B., Jr., and Young, A.B. (1983). Speculations on the functional anatomy of basal ganglia disorders. *Annu Rev Neurosci* 6, 73-94.
- Perez, X.A., Zhang, D., Bordia, T., and Quirk, M. (2017). Striatal D1 medium spiny neuron activation induces dyskinesias in parkinsonian mice. *Mov Disord* 32, 538-548.
- Picconi, B., Centonze, D., Hakansson, K., Bernardi, G., Greengard, P., Fisone, G., Cenci, M.A., and Calabresi, P. (2003). Loss of bidirectional striatal synaptic plasticity in L-DOPA-induced dyskinesia. *Nat Neurosci* 6, 501-506.
- Planert, H., Berger, T.K., and Silberberg, G. (2013). Membrane Properties of Striatal Direct and Indirect Pathway Neurons in Mouse and Rat Slices and Their Modulation by Dopamine. *Plos One* 8.
- Plotkin, J.L., and Surmeier, D.J. (2015). Corticostriatal synaptic adaptations in Huntington's disease. *Curr Opin Neurobiol* 33, 53-62.
- Reiner, A., Albin, R.L., Anderson, K.D., D'Amato, C.J., Penney, J.B., and Young, A.B. (1988). Differential loss of striatal projection neurons in Huntington disease. *Proc Natl Acad Sci U S A* 85, 5733-5737.
- Reiner, A., Medina, L., and Veenman, C.L. (1998). Structural and functional evolution of the basal ganglia in vertebrates. *Brain Res Brain Res Rev* 28, 235-285.
- Rosas, H.D., Goodman, J., Chen, Y.I., Jenkins, B.G., Kennedy, D.N., Makris, N., Patti, M., Seidman, L.J., Beal, M.F., and Koroshetz, W.J. (2001). Striatal volume loss in HD as measured by MRI and the influence of CAG repeat. *Neurology* 57, 1025-1028.
- Ryan, M.B., Bair-Marshall, C., and Nelson, A.B. (2018). Aberrant Striatal Activity in Parkinsonism and Levodopa-Induced Dyskinesia. *Cell Rep* 23, 3438-3446 e3435.
- Shen, W., Flajolet, M., Greengard, P., and Surmeier, D.J. (2008). Dichotomous dopaminergic control of striatal synaptic plasticity. *Science* 321, 848-851.
- Shen, W., Plotkin, J.L., Francardo, V., Ko, W.K., Xie, Z., Li, Q., Fieblinger, T., Wess, J.,

Neubig, R.R., Lindsley, C.W., *et al.* (2015). M4 Muscarinic Receptor Signaling Ameliorates Striatal Plasticity Deficits in Models of L-DOPA-Induced Dyskinesia. *Neuron* 88, 762-773.

Singh, A., Liang, L., Kaneoke, Y., Cao, X., and Papa, S.M. (2015). Dopamine regulates distinctively the activity patterns of striatal output neurons in advanced parkinsonian primates. *J Neurophysiol* 113, 1533-1544.

Smith, Y., Surmeier, D.J., Redgrave, P., and Kimura, M. (2011). Thalamic Contributions to Basal Ganglia-Related Behavioral Switching and Reinforcement. *Journal of Neuroscience* 31, 16102-16106.

Smith, Y., and Villalba, R. (2008). Striatal and extrastriatal dopamine in the basal ganglia: an overview of its anatomical organization in normal and Parkinsonian brains. *Mov Disord* 23 Suppl 3, S534-547.

Soares, J., Kliem, M.A., Betarbet, R., Greenamyre, J.T., Yamamoto, B., and Wichmann, T. (2004). Role of external pallidal segment in primate parkinsonism: comparison of the effects of 1-methyl-4-phenyl-1,2,3,6-tetrahydropyridine-induced parkinsonism and lesions of the external pallidal segment. *J Neurosci* 24, 6417-6426.

Stephenson-Jones, M., Ericsson, J., Robertson, B., and Grillner, S. (2012). Evolution of the basal ganglia: dual-output pathways conserved throughout vertebrate phylogeny. *J Comp Neurol* 520, 2957-2973.

Stout, J.C., Jones, R., Labuschagne, I., O'Regan, A.M., Say, M.J., Dumas, E.M., Queller, S., Justo, D., Santos, R.D., Coleman, A., *et al.* (2012). Evaluation of longitudinal 12 and 24 month cognitive outcomes in premanifest and early Huntington's disease. *J Neurol Neurosurg Psychiatry* 83, 687-694.

Stuber, G.D., Hnasko, T.S., Britt, J.P., Edwards, R.H., and Bonci, A. (2010). Dopaminergic terminals in the nucleus accumbens but not the dorsal striatum corelease glutamate. *J Neurosci* 30, 8229-8233.

Suarez, L.M., Solis, O., Carames, J.M., Taravini, I.R., Solis, J.M., Murer, M.G., and Moratalla, R. (2014). L-DOPA treatment selectively restores spine density in dopamine receptor D2-expressing projection neurons in dyskinetic mice. *Biol Psychiatry* 75, 711-722.

Tepper, J.M., Tecuapetla, F., Koos, T., and Ibanez-Sandoval, O. (2010). Heterogeneity and diversity of striatal GABAergic interneurons. *Frontiers in neuroanatomy* 4, 150.

Tritsch, N.X., Ding, J.B., and Sabatini, B.L. (2012). Dopaminergic neurons inhibit striatal output through non-canonical release of GABA. *Nature* 490, 262-+.

Urs, N.M., Bido, S., Peterson, S.M., Daigle, T.L., Bass, C.E., Gainetdinov, R.R., Bezard, E., and Caron, M.G. (2015). Targeting beta-arrestin2 in the treatment of L-DOPA-induced dyskinesia in Parkinson's disease. *Proc Natl Acad Sci U S A* *112*, E2517-2526.

Villalba, R.M., Lee, H., and Smith, Y. (2009). Dopaminergic denervation and spine loss in the striatum of MPTP-treated monkeys. *Exp Neurol* *215*, 220-227.

Villalba, R.M., and Smith, Y. (2018). Loss and remodeling of striatal dendritic spines in Parkinson's disease: from homeostasis to maladaptive plasticity? *J Neural Transm (Vienna)* *125*, 431-447.

Westin, J.E., Andersson, M., Lundblad, M., and Cenci, M.A. (2001). Persistent changes in striatal gene expression induced by long-term L-DOPA treatment in a rat model of Parkinson's disease. *Eur J Neurosci* *14*, 1171-1176.

Wilson, C.J., Chang, H.T., and Kitai, S.T. (1990). Firing patterns and synaptic potentials of identified giant aspiny interneurons in the rat neostriatum. *J Neurosci* *10*, 508-519.

Zhang, Y., Meredith, G.E., Mendoza-Elias, N., Rademacher, D.J., Tseng, K.Y., and Steece-Collier, K. (2013). Aberrant restoration of spines and their synapses in L-DOPA-induced dyskinesia: involvement of corticostriatal but not thalamostriatal synapses. *J Neurosci* *33*, 11655-11667.

CHAPTER 2

Striatal indirect pathway dysfunction underlies motor deficits in a mouse model of human dyskinesia

2.1 Abstract

Abnormal involuntary movements, or dyskinesias, are seen in many neurological diseases, including disorders where the brain appears grossly normal, suggesting circuit dysfunction may be a root cause. Using unsupervised gene co-expression analysis, we identified co-expression modules in human striatum that are enriched with dyskinesia genes and markers of indirect pathway projection neurons (iMSNs). Among the genes in these dyskinesia modules is PNKD, which is causative for paroxysmal nonkinesigenic dyskinesia (PNKD). We used electrophysiological, optogenetic, and chemogenetic techniques to evaluate basal ganglia circuit function in a transgenic mouse model of PNKD. We find that dyskinesia bouts in PNKD mice are caused by a transient loss of iMSN activity, likely driven by aberrant endocannabinoid-mediated suppression of excitatory presynaptic terminals. These data provide both genetic and functional evidence for dysfunction of striatal iMSNs in the etiology of dyskinesia, and may guide development of new treatments for dyskinesias based on selective modulation of basal ganglia circuitry.

2.2 Introduction

A number of neurological disorders are characterized by abnormal involuntary movements, including neurodegenerative conditions like Huntington's disease and disorders where the brain appears grossly normal, such as many forms of dystonia. While the physiological basis of such abnormal movements, or dyskinesias, is unknown, several lines of evidence suggest that basal ganglia circuit dysfunction may be a key factor. First, in secondary dyskinesias, where anatomical abnormalities are seen on imaging or pathological examination, lesions are most commonly found in the basal ganglia (Albanese et al., 2013). Second, some forms of dyskinesia are triggered by drugs that are believed to act on receptors concentrated in the basal ganglia, such as dopamine receptors (Burkhard, 2014). Third, abnormal neural activity has been found in basal ganglia recordings from humans with involuntary movements, such as dystonia (Schrock et al., 2009) and levodopa-induced dyskinesia (Levy et al., 2001; Lozano et al., 2000; Papa et al., 1999). Finally, in several forms of dyskinesia, basal ganglia deep brain stimulation (DBS) relieves motor symptoms (Deep-Brain Stimulation for Parkinson's Disease Study, 2001; Kumar et al., 1998; Vidailhet et al., 2005), suggesting that circuit dysfunction is a root cause. However, recent studies have also found abnormal activity in the cerebellum (Calderon et al., 2011; Fremont et al., 2017; Fremont et al., 2015), indicating broader network dysfunction in some forms of dystonia.

The standard model of basal ganglia function posits that two main pathways, the direct and indirect pathways, have roughly opposing functions in regulating movement (Albin et al., 1989; DeLong, 1990). These two pathways originate in the input nucleus of the basal ganglia, the striatum. In its simplest formulation, activity in the direct pathway is

hypothesized to promote or invigorate movements, while activity in the indirect pathway broadly suppresses movements. Consistent with this idea, optical stimulation of direct pathway projection neurons (dMSNs) leads to increased movement, while stimulation of indirect pathway projection neurons (iMSNs) causes freezing (Kravitz et al., 2010). *In vivo*, both pathways are co-active (Cui et al., 2013; Isomura et al., 2013), but show decorrelations on rapid timescales that may be critical for action selection (Markowitz et al., 2018). More specific formulations of the classical model have suggested that the indirect pathway mediates a broad suppression of competing motor programs (Mink, 1996) or action-specific suppression of competing movement features (Klaus et al., 2017). In either case, failure to activate the indirect pathway could lead to simultaneous selection of competing movement plans, resulting in both voluntary and involuntary movements. While some electrophysiological recordings from basal ganglia output nuclei are consistent with this hypothesis (Levy et al., 2001; Lozano et al., 2000; Papa et al., 1999), other data suggest that burst firing or oscillatory activity may be a stronger correlate of dyskinesias (Halje et al., 2012; Singh et al., 2015; Swann et al., 2016).

Despite recent advances in understanding basal ganglia circuit function, progress has been hampered on the key question of whether abnormal activity in striatal circuitry causes dyskinesia. This can be attributed both to the diverse set of genes and conditions that give rise to dyskinesia, as well as to a scarcity of mouse models that show the types of involuntary movements seen in human patients. Here, we leveraged the rich human genetics of dyskinesia to identify putative striatal cell types implicated in motor dysfunction, using unsupervised gene co-expression analysis (Kelley et al., 2018). Among the dyskinesia genes most strongly associated with these striatal co-expression

modules was PNKD, mutations in which cause paroxysmal nonkinesigenic dyskinesia (PNKD) in humans, and a similar dyskinetic phenotype in a BAC transgenic mouse model (Lee et al., 2012; Lee et al., 2004; Rainier et al., 2004). PNKD is characterized by attacks of involuntary movements triggered by stress, caffeine, or ethanol. As in many hyperkinetic disorders, the gross brain structure of PNKD patients (Liang et al., 2015) and mice (Lee et al., 2012) appears normal. Although the PNKD protein is widely expressed in neurons and at synapses in the CNS (Lee et al., 2004), its function is unknown.

Evidence suggests that wild-type PNKD protein could play a role in redox status and protein degradation (Shen et al., 2011), and more specifically regulating exocytosis and synaptic transmission via stabilizing interactions with active zone proteins, RIM1 and RIM2 (Shen et al., 2015). Given this potential function, abnormal PNKD protein may trigger circuit dysfunction and dyskinesia at the level of the striatum. The striatum is the site of highest expression for dopamine and adenosine A2a receptors in the brain (Dearry et al., 1990; Rosin et al., 1998; Weiner et al., 1991). In PNKD mutant mice, striatal dopamine signaling is altered (Lee et al., 2012), and the adenosine A2a antagonist, caffeine, triggers dyskinesia. These observations suggest that in PNKD, the combination of pharmacological triggers that target the striatum and baseline abnormalities in synaptic function may create a predisposition to developing abnormal striatal activity and dyskinesia.

Because PNKD is an episodic disorder, it is particularly useful in understanding the physiological changes that occur during the onset of a dyskinetic attack. Therefore, we combined a transgenic mouse model of PNKD with *in vivo* electrophysiology, optogenetics, and chemogenetics to examine whether basal ganglia dysfunction—and

iMSN dysfunction in particular—causes dyskinesia. Using this approach, we found that in PNKD mice, episodes of dyskinesia are associated with a profound loss of iMSN activity. Furthermore, inhibition of iMSNs is both necessary and sufficient for the production of dyskinesia in this model. Finally, we found evidence for dysregulation of endocannabinoid-mediated synaptic plasticity at excitatory inputs to iMSNs, which may underlie their aberrant suppression during dyskinesia.

2.3 Results

Involuntary movements, including dystonia, are a feature of several human neurological disorders, each of which is likely to have distinct pathogenesis. No unifying neuropathological correlate has been identified across these many individual disorders, implying abnormal activity and/or connectivity may lead to dyskinesia. Though we hypothesized that the striatum may be a key region, functional changes in a number of brain regions may be responsible. As a first step in narrowing this focus, we explored whether dyskinesia-associated genes are more strongly enriched among genes that are co-expressed in the striatum, as compared to other brain regions, utilizing existing postmortem gene expression datasets from neurotypical adult humans. We performed unsupervised gene co-expression analysis of 53 datasets representing 6336 human brain samples by aggregating data from nine studies (Table S1) (Kelley et al., 2018). We performed enrichment analysis using a set of previously-published dyskinesia-associated genes (Table S2) in co-expression modules identified in each dataset. Consistent with our hypothesis, this analysis revealed the greatest enrichment of dyskinesia genes in co-expression modules from the human striatum (Figure 1A).

The striatum is composed of multiple cell types, including the principal neurons, direct and indirect pathway medium spiny neurons (dMSNs and iMSNs, respectively), interneurons (including cholinergic and parvalbumin-positive interneurons), and glia. Changes in the function of any one of these cell types might contribute to dyskinesia pathogenesis and/or pathophysiology. To determine whether the striatal co-expression modules that were enriched with dyskinesia genes (i.e. 'dyskinesia modules') were associated with distinct cell types, we analyzed enrichment for known cell-type markers

of dMSNs, iMSNs, cholinergic interneurons, fast-spiking interneurons, and glia. We found that dyskinesia modules were significantly enriched with markers of iMSNs (Figure 1B). These findings indicate that iMSNs may be a key cell type dysregulated across multiple types of dyskinesia.

To determine the affinity of each gene for each dyskinesia module, we calculated the weighted gene coexpression network analysis measure of intramodular connectivity, or k_{ME} (defined as the Pearson correlation between the expression pattern of a gene and the first principal component of a dyskinesia module) (Langfelder & Horvath, 2008). k_{ME} values for significant dyskinesia modules were aggregated over all striatal gene expression datasets to produce a single metric (z-score), which ranks all genes in the genome for their similarity to the consensus dyskinesia module. Several of the dyskinesia-associated genes appear at the upper end of this distribution, including ANO3, a recently identified calcium-activated chloride channel highly expressed in the striatum, mutations in which are associated with cervical dystonia (Charlesworth et al., 2012); PDE10A, a phosphodiesterase highly expressed in striatal neurons, implicated in the mechanisms of levodopa-induced dyskinesia, and mutations in which are associated with childhood onset chorea (Mencacci et al., 2016); and PNKD, a gene associated with paroxysmal nonkinesigenic dyskinesia (Figure 1C). We also found that PNKD gene expression had a higher correlation with iMSN than with dMSN-associated genes (Figure 1D). Together, these genetic data indicate that dyskinesia-related genes are significantly enriched among genes that are co-expressed in the striatum, and specifically point to the indirect pathway as a potential site of dysfunction.

To explore the role of the indirect pathway in dyskinesia, we utilized a PNKD mouse model of dyskinesia. In both patients and mice with this disorder, caffeine, alcohol, or stress triggers attacks of involuntary movements lasting several hours (Lee et al., 2012). Approximately 5-10 minutes after intraperitoneal (IP) injection of caffeine (25 mg/kg), wild-type (WT) mice develop mild hyperactivity, but PNKD mice develop markedly abnormal movement, including repetitive licking, gnawing, choreiform movements of the forepaws, and intermittent dystonic postures (Figure 2A,B), as has been reported previously (Lee et al., 2012). Similarly, after IP administration of ethanol (1.5 g/kg), WT mice show little qualitative change in behavior, but PNKD mice develop severely abnormal movements (Figure S1A). As has been reported previously (Lee et al., 2012), ethanol tends to trigger more severe attacks than does caffeine in PNKD mice, with more prominent and prolonged dystonia. During these more severe ethanol-induced attacks, the overall movement velocity of mice was reduced (Figure S2B), which was rarely observed in caffeine-treated animals (Figure S2C). For this reason, we focused on caffeine-induced attacks in the majority of our subsequent studies. These attacks induced abnormal movements without causing substantive reductions in overall movement. Given the known relationship of neuronal firing or other measures of activity to movement velocity (Cui et al., 2013; Isomura et al., 2013; Jin et al., 2014; Markowitz et al., 2018; Parker et al., 2018), we reasoned that profound reductions in overall movement could be a confound in studying basal ganglia physiology during dyskinesia.

To date, no definitive evidence indicates what site in the brain causes dyskinesia in PNKD. However, current theories regarding the pathophysiology of dyskinesias, our genetic data, as well as clues related to the PNKD protein (Shen et al., 2015), suggest

the striatum may be a key site. To determine whether dyskinesia could be triggered by local caffeine infusion in the striatum, we implanted infusion cannulae in the dorsolateral (sensorimotor) striatum of PNKD mice and WT littermates (Figure 2C). The site and extent of drug diffusion was confirmed postmortem after *in vivo* infusion of a lipophilic dye, FM4-64X (Figure S1D-E). Saline infusion did not trigger dyskinesias in WT or PNKD mice (Figure 2D left). However, caffeine infusion reliably triggered dyskinesia in PNKD mice (Figure 2D right, $p=0.026$ compared to WT mice). The ability of local striatal caffeine to reproduce the behavioral effects of systemic caffeine administration suggested that abnormalities in striatal function are critical for dyskinetic attacks in PNKD.

We took advantage of the paroxysmal nature of this disorder to investigate the activity of striatal neurons during dyskinetic attacks, using multi-electrode arrays implanted in the dorsolateral striatum (Figure 2E; Figure S1F-H). The single-unit activity of striatal MSNs was assessed before and after drug injection in PNKD mice and their WT littermates during open field behavior. In the non-dyskinetic state (prior to any drug injections), the firing rates of MSNs recorded in WT mice (Figure S2I, 1.33 ± 0.18 spikes/sec; $n=376$ units; $N=12$ mice) did not differ from those recorded in PNKD animals (Figure S2J, 1.40 ± 0.10 spikes/sec; $n=350$ units; $N=16$ mice; $p=0.13$, Mann-Whitney). Caffeine injection triggered mild hyperactivity and a modest increase in the average MSN firing rate in WT animals to 1.61 ± 0.09 spikes/sec (Figure 2G, Figure S2I; $n=230$ units; $N=12$ mice; $p=0.0013$, signed-rank), with individual neurons showing both increases and decreases in firing rate (Figure 2F). Surprisingly, in PNKD animals, caffeine triggered a decrease in the average firing rate to 0.79 ± 0.18 spikes/sec (Figure 2G, Figure S2J; $n=205$ units; $N=16$ mice; $p<0.0001$, signed-rank) in parallel with dyskinesia. We next

investigated whether ethanol injection also altered the firing of MSNs in PNKD mice. Though a rapid decrease in firing rate was observed in both WT and PNKD mice following ethanol injection (Figure S2K), a more sustained decrease in firing was observed in PNKD mice (to 0.57 ± 0.10 spikes/sec, $n=139$ units; $N=16$ mice) as compared to WT mice (1.16 ± 0.12 spikes/sec, $n=133$ units; $N=12$ mice). The average firing rate of MSNs was even lower in ethanol- versus caffeine-triggered attacks in PNKD mice (p for comparison here), perhaps related to the severity of attacks. Thus, in contrast to other models of dyskinesia and/or dystonia (Gernert et al., 1999; Liang et al., 2008), reduced striatal single-unit activity was observed during dyskinesia. Given the hypothesis that dyskinesias may be associated with increases in dMSN activity, decreases in iMSN activity, or both, these findings raise the possibility that a reduction in iMSN firing causes abnormal involuntary movements in PNKD.

To specifically record from striatal dMSNs or iMSNs, we used an optogenetic labeling approach (Jin et al., 2014; Kravitz et al., 2013). In Cre recombinase mouse lines that selectively label neurons composing the two pathways (Drd1-Cre (D1-cre) and Adora2a-Cre (A2a-Cre) for the direct and indirect pathway, respectively (Gong et al., 2007), we performed single-unit recordings in freely moving animals previously injected with an AAV encoding Cre-dependent channelrhodopsin-2 (ChR2, Figure 3A, Figure S3A). Positively-identified units showed short-latency firing (<15 msec; see Methods) to blue light pulses (Figure 3B, Figure S3B). Based on classical models of basal ganglia function (DeLong, 1990), the development of hyperactivity and/or involuntary movements is predicted to result from an increase in direct pathway activity, a decrease in indirect pathway activity, or both.

At baseline, the firing rate of optogenetically-identified dMSNs did not differ between WT (Figure S3C; 1.72 ± 0.22 spikes/sec; $n=66$ dMSNs; $N=5$ mice) and PNKD animals (Figure S3D; 1.66 ± 0.31 spikes/sec; $n=32$ dMSNs; $N=6$ mice; $p=0.33$). The baseline firing rate of iMSNs also did not differ between WT (Figure S3E; 1.42 ± 0.28 spikes/sec; $n=34$ iMSNs; $N=4$ mice) and PNKD (Figure S3F; 1.40 ± 0.17 spikes/sec; $n=68$ iMSNs; $N=7$ mice; $p=0.59$). After caffeine injection, individual dMSNs showed increases, decreases, or no change in firing rate in both WT and PNKD animals (Figure 3C, Figure S3C-D). On average, dMSNs showed an increase in firing rate following caffeine injection in WT animals ($p=0.008$), but not in PNKD animals ($p=0.32$). These experiments indicated that changes in striatal dMSN firing rate were not a physiological correlate of caffeine-induced dyskinetic attacks in PNKD mice.

An alternative explanation is that iMSN activity decreases during dyskinetic attacks. In support of this hypothesis, we found significant changes in iMSN activity that developed in parallel with dyskinesia in PNKD mice. In WT iMSNs, a variety of individual responses were seen (Figure S3E), but average firing rate was unchanged after caffeine injection (Figure 3D, $n=21$ iMSNs, $N=4$ mice; $p=0.59$). In contrast, the firing rate of PNKD iMSNs decreased (Figure 3D, Figure S3F), on average to 0.09 ± 0.03 spikes/sec ($n=38$ iMSNs, $N=7$ mice; $p<0.0001$). To investigate how the caffeine-triggered decrease in iMSN activity might be related to dyskinesia in PNKD mice, we looked more closely at the timing of firing rate and behavioral changes. In all but one PNKD iMSN recorded, the firing rate decreased significantly (see Supplementary Methods) *prior* to the onset of dyskinesia (Figure 3F). In extended recording sessions lasting 4-6 hours, the timing of iMSN firing rate changes closely paralleled both the onset and offset of dyskinesia, with decreased

firing rate during dyskinesias and restoration of baseline firing rate at the time of behavioral recovery (Figure 3E, Figure S3G). These findings indicate that in PNKD mice, caffeine-induced dyskinesia is tightly correlated with suppression of iMSN firing.

We also recorded from optically-identified dMSNs and iMSNs before and after ethanol treatment. In WT mice, ethanol induced a modest reduction in the firing rate of dMSNs (Figure S2H, $n=28$, $N=5$, $p=0.005$), but did not significantly alter iMSN firing rate (Figure S2I, $n=13$, $N=4$, $p=0.13$). Like caffeine, ethanol triggered profound decreases in iMSN firing in PNKD mice (S2I, $n=30$, $N=7$, $P=0.0005$). Though variable, we found that ethanol-induced attacks were also accompanied by decreases in the activity of dMSNs (Figure S2H, $n=14$, $N=4$, $p=0.02$). These differences between the effects of ethanol and caffeine on physiology may reflect the differences in the effects of the two drugs on normal locomotion (in both WT and PNKD mice), and the severity of ethanol-induced attacks in PNKD mice (see Figure 2A, Figure S1A). Ethanol reduces movement modestly in wild-type mice, and more profoundly reduces overall movement in PNKD mice (Figure S1B). In healthy animals, the activity of both dMSNs and iMSNs is known to correlate with movement velocity over a variety of timescales (Klaus et al., 2017; Markowitz et al., 2018) (Ryan et al., 2018). Thus, the activity of both dMSNs and iMSNs would be expected to decrease during the periods of reduced movement seen following ethanol treatment. Such a reduction in overall movement was not observed during caffeine-induced attacks (Figure S1C).

Loss of iMSN activity and dyskinesia are strongly correlated in PNKD, but these findings do not demonstrate causality. Indeed, dyskinesia may be characterized by changes in activity in many brain regions, some causative and others the result of the

altered experience of a dyskinetic animal. To determine whether inhibition of iMSN activity is sufficient to cause dyskinesia in the absence of caffeine, we employed a chemogenetic approach. We expressed the inhibitory DREADD, hM4D(G_i-coupled) or a control fluorophore (mCherry) in iMSNs of the dorsolateral striatum of both WT;A2a-Cre and PNKD;A2a-Cre mice (Figure 4A,F). To validate the use of hM4D, we first performed whole-cell *ex vivo* recordings in brain slices from a subset of mice co-injected with Cre-dependent ChR2-eYFP (Figure 4A). Brief blue light pulses evoked spiking in ChR2-eYFP positive iMSNs (Figure 4B). Voltage-clamp recordings in postsynaptic eYFP-negative MSNs (Figure 4C) or globus pallidus pars externa neurons (GPe, Figure 4D) showed light-evoked inhibitory currents. As expected (Bock et al., 2013; Stachniak et al., 2014), application of the DREADD agonist clozapine-N-oxide (CNO, 1 μ M) inhibited iMSN synaptic output onto both intrastriatal and pallidal targets (Figure 3C-E; n=13 striatal, n=5 GPe cells, N=5 mice, p=0.0016). We repeated these experiments in slices from PNKD;A2a-Cre mice, and found that CNO also reduced light-evoked IPSC amplitude in the striatum and GPe (Figure 3E; n=7 striatal, n=5 GPe cells, N=3 mice, p=0.03), confirming that the G_i-coupled DREADD worked at least as well in PNKD animals. Using whole-cell current-clamp recordings, we also observed a modest hyperpolarization of resting membrane potential in mCherry-positive iMSNs after CNO application (Figure 3E; 2.7 \pm 1.1 mV; n=7 iMSNs, N=2 mice), as has been seen in other studies using the G_i-DREADD in the striatum (Kozorovitskiy et al., 2012).

To determine whether activating G_i-DREADDs in striatal iMSNs could cause dyskinesia, we tested the effects of CNO on animals in the open field. After habituation to daily IP saline injections (Figure 4G), we scored motor behavior after injection of saline

or CNO. Administration of saline did not alter behavior in any of the four groups (N=6-10 mice per group; Figure 4H,I, left). CNO administration (1 mg/kg) did not result in abnormal movements in mCherry-injected WT;A2a-Cre or PNKD;A2a-Cre mice (N=6-8 mice per group, $p=0.373$, 0.17 , respectively) or in Gi-DREADD-injected WT mice (N=8 mice, $p=0.9$), but in Gi-DREADD-injected PNKD;A2a-Cre mice, CNO triggered dyskinesia (N=9 mice, $p<0.0001$; Figure 4H,I, right). Though they showed qualitatively similar changes in movement to those seen in PNKD mice treated with caffeine, CNO treatment in PNKD;A2a-Cre Gi-DREADD mice produced less severe dyskinesia (average dyskinesia scores at 40-60 minutes 6.7 vs 8.1; $p=0.008$). These results demonstrate that reducing cAMP levels in iMSNs is *sufficient* to cause dyskinesia in PNKD mice, but not WT mice.

To determine whether enhancing iMSN cAMP signaling might blunt dyskinesia, we used the activating DREADD hM3D(G_s -coupled) in PNKD;A2a-Cre mice (Figure 5A). After habituation to IP injections, saline or CNO was administered 20 minutes prior to injection with caffeine (Figure 5B, top). If reductions in iMSN activity are required for dyskinesia in PNKD mice, then pretreatment with CNO should reduce the severity of caffeine-induced dyskinetic attacks. While pretreatment with saline did not prevent caffeine-induced attacks, pretreatment with CNO reduced dyskinesia in G_s -DREADD-expressing mice, as compared to mCherry-expressing controls (N=9-10 mice per group; $p=0.00028$ Figure 5B, bottom), suggesting that reductions in iMSN activity are *necessary* for dyskinesia in PNKD.

To determine whether activating the G_s -DREADD prevented caffeine-induced reductions in iMSN firing in PNKD mice, we injected PNKD;A2a-Cre mice with bilateral Cre-dependent G_s -DREADD as well as unilateral Cre-dependent ChR2, and implanted

optrode arrays (Figure 5C top, Figure S5A). We then performed single-unit recordings from the DLS during experiments in which saline or CNO was administered prior to caffeine (Figure 5C). Saline injection alone did not significantly impact the firing of unidentified MSNs (Figure S5B-C, $n=64$, $N=3$, $p=0.76$) or optically-identified iMSNs (Figure S5D, $n=16$, $N=3$, $p=0.89$). Saline pretreatment did not prevent caffeine-induced reductions in the firing rate of unidentified MSNs or iMSNs (Figure 5C bottom, $n=22$, $N=3$, $p=0.005$ and $n=6$, $N=3$, $p=0.01$, respectively). CNO treatment alone did not significantly alter the firing of MSNs overall (Figure S5C, $n=41$, $N=3$, $p=0.38$), but CNO pretreatment prevented caffeine-induced reductions in firing rate in both unidentified MSNs (Figure 5C middle, $n=36$, $N=3$, $p=0.59$) and identified iMSNs (Figure 5C bottom, $n=6$, $N=3$, $p=0.60$). These results demonstrate that chemogenetic activation of iMSNs can prevent both the physiological and behavioral effects of caffeine on iMSNs.

To further investigate the mechanism underlying onset of dyskinesia, we reasoned that caffeine—an antagonist at G_s -coupled adenosine A2a receptors—might trigger dyskinetic attacks in PNKD through regulation of either the intrinsic excitability of iMSNs or the strength of their excitatory inputs. Within the basal ganglia and its connections, G-protein-coupled A2a receptors are selectively expressed on striatal iMSNs (Schiffmann et al., 1991), which might account for the cell-type selectivity of the inhibition we observed during caffeine-induced attacks in PNKD mice. In order to test whether the intrinsic excitability of dMSNs or iMSNs was altered in PNKD mice, we performed whole-cell *ex vivo* recordings in slices of PNKD;D1-tdTomato mice or WT controls, in which dMSNs and iMSNs can be visually identified (Figure S4A,5A)(Shuen et al., 2008). In order to reduce the likelihood of stress-induced dyskinetic attacks around the time of sacrifice, we

habituated animals to daily saline injections prior to preparation of brain slices. As these brain slices should represent the non-dyskinetic state in PNKD mice, we hypothesized that basic electrophysiological properties would not differ between neurons in PNKD and WT mice. We found that input resistance did not differ between dMSNs from WT (104 ± 10 Mohms, $n=24$ cells, $N=7$ mice) and PNKD slices (118 ± 18 Mohms, $n=20$ cells, $N=4$ mice, $p=0.25$). Resting membrane potential was also comparable in dMSNs from WT (-85.1 ± 1.6 mV) and PNKD slices (-86.1 ± 1.3 mV, $p=0.95$). To measure excitability, we injected current steps of varying amplitude, and measured the output firing rate (Figure S4A). The rheobase (minimum current to evoke a spike) was similar in dMSNs from WT (400 ± 30 pA) and PNKD slices (355 ± 22 pA, $p=0.26$). The average slope of the input current-output firing relationship (firing response gain) was not significantly different between dMSNs recorded in WT (Figure S4B; 53 ± 4 spikes/sec/nA) versus PNKD slices (49 ± 4 spikes/sec/nA, $p=0.25$). The similar *ex vivo* physiological properties of WT and PNKD dMSNs are consistent with the comparable baseline firing rates we observed in dMSNs in freely moving mice.

We next examined whether acute caffeine application could evoke changes in the excitability of dMSNs in WT or PNKD slices. As dMSNs do not express A2a receptors (Schiffmann et al., 1991), we reasoned caffeine was unlikely to trigger significant changes in excitability. Indeed, acute caffeine application did not alter dMSN firing response gain in WT (Figure S4C-D; $n=7$, $N=5$, $p>0.05$) or PNKD slices (Figure S4E-F; $n=7$, $N=4$, $p>0.05$). These results are consistent with the hypothesis that dMSNs are minimally modulated by caffeine.

We next examined the intrinsic excitability of iMSNs from WT and PNKD mice, using the same methods. Resting membrane potential did not differ between iMSNs recorded in WT (-89.2 +/- 1.9 mV, n=22, N=8) and PNKD mice (-89.4 +/- 1.6 mV, n=22, N=4, p=0.66). Input resistance was also similar in iMSNs from WT (160 +/- 15 Mohms) and PNKD slices (136 +/- 10 Mohms, p=0.25). We were able to confirm the previously reported finding (Day et al., 2008; Kreitzer and Malenka, 2007; Planert et al., 2013) that iMSNs are more excitable than dMSNs (here measured by rheobase; compare Figure S4B, S5B, p=0.04), but we did not observe differences in the rheobase (p=0.87) or firing response gain (p=0.16) of WT and PNKD iMSNs (Figure S5A-B). If the dyskinesia-associated reductions in the firing rate of PNKD iMSNs *in vivo* were mediated by reductions in intrinsic excitability, we would expect to see a decrease in intrinsic excitability in response to caffeine application. However, caffeine did not trigger notable differences in the evoked firing of iMSNs in WT (Figure S5C-D, n=12, N=4, p=0.39) or PNKD slices (Figure S5E-F, n=7, N=4, p>0.05). The negligible effects of caffeine on intrinsic excitability of iMSNs are consistent with previously published evidence suggesting that A2a receptors primarily modulate excitatory synaptic inputs onto iMSNs (Higley and Sabatini, 2010).

A2a receptors are known to regulate endocannabinoid release, which is implicated in synaptic depression on both short and long timescales (Gerdeman et al., 2002; Lerner and Kreitzer, 2012; Narushima et al., 2006; Shen et al., 2008). Endocannabinoid-dependent long-term depression (LTD) is presynaptically expressed and characterized by a reduction in the probability of transmitter release and decreased miniature excitatory postsynaptic current (mEPSC) frequency, but not amplitude (Choi and Lovinger, 1997a,

b). To test whether excitatory synaptic transmission is altered onto dMSNs or iMSNs in PNKD mice, we performed whole-cell voltage-clamp recordings from dMSNs and iMSNs, as described above (Figure 6A, 7A). We compared slices from mice representing three conditions: WT mice, PNKD mice in the non-dyskinetic state, and PNKD mice in the dyskinetic state (a dyskinetic attack was induced just prior to preparation of brain slices). In one set of experiments, we measured miniature excitatory postsynaptic currents (mEPSCs) in dMSNs (Figure 6B). We saw no significant differences in mEPSC amplitude (Figure 6C, $p=0.45$ ANOVA) or frequency ($p=0.42$ ANOVA; Figure 6D) between the three groups ($n=21-31$ neurons and $N=6-13$ mice per group). Furthermore, we did not observe acute changes in dMSN mEPSC amplitude or frequency after application of caffeine in PNKD slices (data not shown, $n=9$, $N=4$, $p>0.05$). We observed similar evoked EPSCs in dMSNs from WT and PNKD slices (Figure 6E), as measured by pulse ratio (PPR; Figure 6E; $n=22,24$ cells, $N=5,6$ mice respectively; $p=0.83$). These findings in *ex vivo* recordings indicate PNKD is not associated with marked changes in dMSN excitability or synaptic function.

Based on our *in vivo* recordings, we predicted marked changes in iMSN synaptic function in *ex vivo* slices from PNKD mice in the dyskinetic state. We first measured mEPSCs in iMSNs from WT mice, non-dyskinetic PNKD mice, and dyskinetic PNKD mice (Figure 7B). Though mEPSC amplitude was similar across the groups (Figure 7C), we observed small (9-12%), but significant differences between cells from WT mice ($n=37$, $N=15$), non-dyskinetic PNKD mice ($n=21$, $N=5$) and dyskinetic PNKD mice ($n=22$, $N=7$, $p=0.0018$, Kruskal Wallis). However, iMSN mEPSC frequency was more substantially (25-38%) reduced in slices from dyskinetic PNKD mice as compared to WT littermates or

non-dyskinetic PNKD mice (Figure 7D; $p=0.0003$). We could elicit similar acute reductions in mEPSC frequency by applying caffeine on slices from non-dyskinetic PNKD mice (Figure 7B-C, $n=8$, $N=3$, $p<0.05$). Together, these results support the idea that there may be a reduction in the number of excitatory synapses and/or probability of release onto iMSNs in dyskinetic PNKD animals, consistent with observations of altered exocytosis in PNKD (Shen et al., 2015). Also consistent with a reduction in the probability of release, we found increased PPR of evoked EPSCs in PNKD iMSNs (Figure 7E; $n=23$ cells per group; $N=8,11$ mice; $p=0.016$). If these reductions in excitatory synaptic input onto iMSNs were the result of *in vivo* LTD, we predicted LTD might be occluded in *ex vivo* slices from dyskinetic animals. To test this hypothesis, we recorded evoked EPSCs before and after a standard high frequency (HFS) LTD protocol (Kreitzer and Malenka, 2007; Lerner and Kreitzer, 2012). In iMSNs from WT slices, LTD was robust (Figure 7F; $n=10$ cells; $N=6$ mice; $p=0.008$), but in iMSNs from PNKD animals, LTD was absent ($n=8$ cells; $N=7$ mice; $p=0.15$), suggesting it might be occluded. One of the major cellular mechanisms in presynaptic striatal LTD is release of endocannabinoids and CB1 receptor-dependent alterations in the probability of vesicle release at the presynaptic terminal (Kreitzer and Malenka, 2007). If this machinery had already been engaged in PNKD mice *in vivo*, then further endocannabinoid-mediated reductions in synaptic responses would be smaller than otherwise predicted. Indeed, the endocannabinoid agonist WIN55,212 (1 μM) produced less synaptic depression in PNKD as compared to WT iMSNs (Figure 7G; $n=7,9$ cells; $N=5,7$ mice; $p<0.0001$ for comparison). These findings show a pathway-specific disruption in excitatory neurotransmission onto iMSNs in symptomatic PNKD animals, which may be a cellular and synaptic substrate of dyskinesia.

If depression of iMSN synaptic inputs leads to reduced iMSN activity, in turn causing dyskinesia, then preventing endocannabinoid signaling should reduce or prevent dyskinetic attacks. To test this hypothesis, we administered the CB1 antagonist AM251 (5 mg/kg) to PNKD mice, prior to caffeine treatment (Figure 8A). In vehicle-pretreated animals, caffeine triggers dyskinetic attacks, as expected (Figure 8B, N=10 mice, $p < 0.0001$). However, in AM251-pretreated mice, attack severity was strongly reduced (N=10 mice, $p < 0.0001$), suggesting that endocannabinoid signaling is necessary for caffeine-induced dyskinesia. To explore whether AM251 might prevent dyskinetic attacks by blunting or preventing a loss of iMSN activity, we performed additional striatal single-unit recordings in PNKD animals during behavioral sessions. In contrast to control experiments, in which caffeine induced robust dyskinetic attacks and decreases in both unidentified and iMSN firing rates (Figures 2G, 3D), caffeine did not cause a significant change in unidentified MSN or iMSN firing rates after AM251 pretreatment (Figure 8C-D; $n = 18, 8$ units; $N = 4$ mice; $p = 0.11$ and 0.643 , respectively). These results further bolster our main hypothesis that reductions in indirect pathway activity are critical for the expression of dyskinesia.

2.4 Discussion

This study tested the hypothesis that striatal circuit dysfunction contributes to dyskinesias. Enrichment analysis of human brain gene co-expression modules with known dyskinesia genes led us to focus in on the striatum, and then on striatal indirect pathway neurons, as a potential locus of neuronal dysfunction. We found that in the PNKD mouse model, caffeine-induced dyskinetic attacks were paralleled by a profound reduction in the firing rate of optogenetically-identified striatal indirect pathway MSNs (iMSNs), with little change in direct pathway MSNs (dMSNs). A reduction in indirect pathway efficacy appears to be necessary and sufficient for the generation of dyskinesia in this PNKD model, as chemogenetic manipulations of iMSNs yielded bidirectional regulation of dyskinesia. Further, using *ex vivo* slice recordings, a potential cellular mechanism for this loss of iMSN activity in dyskinetic PNKD animals was identified: endocannabinoid-mediated synaptic depression of excitatory synapses onto iMSNs. Indeed, pharmacological blockade of endocannabinoid-mediated LTD *in vivo* blunted or prevented caffeine-induced dyskinetic attacks in PNKD mice. Our findings represent the first example in which selective modulation of the indirect pathway appears to underlie symptoms of dyskinesia.

One important aspect of our study is the analysis of human genetic and gene expression data to discover neuronal cell types implicated in disease. While the vast majority of data on human disease genetics is used to identify specific molecules or pathways that relate to disease, we tested the hypothesis that the genes implicated in human disease can also give insights into specific cell types that are dysfunctional (Skene et al., 2018; Skene and Grant, 2016) (Kelly et al., 2018). Such insight is particularly

important for understanding the pathophysiology of brain disorders in which no gross abnormalities of the brain are present, such as many movement disorders and neuropsychiatric illnesses. Here, we establish the feasibility of this approach using gene co-expression analysis of human brain tissue to narrow in on a key brain region and cell type implicated in some forms of dyskinesia.

In some ways, the key role of iMSNs in dyskinesia is not surprising. In the classic hyperkinetic movement disorder, Huntington's Disease, postmortem studies suggest that early neurodegeneration may target iMSNs over dMSNs (Reiner et al., 1988). Recent work has implicated iMSN activity in a phenotypically similar condition, levodopa-induced dyskinesia (Alcacer et al., 2017), though in this form of dyskinesia there are coincident increases in dMSN activity and decreases in iMSN activity (Parker et al., 2018; Ryan et al., 2018). One reason that iMSN activity may be critical for normal movements is that, by virtue of their extensive inhibitory collaterals within the striatum (Dobbs et al., 2016; Smith et al., 1998; Taverna et al., 2008; Wei et al., 2017), and through their downstream regulation of brainstem and thalamocortical motor circuits (Oldenburg and Sabatini, 2015; Roseberry et al., 2016), they are key to the normal ability to suppress competing motor programs (Cui et al., 2013; Tecuapetla et al., 2016; Tecuapetla et al., 2014). Broad loss of the inhibitory influence of iMSNs, either through neurodegeneration (as in Huntington's Disease) or through reductions in firing rate or synchronization (as in PNKD and other "functional" forms of dyskinesia), could lead to increased activity in neighboring dMSN ensembles, decreasing the threshold for triggering movements facilitated by these ensembles. This phenomenon could account for the clinical observation that many involuntary movements, including chorea and dystonia, are exacerbated by voluntary

movement (or even the planning of voluntary movement) in the same body segment (Albanese et al., 2013; Berardelli et al., 1998). Dyskinesias may thus represent an “overflow” of normal motor commands (Mink, 1996).

In PNKD mice, both caffeine and ethanol trigger dyskinetic attacks and reductions in iMSN firing. Though both agents may have some shared targets, including the endocannabinoid system (Lerner et al., 2010; Pava and Woodward, 2012), ethanol acts at several additional targets within the brain, including the dopamine system (Lovinger and Alvarez, 2017; Mereu et al., 1984; Yim et al., 1998) and even on adenosine (Ruby et al., 2010). This less specific pharmacology may be one reason why ethanol also caused reductions in dMSN activity (both in WT and PNKD mice). Additionally, this difference in physiology may be related to two key differences in the behavioral response to ethanol. First, while caffeine did not substantially change gross locomotor activity, ethanol caused more significant reductions in overall movement. Given the known correlation between dMSN and iMSN firing and movement (Klaus et al., 2017; Markowitz et al., 2018; Parker et al., 2018), a reduction in overall movement could cause a confounding reduction in MSN firing in ethanol-treated animals. Second, at the doses used in this study, ethanol triggered more severe dyskinetic attacks, as we reported previously (Lee et al., 2012). If indeed ethanol taps into the same endocannabinoid machinery as caffeine, but more potently, there may be enough endocannabinoid release to trigger LTD of inputs onto both iMSNs and dMSNs.

Interestingly, we found that chemogenetic suppression of iMSNs triggered dyskinesia in PNKD mice, but not in their WT littermates. This suggests that iMSN suppression (to the extent possible with our manipulations) alone is not sufficient to cause

involuntary movement in otherwise normal basal ganglia circuitry, consistent with recent findings (Alcacer et al., 2017). Additional cellular or circuit changes in PNKD, such as altered circuit organization or aberrant neuromodulation, may amplify the effects of chemogenetic inhibition, leading to increased vulnerability to dyskinesia. Precedent for downstream amplification of striatal signaling has been observed in levodopa-induced dyskinesia, at striato-nigral synapses (Borgkvist et al., 2015).

Activating the “excitatory” G_s DREADD largely prevented caffeine-induced reductions in iMSN firing and dyskinetic attacks in PNKD mice. By itself, activation of the DREADD had modest impacts on membrane potential in *ex vivo* slices, and almost no impact on the average firing rate of MSNs *in vivo*. On the other hand, activation of the DREADD may have more marked impact in preventing long-term depression of excitatory inputs and/or decreases in synaptic output. Future experiments might examine relative changes in these two synapses.

We found that excitatory inputs, but not intrinsic excitability, were altered in iMSNs in brain slices from dyskinetic PNKD animals as compared to their wild-type littermates. Interestingly, excitatory inputs onto iMSNs from carefully habituated, non-dyskinetic PNKD mice were similar to those onto wild-type iMSNs, and acute application of caffeine induced a reduction in mEPSC frequency. dMSNs, in contrast, showed little to no differences between wild-type and PNKD mice. These observations are consistent with the idea that aberrant synaptic plasticity may contribute to movement disorders (Deffains and Bergman, 2015). Alterations in striatal LTD have been observed in other animal models of hyperkinetic disorders (Avshalumov et al., 2013; Martella et al., 2009; Picconi et al., 2003; Picconi et al., 2006), suggesting it may be a key cellular mechanism

mediating circuit dysfunction. Though the normal function of the PNKD protein is unknown, it is located at synapses and appears to participate in regulation of synaptic release *in vitro* (Shen et al., 2015). In the context of either increased excitatory input (stress) or adenosine antagonism (caffeine), iMSNs expressing mutant PNKD protein may have a lower threshold for LTD induction, perhaps by amplification of normal postsynaptic signaling pathways or presynaptic endocannabinoid signaling. As ethanol has multiple pharmacological targets, it is hard to be definitive about shared versus convergent mechanisms in caffeine- versus alcohol-induced attacks, but endocannabinoid signaling seems a likely culprit. Given that chemogenetic inhibition of iMSNs triggered dyskinesia only in PNKD animals, our results suggest that there is an underlying cellular or circuit vulnerability in PNKD animals not present in wild-type mice.

Together, these findings highlight a key role for the striatal indirect pathway in the development of dyskinesia episodes in PNKD. While studies in other animal models have stressed the potential importance of the direct pathway (Cenci et al., 1999; Perez et al., 2017), we found that reduced indirect pathway activity may be an alternate physiological correlate, consistent with the idea that the two pathways act in concert to help select appropriate movements, while at the same time suppressing competing movements. Thus, targeting the striatal indirect pathway and endocannabinoid-mediated synaptic plasticity may represent a promising new strategy for the focused treatment of hyperkinetic disorders.

2.5 Experimental Procedures

Animals:

Hemizygous PNKD mice were maintained on a C57Bl/6 background. For *in vivo* experiments, hemizygous PNKD mice were bred to wild-type C57Bl/6, Adora2a-Cre (A2a-Cre) or Drd1-Cre (D1-cre line 217) hemizygous mice, to generate PNKD mice for pharmacological manipulations, PNKD;A2a-Cre mice for indirect pathway manipulations or PNKD;D1-Cre mice for direct pathway manipulations. PNKD negative littermates were used as wild-type (WT) controls. For slice physiology experiments, hemizygous PNKD mice were bred to hemizygous Drd1a-tdTomato mice, to generate Drd1a-tdTomato (WT control) and PNKD;Drd1a-tdTomato (PNKD) mice. Mice of either sex were used. All experiments were performed in mice aged 2-4 months. We complied with local and national ethical and legal regulations regarding the use of mice in research. All experimental protocols were approved by the UC San Francisco Institutional Animal Care and Use Committee.

Behavior:

Mice were administered intraperitoneal (IP) saline and habituated to the open field (a clear acrylic cylinder, 25 cm diameter) for a minimum of 1 hour daily for 2 days prior to experiments. Mice implanted with infusion cannulae were habituated to tethering and infusion (of saline) for a minimum of 2 days, to confirm that the infusion process alone did not trigger dyskinesia. In experiments involving chemogenetic manipulation of iMSNs in PNKD mice, both PNKD and WT control mice were habituated to saline injections daily for approximately 2 weeks, to minimize the likelihood of a stress-induced dyskinetic attack in response to IP injection of a drug or its vehicle in subsequent experiments.

During experiments, mice were placed in the open field chamber and monitored by two cameras, one mounted directly above the chamber to capture overall locomotor activity, another in front of the chamber to capture qualitative aspects of movement, particularly dyskinesia. Video-tracking software (Noldus Ethovision) was used to quantify movement. Manual scoring was performed live during experiments, using a slight modification of a previously published dyskinesia scale (Lee et al., 2012). In this modified scale, numerical ratings indicate the following behaviors: 1 (asleep, inactive); 2 (normal activity); 3 (increased activity); 4 (hyperactivity, running); 5 (jerky movement and slow patterned movement; repetitive exploration); 6 (fast patterned movement; repetitive exploration with hyperactivity); 7 (stereotyped movements; repetitive sniffing/rearing in one location); 8 (continuous purposeless gnawing, sniffing and/or licking); and 9 (chorea -- observed as irregular purposeless jaw or tongue movements or forepaw movements; dystonia). Two seizure episodes were observed after caffeine administration during the study, and were excluded from the dataset. A score of 7 was used for animals with frequent, but not continuous, gnawing, sniffing, or licking movements. For chemogenetic and pharmacological experiments, dyskinesia was scored for 1 minute every 5 minutes. For *in vivo* electrophysiology experiments, dyskinesia was scored for 1 minute every 5 minutes, except for the period between drug injection and the onset of involuntary movements (here defined as a score of 7 or above), when it was scored continuously in 1-minute bins. In AM251 (5 mg/kg) prophylaxis experiments, animals were randomized to the drug or vehicle, one of which were administered IP 30 minutes prior to administration of caffeine (25 mg/kg). On another experimental day, the mice received the other treatment. The experimenter was blinded to the drug being administered until

after acquisition and analysis had been performed. Dyskinesia scores were compared within-group at baseline (-30 to 0 minutes prior to caffeine) and 30-60 minutes after caffeine injection.

Pharmacology:

For *in vivo* experiments, caffeine (Tocris) was dissolved in normal saline at 2 mg/mL, and injected IP at a final dose of 25 mg/kg. Ethanol was administered IP (20% solution in water) at a dose of 1.5 g/kg. AM251 (Tocris) was dissolved in DMSO (Sigma) at 10 mg/mL, then diluted to 0.5 mg/mL in a 1:1 solution of polyethylene glycol (Sigma) and normal saline prior to IP injection at a final dose of 5 mg/kg. Clozapine-N-oxide (Sigma) was dissolved in normal saline at 0.1 mg/mL and injected IP at a final dose of 1 mg/kg. For intracranial infusions, caffeine was dissolved in normal saline at a concentration of 100 mM.

For *ex vivo* slice experiments, picrotoxin (Sigma) was dissolved in warm water at 5 mM, and added to ACSF for a final concentration of 50 μ M. Tetrodotoxin (TTX, Abcam) was dissolved in water at a stock concentration of 1 mM and added to ACSF for a final concentration of 1 μ M. WIN55,212 was dissolved in DMSO at 10 mM, and added to ACSF for a final concentration of 1 μ M. Clozapine-N-oxide (CNO, Sigma) was dissolved in DMSO at 10 mM then diluted in ACSF for a final concentration of 1 μ M.

Intracranial infusion:

2-4 month old mice were implanted with bilateral infusion cannulae. Anesthesia was induced with intraperitoneal ketamine/xylazine and maintained with inhaled isoflurane. After opening the scalp, two small holes were drilled over the dorsolateral striatum (+0.8 AP, +2.2 mm DV from bregma) on either side of the skull using a stereotax-

mounted drill. The exposed skull surface was scored with a scalpel to maximize adhesion of dental cement. Dental cement (Metabond) was applied to the exposed skull surface and the double infusion cannula (PlasticsOne). The infusion cannula (with inner dummy cannula with cap screwed into place) was then lowered into the brain, with the tip of the inner cannula lowered to -2 mm DV from the brain surface. The cannula was then secured to the skull by application of dental acrylic (Ortho-Jet). After the acrylic had set, the scalp was closed with suture, and the mouse was allowed to recover from anesthesia. Buprenorphine (IP, 0.05 mg/kg) and ketoprofen (subcutaneous injection, 5 mg/kg) were administered for postoperative analgesia.

Behavioral experiments began 1 week following surgery. The experimenter was blinded to the genotype of the animal. In each session, the dummy inner cannula was removed, and a drug infusion inner cannula was placed inside the outer cannula, and screwed into place. The mouse was then returned to its home cage with the top removed, and could move freely during drug infusion. Drug or saline was infused bilaterally using a Hamilton double syringe pump (WPI) at a rate of 0.1 μ L per minute for a total volume of 0.5 μ L per side. The cannula was left in place for an additional three minutes, then both infusion cannulae were removed. The mouse was then transferred to the open field behavioral chamber for simultaneous video tracking (for locomotion) and manual scoring (for dyskinesia). Infusion experiments were performed a minimum of 24 hours apart.

To verify cannula function and to mark the location and estimate the extent of drug infusions, a lipophilic fluorescent dye was infused prior to sacrifice. After the final infusion experiments, 0.5 μ L of the dye (FM4-64X, ThermoFisher Scientific) was infused in the

same fashion, after which terminal anesthesia was administered and transcardial fixative perfusion was performed. Tissue was processed as indicated below (Histology).

In vivo electrophysiology/optogenetics:

To construct optrode arrays, optical fiber-ferrule assemblies were cemented onto 32 channel microelectrode arrays (Innovative Neurophysiology). Optical fiber-ferrule assemblies consisted of a 200 μm optical fiber (Thorlabs) threaded through a ceramic ferrule (Thorlabs) and cemented with epoxy. The tip of the optical fiber was positioned in the center of the array, approximately 0.5 mm above the tips of the microelectrodes. Surgical implantation of optrode arrays was performed at 2-4 months of age. Anesthesia was induced with IP ketamine/xylazine and maintained with inhaled isoflurane. Mice were stereotaxically injected with AAV5-DIO-ChR2-mCherry (UPenn Vector Core, 1.5 μL of 1:1 diluted virus) in the left dorsolateral striatum (+0.8 AP, +2.25 ML, and -2.5 mm DV from bregma) through a small hole in the skull. Using a stereotax-mounted drill, this hole was later enlarged into a rectangular craniectomy and the dura was removed to permit implantation of the optrode. Small holes were also made in the right frontal and right posterior areas for later insertion of a skull screw (FST) and the ground wire, respectively. The exposed skull surface was scored with a scalpel to maximize adhesion of dental cement. Dental cement (Metabond) was applied to the exposed skull surface and the base of the optrode array connector. The optrode array was then slowly lowered into the center of the craniectomy to a depth of 2.3 to 2.4 mm from the brain surface. The array, ground wire, and skull screw were secured to the skull by application of dental acrylic (Ortho-Jet). After the acrylic had set, the scalp was closed with suture, and the mouse was allowed to recover from anesthesia. Buprenorphine (IP injection, 0.05 mg/kg) and

ketoprofen (subcutaneous injection, 5 mg/kg) were administered for postoperative analgesia.

2 weeks after implantation, mice were habituated to tethering, the recording chamber, and IP saline injection for a minimum of 1 hour daily for two days. After habituation, experimental sessions occurred approximately twice weekly for 2-6 weeks. During each session, electrical signals (single-unit and LFP data from each of 32 channels) were collected using a multiplexed 32 channel headstage (Triangle Biosystems), an electrical commutator equipped with a fluid bore (Dragonfly), filtered, amplified, and recorded on a MAP system, using RASPUTIN 2.4 HLK3 acquisition software (Plexon).

During recording sessions, after a baseline period, caffeine (25 mg/kg) or ethanol (1.5 g/kg) was injected IP. If a mouse developed stress-induced dyskinesia after tethering, but prior to drug administration, the experiment was terminated. After a period of 2-6 hours of recording spontaneous activity in the open field, an optogenetic cell identification protocol was applied (Kravitz et al., 2013), consisting of 100 ms blue light pulses, given at 1 Hz. At each of 4 light powers (0.5, 1, 2, and 4 mW, typically), 1000 light pulses were delivered via a lightweight patch cable (Doric Lenses) connected to a blue laser (Shanghai Laser and Optics Century), via an optical commutator (Doric Lenses), and controlled by TTL pulses from a behavioral monitoring system (Noldus Ethovision). At the end of this cell identification protocol, the animal was detached from the electrical and optical cables and returned to its home cage.

Single units were identified offline by manual sorting using Offline Sorter 3.3.5 (Plexon) and principle components analysis (PCA). Clusters were considered to

represent a single unit if (1) the unit's waveforms were statistically different from multiunit activity and any other single units on the same wire, in 3D PCA space, (2) no interspike interval <1 ms was observed. Single units were classified as putative MSNs based on waveform and interspike interval distribution, using previously published criteria (Gage et al., 2010) to exclude fast-spiking interneurons.

After single units had been selected for further study, their firing activity was analyzed using NeuroExplorer 4.133 (Nex Technologies). To determine if a unit was optogenetically identified, a peristimulus time histogram was constructed around the onset of laser pulses. To be considered optogenetically identified, a unit had to fulfill 3 criteria: (1) the unit had to increase firing rate above the 99% confidence interval of the baseline within 15 ms of laser onset; (2) the unit's firing was above this threshold for at least 20 ms; (3) the unit's laser-activated waveforms were not statistically distinguishable from spontaneous waveforms.

For display and analysis purposes, the firing rate of single units was averaged in one-minute bins. For comparisons of baseline firing rates between genotypes, a Wilcoxon Rank Sum Test was employed. For analyses of firing rate before, during, and after dyskinetic periods, the average firing rate from 0-30 minutes prior to injection, 30-60 minutes after injection, and 0-20 minutes after behavioral recovery (dyskinesia score of 2) were calculated. To determine whether a unit's firing rate significantly changed after caffeine injection, the firing rates during the baseline period were compared with the firing rates between 30-60 minutes after caffeine injection, using a Wilcoxon Signed Rank test.

Chemogenetics:

AAVs encoding Cre-dependent constructs were stereotaxically injected 2-4 weeks prior to the first behavioral or slice physiology experiments. For chemogenetic inhibition of iMSNs, A2a-Cre mice (either PNKD or WT littermates) were stereotaxically injected with either AAV5-DIO-hM4D(G_i)-mCherry or AAV5-DIO-mCherry (UNC Vector Core, 1 μ L) at 4 sites to cover the bilateral dorsolateral striatum (\pm 1.0 AP, \pm 2.2 ML, -2.5 mm DV). For chemogenetic activation of iMSNs, PNKD;A2a-Cre mice were injected with either AAV5-DIO-hM3D(G_s)-mCherry or AAV5-DIO-mCherry (UNC Vector Core, 1 μ L) at 8 sites per side to cover the majority of the striatum, bilaterally (+0.8 AP, \pm 2.2 ML, -2.5, -4.0 DV; +0.8 AP, \pm 1.2 ML, -2.5, -4.0 DV; 0.0 AP, \pm 2.0 ML, -2.5, -3.7 DV; -0.5 AP, \pm 2.5 ML, -2.0, -3.0 DV). After a recovery period, mice were then habituated daily to the behavioral chamber and to IP injection of saline, so as to reduce the chance of stress-induced dyskinetic attacks when later injected with an experimental agent.

During chemogenetic inhibition experiments, on interleaved days mice were injected IP with either saline (10 μ L/g) or CNO (1 mg/kg), after which their behavior was monitored with both video-tracking of locomotor activity and manual scoring of dyskinesia (see Behavior, above). During chemogenetic activation experiments, on interleaved days mice were injected IP with either saline (10 μ L/g) or CNO (1 mg/kg) 20 minutes prior to injection of caffeine (25 mg/kg), and behavior was monitored. Dyskinesia scores were compared at baseline (0-10 min) and at 40-60 minutes following CNO administration, using a Wilcoxon Signed Rank Test.

Slice electrophysiology:

Prior to terminal anesthesia and preparation of brain slices, animals (1.5-4 months old) were handled, then placed in a 500 mL glass beaker for 5 minutes. In PNKD mice, such handling in unhabituated animals produced stress-induced dyskinetic attacks, as has been previously described (Lee et al., 2012). Mice were deeply anesthetized with an intraperitoneal ketamine-xylazine injection, transcardially perfused with ice-cold sucrose- or glycerol-based slicing solution, decapitated, and the brain was removed and placed in the slicing chamber with ice-cold slicing solution. Sucrose slicing solution contained (in mM): 79 NaCl, 23 NaHCO₃, 68 sucrose, 12 glucose, 2.3 KCl, 1.1 NaH₂PO₄, 6 MgCl₂, and 0.5 CaCl₂. Glycerol slicing solution contained (in mM): 250 glycerol, 2.5 KCl, 1.2 NaH₂PO₄, 10 HEPES, 21 NaHCO₃, 5 glucose, 2 MgCl₂, 2 CaCl₂. The brain was mounted on a submerged chuck, and sequential 300 μm coronal slices were cut on a vibrating microtome (Leica), transferred to a chamber of warm (34° C) carbogenated ACSF containing (in mM) 125 NaCl, 26 NaHCO₃, 2.5 KCl, 1 MgCl₂, 2 CaCl₂, 1.25 NaH₂PO₄, 12.5 glucose for 30-60 minutes, then stored in carbogenated ACSF at room temperature. Each slice was then submerged in a chamber superfused with carbogenated ACSF at 31-33° C for recordings.

Medium spiny neurons were targeted for recordings using differential interference contrast (DIC) optics in PNKD;Drd1a-tdTomato or PNKD;D2-GFP mice. In PNKD;Drd1a-tdTomato mice, direct pathway neurons were identified by their tdTomato-positive somata, and indirect pathway neurons were identified by their tdTomato-negative medium-sized somata. In PNKD;D2-GFP mice, indirect pathway neurons were identified by their GFP-positive somata, and direct pathway cells were identified by their GFP-

negative medium-sized somata. Fluorescence-negative neurons with GABAergic interneuron physiological properties (membrane tau decay <1 ms for both fast-spiking and persistent low-threshold spiking subtypes; input resistance >500 M Ω in persistent low-threshold spiking subtype) were excluded from the analysis. Neurons were patched in whole-cell current-clamp or voltage-clamp configurations using borosilicate glass electrodes (3-5 M Ω) filled with either potassium-based (current-clamp) or cesium-based (voltage-clamp) internal solution containing (in mM) respectively: 130 KMeSO₃, 10 NaCl, 2 MgCl₂, 0.16 CaCl₂, 0.5 EGTA, 10 HEPES, 2 MgATP, 0.3 NaGTP or 120 CsMeSO₃, 15 CsCl, 8 NaCl, 0.5 EGTA, 10 HEPES, 2 MgATP, 0.3 NaGTP, 5 QX-314, pH 7.3. Picrotoxin (50 μ M) was added to the external solution to block synaptic currents mediated by GABA_A receptors. Drugs were prepared as stock solutions and added to the ACSF to yield the final concentration.

Whole-cell recordings were made using a MultiClamp 700B amplifier (Molecular Devices) and ITC-18 A/D board (HEKA). Data was acquired using Igor Pro 6.0 software (Wavemetrics) and custom acquisition routines (mafPC, courtesy of M. A. Xu-Friedman). Whole-cell recordings were filtered at 2 kHz and digitized at 10 kHz. All recorded neurons exhibited electrophysiological characteristics of medium spiny neurons. In current-clamp recordings to measure intrinsic properties, membrane potential was measured as the average V_m 5-10 minutes after break-in. A series of small negative current steps were delivered from rest to calculate the input resistance of each cell. Rheobase and other input-output properties were obtained by giving a series of square-wave current steps, ranging from 100 pA to 800 pA (or the maximum current at which a cell could sustain spiking across the step), in 100 pA increments, with a 10 sec interstimulus interval.

Synaptic currents were monitored at a holding potential of -70 mV. Series resistance and leak currents were monitored continuously. Miniature EPSCs were recorded at -70 mV in 1 μ M TTX and 50 μ M picrotoxin. Only cells with at least 500 events were included in the analysis. Cumulative probability plots were generated from 500 randomly selected mEPSC events. Evoked EPSCs onto medium spiny neurons were elicited in the presence of picrotoxin (50 μ M) with a stimulus isolator (IsoFlex, AMPI) and a glass electrode placed dorsolateral to the recorded neuron, typically 100-200 μ m away. Stimulus intensity was adjusted to yield EPSC amplitudes of approximately 400 pA. Stimulus duration was 300 μ s. For evaluation of the paired pulse ratio, two stimuli were given at variable interstimulus intervals (ISIs; 25, 50, 100, 200, 500 ms) with a 20 sec intertrial interval. Three repetitions at each ISI were averaged to yield the PPR for that ISI. For monitoring of EPSC amplitude over time, two pulses delivered with 50 ms interstimulus interval were given every 20 seconds. Our high-frequency stimulation (HFS) protocol for induction of long-term depression consisted of 4 trials (1 second each, 10 second intertribal interval) of 100 Hz afferent stimulation (stimulation intensity calibrated to produce a 1.5 nA EPSC at -70 mV) paired with depolarization to -10 mV (Kreitzer and Malenka, 2007; Lerner and Kreitzer, 2012). Following the HFS protocol, the stimulation intensity was returned to the baseline level and EPSCs were monitored for a minimum of 30 additional minutes.

For analyses of basic excitability measures, a Wilcoxon Rank Sum test was used to compare between genotypes. For analyses of paired pulse ratio, mEPSC frequency and amplitude, an unpaired two-tailed T-test was employed. Synaptic depression was analyzed by calculating the average EPSC amplitude during the 10 minute baseline and 20 to 30 minutes following a manipulation (HFS or WIN55,212 application). Changes in

excitability or mEPSC frequency in response to acute caffeine application was analyzed by comparing a 10 minute baseline period with the value 20-30 minutes after drug application. For these analyses, a Wilcoxon Signed-Rank test was used.

In slice experiments to validate use of the inhibitory DREADD hM4D (Gi), we prepared acute slices from animals coinjected with AAV5-DIO-ChR2-eYFP (UPenn Vector Core, 1 μ L of 1:1 dilution) and AAV5-DIO-hM4D(Gi)-mCherry (UNC Vector Core, 1 μ L). eYFP positive striatal neurons were patched in the whole-cell current clamp mode, with a potassium-based internal solution (see above). Optogenetic stimulation was delivered to the slice by a TTL-controlled LED (Olympus), passed through a ChR2 (473 nm) filter (Chroma) and the 40X immersion objective. LED intensity was adjusted to yield an output of approximately 1-2 mW at the slice. Light pulses were 5 ms in duration. To measure acute effects of CNO in slice physiology experiments, we targeted eYFP-negative neurons in the striatum or GPe, in an area of mCherry fluorescence indicating local striatal axons were infected. These neurons were patched in whole-cell voltage-clamp mode, with a cesium chloride-based internal solution containing (in mM): 120 CsCl, 15 CsMeSO₃, 8 NaCl, 0.5 EGTA, 10 HEPES, 2 MgATP, 0.3 NaGTP, pH 7.3. IPSCs were elicited with optogenetic stimulation every 30 seconds, and IPSC amplitude was compared before and 10-15 minutes after addition of CNO (1 μ M) to the ACSF, using the Wilcoxon Signed-Rank Test.

Histology:

Following behavioral, *in vivo* physiology and chemogenetic experiments, mice were deeply anesthetized with IP ketamine-xylazine and transcardially perfused with 4% paraformaldehyde in PBS. Prior to perfusion, electrode location was marked in implanted

mice by electrolytic lesioning. After deep anesthesia, the implant was connected to a solid state, direct current (DC) Lesion Maker (Ugo Basile). A current of 100 μ A was passed through each microwire for 5 seconds. After perfusion, the brain was dissected from the skull and post-fixed overnight in 4% paraformaldehyde, then placed in 30% sucrose at 4° C for 2-3 days for cryoprotection. The brain was then cut into 30 μ m coronal sections on a freezing microtome (Leica), prior to washing in PBS and mounting in Vectashield Mounting Medium onto glass slides for subsequent imaging. All images were taken on a Nikon 6D conventional widefield microscope.

Human gene expression studies:

Integrative analysis of human CNS transcriptomes was performed essentially as described (Kelley et al., 2018). We obtained publicly available gene expression data from eight studies (Berchtold et al., 2008; GTExConsortium, 2015; Hawrylycz et al., 2015; Hernandez et al., 2012; Hodges et al., 2006; Kang et al., 2011; Li et al., 2013; Ramasamy et al., 2014a) and one resource (<http://www.brainspan.org/>) that profiled large numbers of postmortem CNS bulk tissue samples from neurotypical humans. Expression profiling was performed on six technology platforms, including RNA-seq and various commercial microarrays. Samples from each of the nine sources were separated into 53 datasets representing 11 major neuroanatomical regions. Each regional dataset consisted of at least 25 samples, all of which came from adults (≥ 18 years). After removing outliers (see below), we analyzed a total of 6336 transcriptomes (Table S1).

Data preprocessing and quality control: Preprocessing was performed from raw data when possible. Affymetrix microarray raw data (.CEL files) were downloaded from Gene Expression Omnibus (GEO: <http://www.ncbi.nlm.nih.gov/geo/>) using the following

accession IDs: GSE11882 (Berchtold et al., 2008), GSE25219 (Kang et al., 2011), GSE3790 (Hodges et al., 2006), GSE45642 (Li et al., 2013), and GSE46706 (Ramasamy et al., 2014b). Probe-level data from Affymetrix Exon 1.0 microarrays (GSE25219 and GSE46706) were summarized using the Robust Multi-Array (RMA) algorithm (Irizarry et al., 2003) at the gene level with Affymetrix Power Tools software (APT 1.15.2) and reverse log-transformed for further processing.

Affymetrix U133A and U133Plus2 microarray probes from GSE3790, GSE45642, and GSE11882 were pruned to eliminate non-specific and mis-targeted probes using the ProbeFilter R package (Dai et al., 2005) with mask files obtained from <http://masker.nci.nih.gov/ev/> (Zhang et al., 2005). After applying the mask files, only probe sets with at least seven remaining probes were retained for further analysis. Expression values were generated in R using the `expresso` function of the `affy` R package (Gautier et al., 2004) with "mas" settings and no normalization, followed by scaling of arrays to the same average intensity (200). For GSE45642, gene expression was not scaled and technical replicates were removed (AMY samples restricted to site I; DLPFC samples restricted to site D; HIP and NUAC samples restricted to site M). Non-normalized Illumina microarray data were obtained from GEO for GSE36192 (Hernandez et al., 2012). Normalized expression data from GTEx, BrainSpan, and the Allen Brain Institute (ABI) were downloaded from their respective websites (<http://www.gtexportal.org/>, V6 data release; <http://www.brainspan.org/>, Oct2013 data release; and <http://human.brain-map.org/>, March2013 data release). For the RNA-seq datasets (GTEx and BrainSpan), RPKM gene expression values were used.

Sample information for datasets with GEO accession IDs was obtained using the GEOquery R package (Davis and Meltzer, 2007) with the exception of hybridization batch information, which was extracted from the header information of Affymetrix .CEL files when available. Each of the 53 regional datasets was individually processed using the SampleNetwork R function (Oldham et al., 2012), which is designed to identify and remove sample outliers, perform data normalization, and adjust for batch effects (Johnson et al., 2007). We defined sample outliers as those that were more than four standard deviations below the mean connectivity of all samples measured over all features ($Z.K < -4$). Iterative pruning was applied for each regional dataset to remove all samples with $Z.K < -4$ (Table S1). For non-normalized data (GSE11882, GSE3790, GSE4542, and GSE36192), quantile normalization (Bolstad et al., 2003) was then performed. If a batch effect was present (defined as a significant association between the 1st principal component of the expression data and a technical batch covariate), batch correction was performed using the ComBat R function (Johnson et al., 2007), which is implemented in SampleNetwork. For GTEx data, we detected a large batch effect due to center site. We therefore restricted our analysis to samples acquired by centers 'B1, A1' or 'C1, A1'. Lastly, prior to coexpression analysis, probes / genes that had zero variance across all samples were removed. For GTEx, we further restricted our analysis to 27,540 transcripts that were detected (≥ 0.1 RPKM) in at least 200 CNS samples. Table S1 provides additional details on data preprocessing and quality control.

Unsupervised gene coexpression module detection: We analyzed gene coexpression relationships in each regional dataset in the R statistical computing environment (<http://cran.us.r-project.org>) using a four-step approach (Lui et al., 2014;

Molofsky et al., 2013). First, pairwise biweight midcorrelations (bicor) were calculated for all possible pairs of probes / genes over all samples in each dataset using the bicor function in the WGCNA R package (Langfelder and Horvath, 2008). Bicor is a robust correlation metric that is less sensitive to outliers than Pearson correlation but often more powerful than Spearman correlation (Hardin et al., 2007; Song et al., 2012). Second, probes / genes were clustered using the flashClust (Langfelder and Horvath, 2008) implementation of a hierarchical clustering procedure with complete linkage and $1 - \text{bicor}$ as a distance measure. Third, the resulting dendrogram was cut at a series of heights corresponding to the top 0.01%, 0.1%, 1%, 2%, 3%, 4%, or 5% of pairwise correlations for the entire dataset. Moreover, for each of these thresholds, we modified the minimum module size to require 8, 10, 12, 15, or 20 members. This approach yielded $7 \times 5 = 35$ different gene coexpression networks for each regional dataset. Third, initial modules in each network were summarized by their module eigengenes, which is defined as the first principal component obtained by singular value decomposition of the coexpression module (Horvath and Dong, 2008). Fourth, highly similar modules were merged if the correlations of their module eigengenes exceeded an arbitrary threshold (0.85). This procedure was performed iteratively for each network such that the pair of modules with the highest correlation (> 0.85) was merged first, followed by recalculation of module eigengenes, followed by recalculation of all correlations, until no pairs of modules exceeded the threshold. The WGCNA measure of intramodular connectivity (k_{ME}) was then calculated for each probe / gene with respect to all modules by correlating its expression pattern across all samples with each module eigengene (Horvath and Dong, 2008; Oldham et al., 2008).

Module enrichment analysis with a dyskinesia gene set: To identify ‘dyskinesia gene coexpression modules’ (i.e. groups of coexpressed genes that are enriched with genes involved in human dyskinesias), we cross-referenced coexpression modules from each regional dataset with a manually curated list of genes implicated in human dyskinesias (Table S2). Modules were defined as all unique genes with positive k_{ME} values that were significant after applying a Bonferroni correction for multiple comparisons ($p < 0.05 / (\# \text{ probes or genes in the regional dataset} \times \# \text{ of modules in the network})$). If a probe / gene was significantly correlated with more than one module it was assigned to the module for which it had the highest k_{ME} value. For each regional dataset, enrichment analysis was performed for all modules in all ($n = 35$) networks using a one-sided Fisher's exact test as implemented by the `fisher.test` R function. The module with the most significant enrichment for the dyskinesia gene set was identified in each regional dataset.

Data integration and calculation of striatum dyskinesia module membership: Operationally, we define the transcriptional ‘profile’ of the dyskinesia module in a given dataset as a list of probes / genes ranked by descending k_{ME} values. To create a ‘consensus’ dyskinesia transcriptional profile, we used the following approach. First, datasets that did not contain a module that was significantly enriched with the dyskinesia gene set after applying a Bonferroni correction for multiple comparisons ($p < 0.05 / \# \text{ modules}$) were excluded (GSE3790). Second, probe / gene identifiers from all datasets were mapped to a common identifier (HomoloGene ID data build 68). Third, k_{ME} vectors for each module in microarray datasets (in which individual transcripts are often targeted by multiple probes) were collapsed to unique identifiers by retaining for each

HomoloGene ID the probe with the highest k_{ME} value. Because k_{ME} values are correlation coefficients, they cannot be averaged directly over independent datasets of different sample sizes. Therefore, to aggregate k_{ME} values for a given HomoloGene ID across regional datasets, we used Fisher's method for combining correlation coefficients from independent datasets (Fisher, 1970). We implemented this method by initially transforming k_{ME} values using the Fisher transformation:

$$z_{gd} = \frac{1}{2} \ln \left(\frac{1+k_{ME.gd}}{1-k_{ME.gd}} \right)$$

(1)

where g indexes the gene and d indexes the regional dataset. An average of the resulting z-scores (weighted by sample size) was then determined with the following equation:

$$\bar{z}_g = \frac{\sum_{d=1}^D z_{gd}(n_d-3)}{\sum_{d=1}^D (n_d-3)}$$

(2)

where n denotes the number of samples in dataset d . The sampling standard deviation of \bar{z}_g is:

$$SD(\bar{z}_{gc}) = \sqrt{\frac{1}{\sum_{d=1}^D (n_d-3)}} .$$

(3)

Dividing the 'average' z-scores by the sampling standard deviation yields the genome-wide statistics displayed in Fig. 1C.

Enrichment analysis with cell-type markers: The following cell-type marker gene sets were used to perform enrichment analyses of the top dyskinesia module in each striatal dataset: direct and indirect medium spiny neurons (Gokce et al., 2016); astrocytes,

oligodendrocytes, and microglia: (Zhang et al., 2014); for cholinergic and parvalbumin interneurons, we created sets of genes based on the top 50 genes ranked by correlation to *CHAT* and *PVALB*, respectively, across our human striatum expression datasets.

PNKD correlation aggregation: We averaged *PNKD* correlation coefficients with DRD1 or DRD2 across striatum datasets using Fisher's method (as described above) by calculating Fisher transformed z-scores, \bar{z}_g (weighted by sample size). We converted \bar{z}_g into an 'average' correlation coefficient by performing the reverse Fisher transformation:

$$\bar{r}_g = \frac{\exp(2\bar{z}_g) - 1}{\exp(2\bar{z}_g) + 1} \quad .$$

(4)

2.6 Author Contributions & Acknowledgments

Author Contributions

ABN and ACK designed the experiments. ABN performed and analyzed the *in vivo* physiology and chemogenetic experiments. ABN and AEG performed and analyzed the slice physiology experiments. MO and KK analyzed gene expression datasets from postmortem human tissue. HSY and LP generated and characterized the PNKD mouse model, and consulted regarding behavioral experiments. ABN and ACK wrote the manuscript with contributions from all authors.

Acknowledgments

This work was supported by K08 NS081001 (ABN), R01 MH113896 (MCO), R01 NS064984 (ACK), R01 NS078435 (ACK), and the William Bowes Neurogenetics Fund (LJP). ABN is the Richard and Shirley Cahill Endowed Chair in Parkinson's Disease Research. MCO is supported by a Scholar Award from the UCSF Weill Institute for Neurosciences. AEG is supported by the National Science Foundation Graduate Research Fellowship and the UCSF Discovery Fellows Program. KWK was supported by the UCSF Medical Scientist Training Program, NIGMS T32GM007618. We thank the UCSF NIAAA P50 Histology Core for sharing equipment. We thank Philip Starr for valuable discussion, and Chloe Bair-Marshall and Matthew Lum for technical assistance.

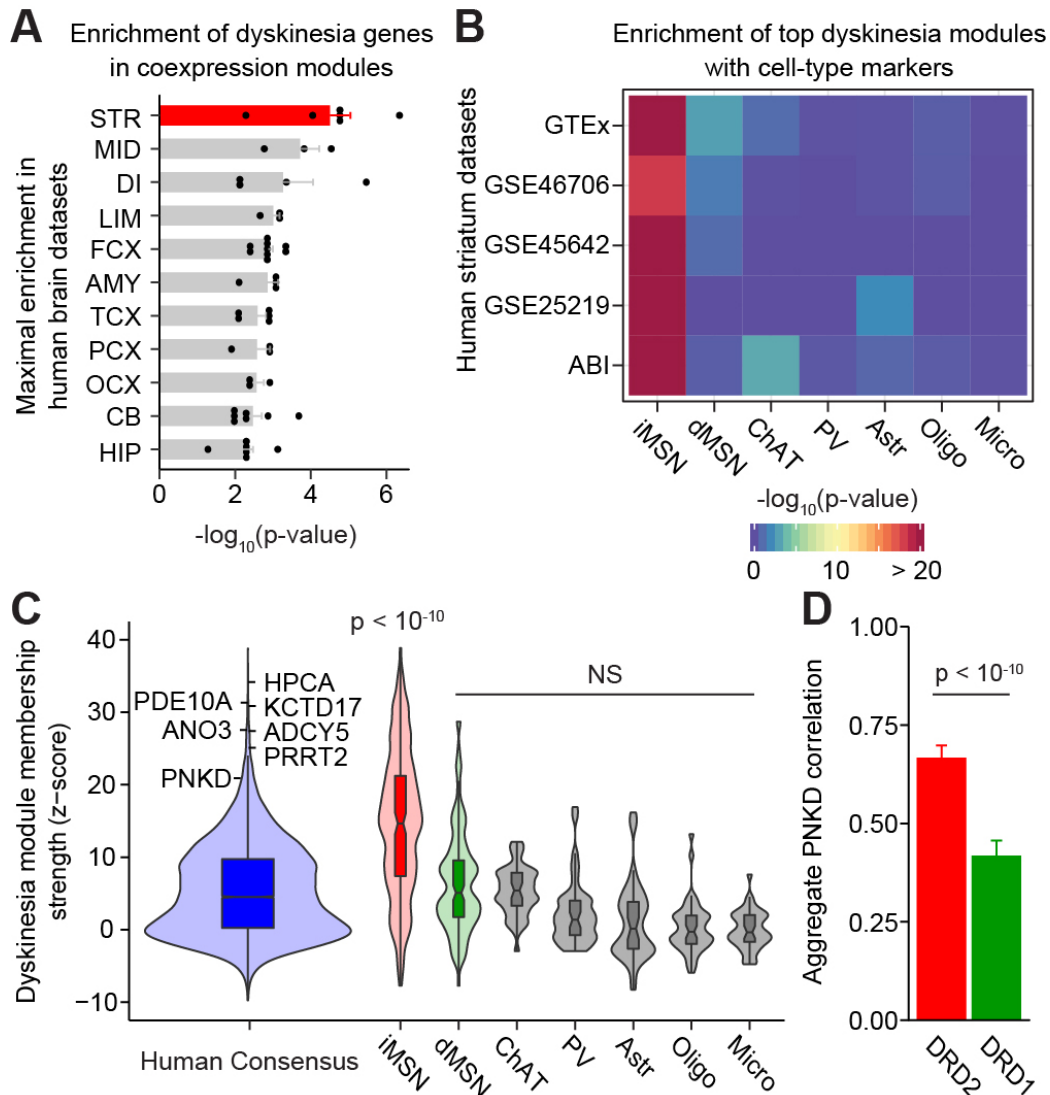


Figure 1: Dyskinesia-associated genes are co-expressed with markers of indirect pathway neurons in human striatum. Analysis of gene expression data from neurotypical adult human brains. A. Enrichment p-values for the most significant dyskinesia gene module from each brain region and dataset (each dot represents one dataset). B. Enrichment of striatal dyskinesia modules with cell-type markers (see methods): indirect pathway MSNs (iMSN), direct pathway MSNs (dMSN), cholinergic interneurons (ChAT), parvalbumin-positive fast-spiking interneurons (PV), astrocytes (Astr), oligodendrocytes (Oligo), and microglia (Micro). Striatal dyskinesia modules consistently showed significant enrichment for iMSN marker genes, but not markers of other cell types. C. Genome-wide distribution of consensus striatal dyskinesia module membership strength. Dyskinesia genes with z-score >20 are labeled. The distributions for the cell-type genes from (B) were cross-referenced with genes with high consensus dyskinesia module membership (z-score >20). D. The aggregate correlation of PNKD expression with iMSNs and dMSNs signatures across the human striatum datasets from (B). Abbreviations: STR = striatum; MID = midbrain; DI = diencephalon; LIM = limbic cortex; FCX = frontal cortex; AMY = amygdala; TCX = temporal cortex; CB = cerebellum; OXC = occipital cortex; HIP = hippocampus. Error bars denote the SEM.

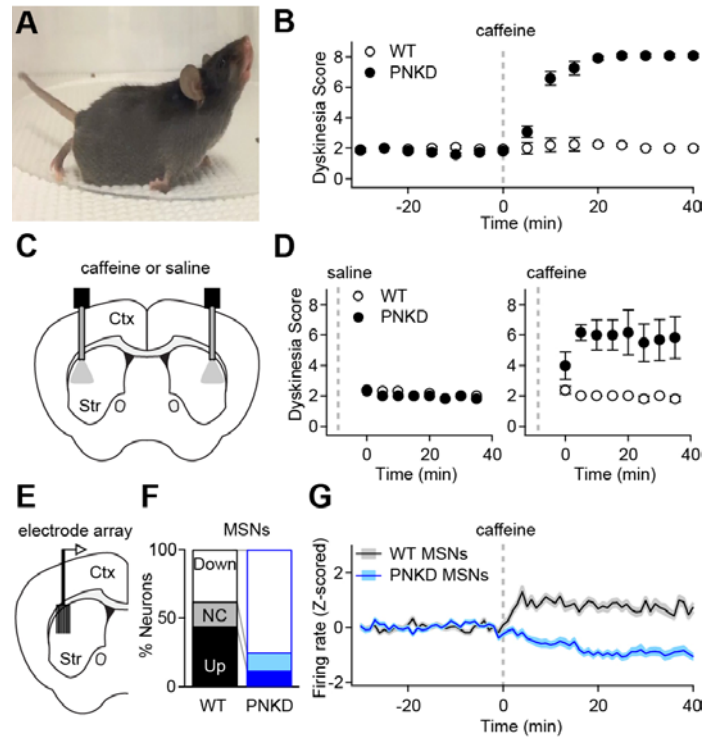


Figure 2. Dyskinetic attacks in PNKD mice are accompanied by decreased firing rates in striatal projection neurons. A. Dystonic posturing in a PNKD mouse treated with caffeine (25 mg/kg). B. Dyskinesia scores of WT and PNKD mice treated with systemic (intraperitoneal, IP) caffeine (dotted line). C. Schematic diagram showing bilateral infusion cannulae in the dorsolateral striatum. D. Dyskinesia scores for WT and PNKD mice treated with intra-striatal saline (left) or caffeine (right). E. Schematic diagram showing multielectrode array implantation in left dorsolateral striatum. F. Percentage of units whose firing rates went up, down, or had no change (NC) after IP caffeine. G. Average Z-scored firing rates of unidentified MSNs before and after IP caffeine administration (T=0) in WT and PNKD mice. All values are displayed as average \pm SEM.

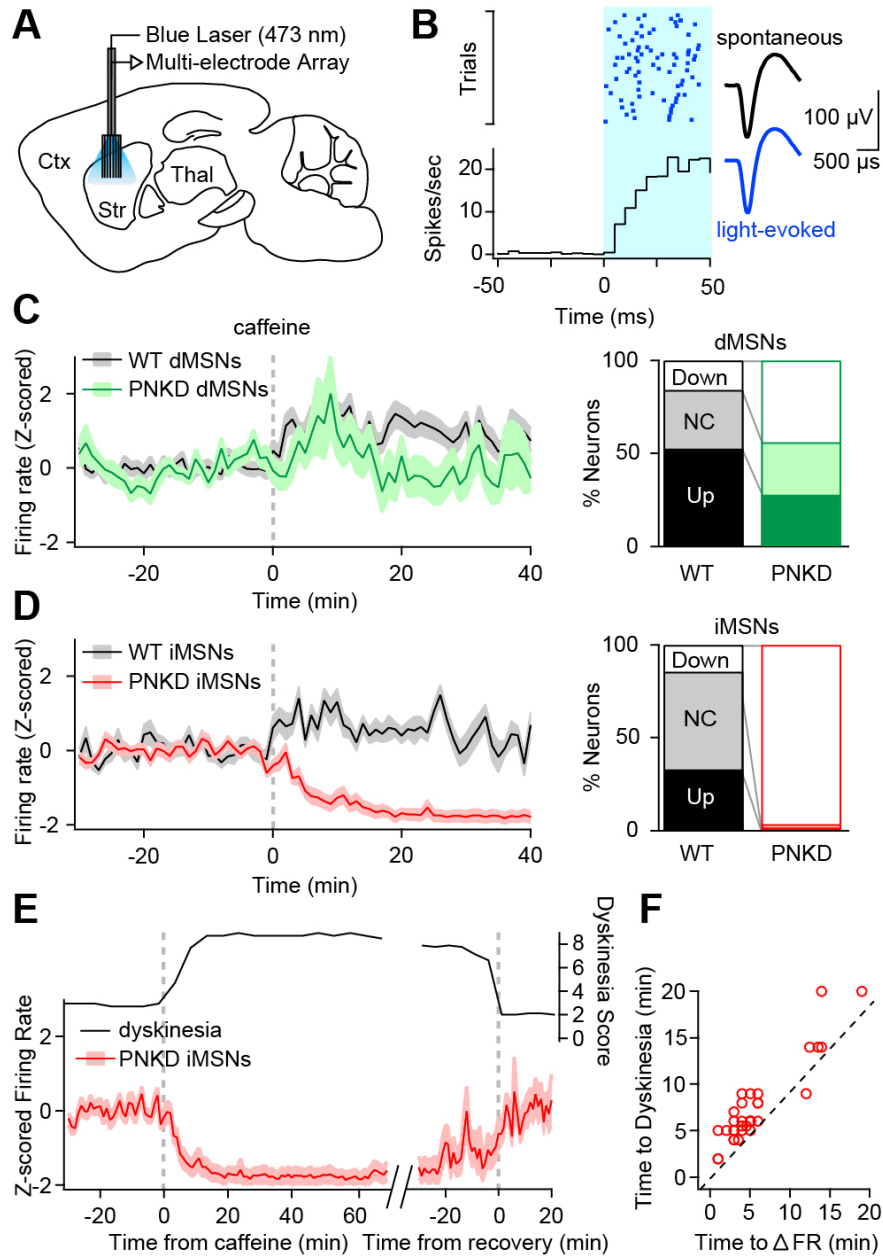


Figure 3. iMSNs are differentially suppressed during caffeine-triggered dyskinesia. A. Schematic diagram of optrode recording configuration in sagittal view. B. Representative optogenetically-identified unit, showing responses to blue light pulses (left) and average spontaneous and light-evoked waveforms (right). C, D. Average Z-scored firing rates of optogenetically-identified direct pathway MSNs (dMSNs, C) or indirect pathway MSNs (iMSNs, D) in WT and PNKD mice before and after caffeine administration (T=0). Right: Percentage of units whose firing rates went up, down, or had no change (NC) after caffeine. E. Dyskinesia score (black line) and Z-scored iMSN firing rates (red line) from PNKD animals monitored until recovery. F. Plot of time to change in firing rate of iMSNs vs time to dyskinesia. All values are displayed as average \pm SEM.

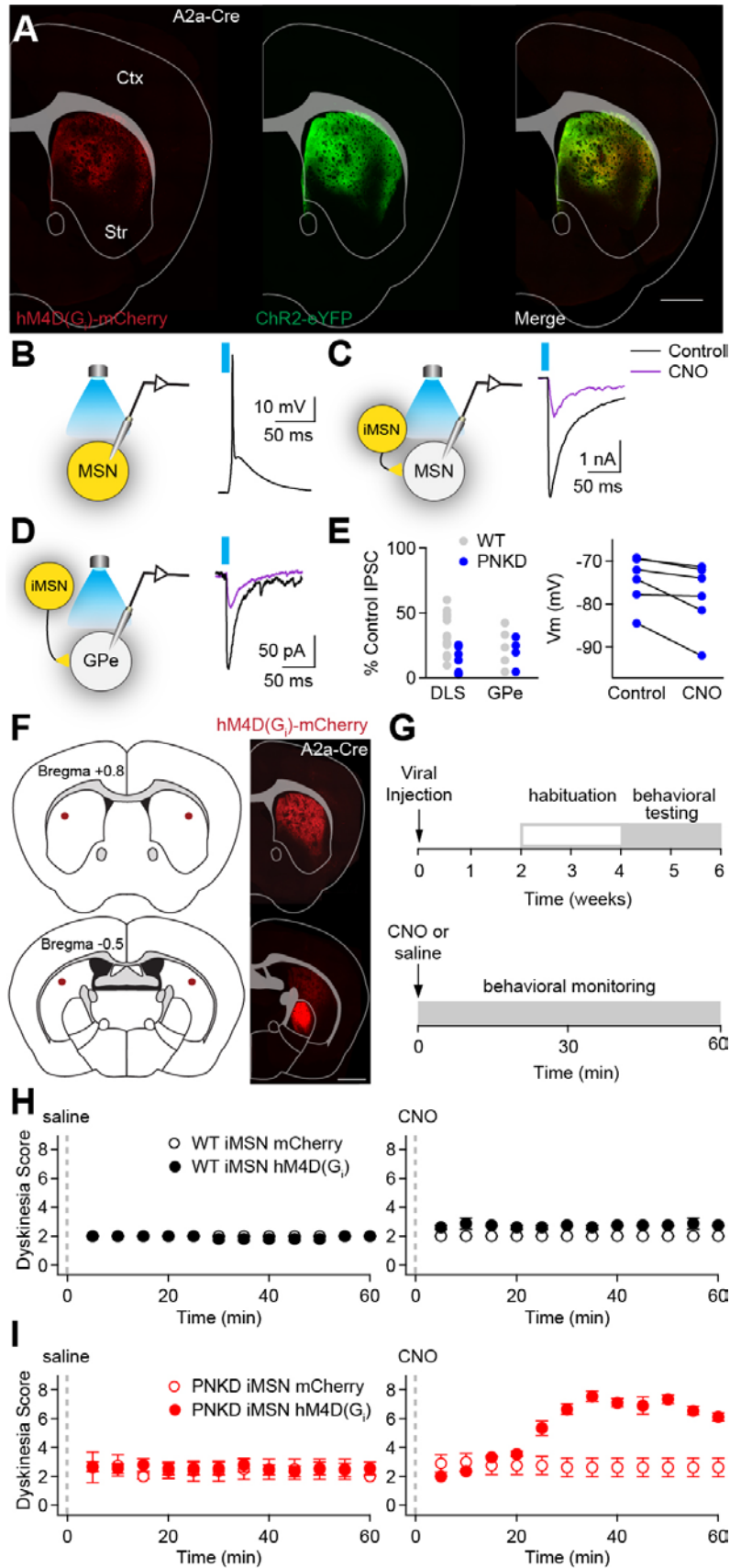


Figure 4. Chemogenetic inhibition of iMSNs causes dyskinesia in PNKD mice. A-E. The DLS of A2a-Cre mice was injected at a single site with AAVs encoding Cre-dependent hM4D(G_i)-mCherry and ChR2-eYFP. Acute coronal sections were prepared for histology (A) and slice electrophysiology (B-E). A. Coronal section of DLS showing expression of hM4D(G_i)-mCherry (left), ChR2-eYFP (center), and merged (right). B-E. Whole-cell recordings of striatal MSNs (B-C) and globus pallidus pars externa (GPe) neurons. Recording configurations are schematized at left in each panel. B. Representative current clamp recording from an eYFP-positive striatal neuron (putative iMSN), showing a light-evoked action potential in response to a 5 ms pulse of blue light (1 mW). C. Representative voltage-clamp recording from an eYFP-negative striatal neuron (MSN), showing a light-evoked inhibitory postsynaptic current (IPSC) before (black) and after (purple) application of clozapine-N-oxide (CNO, 1 μM). D. Representative voltage clamp recording from a GPe neuron, showing a light-evoked IPSC before and after application of CNO. E. Left: summary of IPSC amplitude in the DLS and GPe after CNO application. Right: resting V_m of iMSNs before and after CNO application. F. Left: schematic diagram showing 4 DLS injection sites in A2a-Cre mice. Right: Representative coronal sections from a mouse injected with AAV-DIO-hM4D(G_i)-mCherry. G. Experimental timeline. Mice were injected with AAVs encoding Cre-dependent mCherry or hM4D-mCherry. After habituation to daily saline injections, mice were administered either IP saline or CNO on interleaved testing days. H,I. Dyskinesia score in WT;A2a-Cre (H) or PNKD;A2a-Cre (I) animals administered saline (left) or CNO (1 mg/kg; right). All values are displayed as average ± SEM. Scale bars = 1 mm.

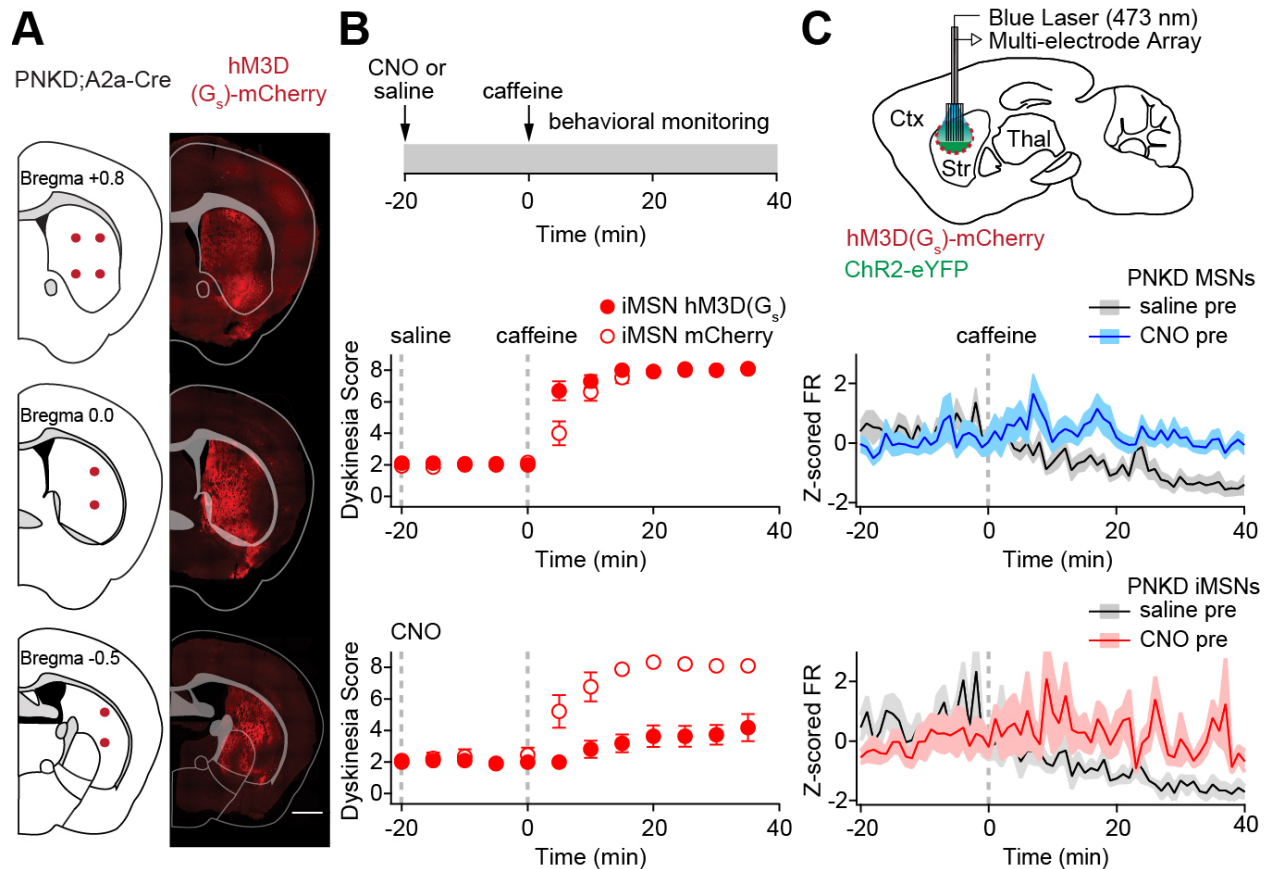


Figure 5. Chemogenetic activation of iMSNs blunts dyskinesia in PNKD mice. A. Left: Schematic diagram showing 8 striatal injection sites per side in PNKD;A2a-Cre mice. Right: representative coronal sections from a mouse injected with AAV-DIO-hM3D(G_s)-mCherry. B. Top: Experimental design. Middle/Bottom: Dyskinesia score in PNKD;A2a-Cre mice pretreated with saline (middle) or CNO (bottom) prior to caffeine. C. Top: Sagittal schematic diagram of optrode recording configuration. ChR2-eYFP and hM3D(G_s)-mCherry were injected in the dorsolateral striatum of PNKD;A2a-Cre mice. Middle: Average Z-scored firing rates of unidentified MSNs in WT or PNKD mice pretreated with saline or CNO before and after caffeine administration. Bottom: Average Z-scored firing rates of optogenetically-identified indirect pathway MSNs (iMSNs) in WT and PNKD mice pretreated with saline or CNO before and after caffeine administration. All values are displayed as average ± SEM. Scale bars = 1 mm.

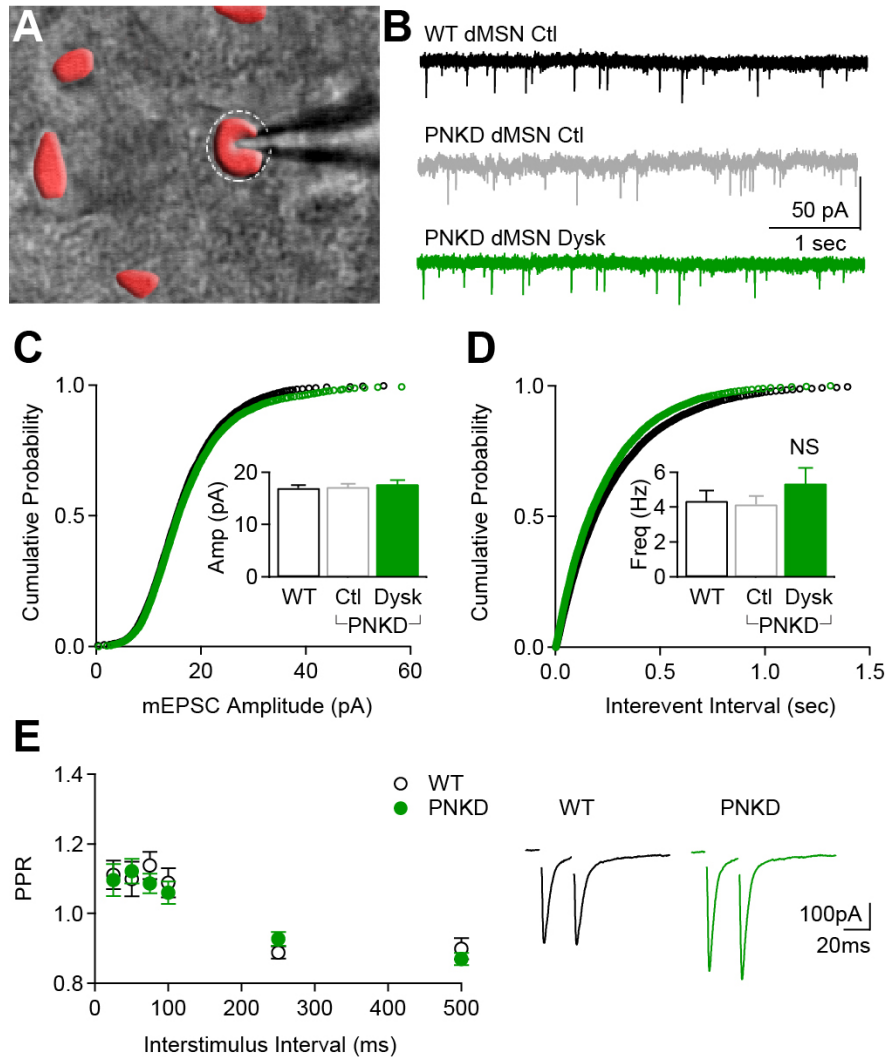


Figure 6. Excitatory transmission unchanged onto dMSNs in dyskinetic PNKD mice. A. Overlaid DIC and fluorescence images of a striatal slice from PNKD;Drd1a-tdTomato mouse, illustrating targeting of tdTomato-positive dMSNs. B. Representative traces of miniature excitatory postsynaptic currents (mEPSCs) from WT (black), non-dyskinetic PNKD (grey), and dyskinetic PNKD (green) dMSNs. C. mEPSC amplitude cumulative histogram from WT and PNKD iMSNs. Inset: Average mEPSC amplitudes from WT (black open), non-dyskinetic (grey open), and dyskinetic (green closed) PNKD mice. D. mEPSC frequency cumulative histogram. Inset: Average mEPSC frequencies from WT (black open), non-dyskinetic (grey open), and dyskinetic (green closed) PNKD mice. E. Left: Average paired pulse ratio (PPR) of evoked EPSCs. Right: Representative EPSCs with 25 ms ISI. All values are displayed as average \pm SEM.

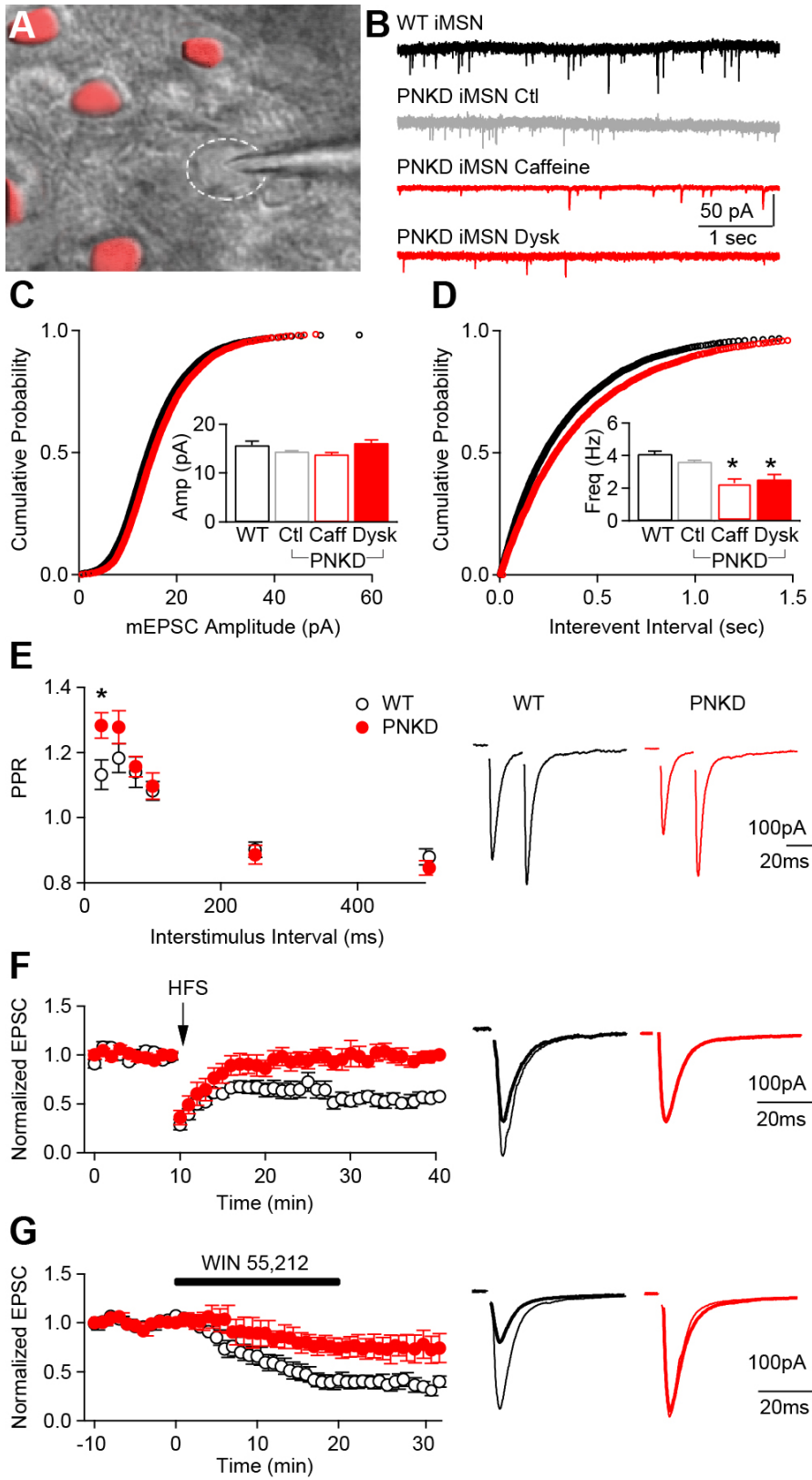


Figure 7. Excitatory transmission reduced onto iMSNs in dyskinetic PNKD mice. A. Overlaid DIC and fluorescence images of a striatal slice from PNKD;*Drd1a*-tdTomato mouse, illustrating targeting of tdTomato-negative iMSNs. B. Representative traces of miniature excitatory postsynaptic currents (mEPSCs) from WT (black), non-dyskinetic PNKD (grey), non-dyskinetic PNKD with caffeine (red), and dyskinetic PNKD (red) iMSNs. C. mEPSC amplitude cumulative histogram from WT (black) and PNKD (red) iMSNs. Inset: Average mEPSC amplitudes from WT (black open), non-dyskinetic PNKD (grey open), non-dyskinetic PNKD with caffeine (red open), and dyskinetic PNKD (red filled) mice. D. mEPSC frequency cumulative histogram. Inset: Average mEPSC frequencies from WT, non-dyskinetic PNKD, non-dys kinetic PNKD with caffeine, and dyskinetic PNKD mice. E-G. Electrically evoked EPSCs in slices from WT and dyskinetic PNKD mice. E. Left: Average paired pulse ratio (PPR) of evoked EPSCs. Right: Representative EPSCs with 25 ms interspike interval (ISI). F. Left: Normalized evoked EPSC amplitude in iMSNs subjected to high frequency stimulation (HFS, arrow) to elicit long-term depression. Right: Representative EPSCs before (thin line) and after (thick line) HFS. G. Left: Normalized evoked EPSC amplitude in iMSNs treated with WIN 55,212. Right: Representative EPSCs before (thin line) and after (thick line) WIN 55,212. All values are displayed as average \pm SEM.

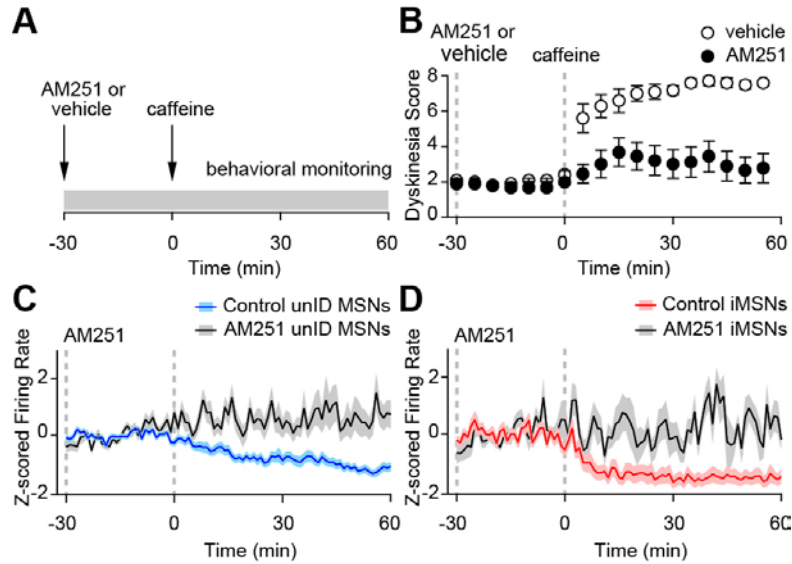
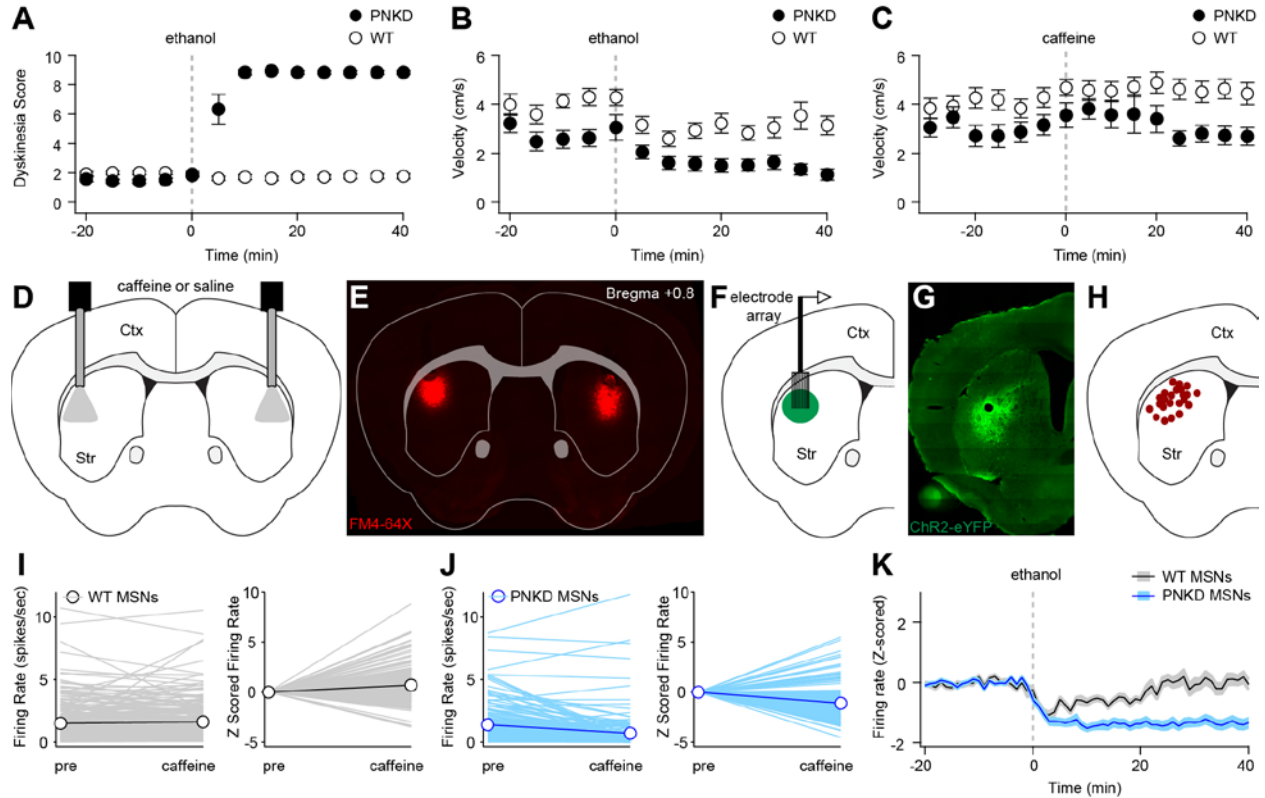
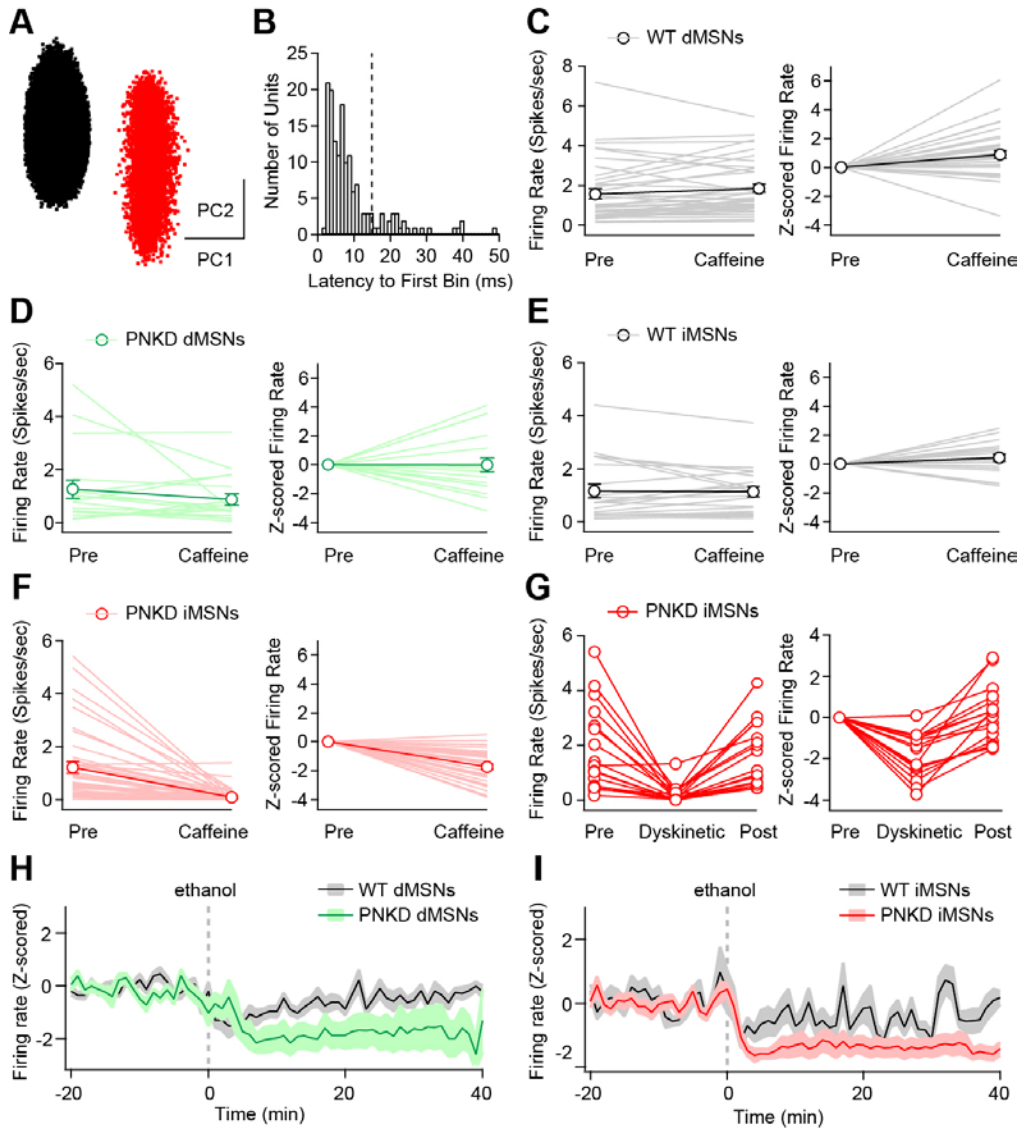


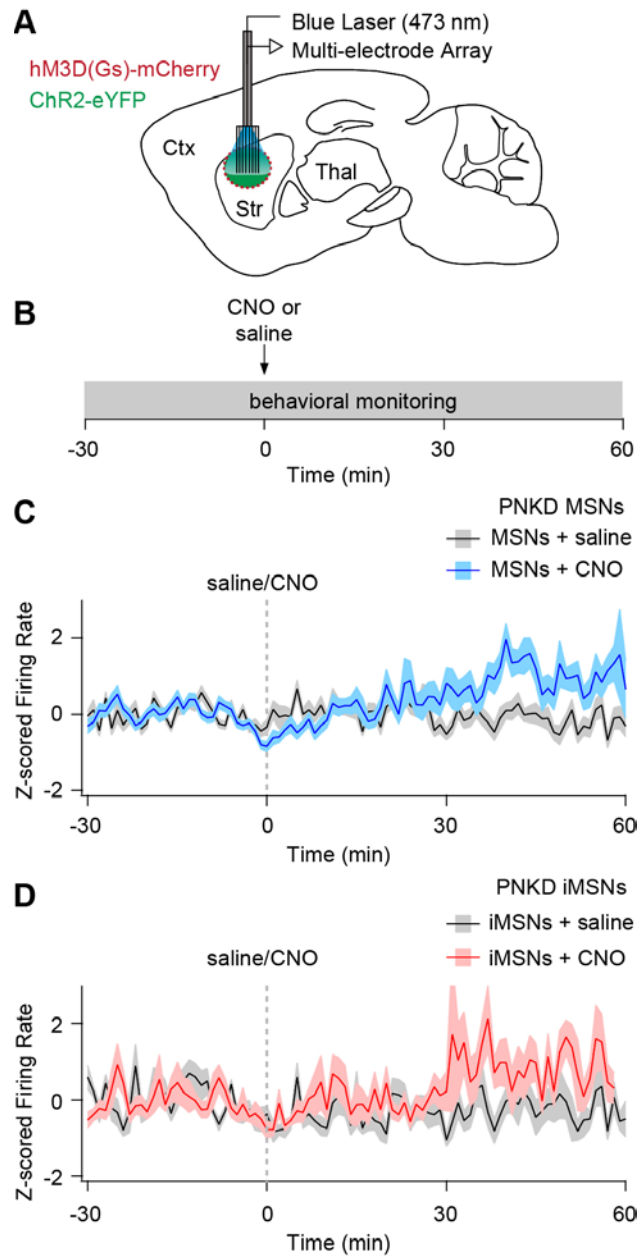
Figure 8. Cannabinoid CB1 antagonists block iMSN suppression and dyskinesia in PNKD mice. A. Experimental timeline. PNKD mice were pretreated with the endocannabinoid antagonist AM251 (5 mg/kg) or vehicle prior to caffeine injection. B. Dyskinesia score in PNKD mice during these trials. C, D. Average Z-scored firing rates from PNKD mice treated with caffeine, with or without AM251 pretreatment. C. Unidentified striatal units. D. Optogenetically identified iMSNs. All values are displayed as average \pm SEM.



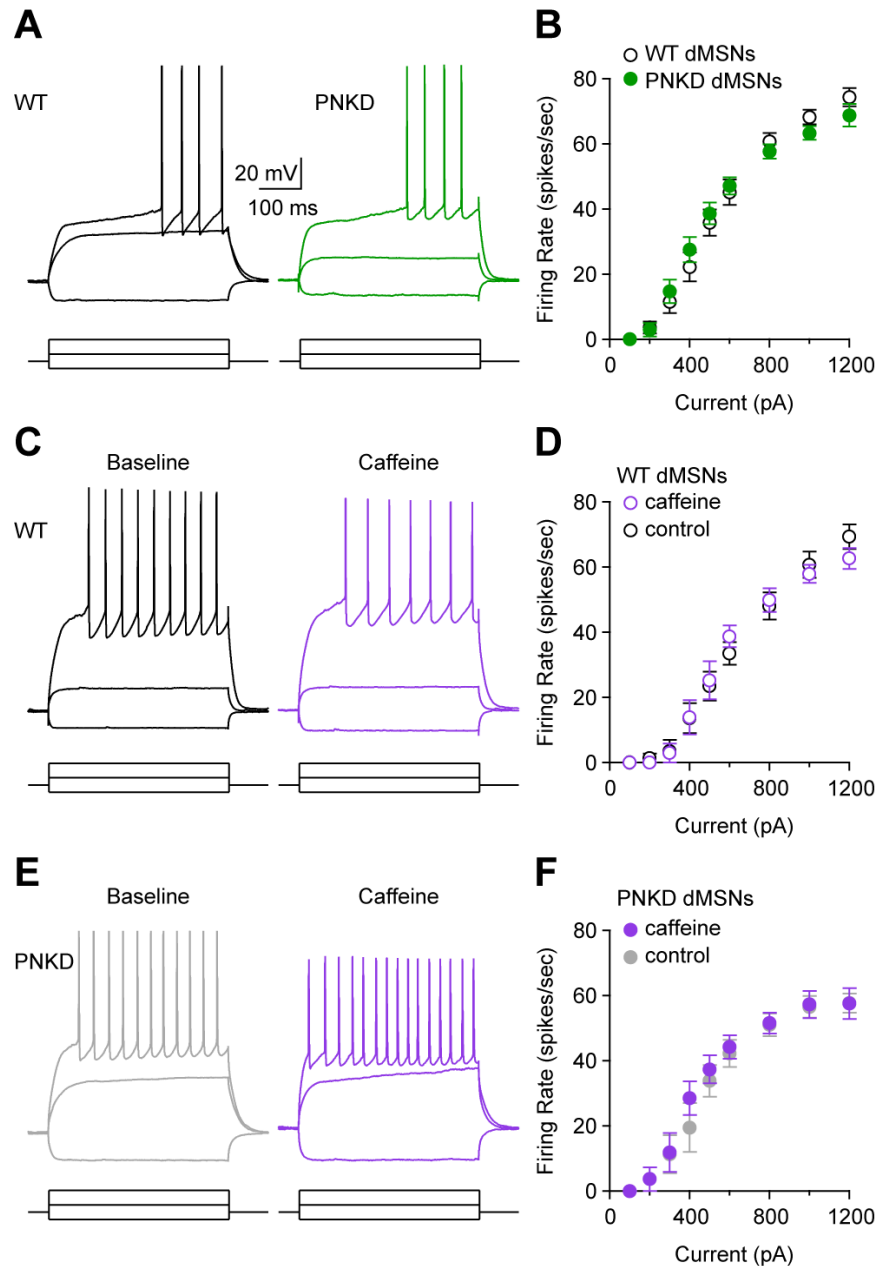
Supplemental Figure 1 (related to Figure 2). Dyskinesia alters striatal firing rates in PNKD mice. A. Dyskinesia scores of WT and PNKD mice treated with systemic (intraperitoneal, IP) ethanol (1.5 g/kg; dotted line) B. Velocity of WT and PNKD mice treated with IP ethanol. C. Velocity of WT and PNKD mice treated with IP caffeine (25 mg/kg; dotted line). D. Schematic diagram showing (in coronal section) infusion cannulae implanted in the bilateral dorsolateral striatum (DLS). E. Representative postmortem histological section from a mouse implanted with bilateral infusion cannulae, estimating the sites of drug infusion by the lipophilic dye FM4-64X, which was infused just prior to sacrifice. F. Schematic diagram showing microelectrode array implant in the left DLS. The DLS was also injected with AAV-DIO-ChR2-eYFP. G. Representative postmortem histological section showing region of ChR2-eYFP expression (green) around the recording sites (electrolytic lesion is small hole in tissue). H. Summary of recording sites, as marked by electrolytic lesions. I, J. Firing rate changes of individual unidentified striatal units (putative MSNs) between baseline (pre) and 30-60 minutes following caffeine administration (caffeine). Absolute firing rates are shown at left and Z-scored firing rate is shown at right. I. Firing rates in wild-type (WT) animals. J. Firing rates in PNKD animals. K. Average Z-scored firing rates of unidentified MSNs before and after IP ethanol administration (T=0) in WT and PNKD mice.



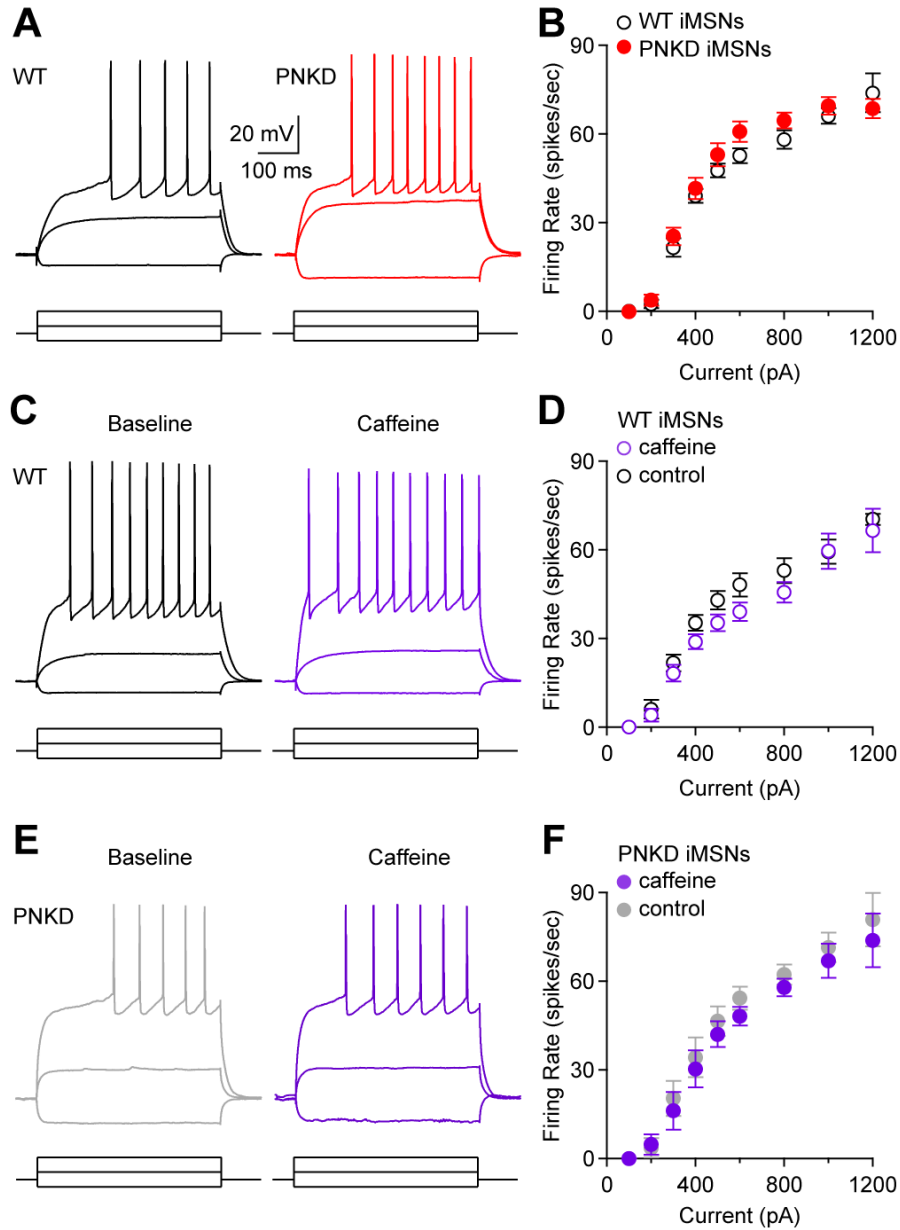
Supplemental Figure 2 (related to Figure 2). Recordings from optogenetically-identified dMSNs and iMSNs in wild-type and PNKD mice. A. Example of typical single-unit (red) and multiunit (black) waveforms as displayed in PCA space. B. Histogram showing the latency of individual optogenetically labeled MSNs to laser pulses. Latency was calculated as time to the first (of at least 20) 1 ms bin in which firing rate exceeded the 99% confidence interval of the baseline. C-F. Individual firing rate changes between baseline (pre) and 30-60 minutes following caffeine administration (caffeine). Absolute firing rates are shown at left and Z-scored firing rate is shown at right for WT dMSNs (C), PNKD dMSNs (D), WT iMSNs (E), and PNKD iMSNs (F). G. Individual PNKD iMSN firing rate changes observed during prolonged sessions, between baseline (pre), 30-60 minutes following caffeine administration (dyskinetic) and after full behavioral recovery (post). Absolute firing rates are shown at left, and Z-scored firing rate at right. H, I. Average Z-scored firing rates of optogenetically-identified direct pathway MSNs (dMSNs, H) or indirect pathway MSNs (iMSNs, I) in WT and PNKD mice before and after ethanol administration (T=0).



Supplemental Figure 3 (related to Figure 5). Chemogenetic activation of iMSNs blunts dyskinesia in PNKD mice. A. Schematic diagram of optrode recording configuration in sagittal view with ChR2-eYFP and hM3D(G_s)-mCherry injected in the dorsolateral striatum. B. Experimental design. C. Average Z-scored firing rates of MSNs in WT or PNKD before and after saline or CNO administration. D. Average Z-scored firing rates of optogenetically-identified indirect pathway MSNs (iMSNs) in WT and PNKD before and after saline or CNO administration. All values are displayed as average \pm SEM.



Supplemental Figure 4 (related to Figure 6). Caffeine does not modulate intrinsic excitability in WT or PNKD dMSNs. A. Current-clamp recordings from a representative WT (black) or PNKD (green) dMSN displaying responses to injected current steps (100-pA steps). B. Summary of firing frequency in response to injected current in WT (black open circles) and PNKD (green filled circles) dMSNs. C. Current-clamp recordings from a representative WT dMSN displaying responses to injected current steps before (black) and after (purple) caffeine application. D. Summary of firing frequency in response to injected current in WT dMSNs before (black open circles) and after (purple open circles) caffeine application. E. Current-clamp recordings from a representative PNKD dMSN displaying responses to injected current steps before (grey) and after (purple) caffeine application. F. Summary of firing frequency in response to injected current in PNKD dMSNs before (grey filled circles) and after (purple filled circles) caffeine. All values are displayed as average \pm SEM.



Supplemental Figure 5 (related to Figure 7). Caffeine does not modulate intrinsic excitability in WT or PNKD iMSNs. A. Current clamp recordings from a representative WT (black) or PNKD (red) iMSN displaying responses to injected current steps (100-pA steps). B. Summary of firing frequency in response to injected current in WT (black open circles) and PNKD (red filled circles) iMSNs. C. Current clamp recordings from a representative WT iMSN displaying responses to injected current steps before (black) and after (purple) caffeine application. D. Summary of firing frequency in response to injected current in WT iMSNs before (black open circles) and after (purple open circles) caffeine application. E. Current clamp recordings from a representative PNKD iMSN displaying responses to injected current steps before (grey) and after (purple) caffeine application. F. Summary of firing frequency in response to injected current in PNKD iMSN before (grey filled circles) and after (purple filled circles) caffeine. All values are displayed as average \pm SEM.

CNS transcriptomes analyzed in this study											
Dataset_name	Source	Species	Region	Sample Prep	Age	Platform	Outliers	Samples	Post-QC	Batch Correction	Reference
Hs.AMY.ABI	ABI	Human	AMY	Dissection / LMD	Adult	Agilent	0	72		NO	(lawrylycz et al., 2015)
Hs.CB.ABI	ABI	Human	CB	Dissection / LMD	Adult	Agilent	4	364		NO	(lawrylycz et al., 2015)
Hs.DI.ABI	ABI	Human	DI	Dissection / LMD	Adult	Agilent	7	333		NO	(lawrylycz et al., 2015)
Hs.FCX.ABI	ABI	Human	FCX	Dissection / LMD	Adult	Agilent	12	533		NO	(lawrylycz et al., 2015)
Hs.HIP.ABI	ABI	Human	HIP	Dissection / LMD	Adult	Agilent	0	188		NO	(lawrylycz et al., 2015)
Hs.LIM.ABI	ABI	Human	LIM	Dissection / LMD	Adult	Agilent	6	195		NO	(lawrylycz et al., 2015)
Hs.MID.ABI	ABI	Human	MID	Dissection / LMD	Adult	Agilent	0	182		NO	(lawrylycz et al., 2015)
Hs.OCX.ABI	ABI	Human	OCX	Dissection / LMD	Adult	Agilent	2	210		NO	(lawrylycz et al., 2015)
Hs.PCX.ABI	ABI	Human	PCX	Dissection / LMD	Adult	Agilent	5	285		NO	(lawrylycz et al., 2015)
Hs.STR.ABI	ABI	Human	STR	Dissection / LMD	Adult	Agilent	5	165		NO	(lawrylycz et al., 2015)
Hs.TCX.ABI	ABI	Human	TCX	Dissection / LMD	Adult	Agilent	5	465		NO	(lawrylycz et al., 2015)
Hs.FCX.GSE11882	GSE11882	Human	FCX	Dissection	Adult	AffyU133Plus2	0	48		NO	(Berchtold et al 2008)
Hs.HIP.GSE11882	GSE11882	Human	HIP	Dissection	Adult	AffyU133Plus2	1	42		NO	(Berchtold et al 2008)
Hs.PCX.GSE11882	GSE11882	Human	PCX	Dissection	Adult	AffyU133Plus2	0	43		NO	(Berchtold et al 2008)
Hs.TCX.GSE11882	GSE11882	Human	TCX	Dissection	Adult	AffyU133Plus2	0	39		NO	(Berchtold et al 2008)
Hs.AMY.GSE25219	GSE25219	Human	AMY	Dissection	Adult	AffyExon1.0	0	26		NO	(Kang et al., 2011)
Hs.CB.GSE25219	GSE25219	Human	CB	Dissection	Adult	AffyExon1.0	0	25		NO	(Kang et al., 2011)
Hs.DI.GSE25219	GSE25219	Human	DI	Dissection	Adult	AffyExon1.0	0	27		NO	(Kang et al., 2011)
Hs.FCX.GSE25219	GSE25219	Human	FCX	Dissection	Adult	AffyExon1.0	3	141		NO	(Kang et al., 2011)
Hs.HIP.GSE25219	GSE25219	Human	HIP	Dissection	Adult	AffyExon1.0	1	25		NO	(Kang et al., 2011)
Hs.OCX.GSE25219	GSE25219	Human	OCX	Dissection	Adult	AffyExon1.0	0	29		NO	(Kang et al., 2011)
Hs.PCX.GSE25219	GSE25219	Human	PCX	Dissection	Adult	AffyExon1.0	0	56		NO	(Kang et al., 2011)
Hs.STR.GSE25219	GSE25219	Human	STR	Dissection	Adult	AffyExon1.0	0	27		NO	(Kang et al., 2011)
Hs.TCX.GSE25219	GSE25219	Human	TCX	Dissection	Adult	AffyExon1.0	0	86		NO	(Kang et al., 2011)
Hs.CB.GSE36192	GSE36192	Human	CB	Dissection	Adult	Ilmn112v3	29	356		YES	(Ilemendez et al., 2012)
Hs.FCX.GSE36192	GSE36192	Human	FCX	Dissection	Adult	Ilmn112v3	25	362		YES	(Ilemendez et al., 2012)
Hs.CB.GSE3790	GSE3790	Human	CB	Dissection	Adult	AffyU133A	0	27		YES	(Hodges et al., 2006)
Hs.FCX.GSE3790	GSE3790	Human	FCX	Dissection	Adult	AffyU133A	0	28		YES	(Hodges et al., 2006)
Hs.STR.GSE3790	GSE3790	Human	STR	Dissection	Adult	AffyU133A	0	32		YES	(Hodges et al., 2006)
Hs.AMY.GSE45642	GSE45642	Human	AMY	Dissection	Adult	AffyU133A	0	32		YES	(Li et al., 2013)
Hs.CB.GSE45642	GSE45642	Human	CB	Dissection	Adult	AffyU133A	0	42		YES	(Li et al., 2013)
Hs.FCX.GSE45642	GSE45642	Human	FCX	Dissection	Adult	AffyU133A	1	75		YES	(Li et al., 2013)
Hs.HIP.GSE45642	GSE45642	Human	HIP	Dissection	Adult	AffyU133A	2	59		YES	(Li et al., 2013)
Hs.LIM.GSE45642	GSE45642	Human	LIM	Dissection	Adult	AffyU133A	0	64		YES	(Li et al., 2013)
Hs.STR.GSE45642	GSE45642	Human	STR	Dissection	Adult	AffyU133A	2	63		YES	(Li et al., 2013)
Hs.CB.GSE46706	GSE46706	Human	CB	Dissection	Adult	AffyExon1.0	0	94		NO	(Ramasamy et al., 2014)
Hs.DI.GSE46706	GSE46706	Human	DI	Dissection	Adult	AffyExon1.0	0	93		NO	(Ramasamy et al., 2014)
Hs.FCX.GSE46706	GSE46706	Human	FCX	Dissection	Adult	AffyExon1.0	5	90		NO	(Ramasamy et al., 2014)
Hs.HIP.GSE46706	GSE46706	Human	HIP	Dissection	Adult	AffyExon1.0	2	92		NO	(Ramasamy et al., 2014)
Hs.MID.GSE46706	GSE46706	Human	MID	Dissection	Adult	AffyExon1.0	0	71		NO	(Ramasamy et al., 2014)
Hs.OCX.GSE46706	GSE46706	Human	OCX	Dissection	Adult	AffyExon1.0	6	90		NO	(Ramasamy et al., 2014)
Hs.STR.GSE46706	GSE46706	Human	STR	Dissection	Adult	AffyExon1.0	0	97		NO	(Ramasamy et al., 2014)
Hs.TCX.GSE46706	GSE46706	Human	TCX	Dissection	Adult	AffyExon1.0	8	76		NO	(Ramasamy et al., 2014)
Hs.AMY.GTeX	GTeX	Human	AMY	Dissection	Adult	RNA-seq	6	59		NO	(The GTeX Consortium et al 2015)
Hs.CB.GTeX	GTeX	Human	CB	Dissection	Adult	RNA-seq	7	93		NO	(The GTeX Consortium et al 2015)
Hs.DI.GTeX	GTeX	Human	DI	Dissection	Adult	RNA-seq	5	82		NO	(The GTeX Consortium et al 2015)
Hs.FCX.GTeX	GTeX	Human	FCX	Dissection	Adult	RNA-seq	5	95		NO	(The GTeX Consortium et al 2015)
Hs.HIP.GTeX	GTeX	Human	HIP	Dissection	Adult	RNA-seq	3	84		NO	(The GTeX Consortium et al 2015)
Hs.MID.GTeX	GTeX	Human	MID	Dissection	Adult	RNA-seq	7	48		NO	(The GTeX Consortium et al 2015)
Hs.STR.GTeX	GTeX	Human	STR	Dissection	Adult	RNA-seq	27	280		NO	(The GTeX Consortium et al 2015)
Hs.LIM.GTeX	GTeX	Human	LIM	Dissection	Adult	RNA-seq	4	76		NO	(The GTeX Consortium et al 2015)
Hs.FCX.RNAseq	Brainspan.org	Human	FCX	Dissection	Adult	RNA-seq	0	44		NO	Brainspan.org
Hs.TCX.RNAseq	Brainspan.org	Human	TCX	Dissection	Adult	RNA-seq	1	26		NO	Brainspan.org

Table 1. Human CNS transcriptomes analyzed in this study. Dataset_name: Dataset (Hs = human); Source: Gene Expression Omnibus identifier or resource name (ABI = Allen Brain Institute, GTeX = Genotype-Tissue Expression project); Species: human; Region: CNS region (AMY = amygdala, CB = cerebellum, CTX = cortex, DI = diencephalon, FCX = frontal cortex, HIP = hippocampus, LIM = limbic cortex, MID = midbrain, OCX = occipital cortex, PCX = parietal cortex, STR = striatum, TCX = temporal cortex); Sample Prep: dissection = macro-dissection; Adult: >= 18 years of age; Technology Platform: Affy = Affymetrix; Outliers: Number of outlier samples that were removed; Samples Post-QC: Number of samples remaining after quality control (QC); Batch Correction: Whether batch correction was performed; Reference: Reference or website of the dataset.

Gene	Entrez ID	# Datasets	# Samples	Mean r	Z-Score	Reference
HPCA	3208	5	632	0.88	34.2	Charlesworth et al, Am J Hum Genet 2015
PDE10A	10846	5	632	0.85	31.3	Mencacci et al, Am J Hum Genet 2016
KCTD17	79734	5	632	0.85	30.8	Mencacci et al, Am J Hum Genet 2015
ANO3	63982	5	632	0.8	27.5	Charlesworth et al, Am J Hum Genet 2015
ADCY5	111	4	569	0.82	27.4	Chen et al, Arch Neurol 2012
PRRT2	112476	4	569	0.79	25.1	Chen et al, Nat Genet 2011
PNKD	25953	4	569	0.71	20.9	Lee et al, Hum Mol Genet 2004
GNAL	2774	5	632	0.62	18.1	Fuchs et al, Nat Genet 2013
TOR1A	1861	5	632	0.6	17.2	Ozelius et al, Nat Genet 1997
TUBB4A	10382	5	632	0.52	14.2	Hersheson et al, Ann Neurol 2013
GCH1	2643	5	632	0.41	10.9	Ichinose et al, Nat Genet 1994
CIZ1	25792	5	632	0.41	10.7	Xiao et al, Ann Neurol 2012
THAP1	55145	5	632	0.35	9.08	Fuchs et al, Nat Genet 2009
CYP2U1	113612	4	569	0.28	6.89	Citterio et al, J Neurol 2013
PRKRA	8575	5	632	0.25	6.4	Zech et al, Mov Disord 2014
KMT2B	9757	5	632	0.24	6.16	Zech et al, Am J Hum Genet 2016
VPS16	64601	3	508	0.24	5.37	Cai et al, Sci Rep 2016
COMT	1312	5	632	0.0089	0.221	Gu et al, Neurol Sci 2016
ECHS1	1892	5	632	0.0054	0.134	Olgiatei et al, Mov Disord 2016
POC1B	282809	4	569	-0.016	-0.375	Gu et al, Neurol Sci 2016
ACY1	95	4	569	-0.029	-0.677	Sass et al, Metab Brain Dis 2016
COL6A3	1293	5	632	-0.062	-1.55	Zech et al, Am J Hum Genet 2015
GCDH	2639	5	632	-0.11	-2.64	Marti-Masso et al, Hum Genet, 2012

Table 2. Dyskinesia Gene Set. Gene: HGNC gene symbol; Entrez ID: Entrez identifier; Number of Datasets: The number of gene expression datasets from human striatum that included data for each gene; Number of Samples: The total number of human striatal samples in these datasets; Dyskinesia Mean R: The aggregate correlation (Methods) between the expression of each gene and the dyskinesia module eigengene over all samples from all human striatal datasets; Dyskinesia Z-Score: Z-score of the association of each gene with the dyskinesia module over all human striatal datasets; Reference: Published study that implicates each gene in human dyskinesia.

2.10 References

- Albanese, A., Bhatia, K., Bressman, S.B., DeLong, M.R., Fahn, S., Fung, V.S., Hallett, M., Jankovic, J., Jinnah, H.A., Klein, C., et al. (2013). Phenomenology and classification of dystonia: a consensus update. *Movement disorders: official journal of the Movement Disorder Society* 28, 863-873.
- Albin, R.L., Young, A.B., and Penney, J.B. (1989). The functional anatomy of basal ganglia disorders. *Trends in neurosciences* 12, 366-375.
- Alcacer, C., Andreoli, L., Sebastianutto, I., Jakobsson, J., Fieblinger, T., and Cenci, M.A. (2017). Chemogenetic stimulation of striatal projection neurons modulates responses to Parkinson's disease therapy. *J Clin Invest* 127, 720-734.
- Avshalumov, Y., Volkman, C.E., Ruckborn, K., Hamann, M., Kirschstein, T., Richter, A., and Kohling, R. (2013). Persistent changes of corticostriatal plasticity in dt(sz) mutant hamsters after age-dependent remission of dystonia. *Neuroscience* 250, 60-69.
- Berardelli, A., Rothwell, J.C., Hallett, M., Thompson, P.D., Manfredi, M., and Marsden, C.D. (1998). The pathophysiology of primary dystonia. *Brain: a journal of neurology* 121 (Pt 7), 1195-1212.
- Berchtold, N.C., Cribbs, D.H., Coleman, P.D., Rogers, J., Head, E., Kim, R., Beach, T., Miller, C., Troncoso, J., Trojanowski, J.Q., et al. (2008). Gene expression changes in the course of normal brain aging are sexually dimorphic. *PNAS* 105, 15605-15610.
- Bock, R., Shin, J.H., Kaplan, A.R., Dobi, A., Markey, E., Kramer, P.F., Gremel, C.M., Christensen, C.H., Adrover, M.F., and Alvarez, V.A. (2013). Strengthening the accumbal indirect pathway promotes resilience to compulsive cocaine use. *Nature neuroscience* 16, 632-638.
- Bolstad, B.M., Irizarry, R.A., Astrand, M., and Speed, T.P. (2003). A comparison of normalization methods for high density oligonucleotide array data based on variance and bias. *Bioinformatics* 19, 185-193.
- Borgkvist, A., Avegno, E.M., Wong, M.Y., Kheirbek, M.A., Sonders, M.S., Hen, R., and Sulzer, D. (2015). Loss of Striatonigral GABAergic Presynaptic Inhibition Enables Motor Sensitization in Parkinsonian Mice. *Neuron* 87, 976-988.
- Burkhard, P.R. (2014). Acute and subacute drug-induced movement disorders. *Parkinsonism Relat Disord* 20 Suppl 1, S108-112.
- Calderon, D.P., Fremont, R., Kraenzlin, F., and Khodakhah, K. (2011). The neural substrates of rapid on set Dystonia-Parkinsonism. *Nature neuroscience* 14, 357-365.

Cenci, M.A., Tranberg, A., Andersson, M., and Hilbertson, A. (1999). Changes in the regional and compartmental distribution of FosB- and JunB-like immunoreactivity induced in the dopamine denervated rat striatum by acute or chronic L-dopa treatment. *Neuroscience* 94, 515-527.

Charlesworth, G., Plagnol, V., Holmstrom, K.M., Bras, J., Sheerin, U.M., Preza, E., Rubio-Agusti, I., Ryten, M., Schneider, S.A., Stamelou, M., et al. (2012). Mutations in ANO3 cause dominant craniocervical dystonia: ion channel implicated in pathogenesis. *Am J Hum Genet* 91, 1041-1050.

Choi, S., and Lovinger, D.M. (1997a). Decreased frequency but not amplitude of quantal synaptic responses associated with expression of corticostriatal long-term depression. *The Journal of neuroscience: the official journal of the Society for Neuroscience* 17, 8613-8620.

Choi, S., and Lovinger, D.M. (1997b). Decreased probability of neurotransmitter release underlies striatal long-term depression and postnatal development of corticostriatal synapses. *Proceedings of the National Academy of Sciences of the United States of America* 94, 2665-2670.

Cui, G., Jun, S.B., Jin, X., Pham, M.D., Vogel, S.S., Lovinger, D.M., and Costa, R.M. (2013). Concurrent activation of striatal direct and indirect pathways during action initiation. *Nature* 494, 238-242.

Dai, M., Wang, P., Boyd, A.D., Kostov, G., Athey, B., Jones, E.G., Bunney, W.E., Myers, R.M., Speed, T.P., Akil, H., et al. (2005). Evolving gene/transcript definitions significantly alter the interpretation of Gene Chip data. *Nucleic Acids Res* 33, e175.

Davis, S., and Meltzer, P.S. (2007). GEOquery: a bridge between the Gene Expression Omnibus (GEO) and BioConductor. *Bioinformatics* 23, 1846-1847.

Day, M., Wokosin, D., Plotkin, J.L., Tian, X., and Surmeier, D.J. (2008). Differential excitability and modulation of striatal medium spiny neuron dendrites. *The Journal of neuroscience: the official journal of the Society for Neuroscience* 28, 11603-11614.

Dearry, A., Gingrich, J.A., Falardeau, P., Fremeau, R.T., Jr., Bates, M.D., and Caron, M.G. (1990). Molecular cloning and expression of the gene for a human D1 dopamine receptor. *Nature* 347, 72-76.

Deep-Brain Stimulation for Parkinson's Disease Study, G. (2001). Deep-brain stimulation of the subthalamic nucleus or the pars interna of the globus pallidus in Parkinson's disease. *The New England journal of medicine* 345, 956-963.

Deffains, M., and Bergman, H. (2015). Striatal cholinergic interneurons and cortico-striatal synaptic plasticity in health and disease. *Movement disorders: official journal of the Movement Disorder Society* 30, 1014-1025.

- DeLong, M.R. (1990). Primate models of movement disorders of basal ganglia origin. *Trends in neurosciences* 13, 281-285.
- Dobbs, L.K., Kaplan, A.R., Lemos, J.C., Matsui, A., Rubinstein, M., and Alvarez, V.A. (2016). Dopamine Regulation of Lateral Inhibition between Striatal Neurons Gates the Stimulant Actions of Cocaine. *Neuron* 90, 1100-1113.
- Fisher, R.A. (1970). *Statistical Methods for Research Workers*, Fourteenth Edition edn (Hafner Publishing Company).
- Fremont, R., Tewari, A., Angueyra, C., and Khodakhah, K. (2017). A role for cerebellum in the hereditary dystonia DYT1. *eLife* 6.
- Fremont, R., Tewari, A., and Khodakhah, K. (2015). Aberrant Purkinje cell activity is the cause of dystonia in a shRNA-based mouse model of Rapid Onset Dystonia-Parkinsonism. *Neurobiology of disease* 82, 200-212.
- Gage, G.J., Stoetzer, C.R., Wiltschko, A.B., and Berke, J.D. (2010). Selective activation of striatal fastspiking interneurons during choice execution. *Neuron* 67, 466-479.
- Gautier, L., Cope, L., Bolstad, B.M., and Irizarry, R.A. (2004). affy--analysis of Affymetrix GeneChip data at the probe level. *Bioinformatics* 20, 307-315.
- Gerdeman, G.L., Ronesi, J., and Lovinger, D.M. (2002). Postsynaptic endocannabinoid release is critical to long-term depression in the striatum. *Nature neuroscience* 5, 446-451.
- Gernert, M., Richter, A., and Loscher, W. (1999). Alterations in spontaneous single unit activity of striatal subdivisions during ontogenesis in mutant dystonic hamsters. *Brain research* 821, 277-285.
- Gokce, O., Stanley, G., Treutlein, B., Neff, N.F., Camp, G.J., Malenka, R.C., Rothwell, P.E., Fuccillo, M.V., Sudhof, T.C., and Quake, S.R. (2016). Cellular Taxonomy of the Mouse Striatum as Revealed by Single-Cell RNA-Seq. *Cell Rep* 16, 1126-1137.
- Gong, S., Doughty, M., Harbaugh, C.R., Cummins, A., Hatten, M.E., Heintz, N., and Gerfen, C.R. (2007). Targeting Cre recombinase to specific neuron populations with bacterial artificial chromosome constructs. *The Journal of neuroscience: the official journal of the Society for Neuroscience* 27, 9817-9823.
- GTEX Consortium (2015). Human genomics. The Genotype-Tissue Expression (GTEx) pilot analysis: multitissue gene regulation in humans. *Science* 348, 648-660.
- Halje, P., Tamte, M., Richter, U., Mohammed, M., Cenci, M.A., and Petersson, P. (2012). Levodopa induced dyskinesia is strongly associated with resonant cortical oscillations.

The Journal of neuroscience: the official journal of the Society for Neuroscience 32, 16541-16551.

Hardin, J., Mitani, A., Hicks, L., and VanKoten, B. (2007). A robust measure of correlation between two genes on a microarray. *BMC Bioinformatics* 8, 220.

Hawrylycz, M., Miller, J.A., Menon, V., Feng, D., Dolbeare, T., Guillozet-Bongaarts, A.L., Jegga, A.G., Aronow, B.J., Lee, C.K., Bernard, A., et al. (2015). Canonical genetic signatures of the adult human brain. *Nat Neurosci* 18, 1832-1844.

Hernandez, D.G., Nalls, M.A., Moore, M., Chong, S., Dillman, A., Trabzuni, D., Gibbs, J.R., Ryten, M., Arepalli, S., Weale, M.E., et al. (2012). Integration of GWAS SNPs and tissue specific expression profiling reveal discrete eQTLs for human traits in blood and brain. *Neurobiol Dis* 47, 20-28.

Higley, M.J., and Sabatini, B.L. (2010). Competitive regulation of synaptic Ca²⁺ influx by D2 dopamine and A2A adenosine receptors. *Nature neuroscience* 13, 958-966.

Hodges, A., Strand, A.D., Aragaki, A.K., Kuhn, A., Sengstag, T., Hughes, G., Elliston, L.A., Hartog, C., Goldstein, D.R., Thu, D., et al. (2006). Regional and cellular gene expression changes in human Huntington's disease brain. *Hum Mol Genet* 15, 965-977.

Horvath, S., and Dong, J. (2008). Geometric interpretation of gene coexpression network analysis. *PLoS Comput Biol* 4, e1000117.

Irizarry, R.A., Hobbs, B., Collin, F., Beazer-Barclay, Y.D., Antonellis, K.J., Scherf, U., and Speed, T.P. (2003). Exploration, normalization, and summaries of highdensity oligonucleotide array probe level data. *Biostatistics* 4, 249-264.

Isomura, Y., Takekawa, T., Harukuni, R., Handa, T., Aizawa, H., Takada, M., and Fukai, T. (2013). Reward modulated motor information in identified striatum neurons. *The Journal of neuroscience: the official journal of the Society for Neuroscience* 33, 10209-10220.

Jin, X., Tecuapetla, F., and Costa, R.M. (2014). Basal ganglia subcircuits distinctively encode the parsing and concatenation of action sequences. *Nature neuroscience* 17, 423-430.

Johnson, W.E., Li, C., and Rabinovic, A. (2007). Adjusting batch effects in microarray expression data using empirical Bayes methods. *Biostatistics* 8, 118-127.

Kang, H.J., Kawasawa, Y.I., Cheng, F., Zhu, Y., Xu, X., Li, M., Sousa, A.M., Pletikos, M., Meyer, K.A., Sedmak, G., et al. (2011). Spatio-temporal transcriptome of the human brain. *Nature* 478, 483-489.

- Kelley, K.W., Nakao-Inoue, H., Molofsky, A.V., and Oldham, M.C. (2018). Variation among intact tissue samples reveals the core transcriptional features of human CNS cell classes. *Nature neuroscience* 21, 1171-1184.
- Klaus, A., Martins, G.J., Paixao, V.B., Zhou, P., Paninski, L., and Costa, R.M. (2017). The Spatiotemporal Organization of the Striatum Encodes Action Space. *Neuron* 96, 949.
- Kozorovitskiy, Y., Saunders, A., Johnson, C.A., Lowell, B.B., and Sabatini, B.L. (2012). Recurrent network activity drives striatal synaptogenesis. *Nature* 485, 646-650.
- Kravitz, A.V., Freeze, B.S., Parker, P.R., Kay, K., Thwin, M.T., Deisseroth, K., and Kreitzer, A.C. (2010). Regulation of parkinsonian motor behaviours by optogenetic control of basal ganglia circuitry. *Nature* 466, 622-626.
- Kravitz, A.V., Owen, S.F., and Kreitzer, A.C. (2013). Optogenetic identification of striatal projection neuron subtypes during in vivo recordings. *Brain research* 1511, 21-32.
- Kreitzer, A.C., and Malenka, R.C. (2007). Endocannabinoid-mediated rescue of striatal LTD and motor deficits in Parkinson's disease models. *Nature* 445, 643-647.
- Kumar, R., Lozano, A.M., Kim, Y.J., Hutchison, W.D., Sime, E., Halket, E., and Lang, A.E. (1998). Doubleblind evaluation of subthalamic nucleus deep brain stimulation in advanced Parkinson's disease. *Neurology* 51, 850-855.
- Langfelder, P., and Horvath, S. (2008). WGCNA: an R package for weighted correlation network analysis. *BMC Bioinformatics* 9, 559.
- Lee, H.Y., Nakayama, J., Xu, Y., Fan, X., Karouani, M., Shen, Y., Pothos, E.N., Hess, E.J., Fu, Y.H., Edwards, R.H., et al. (2012). Dopamine dysregulation in a mouse model of paroxysmal nonkinesigenic dyskinesia. *J Clin Invest* 122, 507-518.
- Lee, H.Y., Xu, Y., Huang, Y., Ahn, A.H., Auburger, G.W., Pandolfo, M., Kwiecinski, H., Grimes, D.A., Lang, A.E., Nielsen, J.E., et al. (2004). The gene for paroxysmal non-kinesigenic dyskinesia encodes an enzyme in a stress response pathway. *Hum Mol Genet* 13, 3161-3170.
- Lerner, T.N., Horne, E.A., Stella, N., and Kreitzer, A.C. (2010). Endocannabinoid signaling mediates psychomotor activation by adenosine A2A antagonists. *The Journal of neuroscience: the official journal of the Society for Neuroscience* 30, 2160-2164.
- Lerner, T.N., and Kreitzer, A.C. (2012). RGS4 is required for dopaminergic control of striatal LTD and susceptibility to parkinsonian motor deficits. *Neuron* 73, 347-359.
- Levy, R., Dostrovsky, J.O., Lang, A.E., Sime, E., Hutchison, W.D., and Lozano, A.M. (2001). Effects of apomorphine on subthalamic nucleus and globus pallidus internus neurons in patients with Parkinson's disease. *Journal of neurophysiology* 86, 249-260.

Li, J.Z., Bunney, B.G., Meng, F., Hagenauer, M.H., Walsh, D.M., Vawter, M.P., Evans, S.J., Choudary, P.V., Cartagena, P., Barchas, J.D., et al. (2013). Circadian patterns of gene expression in the human brain and disruption in major depressive disorder. *PNAS* 110, 9950-9955.

Liang, L., DeLong, M.R., and Papa, S.M. (2008). Inversion of dopamine responses in striatal medium spiny neurons and involuntary movements. *The Journal of neuroscience: the official journal of the Society for Neuroscience* 28, 7537-7547.

Liang, S., Yu, X., Zhang, S., and Tai, J. (2015). A case of familial paroxysmal nonkinesigenic dyskinesia due to mutation of the PNKD gene in Chinese Mainland. *Brain research* 1595, 120-126.

Lovinger, D.M., and Alvarez, V.A. (2017). Alcohol and basal ganglia circuitry: Animal models. *Neuropharmacology* 122, 46-55.

Lozano, A.M., Lang, A.E., Levy, R., Hutchison, W., and Dostrovsky, J. (2000). Neuronal recordings in Parkinson's disease patients with dyskinesias induced by apomorphine. *Annals of neurology* 47, S141-146.

Lui, J.H., Nowakowski, T.J., Pollen, A.A., Javaherian, A., Kriegstein, A.R., and Oldham, M.C. (2014). Radial glia require PDGFD-PDGFRbeta signalling in human but not mouse neocortex. *Nature* 515, 264-268.

Markowitz, J.E., Gillis, W.F., Beron, C.C., Neufeld, S.Q., Robertson, K., Bhagat, N.D., Peterson, R.E., Peterson, E., Hyun, M., Linderman, S.W., et al. (2018). The Striatum Organizes 3D Behavior via Moment to-Moment Action Selection. *Cell* 174, 44-58 e17.

Martella, G., Tassone, A., Sciamanna, G., Platania, P., Cuomo, D., Viscomi, M.T., Bonsi, P., Cacci, E., Biagioni, S., Usiello, A., et al. (2009). Impairment of bidirectional synaptic plasticity in the striatum of a mouse model of DYT1 dystonia: role of endogenous acetylcholine. *Brain: a journal of neurology* 132,2336-2349.

Mencacci, N.E., Kamsteeg, E.J., Nakashima, K., R'Bibo, L., Lynch, D.S., Balint, B., Willemsen, M.A., Adams, M.E., Wiethoff, S., Suzuki, K., et al. (2016). De Novo Mutations in PDE10A Cause Childhood-Onset Chorea with Bilateral Striatal Lesions. *Am J Hum Genet* 98, 763-771.

Mereu, G., Fadda, F., and Gessa, G.L. (1984). Ethanol stimulates the firing rate of nigral dopaminergic neurons in unanesthetized rats. *Brain research* 292, 63-69.

Mink, J.W. (1996). The basal ganglia: focused selection and inhibition of competing motor programs. *Progress in neurobiology* 50, 381-425.

Molofsky, A.V., Glasgow, S.M., Chaboub, L.S., Tsai, H.H., Murnen, A.T., Kelley, K.W., Fancy, S.P., Yuen, T.J., Madireddy, L., Baranzini, S., et al. (2013). Expression profiling of

Aldh1l1-precursors in the developing spinal cord reveals glial lineage-specific genes and direct Sox9-Nfe2l1 interactions. *Glia* 61, 1518-1532.

Narushima, M., Hashimoto, K., and Kano, M. (2006). Endocannabinoid-mediated short term suppression of excitatory synaptic transmission to medium spiny neurons in the striatum. *Neuroscience research* 54,159-164.

Oldenburg, I.A., and Sabatini, B.L. (2015). Antagonistic but Not Symmetric Regulation of Primary Motor Cortex by Basal Ganglia Direct and Indirect Pathways. *Neuron* 86, 1174-1181.

Oldham, M.C., Konopka, G., Iwamoto, K., Langfelder, P., Kato, T., Horvath, S., and Geschwind, D.H. (2008). Functional organization of the transcriptome in human brain. *Nat Neurosci* 11, 1271-1282.

Oldham, M.C., Langfelder, P., and Horvath, S. (2012). Network methods for describing sample relationships in genomic datasets: application to Huntington's disease. *BMC Syst Biol* 6, 63.

Papa, S.M., Desimone, R., Fiorani, M., and Oldfield, E.H. (1999). Internal globus pallidus discharge is nearly suppressed during levodopa-induced dyskinesias. *Annals of neurology* 46, 732-738.

Parker, J.G., Marshall, J.D., Ahanonu, B., Wu, Y.W., Kim, T.H., Grewe, B.F., Zhang, Y., Li, J.Z., Ding, J.B., Ehlers, M.D., et al. (2018). Diametric neural ensemble dynamics in parkinsonian and dyskinetic states. *Nature* 557, 177-182.

Pava, M.J., and Woodward, J.J. (2012). A review of the interactions between alcohol and the endocannabinoid system: implications for alcohol dependence and future directions for research. *Alcohol* 46, 185-204.

Perez, X.A., Zhang, D., Bordia, T., and Quik, M. (2017). Striatal D1 medium spiny neuron activation induces dyskinesias in parkinsonian mice. *Movement disorders: official journal of the Movement Disorder Society*.

Picconi, B., Centonze, D., Hakansson, K., Bernardi, G., Greengard, P., Fisone, G., Cenci, M.A., and Calabresi, P. (2003). Loss of bidirectional striatal synaptic plasticity in L-DOPA-induced dyskinesia. *Nature neuroscience* 6, 501-506.

Picconi, B., Passino, E., Sgobio, C., Bonsi, P., Barone, I., Ghiglieri, V., Pisani, A., Bernardi, G., Ammassari-Teule, M., and Calabresi, P. (2006). Plastic and behavioral abnormalities in experimental Huntington's disease: a crucial role for cholinergic interneurons. *Neurobiology of disease* 22, 143-152.

Planert, H., Berger, T.K., and Silberberg, G. (2013). Membrane properties of striatal direct and indirect pathway neurons in mouse and rat slices and their modulation by dopamine. *PloS one* 8, e57054.

Rainier, S., Thomas, D., Tokarz, D., Ming, L., Bui, M., Plein, E., Zhao, X., Lemons, R., Albin, R., Delaney, C., et al. (2004). Myofibrillogenesis regulator 1 gene mutations cause paroxysmal dystonic choreoathetosis. *Archives of neurology* 61, 1025-1029.

Ramasamy, A., Trabzuni, D., Guelfi, S., Varghese, V., Smith, C., Walker, R., De, T., Coin, L., de Silva, R., Cookson, M.R., et al. (2014a). Genetic variability in the regulation of gene expression in ten regions of the human brain. *Nat Neurosci* 17, 1418-1428.

Ramasamy, A., Trabzuni, D., Guelfi, S., Varghese, V., Smith, C., Walker, R., De, T., Consortium, U.K.B.E., North American Brain Expression, C., Coin, L., et al. (2014b). Genetic variability in the regulation of gene expression in ten regions of the human brain. *Nature neuroscience* 17, 1418-1428.

Reiner, A., Albin, R.L., Anderson, K.D., D'Amato, C.J., Penney, J.B., and Young, A.B. (1988). Differential loss of striatal projection neurons in Huntington disease. *Proc Natl Acad Sci U S A* 85, 5733-5737.

Roseberry, T.K., Lee, A.M., Lalive, A.L., Wilbrecht, L., Bonci, A., and Kreitzer, A.C. (2016). Cell-Type-Specific Control of Brainstem Locomotor Circuits by Basal Ganglia. *Cell* 164, 526-537.

Rosin, D.L., Robeva, A., Woodard, R.L., Guyenet, P.G., and Linden, J. (1998). Immunohistochemical localization of adenosine A2A receptors in the rat central nervous system. *The Journal of comparative neurology* 401, 163-186.

Ruby, C.L., Adams, C.A., Knight, E.J., Nam, H.W., and Choi, D.S. (2010). An essential role for adenosine signaling in alcohol abuse. *Curr Drug Abuse Rev* 3, 163-174.

Ryan, M.B., Bair-Marshall, C., and Nelson, A.B. (2018). Aberrant Striatal Activity in Parkinsonism and Levodopa-Induced Dyskinesia. *Cell Rep* 23, 3438-3446 e3435.

Schiffmann, S.N., Jacobs, O., and Vanderhaeghen, J.J. (1991). Striatal restricted adenosine A2 receptor (RDC8) is expressed by enkephalin but not by substance P neurons: an in situ hybridization histochemistry study. *J Neurochem* 57, 1062-1067.

Schrock, L.E., Ostrem, J.L., Turner, R.S., Shimamoto, S.A., and Starr, P.A. (2009). The subthalamic nucleus in primary dystonia: single-unit discharge characteristics. *Journal of neurophysiology* 102, 3740-3752.

Shen, W., Flajolet, M., Greengard, P., and Surmeier, D.J. (2008). Dichotomous dopaminergic control of striatal synaptic plasticity. *Science* 321, 848-851.

Shen, Y., Ge, W.P., Li, Y., Hirano, A., Lee, H.Y., Rohlmann, A., Missler, M., Tsien, R.W., Jan, L.Y., Fu, Y.H., et al. (2015). Protein mutated in paroxysmal dyskinesia interacts with the active zone protein RIM and suppresses synaptic vesicle exocytosis. *Proc Natl Acad Sci U S A* 112, 2935-2941.

Shen, Y., Lee, H.Y., Rawson, J., Ojha, S., Babbitt, P., Fu, Y.H., and Ptacek, L.J. (2011). Mutations in PNKD causing paroxysmal dyskinesia alters protein cleavage and stability. *Hum Mol Genet* 20, 2322-2332.

Shuen, J.A., Chen, M., Gloss, B., and Calakos, N. (2008). *Drd1a*-tdTomato BAC transgenic mice for simultaneous visualization of medium spiny neurons in the direct and indirect pathways of the basal ganglia. *The Journal of neuroscience: the official journal of the Society for Neuroscience* 28, 2681-2685.

Singh, A., Liang, L., Kaneoke, Y., Cao, X., and Papa, S.M. (2015). Dopamine regulates distinctively the activity patterns of striatal output neurons in advanced parkinsonian primates. *Journal of neurophysiology* 113, 1533-1544.

Skene, N.G., Bryois, J., Bakken, T.E., Breen, G., Crowley, J.J., Gaspar, H.A., Giusti-Rodriguez, P., Hodge, R.D., Miller, J.A., Munoz-Manchado, A.B., et al. (2018). Genetic identification of brain cell types underlying schizophrenia. *Nat Genet* 50, 825-833.

Skene, N.G., and Grant, S.G. (2016). Identification of Vulnerable Cell Types in Major Brain Disorders Using Single Cell Transcriptomes and Expression Weighted Cell Type Enrichment. *Front Neurosci* 10, 16.

Smith, Y., Bevan, M.D., Shink, E., and Bolam, J.P. (1998). Microcircuitry of the direct and indirect pathways of the basal ganglia. *Neuroscience* 86, 353-387.

Song, L., Langfelder, P., and Horvath, S. (2012). Comparison of co-expression measures: mutual information, correlation, and model based indices. *BMC Bioinformatics* 13, 328.

Stachniak, T.J., Ghosh, A., and Sternson, S.M. (2014). Chemogenetic synaptic silencing of neural circuits localizes a hypothalamus-->midbrain pathway for feeding behavior. *Neuron* 82, 797-808.

Swann, N.C., de Hemptinne, C., Miocinovic, S., Qasim, S., Wang, S.S., Ziman, N., Ostrem, J.L., San Luciano, M., Galifianakis, N.B., and Starr, P.A. (2016). Gamma Oscillations in the Hyperkinetic State Detected with Chronic Human Brain Recordings in Parkinson's Disease. *The Journal of neuroscience: the official journal of the Society for Neuroscience* 36, 6445-6458.

Taverna, S., Ilijic, E., and Surmeier, D.J. (2008). Recurrent collateral connections of striatal medium spiny neurons are disrupted in models of Parkinson's disease. *The Journal of neuroscience: the official journal of the Society for Neuroscience* 28, 5504-5512.

Tecuapetla, F., Jin, X., Lima, S.Q., and Costa, R.M. (2016). Complementary Contributions of Striatal Projection Pathways to Action Initiation and Execution. *Cell* 166, 703-715.

Tecuapetla, F., Matias, S., Dugue, G.P., Mainen, Z.F., and Costa, R.M. (2014). Balanced activity in basal ganglia projection pathways is critical for contraversive movements. *Nature communications* 5, 4315.

Vidailhet, M., Vercueil, L., Houeto, J.L., Krystkowiak, P., Benabid, A.L., Cornu, P., Lagrange, C., Tezenas du Montcel, S., Dormont, D., Grand, S., et al. (2005). Bilateral deep-brain stimulation of the globus pallidus in primary generalized dystonia. *The New England journal of medicine* 352, 459-467.

Wei, W., Ding, S., and Zhou, F.M. (2017). Dopaminergic treatment weakens medium spiny neuron collateral inhibition in the parkinsonian striatum. *Journal of neurophysiology* 117, 987-999.

Weiner, D.M., Levey, A.I., Sunahara, R.K., Niznik, H.B., O'Dowd, B.F., Seeman, P., and Brann, M.R. (1991). D1 and D2 dopamine receptor mRNA in rat brain. *Proceedings of the National Academy of Sciences of the United States of America* 88, 1859-1863.

Yim, H.J., Schallert, T., Randall, P.K., and Gonzales, R.A. (1998). Comparison of local and systemic ethanol effects on extracellular dopamine concentration in rat nucleus accumbens by microdialysis. *Alcohol Clin Exp Res* 22, 367-374.

Zhang, J., Finney, R.P., Clifford, R.J., Derr, L.K., and Buetow, K.H. (2005). Detecting false expression signals in high-density oligonucleotide arrays by an in silico approach. *Genomics* 85, 297-308.

Zhang, Y., Chen, K., Sloan, S.A., Bennett, M.L., Scholze, A.R., O'Keefe, S., Phatnani, H.P., Guarnieri, P., Caneda, C., Ruderisch, N., et al. (2014). An RNA-sequencing transcriptome and splicing database of glia, neurons, and vascular cells of the cerebral cortex. *J Neurosci* 34, 11929-11947.

CHAPTER 3

A subset of striatal neurons mediates levodopa-induced dyskinesia

3.1 Abstract

Parkinson's disease is characterized by the progressive loss of midbrain dopamine neurons. Dopamine replacement therapy with levodopa alleviates parkinsonian motor symptoms, but is complicated by the development of involuntary movements, termed levodopa-induced dyskinesia (LID). Aberrant activity in the striatum has been hypothesized to cause LID. Here, to establish a direct link between striatal activity and dyskinesia, we combine optogenetics and a method to manipulate dyskinesia-associated neurons, Targeted Recombination in Active Populations (TRAP). We find that TRAPed cells are a stable subset of sensorimotor striatal neurons, predominantly from the direct pathway, and that reactivation of TRAPed striatal neurons causes dyskinesia in the absence of levodopa. Inhibition of TRAPed cells, but not a nonspecific subset of direct pathway neurons, ameliorates LID. These results establish that a distinct subset of striatal neurons is causally involved in LID and indicate that successful therapeutic strategies for treating LID may require targeting functionally-selective neuronal subtypes.

3.2 Introduction

In Parkinson's disease (PD), degeneration of midbrain dopamine neurons leads to slowing of movement (bradykinesia), rigidity, and tremor. Levodopa, the gold standard dopamine replacement therapy, alleviates motor symptoms for many years, but eventually triggers abnormal involuntary movements, termed levodopa-induced dyskinesia (LID). Pharmacological treatment for LID is limited. Development of new therapies has been hampered by limited understanding of the relationship of specific brain areas and cell types to dyskinesia.

LID-associated aberrant activity has been observed in several brain regions, but which area and/or cell types cause dyskinesia is unknown. One hypothesis is that by increasing dopamine release, levodopa evokes abnormal activity in the striatum, the primary input nucleus of the basal ganglia, and a major target of midbrain dopaminergic neurons. Compelling pharmacological, biochemical, and electrophysiological data from rodent and nonhuman primate models of LID indirectly support this hypothesis: local striatal infusion of levodopa triggers dyskinesia in parkinsonian rats (Buck et al., 2010), striatal firing rate and pattern change markedly in parkinsonian monkeys with LID (Liang et al., 2008; Singh et al., 2015), and biochemical changes are seen in parkinsonian rodents treated with levodopa. Immediate early genes (IEGs) such as c-Fos, FosB, and Δ FosB are consistently upregulated in the striatum of animals with LID (Jenner, 2008). However, other brain regions have also been implicated, including primary motor cortex (M1) (Halje et al., 2012; Lindenbach and Bishop, 2013; Swann et al., 2016) and primary somatosensory cortex (S1) (Alam et al., 2017). Interconnections between these brain

regions add uncertainty regarding the origin of aberrant activity and heighten the need to look brain-wide to find the specific cell types and patterns of activity that cause LID.

Striatal IEG expression correlates with dyskinesia severity in parkinsonian primates (Berton et al., 2009), but these findings do not indicate whether striatal activation is causal. To investigate which brain regions and cell types cause LID, we used a transgenic mouse tool, Targeted Recombination in Active Populations (TRAP) (Guenther et al., 2013), in combination with a well-established mouse model of LID (Cenci and Lundblad, 2007). Based on Fos-driven CreER, TRAP allows identification and subsequent manipulation of activated neurons, captured during a time window defined by tamoxifen administration. Using TRAP, we find LID-associated neurons in several brain regions, including M1, S1, and striatum. Optical reactivation of LID-associated *striatal* neurons, but not LID-associated neurons in other brain regions, triggered dyskinesia in the absence of levodopa. Furthermore, inhibiting striatal LID-associated neurons, but not nonspecifically labeled neurons in the same region, reduced dyskinesia, indicating that a distinct subpopulation of striatal neurons mediates LID.

3.3 Results

Targeted recombination in active populations (TRAP) captures levodopa-induced dyskinesia (LID)-associated neurons

We first validated the mouse model of LID in wild-type (WT) mice, examining behavior and IEG expression (Figure S1A). To control for the effects of parkinsonism and levodopa treatment itself, we divided mice (N=34) into four experimental groups, based on parkinsonian state (unilateral intrastriatal injection of saline or the neurotoxin 6-OHDA, the latter to deplete dopamine neurons, Figure S1B) and systemic treatment (daily intraperitoneal saline or levodopa/benserazide). During behavioral sessions, a blinded experimenter measured open field locomotor behavior (drug-induced rotations) or scored dyskinesia in response to saline or levodopa injection. While parkinsonian animals rotate ipsilateral to the dopamine depleted side, levodopa evokes contralateral rotations (6-OHDA/levodopa group, Figure S1E). Dyskinesia was quantified using a validated rating scale for abnormal involuntary movements (AIMs) (Cenci and Lundblad, 2007). Nonparkinsonian animals treated with systemic saline (saline/saline, N=6) or levodopa (saline/levodopa, N=6) did not develop dyskinesia (Figure S1C). Similarly, parkinsonian animals treated with systemic saline (6-OHDA/saline, N=6) did not develop dyskinesia (Figure S1C). However, parkinsonian mice receiving levodopa (6-OHDA/levodopa, N=16) developed dyskinesia, peaking 20-40 minutes after injection (Figure S1C). LID was reliably evoked over 3 weeks of treatment (Figure S1D). To evaluate IEG expression in LID, we sacrificed animals 2 hours after saline or levodopa injection and immunostained for c-Fos (Figure S1F-I). As expected, c-Fos positive nuclei were markedly increased in the sensorimotor, or dorsolateral striatum (DLS) of 6-OHDA/levodopa-treated mice

(Figure S1I). However, striatal expression of c-Fos was not increased in other groups (Figure S1J), consistent with other studies employing intrastriatal dopamine depletion (Pavon et al., 2006).

We repeated these experiments in FosTRAP ($Fos^{CreER/+}R26^{Ai14/+}$) mice (N=39), again in four experimental groups based on intrastriatal injection (Figure 1A) and systemic treatment (Figure 1B). Postmortem staining for tyrosine hydroxylase (TH) was used to confirm dopamine depletion (Figure 1C). As in WT mice, FosTRAP mice treated with 6-OHDA and levodopa (N=11) showed contralateral rotations (Figure 1F) and dyskinesia (Figure 1D-E,G), while the three control groups did not (N=10 saline/saline, N=9 saline/levodopa, and N=9 6-OHDA/saline mice). We then used FosTRAP to capture neurons activated during LID by administering the short-acting tamoxifen metabolite, 4-hydroxytamoxifen (4-OHT), during a single levodopa or saline treatment session. In FosTRAP mice, the pairing of 4-OHT and a behavioral state which activates c-Fos, such as dyskinesia, leads to Cre-dependent expression of tdTomato (Guenthner et al., 2013). We captured activated cells one week into daily saline or levodopa treatment (Figure 1B) and sacrificed animals two weeks later to quantify tdTomato expression (henceforth called "TRAPed cells") brain-wide (Figure 1H). We focused on three candidate brain areas: the striatum, primary somatosensory cortex (S1), and primary motor cortex (M1). TRAPed cells were found in each region (Figure S1K), but differed in abundance. As with c-Fos immunostaining, we found a marked increase in TRAPed cells in the DLS of 6OHDA/levodopa-treated mice (Figure 1H, right panel). The density and number of TRAPed cells was increased in the striatum of these mice as compared to the three control groups (Figure 1I, S1L, $p < 0.01$, N=10 animals). TRAPed cells were also observed

in S1 and M1, but were not significantly enriched in 6-OHDA/levodopa treated mice over control groups (Figure 1I, S1L, N=10 animals each). These results are consistent with previous studies showing strong striatal IEG activation in rodents with LID (Jenner, 2008).

As FosTRAP requires time for Cre-dependent fluorophore expression, and c-Fos labeling reflects activation just prior to sacrifice, it is not possible to confirm whether FosTRAP and c-Fos label the same cells in a given levodopa session. However, we examined whether FosTRAP and c-Fos capture a similar group of cells across two sessions by c-Fos immunostaining tissue from FosTRAP mice administered levodopa 2 hours prior to sacrifice. TRAPed and c-Fos positive cells reflect activation of cells from levodopa sessions 2-3 weeks prior and just prior to perfusion, respectively. Remarkably, we saw extensive overlap between striatal TRAPed and c-Fos-positive cells (Figure 1J-L, $98.1\% \pm 0.4$, N=7 animals). As individual IEGs differ in their pattern of activation, we also examined the expression of two other LID-associated IEGs, Δ FosB and Erg-1, in TRAPed cells (Figure S1M,O). As with c-Fos, we saw extensive overlap between TRAPed cells and these cellular markers (Figure S1N,P, Δ FosB, $83.3\% \pm 1.9$, Erg-1, $83.4\% \pm 1.7$, N=3 animals each). Together, these results suggested that TRAP and IEGs capture overlapping populations of neurons, but further, that LID-associated striatal cells represent a consistent, nonrandom population session to session (Figure S1Q).

TRAPed cells are primarily direct pathway medium spiny neurons

We next investigated which striatal cell types were TRAPed during LID, using confocal imaging to quantify colocalization of tdTomato and neuronal markers in postmortem tissue from 6-OHDA/levodopa-treated mice. Not surprisingly, we found that

99.0 ± 0.10% of activated cells were neurons, by colocalization with the marker NeuN (Figure 2A,G, N=4 animals). Next, we focused on whether TRAPed cells were striatal projection neurons (medium spiny neurons, MSNs), cholinergic interneurons, or GABAergic interneurons. We hypothesized that levodopa-evoked striatal dopamine release activates neurons via “excitatory” D1-like receptors (Surmeier et al., 2011), which are expressed on a subset of MSNs and parvalbumin (PV)-positive GABAergic interneurons. Other cell types express “inhibitory” D2-like receptors and would be less likely to be activated by levodopa. Cholinergic interneurons express both D5 (Bergson et al., 1995) and D2 receptors, so it was difficult to predict whether they would be activated by levodopa. Immunohistochemistry for the markers of major striatal cell types revealed that none of the TRAPed cells expressed choline acetyltransferase (ChAT, Figure 2B,G, N=3 animals), 1.0 ± 1.0% expressed Neuropeptide Y (NPY, Figure 2C,G, N=3 animals), and 5.0 ± 2.0% expressed PV (Figure 2D,G, N=3 animals). From these results, we reasoned that most TRAPed cells are MSNs. To confirm this hypothesis, we examined colocalization of the MSN marker DARPP-32 (dopamine- and cAMP-regulated phosphoprotein Mr~32,000) (Figure 2E, N=4 animals). 93.0 ± 2.0% of all TRAPed cells were DARPP-32 positive (Figure 2G), confirming the vast majority of TRAPed neurons are MSNs.

Based on their expression of D1 receptors (Gerfen et al., 1990), many have hypothesized that in parkinsonian animals, levodopa treatment leads to increased activity of D1-bearing direct pathway MSNs (dMSNs), and excessive activity in the case of dyskinesia. Physiological recordings in downstream basal ganglia nuclei are consistent with, but cannot directly confirm this hypothesis (Boraud et al., 2001; Fillion et al., 1991;

Levy et al., 2001; Lozano et al., 2000; Papa et al., 1999). It is unclear how D2-bearing indirect pathway MSNs (iMSNs) are involved. To determine whether activated neurons are dMSNs, we repeated similar experiments in two additional cohorts of mice: FosTRAP;Ai14;D2-GFP mice, in which GFP is expressed in iMSNs, and in *Drd1a*-tdTomato mice, in which tdTomato is expressed in dMSNs. In the former cohort, we found that $10.4 \pm 0.1\%$ of TRAPed neurons were D2-GFP positive (Figure 2F-G, N=3 animals), and only $3.7 \pm 0.5\%$ of c-Fos positive neurons were D2-GFP positive (Figure S2F,H), suggesting the majority of TRAPed cells are dMSNs. We further corroborated this hypothesis in the second cohort, by colocalization of D1-tdTomato with c-Fos (Figure S2A-B, N=18 animals). As in previous experiments, 6-OHDA/levodopa-treated *Drd1a*-tdTomato mice showed drug-induced rotations and dyskinesia (Figure S2C-E). In postmortem tissue from levodopa-treated parkinsonian animals, approximately $70.0\% \pm 4.0$ of c-Fos positive nuclei showed colocalization with the dMSN reporter (Figure S2F-G, N=5 animals). Though all dMSNs express D1 receptors, only a subset may be activated by a dopaminergic manipulation. Differential synaptic inputs or sensitivity to dopamine may lead to heterogeneity amongst dMSN responses. We found that only $20.0 \pm 2.0\%$ of all striatal neurons were TRAPed. Indeed, even amongst dMSNs, only $53.0 \pm 4.0\%$ show c-Fos expression (Figure S2G). Together with our earlier results, these findings suggest that LID recruits a stable subset of predominantly striatal dMSNs.

Optogenetic reactivation of TRAPed striatal cells, but not TRAPed S1 or M1 cortical cells, causes dyskinesia in the absence of levodopa

TRAPed striatal neurons may be the cause or the effect of dyskinesia, or they may be activated by levodopa, but be unrelated to dyskinesia. To investigate the relationship between TRAPed cells and dyskinesia, we asked whether the number or density of activated neurons correlated with dyskinesia severity across animals (Figure 3A, S3A). The density and number of TRAPed cells strongly correlated with AIM score in the striatum, more than in S1 and M1 (Figure 3B, S3B; N=10 animals per area), consistent with, but not proving, the hypothesis that TRAPed cells cause dyskinesia.

We next wondered how levodopa altered the firing rate of TRAPed striatal neurons, hypothesizing that levodopa increases the firing rate of TRAPed neurons. To confirm and further characterize this change in firing rate of TRAPed neurons, we performed optrode recordings in freely moving mice. We expressed Cre-dependent Channelrhodopsin (ChR2) in the DLS of dopamine-depleted FosTRAP mice, who were subsequently implanted with fixed 32-channel optrode arrays (Figure 3C). Animals developed levodopa-evoked contralateral rotations and dyskinesia as in other cohorts of FosTRAP mice (data not shown), and single-unit recordings commenced 1-2 weeks following 4-OHT administration, to allow for ChR2 expression. During each session, we recorded striatal activity before and after levodopa administration, and at the end of the session, delivered a series of blue light pulses to determine if the unit expressed ChR2 (and thus was TRAPed) (Kravitz et al., 2013). Those units with short-latency responses to blue light pulses (Figure 3D) were classified as optically-identified TRAPed neurons. As expected, we found that all optically labeled TRAPed putative MSNs showed a significant levodopa-evoked increase in firing rate (Figure 3E, baseline: 0.27 ± 0.1 spikes/sec, levodopa: 4.51 ± 1.3 spikes/sec, n=8 cells, N=4 animals). These results suggest that the majority of

TRAPed neurons are positively modulated by dopamine, and that increased activity of such neurons parallels dyskinesia following levodopa administration.

Given both the increase in TRAPed striatal neuron firing rate during dyskinesia and the correlation between the number of TRAPed striatal neurons and dyskinesia severity, we next wanted to determine whether reactivating LID-associated neuronal ensembles in the striatum, *in the absence of levodopa*, causes dyskinesia. As in previous experiments, we expressed ChR2 or eYFP in the DLS of FosTRAP mice and implanted optical fibers (Figure 3F, S3D). Animals showed levodopa-evoked contralateral rotations and dyskinesia over 3 weeks of levodopa treatment as in previous cohorts (data not shown). ChR2-eYFP expression in TRAPed cells was confirmed by postmortem histology (Figure 3F, S3E) and current clamp recordings showing light-evoked spiking (Figure S3F). After 4-OHT administration and Cre-dependent opsin expression, two blinded raters scored behavior during optical stimulation (1 mW blue light). Based on optrode recordings, we found that 30 second, 1 mW light stimulation transiently evoked firing rates of 3.9 ± 1.6 spikes/sec (Figure S3C) in TRAPed striatal neurons, similar to peak firing rates in TRAPed striatal neurons in response to levodopa (Figure 3E). In FosTRAP-ChR2 mice, blue light qualitatively reproduced the motor effects of levodopa, including contralateral rotations and dyskinesia (Figure 3G left; S3G and Movie S1). While in FosTRAP-eYFP animals, light did not evoke dyskinesia (N=14 mice; p=1.0), in FosTRAP-ChR2 mice, light increased dyskinesia (N=14 mice; p=0.001). The light-evoked change in both dyskinesia and rotations was larger in FosTRAP-ChR2 mice than in eYFP animals (3G middle: p=0.0002; 3G right: p=0.01). These results suggest that reactivation of striatal LID-associated neurons is sufficient to cause dyskinesia in the absence of levodopa.

In contrast, we found that reactivation of TRAPed neurons in other LID-associated brain regions, S1 and M1, did not evoke dyskinesia. Using a similar approach, we expressed ChR2 or eYFP in S1 or M1 TRAPed cortical cells (Figure 3H,J, S3H,I,L,M), which showed light-evoked spiking (Figure S3J,N). We then administered, in separate sessions, either continuous or pulsatile (10 Hz) blue light, to activate S1 or M1 TRAPed neurons (p values for each condition are noted). In FosTRAP-ChR2 mice (N=10), optical stimulation in S1, with continuous or pulsatile blue light, failed to increase rotational behavior (Figure 3I right; $p=0.77$ and 0.89 , respectively) or dyskinesia (Figure 3I, left; $p=0.25$ and 0.31 , respectively). In FosTRAP-eYFP mice (N=8), S1 light also failed to change rotations ($p=0.52$ and 0.91 , respectively) or dyskinesia ($p=0.25$ and 0.25 , respectively). There were also no differences noted in the light-evoked rotations in FosTRAP-ChR2 and eYFP cohorts ($p=0.81$ and 0.11), nor in light-evoked changes in dyskinesia (Figure 3I, middle; S3K; $p=0.86$ and 0.83).

Optical stimulation of M1, with continuous or 10 Hz pulsatile stimulation, also failed to evoke rotations (Figure 3K, right; $p=0.89$ and $p=0.96$, respectively) or dyskinesia (Figure 3K, left; S3O; $p=1.0$ and $p=1.0$, respectively) in FosTRAP-ChR2 mice (N=6). As predicted, in M1 FosTRAP-eYFP mice (N=5), light administration also did not evoke changes in rotations ($p=0.55$ and $p=0.65$) or dyskinesia ($p=0.5$ and $p=0.25$). Finally, there were no differences in the light-evoked change in rotations ($p=0.34$ and $p=0.53$, respectively) or dyskinesia between the M1 ChR2 and eYFP groups ($p=0.85$ and $p=0.12$, respectively). We did, however, see a significant increase in velocity and total distance traveled with M1 activation (baseline distance eYFP: 462.3 ± 130.0 cm, baseline distance ChR2: 679.2 ± 236.8 cm, light on epochs distance eYFP: 450.5 ± 116.6 cm, light on

epochs distance ChR2: 846.7 ± 257.2 cm, $p=0.009$, baseline velocity eYFP: 3.7 ± 1.1 cm, baseline velocity ChR2: 5.5 ± 1.9 cm, light on epochs velocity eYFP: 3.6 ± 0.9 cm, light on epochs velocity ChR2: 6.9 ± 2.1 cm, $p=0.009$), as would be expected for stimulation of motor cortex. These results confirmed that reactivation of TRAPed striatal cells, but not S1 or M1 cortical cells, is sufficient for dyskinesia in the absence of levodopa.

Optogenetic inhibition of TRAPed striatal neurons, but not nonspecific direct pathway neurons, ameliorates LID

Dyskinesia triggered by optical reactivation of striatal TRAPed cells suggests they may be sufficient for dyskinesia, but does not definitively show that these neurons cause LID under normal conditions. To test whether the activity of TRAPed striatal neurons is required for LID, we expressed the inhibitory opsin eNpHR3.0 or eYFP (Figure 4A, S4A) in the DLS of parkinsonian FosTRAP mice treated with daily levodopa. We confirmed eNpHR3.0 expression with postmortem histology (Figure 4A, S4B) and slice physiology showing light-evoked inhibition of spiking (Figure S4C). To determine whether inhibition of TRAPed neurons reduces LID, green light was delivered during peak LID. In neither eNpHR3.0-expressing animals ($N=12$), nor in eYFP-expressing controls ($N=15$), did green light change rotational behavior (Figure 4B right, $p=0.55$ and 0.52 , respectively). However, in FosTRAP-eNpHR3.0 mice, green light reduced dyskinesia severity during light-on periods (Figure 4B left, S4D and Movie S2, $p=0.0005$). In eYFP controls, green light did not change dyskinesia severity ($p=0.81$). The light-evoked reduction in dyskinesia was greater in eNpHR3.0 animals, as compared to eYFP controls (Figure 4B middle,

$p=0.0002$). These results suggested TRAPed striatal cells are also necessary for dyskinesia, though it remains unclear how they contribute to rotational behavior.

Although LID-associated TRAPed cells are predominantly dMSNs, they represent only a subset of all dMSNs. To determine if this specific subset is necessary for LID, we tested whether inhibiting a random subset of dMSNs (as opposed to TRAPed neurons) could reduce LID, by optically inhibiting DLS dMSNs in parkinsonian D1-Cre animals treated with levodopa. We confirmed striatal eNpHR3.0 expression with histology and slice physiology (Figure 4C, S4E-G). Much to our surprise, optical inhibition of a comparable number of random dMSNs did not alter rotations or dyskinesia in D1-Cre-eNpHR3.0 mice (Figure 4D left and right, S4H; $p=0.48$ and 0.75 , respectively; $N=10$ mice). As expected, green light did not alter rotations or dyskinesia in D1-Cre-eYFP mice ($p=1.0$ and 1.0 , respectively, $N=9$ mice). No differences in light-evoked dyskinesias were observed between the eNpHR3.0 and eYFP groups (4D middle, $p=0.88$). It was somewhat surprising that dyskinesia was not reduced in D1-eNpHR3.0 mice, despite the fact that we were likely manipulating significantly more neurons in D1-eNpHR3.0 mice than FosTRAP-eNpHR3.0 mice (Figure S4I). Taken together, our results suggest that TRAPed cells may represent a specific subset of striatal direct pathway neurons necessary for levodopa-induced dyskinesia (Figure S4J).

3.4 Discussion

We used optogenetics and FosTRAP to investigate the neural populations that cause levodopa-induced dyskinesia (LID). Although LID-associated neurons were found brain-wide, the number of activated neurons in the striatum correlated most strongly with dyskinesia severity, and optogenetic reactivation of these neurons caused dyskinesia in the absence of levodopa. Inhibition of TRAPed striatal neurons, but not a random set of dMSNs, ameliorated LID. While these results corroborate many studies implicating the striatum in LID (Andersson et al., 1999; Berton et al., 2009; Buck et al., 2010; Cao et al., 2010; Engeln et al., 2014; Westin et al., 2001), our study is the first to establish that a specific and stable subset of striatal neurons causally mediates LID.

Many suspect LID is the result of excessive dMSN activity, and previous studies have treated dMSNs as a single group experiencing biochemical and physiological changes during LID. Our results combining FosTRAP with traditional c-Fos immunohistochemistry showed that dyskinetic attacks triggered weeks apart activated a highly overlapping population of striatal neurons. This surprising finding suggests that the dMSNs activated during LID are a highly selective and stable subgroup (Figure S1Q). Within this subpopulation, there were many dMSNs, as has been suggested in previous studies of IEGs in LID. We also found that these TRAPed MSNs showed elevated firing rates in response to levodopa *in vivo*. However, our experiments showed LID recruits a handful of PV-positive interneurons, and somewhat surprisingly, a small number of iMSNs. Taken together, these results suggest LID is mediated by a varied, but specialized ensemble within the striatum.

Optical stimulation may impose non-physiological levels or patterns of activity on brain circuits. Though recent studies demonstrated that optical or chemogenetic stimulation of sensorimotor striatum of parkinsonian animals, either nonspecifically or in dMSNs, can evoke dyskinesia (Alcacer et al., 2017; Hernandez et al., 2017; Perez et al., 2017), dyskinesia has also been reported with dMSN stimulation in healthy animals (Rothwell et al., 2015). These observations suggest synchronous activation of a large number of dMSNs in the sensorimotor striatum may be sufficient to cause dyskinesia, but do not indicate which neurons are normally engaged in LID. Optical reactivation of LID-associated neurons in our study has many of the same methodological caveats, though single-unit recordings of TRAPed striatal neurons suggests light-evoked firing in TRAPed neurons approximated firing rates achieved by TRAPed neurons during LID. In addition, inhibiting LID-associated striatal neurons reduced LID, whereas inhibiting a comparable number of dMSNs did not. This observation suggests (1) TRAPed striatal neurons are necessary and sufficient to produce dyskinesia in parkinsonian animals, and (2) TRAPed neurons represent a more LID-specific subset of neurons than dMSNs overall.

Why is inhibiting TRAPed striatal neurons more effective than inhibiting dMSNs to reduce LID? One explanation may be that circuit reorganization, triggered by parkinsonism itself, or by chronic levodopa treatment, is heterogeneous within the striatum. For example, TRAPed neurons may be particularly vulnerable to aberrant corticostriatal plasticity, which has been reported in rodent models of LID (Bagetta et al., 2012; Fieblinger et al., 2014; Picconi et al., 2003; Shen et al., 2015; Zhang et al., 2013). Alternatively, TRAPed cells may differ from neighboring dMSNs in local inhibitory connections (Gittis et al., 2011a), synaptic output (Borgkvist et al., 2015), or sensitivity to

dopamine (Heiman et al., 2014), which in turn may drive the differences in behavior evoked by manipulating TRAPed versus random dMSNs. Finally, the TRAPed population included a small number of PV-positive striatal neurons and iMSNs, which may contribute to circuit dysfunction and dyskinesia. Though several studies have implicated PV-positive interneurons in dyskinesia (Alberico et al., 2017; Gernert et al., 2000; Gittis et al., 2011b), at this point it is unclear how these interneurons contribute to dyskinesia without cell type-specific experiments directly testing causality.

Our results suggest that LID is caused by a distinct and stable group of striatal neurons. To take full advantage of this observation, these neurons will require further study, including a deeper examination of their activity patterns and behavioral correlates *in vivo*, and their cellular and synaptic properties *in vitro*. Taken together, these results could help identify new pharmacological targets for the prevention and management of LID.

3.5 Experimental Procedures

Animals:

Six different types of transgenic mice, of either sex, aged 3-6 months, all on a C57Bl/6 background, were used in this study. Hemizygous FosTRAP mice (Liqun Luo, Stanford) were bred to either wild-type C57Bl/6 mice (WT, Jackson Labs) or homozygous Ai14 mice (Jackson Labs) to yield FosTRAP;WT or FosTRAP;Ai14 mice. Hemizygous *Drd1a*-tdTomato mice (Shuen et al., 2008) were bred against WT mice to produce *Drd1a*-tdTomato;WT animals. Hemizygous D2-GFP mice (Gong et al., 2003) were bred against WT mice to produce D2-GFP;WT animals. To look for colocalization of FosTRAP and D2-GFP in the striatum, hemizygous FosTRAP;Ai14 mice were bred to hemizygous D2-GFP mice to yield FosTRAP;Ai14;D2-GFP mice. To manipulate direct pathway neurons, hemizygous *Drd1*-Cre (D1-Cre-217) mice were crossed to WT animals to yield D1-Cre;WT mice. Animals were housed 1-5 per cage on a 12-hour light/dark cycle with *ad libitum* access to rodent chow and water. All behavioral manipulations were performed during the light phase. We complied with local and national ethical and legal regulations regarding the use of mice in research. All experimental protocols were approved by the UC San Francisco Institutional Animal Care and Use Committee.

Surgical Procedures:

All surgical procedures were performed at 3-6 months of age. Anesthesia was induced with intraperitoneal (IP) injection ketamine/xylazine and maintained with 0.5%-1.0% inhaled isoflurane. Mice were placed in a stereotaxic frame and a mounted drill was used to create two small holes over the left dorsolateral striatum. The left dorsolateral striatum (DLS, ± 1.0 AP, + 2.4 ML, - 3.0 mm DV) was injected at two sites using a 33-

gauge needle with 2-2.5 μ l per site 6-Hydroxydopamine (6-OHDA)-bromide (to render mice parkinsonian) or normal saline (for control animals). In some experiments, AAV5-DIO-ChR2-eYFP (UPenn Vector Core, 1 μ L of 1:1 diluted virus per site), AAV5-DIO-eYFP (UNC Vector Core, 1 μ l per site), or AAV5-DIO-eNpHR3.0 (UNC Vector Core, 1 μ L per site) was also injected in the DLS (\pm 1.0 AP, + 2.4 ML, - 3.0 mm DV). 6-OHDA, saline, and virus were injected at a rate of 0.15 μ l/min, after which the injection cannula was left in place for 10-15 minutes prior to being withdrawn and the scalp being sutured. For experiments targeting cortical regions, AAV5-DIO-ChR2-eYFP or AAV5-DIO-eYFP was injected at two sites in primary somatosensory cortex (S1, +0.9 AP, +3.0 ML, -0.5 mm DV and -1.1 AP, +3.0 ML, -0.4 mm DV) or primary motor cortex (M1, +1.9 AP, +1.9 ML, -0.75 mm DV and -0.1 AP, +1.15 ML, -0.6 mm DV). For subsequent optical manipulations, the scalp was reopened 4-5 weeks after initial surgeries to implant optical fiber-ferrule assemblies in the DLS, S1, or M1 sites: DLS (\pm 1.0 AP, + 2.4 ML, - 2.8 mm DV), S1 (+0.9 AP, +3.0 ML, -0.2 mm DV and -1.1 AP, +3.0 ML, -0.2 mm DV), and M1 (+1.9 AP, +1.9 ML, -0.55 mm DV and -0.1 AP, +1.15 ML, -0.55 mm DV). Ferrules were secured in place with dental cement (Metabond) and dental acrylic (Ortho-Jet). The scalp was then sutured and the mouse was allowed to recover from anesthesia.

In preparation for *in vivo* single-unit recordings, FosTRAP;Ai14 mice were injected with 6-OHDA and ChR2, as described above, and optrode arrays were implanted in a subsequent surgical procedure. After the skull was reopened, a large craniectomy (1.5 x 1 mm) was created over the DLS, and two additional holes were drilled for placement of a skull screw (Fine Scientific Tools, FST) and ground wire, both over the contralateral hemisphere. A fixed multichannel electrode array (32 tungsten microwires, Innovative

Neurophysiology) coupled to a 200 μm optical fiber (Thorlabs) was slowly lowered through the craniectomy into the DLS. The final location of the array was targeted 100-200 μm above the previous 6-OHDA and ChR2 injection (-2.7-2.8 mm DV). The array was covered and secured into place with dental cement and acrylic, as above. In 2 of 4 mice used for *in vivo* unit recordings, a medial forebrain bundle (MFB) dopamine depletion was used instead of an intrastriatal depletion. In this case, 1 μl of 6-OHDA was injected unilaterally into the MFB (-1.0 AP, +1.0 ML, -4.9 mm DV).

All animals were given Buprenorphine (IP, 0.05 mg/kg) and ketoprofen (subcutaneous injection, 5 mg/kg) for postoperative analgesia. Parkinsonian animals were monitored closely for 1 week following surgery: mouse cages were kept on a heating pad, animals received daily saline injections and were fed nutritional supplements (Diet-Gel Recovery Packs and forage/trail mix).

Behavior:

Postoperatively, parkinsonian mice were monitored in the open field 1-2 times per week for 10 minutes per session. All mice were habituated to the open field (clear acrylic cylinders, 25 cm diameter) for 30 minutes 1-2 days prior to behavioral sessions. The mice were monitored via two cameras, one directly above (to capture overall movement) and one in front of the chamber (to capture fine motor behaviors). Video-tracking software (Noldus Ethovision) was used to quantify locomotor activity, including rotations (full 360° contralateral or ipsilateral turns), distance traveled, and velocity. After a three-week baseline period, daily injections of levodopa commenced. Levodopa-induced dyskinesia (LID) was scored during weekly sessions in which mice were injected, then placed in a clean, clear cage for visualization. Dyskinesia was quantified using a standard scoring

method (Cenci and Lundblad, 2007), which takes into account abnormal involuntary movements (AIMs) in axial, limb, and orofacial (ALO) body segments. Briefly, dyskinesia was quantified every 20 minutes, over a two-hour period, using a scale of 0-4. A score of 0 indicates no abnormal movement, and a score of 4 describes continuous and uninterruptable dyskinetic movements; 12 (4 x 3 body segments) is the maximum score possible for a given time point. For regular weekly dyskinesia scoring, 1-2 blinded experimenters rated AIMs. For optical reactivation or inhibition experiments, 2 blinded raters scored mice.

Pharmacology:

6-OHDA (Sigma Aldrich) for intrastriatal dopamine depletions was prepared at 2.5 $\mu\text{g}/\mu\text{l}$ in normal saline solution. 6-OHDA (Sigma Aldrich) for MFB dopamine depletions was prepared at 5 $\mu\text{g}/\mu\text{l}$ in normal saline solution. Levodopa (Sigma Aldrich) was always co-administered with benserazide (Sigma Aldrich) and prepared in normal saline solution. For cell counts and cell density experiments, (Figure 1 and S1) WT and FosTRAP;Ai14 animals received 20 mg/kg levodopa and 10 mg/kg benserazide. For optical reactivation experiments (Figure 3, S3, and Movie S1), 10 mg/kg levodopa and 5 mg/kg benserazide were used. For optical inhibition experiments (Figure 4, S4, and Movie S2), 5 mg/kg levodopa and 2.5 mg/kg benserazide were administered. Levodopa was given via IP injection 5-7 days per week. On the 7th day of levodopa treatment for FosTRAP;Ai14 mice, animals were given 4-hydroxytamoxifen (4-OHT, 50 mg/kg in Chen oil, IP) exactly one hour post-levodopa injection to capture dyskinesia-associated neurons (Figure 1B). 4-OHT was prepared as previously described (Guenther et al., 2013). Briefly, to prepare a 20 mg/mL stock of 4-OHT, 4-OHT was added to 200 proof ethanol, vortexed, and placed

on a horizontal shaker at 37° C for 30 minutes or until the 4-OHT dissolved. The stock solution was kept covered in foil to minimize light exposure. Next, to prepare a 10 mg/mL working solution in oil, the 4-OHT/ethanol mixture was combined with Chen Oil (a mixture of 4 parts sunflower seed oil and 1 part castor oil) and placed into 1.5 mL Eppendorf tubes. The tubes were vigorously mixed, wrapped in foil, and left on a nutator for 45 min at room temperature, vortexing and shaking periodically. The tubes were then placed in a speed-vac for 2-3 hours to evaporate the ethanol. If necessary, the final volume was adjusted with Chen Oil to 1 mL to reach a final concentration of 10 mg/mL. Both levodopa and 4-OHT were injected in a quiet, familiar environment, and animals were returned to their home cages, to minimize additional stimuli. Daily levodopa injections continued for 2-6 weeks to allow expression of Cre-dependent constructs. For *in vitro* experiments, picrotoxin (Sigma) was dissolved in warm water to prepare a 5 mM stock solution, which was subsequently diluted in ACSF for a final concentration of 50 μ M.

Optogenetic Manipulations:

Prior to optical stimulation experiments, animals were habituated to tethering with lightweight patch cables (components: PrecisionFiber Products and ThorLabs) coupled to an optical commutator (Doric Lenses) in the open field for 30 minutes, over 1-2 days. Optical stimulation experiments consisted of a two-minute baseline followed by 30 seconds light on/30 seconds light off (repeated 5-10x) and then a two-minute post period. TTL-controlled blue (488 nm, 1 mW, Shanghai Laser and Optics Century) or green laser light (593 nm, 5 mW, Shanghai Laser and Optics Century) was delivered continuously for all striatal experiments and either continuously or in pulse trains (5 msec, 10Hz, controlled with Master8, A.M.P.I.) for S1 or M1 experiments. Animals were manually scored for

dyskinetic behavior by raters blinded to the manipulation (eg ChR2 vs eYFP) during the baseline, light on/off, and post period. Video-tracking software was used to measure movement. For optical reactivation experiments, animals had not received levodopa for at least the previous 24 hours. For optical inhibition experiments, levodopa was administered 20-30 minutes before testing, to capture maximal dyskinesia. At the end of experimental procedures, animals were returned to their home cages.

In Vivo Electrophysiology:

Two weeks after optrode array implantation, mice were habituated to tethering and the recording chamber for 1-2 days. After habituation, experimental sessions occurred 3-5 times per week for 2-6 weeks. During each session, electrical signals (single-unit and LFP data from each of 32 channels) were collected using a multiplexed 32 channel headstage (Triangle Biosystems), an electrical commutator equipped with a fluid bore (Dragonfly), filtered, amplified, and recorded on a MAP system, using RASPUTIN 2.4 HLK3 acquisition software (Plexon). Spike waveforms were filtered at 154–8800 Hz and digitized at 40 kHz. The experimenter manually set a threshold for storage of electrical events.

During recording sessions, after a baseline period of 30 minutes, levodopa (5-10 mg/kg) was injected IP. After a period of 2-3 hours of recording spontaneous activity in the open field, an optogenetic cell identification protocol was applied (Kravitz et al., 2013), consisting of 100 msec blue light pulses, given at 1 Hz. At each of 4 light powers (0.5, 1, 2, and 4 mW), 1000 light pulses were delivered via a lightweight patch cable (Doric Lenses) connected to a blue laser (Shanghai Laser and Optics Century), via an optical commutator (Doric Lenses), and controlled by TTL pulses from a behavioral monitoring

system (Noldus Ethovision). In a subset of experiments, an additional cell identification protocol was applied, which consisted of continuous 30 seconds light on/off (repeated 5-10x) blue light pulses given at each light power (0.5, 1, 2, and 4mW). At the end of all cell identification protocols, animals were detached from the electrical and optical cables and returned to their home cages.

Single units were identified offline by manual sorting using Offline Sorter 3.3.5 (Plexon) and principle components analysis (PCA). Clusters were considered to represent a single unit if (1) the unit's waveforms were statistically different from multiunit activity and any other single units on the same wire, in 3D PCA space, (2) no interspike interval <1 msec was observed. Single units were then classified as putative medium spiny neurons (MSNs) as previously described (Berke et al., 2004; Gage et al., 2010; Harris et al., 2000) using features of the spike waveform (peak to valley and peak width), as well as inter-spike interval distribution. Only putative MSNs were included in subsequent analyses.

After single units had been selected for further study, their firing activity was analyzed using NeuroExplorer 4.133 (Nex Technologies). To determine if a unit was optogenetically identified, a peristimulus time histogram was constructed around the onset of laser pulses. To be considered optogenetically identified, a unit had to fulfill 3 criteria: (1) the unit had to increase firing rate above the 99% confidence interval of the baseline within 15 msec of laser onset; (2) the unit's firing was above this threshold for at least 15 msec; (3) the unit's laser-activated waveforms were not statistically distinguishable from spontaneous waveforms.

For display and analysis purposes, the firing rate of single units was averaged in one-minute bins. For analyses of firing rate before and during levodopa administration, the average firing rate from 0-30 minutes prior to injection and 35-65 minutes after injection were calculated. To determine whether a unit's firing rate significantly changed after levodopa injection, the firing rates during the baseline period were compared with the firing rates between 35-65 minutes after levodopa injection, using a Wilcoxon Signed Rank test.

***In Vitro* Electrophysiology:**

To prepare ex vivo slices for whole-cell recordings, mice were deeply anesthetized with an IP ketamine-xylazine injection, transcardially perfused with ice-cold glycerol-based slicing solution, decapitated, and the brain was removed. Glycerol-based slicing solution contained (in mM): 250 glycerol, 2.5 KCl, 1.2 NaH₂PO₄, 10 HEPES, 21 NaHCO₃, 5 glucose, 2 MgCl₂, 2 CaCl₂. The brain was mounted on a submerged chuck, and sequential 300 µm coronal slices were cut on a vibrating microtome (Leica), transferred to a chamber of warm (34° C) carbogenated ACSF containing (in mM) 125 NaCl, 26 NaHCO₃, 2.5 KCl, 1 MgCl₂, 2 CaCl₂, 1.25 NaH₂PO₄, 12.5 glucose for 30-60 minutes, then stored in carbogenated ACSF at room temperature. Each slice was then submerged in a chamber superfused with carbogenated ACSF at 31-33°C for recordings.

Striatal or cortical neurons were targeted for recordings using differential interference contrast (DIC) optics in FosTRAP;Ai14 or D1-Cre mice on a Olympus BX 51 WIF microscope. In FosTRAP;Ai14 mice, TRAPed neurons were identified by their td-Tomato positive somata and D1 positive neurons were identified by eYFP fluorescence from DIO-eYFP or DIO-eNpHR3.0-eYFP. Neurons were patched in the whole-cell

configuration using borosilicate glass electrodes (3-5 M Ω) filled with potassium methanesulfonate-based internal solution containing (in mM): 130 KMeSO₃, 10 NaCl, 2 MgCl₂, 0.16 CaCl₂, 0.5 EGTA, 10 HEPES, 2 MgATP, 0.3 NaGTP, pH 7.3. Picrotoxin was added to all external solutions.

Whole-cell current-clamp recordings were made using a MultiClamp 700B amplifier (Molecular Devices) and digitized with an ITC-18 A/D board (HEKA). Data was acquired using Igor Pro 6.0 software (Wavemetrics) and custom acquisition routines (mafPC, courtesy of M. A. Xu-Friedman). Current-clamp recordings were filtered at 5 kHz and digitized at 10 kHz. To validate ChR2 or eNpHR3.0 function in slice, light pulses were delivered to the slice by a TTL-controlled LED (Olympus), passed through a GFP (473 nm) or TxRed (562 nm) filter (Chroma) and the 40X immersion objective. LED intensity was adjusted to yield an output of approximately 1-10 mW at the slice. Light pulses were 5-2,000 msec in duration. For optogenetic inhibition experiments, cells were given current injections (200-800 pA) to produce stable spiking at roughly 10 Hz. After 500 msec, a 500-1000 msec light pulse was delivered to assess the ability of eNpHR3.0 to inhibit spiking. Holding current and input resistance were continuously monitored as proxies of recording stability.

Histology, Microscopy, and Cell Counting:

After optogenetic or behavioral experiments, mice were deeply anesthetized with IP ketamine-xylazine and transcardially perfused with 4% paraformaldehyde in PBS. After perfusion, the brain was dissected from the skull and post-fixed overnight in 4% paraformaldehyde, then placed in 30% sucrose at 4°C for cryoprotection. The brain was then cut into 35 μ m coronal or sagittal sections on a freezing microtome (Leica) and then

mounted in Vectashield Mounting Medium onto glass slides for imaging. For immunohistochemistry, the tissue was blocked with 3% normal donkey serum (NDS) and permeabilized with 0.1% Triton X-100 for 2 hours at room temperature on a shaker. A subset of stains used 5% normal donkey serum with 1.0% Triton X-100 (anti-ChAT). Primary antibodies were added to 3% NDS and incubated overnight at 4° C on a shaker. Primary antibodies used: Rabbit anti-TH (Pel-Freez, 1:1000), Chicken anti-TH (Sigma, 1:1000), Rabbit anti-c-Fos (Cell Signaling Technology, 1:1000), Rabbit anti-c-Fos (Santa Cruz, 1:1000), Goat anti-ChAT (Millipore, 1:500), Rabbit anti-DARPP-32 (Cell Signaling Technology, 1:1000), Mouse anti-RFP (Rockland Immunochemicals, 1:500), Rabbit anti-NeuN (Millipore, 1:1000), Rabbit anti-NPY (Cell Signaling Technology, 1:1000), Rabbit anti-PV (Swant, 1:2000), Rabbit anti-Erg-1 (Cell Signaling Technology, 1:500), or Goat anti- Δ FosB (Santa Cruz Biotechnology, 1:500). Slices were then incubated in secondary antibodies (donkey anti-rabbit, mouse, goat, or chicken Alexafluor 488, 593, or 647, 1:500, JacksonImmuno Research) for 2-4 hours at 4°C on a shaker, washed, and mounted onto slides for imaging. For a subset of animals (WT LID cohort, Figure S1A-J), development with diaminobenzidine (DAB) was used to visualize c-Fos. After 2-4 hours of incubation with secondary antibodies, the tissue was washed and then incubated for 60 minutes in Avidin-Biotin Complex (ABCVector Elite). After washing in PBS, DAB was prepared and added to each well. The color reaction was monitored under a dissecting microscope. Slices were then washed and mounted onto slides for imaging. 4 or 10x images were acquired on a Nikon 6D conventional widefield microscope.

Quantification and Statistical Analysis

Behavior:

Average AIM score per session (Figure 1E and S1C) is an average ALO score per 20 minutes of scoring. Average AIM score per week (Figure 1G and S1D) is an average ALO score over the entire 120-minute scoring session. Levodopa-induced contralateral rotations were measured weekly using video tracking (Figure 1F and S1E). Mice were placed in the open field 20-30 minutes post-levodopa injection and monitored for 10 minutes in the open field.

Optogenetic Experiments:

For each stimulation experiment, we calculated all behavioral measurements (both AIMS and rotations) during three periods, termed 'OFF (1)', 'ON', and 'OFF (2)'. The 'OFF (1)' period was the 25 seconds preceding the laser. The 'ON' period was the period starting 5 seconds after the illumination of the laser and lasting until the end of laser illumination (25 seconds long). The 'OFF (2)' period was the period between 5 and 30 seconds after the end of the laser illumination. The two-minute baseline preceding stimulation ('pre'), and two-minute baseline after stimulation ('post') was not included in calculations. Rotation data is presented as a rotation ratio (total ipsilateral rotations)/(total contralateral + total ipsilateral rotations). As dyskinesia intensity varied from animal to animal, data was also presented with the baseline subtracted (Figure 3G, I, K, middle panels; Figure 4B, D, middle panels). The Wilcoxon rank-sum test was used to compare animals expressing eYFP versus an opsin (ChR2 or eNpHR3.0). To compare 'OFF' (1) and 'ON' periods within an animal, the Wilcoxon sign-rank test was employed. If postmortem studies showed evidence of inadequate dopamine depletion, viral

expression, or no TRAPed cells (based on user error), its results were excluded from further analysis (N=3 animals excluded from the entire study, 2 based on inadequate viral expression (1 ChR2 and 1 eYFP) and 1 based on improper injection of 4-OHT).

***In Vivo* Electrophysiology:**

For display and analysis purposes, the firing rate of single units was averaged in one-minute bins. For analyses of firing rate before and during levodopa administration, the average firing rate from 0-30 minutes prior to injection and 35-65 minutes after injection were calculated. To determine whether a unit's firing rate significantly changed after levodopa injection, the firing rates during the baseline period were compared with the firing rates between 35-65 minutes after levodopa injection, using a Wilcoxon Signed Rank test.

Histology, Microscopy, and Cell Counting:

To quantify colocalization between TRAPed cells or c-Fos positive nuclei or for high magnification images, confocal imaging was implemented using a Nikon Spinning Disk confocal microscope with a 40x objective. Exposure times were matched between images of the same type.

To quantify the number of TRAPed cells in the striatum, S1, or M1 (Figure S1L) or c-Fos positive nuclei in the striatum (Figure S1J), individual images were stitched together to produce an entire coronal or sagittal image. We consulted the Allen Brain Atlas (<http://www.brain-map.org/>) and the Mouse Brain in Stereotaxic Coordinates (hard copy, 4th edition, by George Paxinos) for anatomy and chose 5-7 representative coronal or sagittal sections (at specified coordinates from bregma) for each brain region. To quantify the number of striatal c-Fos positive nuclei we used the coronal coordinates (+1) - (-1) for

quantification. To quantify the number or density of TRAPed cells in the striatum, S1, or M1 we used the following sagittal coordinates for quantification, striatum: 1.725-3.60 ML, S1: 1.08-3.72 ML, and M1: 1.0-3.1 ML. We used FIJI/ImageJ software to count cells, using both auto-threshold detection and manual counting. Slices were discarded if there was tissue damage to the designated area. One-way ANOVA was used to assess any differences in cell numbers for c-Fos positive nuclei in the striatum (Figure S1J) or TRAPed cell or cell density in the striatum, S1, and M1 (Figure 1I and S1L). For all cohorts, the post-hoc Tukey HSD test was used if the analysis of variance yielded a significant F-ratio. For the WT LID cohort (Figure S1J), we saw no statistical difference in cell numbers between the control groups (saline/saline, saline/levodopa, and 6-OHDA/saline), and pooled the data together to compare to the 6-OHDA/levodopa treated group. To determine correlations between behavior and TRAPed neurons (Figure 3B and S3B), the average number or density of TRAPed cells was calculated by averaging cell counts or density over the defined coordinates for each brain area. The AIM score was calculated by summing all AIM scores over the entire 120 minute scoring session closest to the day of 4-OHT administration.

For immunohistochemical experiments to investigate colocalization between TRAPed cells and markers of striatal cell types (Figure 2 and S2), 5-7 representative coronal or sagittal slices per animal were chosen, focusing next on 5-7 specific fields of view (1x1 screen size) in the DLS. Confocal z-stacks in each field of view were acquired, matching exposure time and laser power for each fluorophore in all images captured. To assess colocalization between TRAPed cells and different neuronal markers, maximum z-projections were made and merged to produce an overlay with TRAPed cells and the

corresponding cellular marker. For each animal, a minimum of 100 cells of each type (TRAP-tdTomato, cellular marker, or c-Fos) were manually counted using custom scripts in FIJI/ImageJ. For a cell to be counted as colocalized, it needed to appear on both individual and merged channels in the z-stack and maximum z-projection showing identical overlap with the other cell. Any cell showing ambiguous overlap was not counted as colocalized. The same procedure was used to assess colocalization of c-Fos and Drd1a-tdTomato (Figure S2F-G) and c-Fos and D2-GFP (Figure S2F,H).

To determine the average number of FosTRAP-eNpHR3.0 vs. D1-eNpHR3.0 per field, confocal images were acquired from at least 2 sagittal or coronal sections where the optical ferrule could be seen. We focused on 5-7 specific fields of view near the ferrule mark and acquired images over a strict depth of 20 μm for each animal. Cells were manually counted, using the outline of the cell body and cell processes as a guide, in FIJI/ImageJ using both the maximum z-projection and individual images within the stack. At least two blinded experimenters validated the presence or absence of an eNpHR3.0 positive cell.

3.6 Author Contributions & Acknowledgments

Author Contributions

AEG, ABN, and ACK designed the experiments. AEG, ABN, MYL, DN, and CJBM performed experiments. CJG and LL generated the FosTRAP mouse line and consulted on related protocols. AEG and ABN wrote the manuscript with contributions from all authors.

Acknowledgments

We thank Viktor Kharazia, Scott Wegner (UCSF ACTG), and DeLaine Larsen (UCSF Nikon Imaging Center) for histological and microscopy assistance, and Kevin Bender, Phillip Starr, Massimo Scanziani, Michael Ryan, and members of the Nelson and Kreitzer laboratories, for valuable discussion. This work was supported by the Brain Research Foundation (ABN), K08 NS081001 (ABN), National Science Foundation Graduate Research Fellowship (AEG), and UCSF Discovery Fellows Program (AEG). ABN is the Richard and Shirley Cahill Endowed Chair in Parkinson's Disease Research.

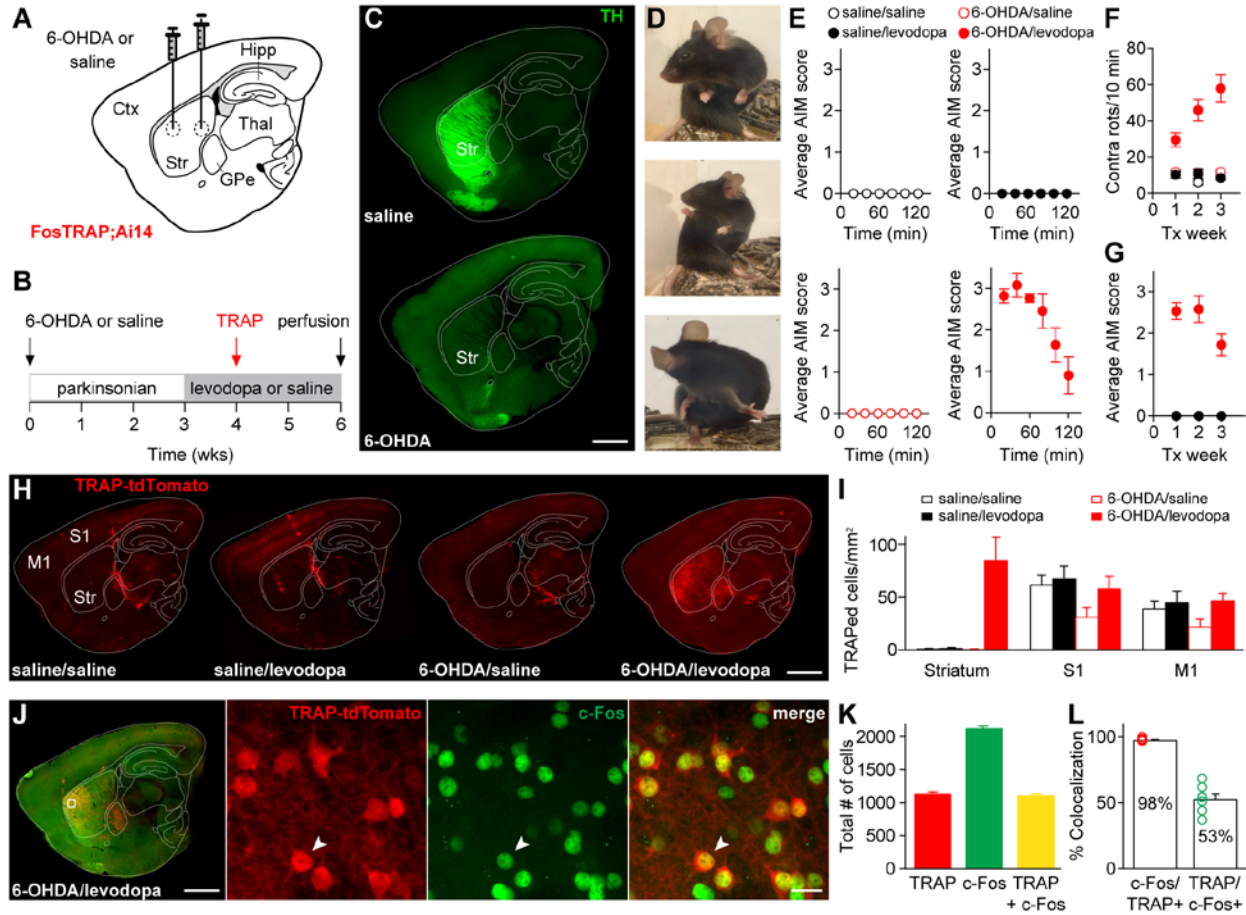


Figure 1. FosTRAP captures levodopa-induced dyskinesia (LID)-associated striatal cells. FosTRAP mice were separated into 4 groups based on intracerebral injections (saline or 6-OHDA) and chronic drug treatment (saline or levodopa). A. Sagittal schematic showing 6-OHDA or saline injections. B. Experimental timeline. C. Sagittal sections from mice injected with saline (top) or 6-OHDA (bottom) stained with anti-tyrosine hydroxylase (TH). D. Still images showing levodopa-induced dyskinesia in a parkinsonian FosTRAP mouse. E. Average abnormal involuntary movement (AIM) score measured after levodopa or saline injection in all groups. F. Contralateral rotations over 3 weeks of treatment. G. Average composite AIM score over 3 weeks of treatment (note: all four groups are displayed, but three groups showed no AIMS). H. Representative sagittal sections from the four experimental groups. Increased striatal expression of TRAP-tdTomato was only observed in 6-OHDA/levodopa treated animals. I. Density of TRAPed cells measured in the striatum, S1, and M1. J-L. FosTRAP mice were administered levodopa 2 hours prior to perfusion. TRAPed cells reflect those activated during a levodopa session approximately 2 weeks prior, while c-Fos positive neurons reflect cells activated during the terminal levodopa session. J. Left, Sagittal section showing TRAP-tdTomato and immunostained for c-Fos. Inset: Confocal images showing colocalization (arrowhead) of TRAP-tdTomato (left), c-Fos (middle), and merged image (right). K. Total number of TRAP-tdTomato, c-Fos, and colocalized cells. L. Percent colocalization of c-Fos with TRAP-tdTomato (left) and TRAP with c-Fos (right). C, H, and J (left): scale bar equals 1 mm. J (inset): scale bar equals 20 μ m. Data is displayed as average \pm SEM. See also Figure S1.

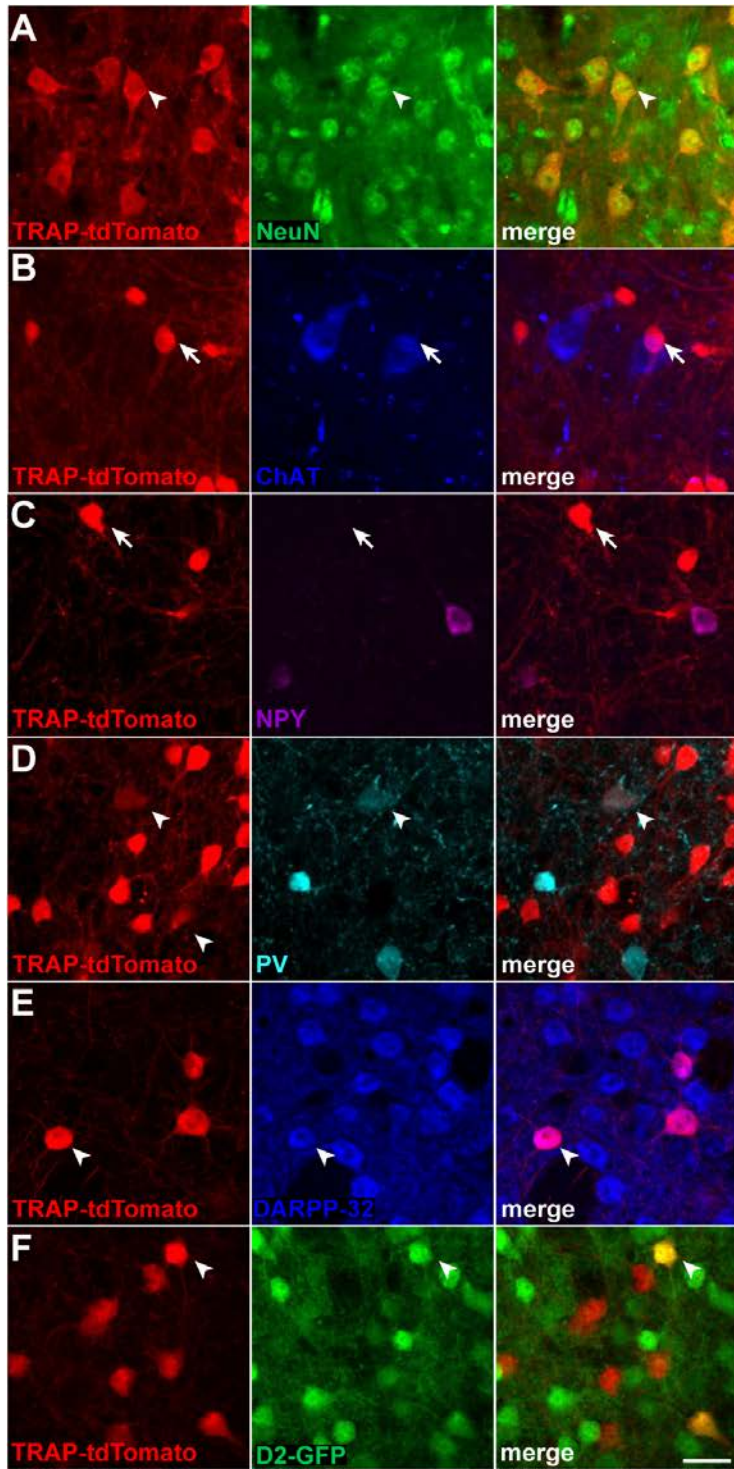


Figure 2. TRAPed cells are primarily direct pathway medium spiny neurons. A-F. Representative 40X confocal images from the striatum of FosTRAP mice treated with 6-OHDA and levodopa, immunostained for different cellular markers. Left columns show TRAP-tdTomato, middle columns show antibody staining for NeuN (A), Choline Acetyltransferase (ChAT, B), Neuropeptide Y (NPY, C), Parvalbumin (PV, D), DARPP-32 (E), D2-GFP (F), and right columns show merged images. White arrowheads denote colocalization, while white arrows show non-colocalized cells. G. Percent of TRAPed striatal cells positive for each cellular marker. A-F scale bar equals 20 μ m. Data is displayed as average \pm SEM. See also Figure S2.

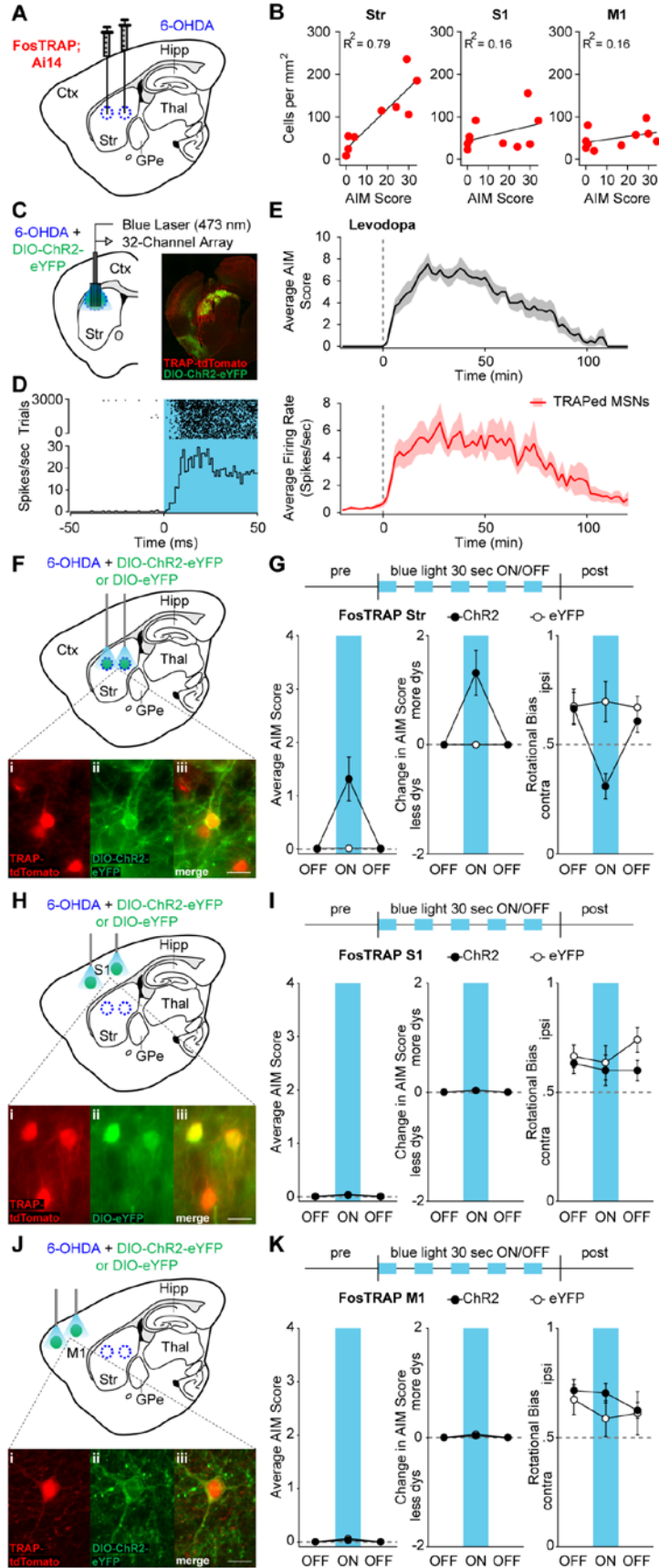


Figure 3. Optogenetic reactivation of TRAPed striatal neurons, but not TRAPed S1 or M1 cortical neurons, causes dyskinesia in the absence of levodopa. A. FosTRAP mice were injected intrastrially with 6-OHDA. B. Correlation between the density of TRAPed cells and total AIM score. C. Coronal schematic of optrode recording configuration (left) and representative postmortem section from a dopamine-depleted FosTRAP mouse injected with DIO-ChR2-eYFP (right). D. Representative optogenetically-identified unit, showing short-latency spiking to blue light pulses. Top: rasterized firing during 3,000 trials. Bottom: peristimulus time histogram. E. Top: Average AIM score from sessions in which a TRAPed neuron was identified. Levodopa was administered at time zero (dotted line). Bottom: Average firing rate of optogenetically identified TRAPed MSNs in response to levodopa. F-K. FosTRAP mice were injected with intrastriatal 6-OHDA and DIO-ChR2-eYFP or DIO-eYFP in either the striatum (Str, F), primary somatosensory cortex (S1, H), or primary motor cortex (M1, J), after which behavioral testing commenced in the absence of levodopa (G,I,K). F,H,J. Sagittal schematics showing sites of injection and light activation. Insets, postmortem histology showing TRAP-tdTomato (i), ChR2-eYFP (ii), and merge (iii) in the striatum, S1, and M1. G, I, K. Top: optical activation protocol (1mW) in Str, S1, and M1. Average (left) and change in (middle) AIM scores before, during, and after blue light in FosTRAP-ChR2 or eYFP mice. Right: rotational bias. F,H,J scale bar equals 20 μ m. Data is displayed as average \pm SEM. See also Figure S3.

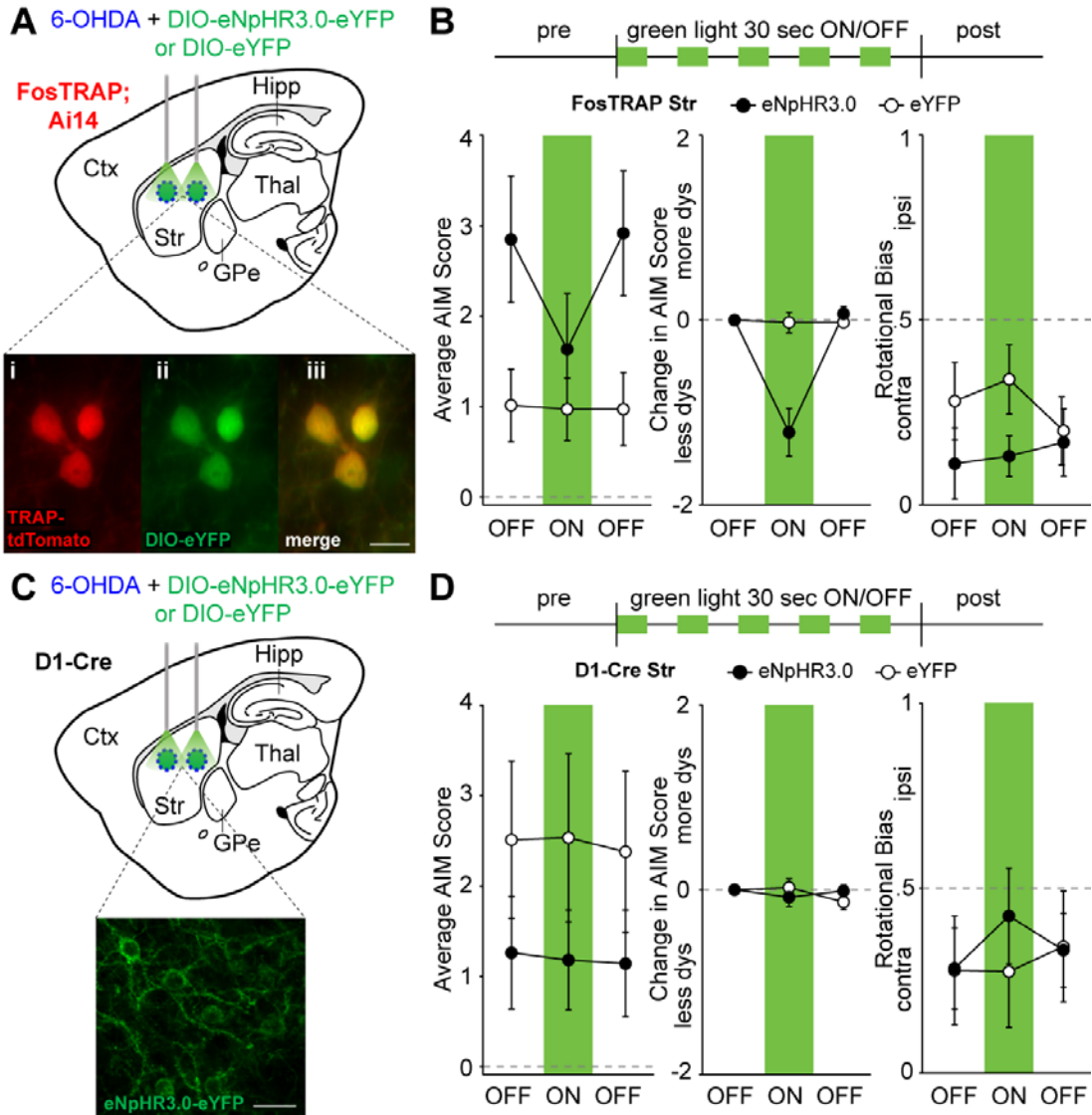
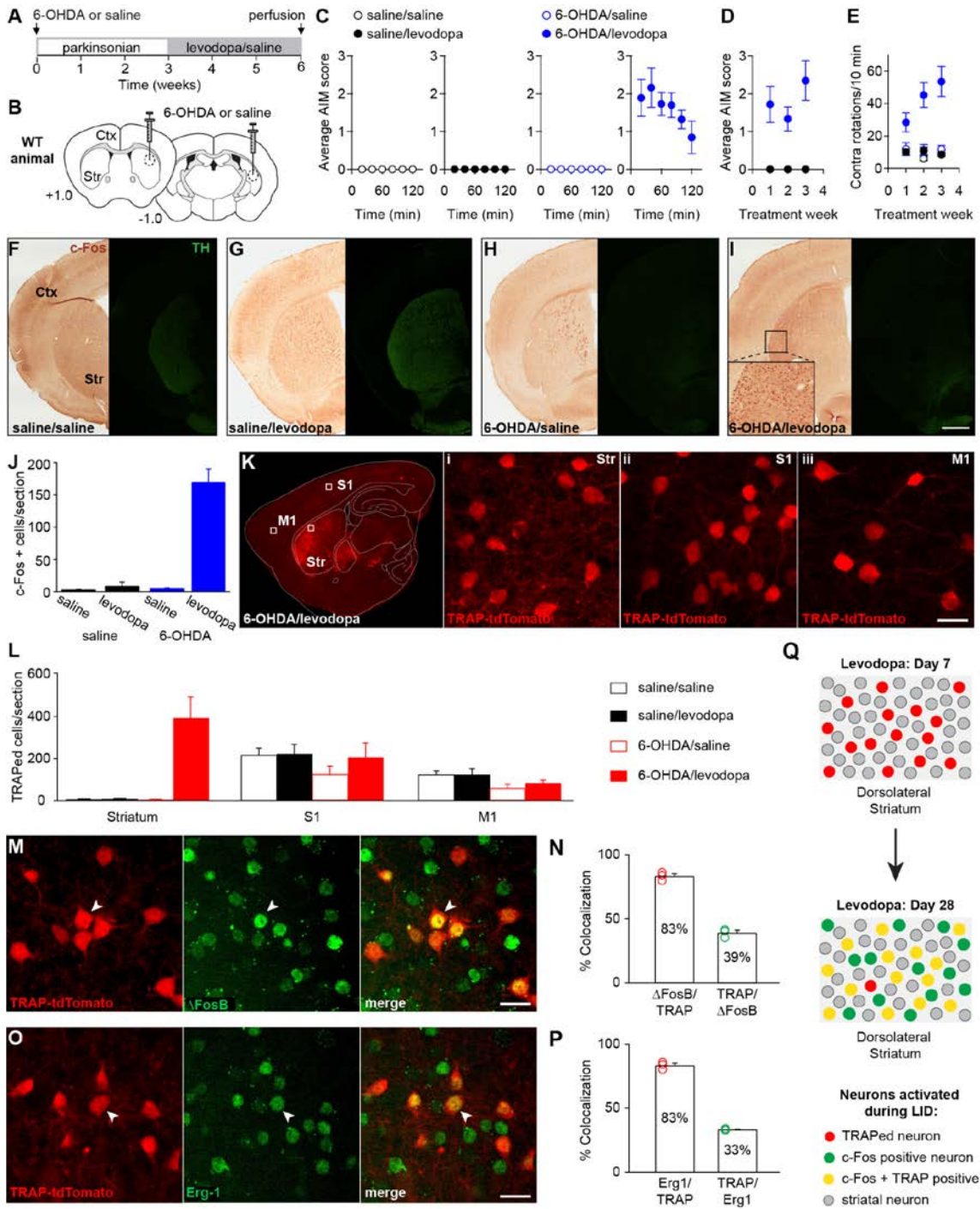
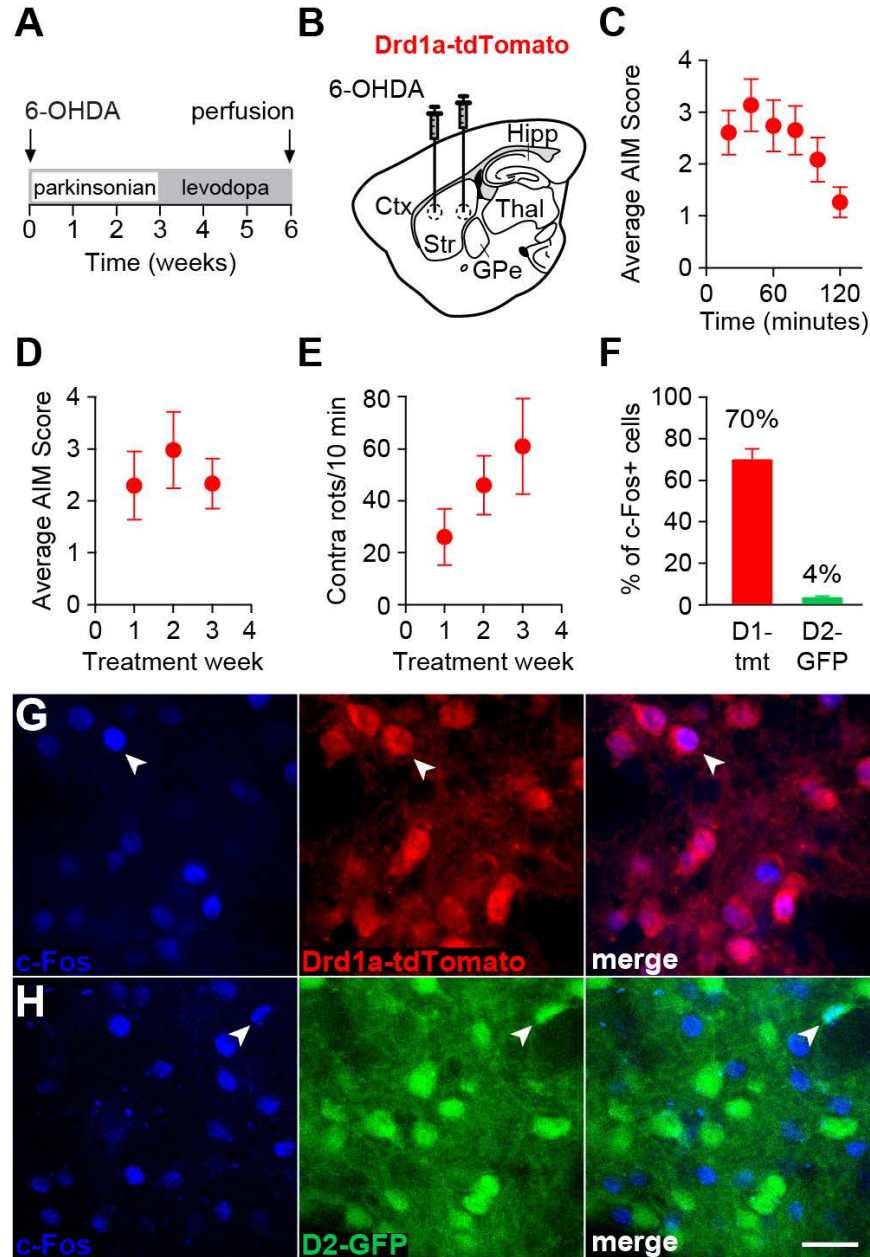


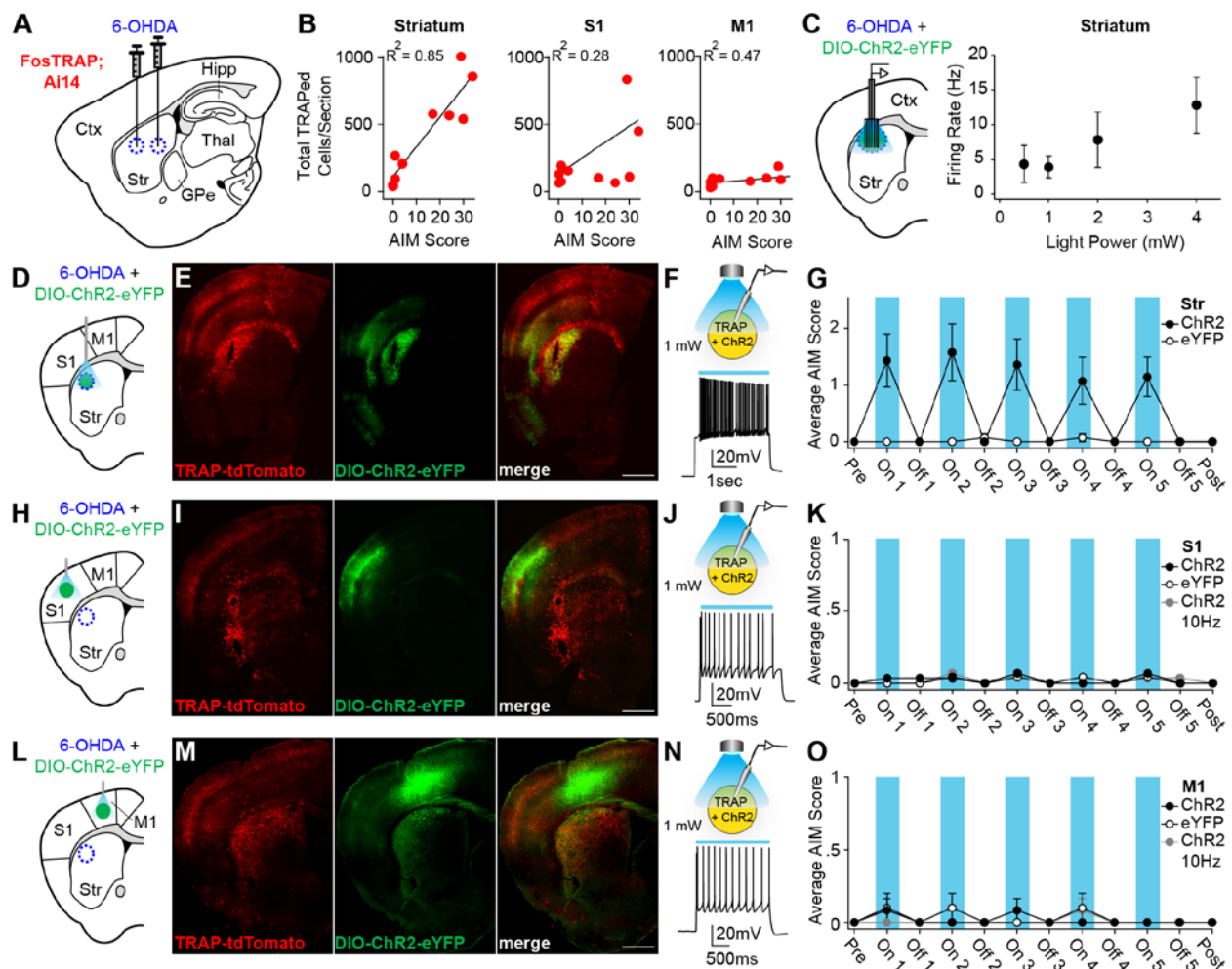
Figure 4. Optogenetic inhibition of TRAPed striatal neurons, but not all direct pathway neurons, ameliorates levodopa-induced dyskinesia. FosTRAP (A-B) or D1-Cre mice (C-D) were injected with intrastriatal 6-OHDA and DIO-eNpHR3.0-eYFP or DIO-eYFP. Behavioral testing was performed after the injection of levodopa. A,C. Sagittal schematics showing sites of injection and light stimulation in FosTRAP (A) and D1-Cre (C) mice. A. Inset: postmortem histology showing TRAP-tdTomato (i), eYFP (ii), and merge (iii). B,D. Top: optogenetic inhibition protocol (5 mW). Average (left) and change in (middle) AIM scores before, during, and after striatal green light in eNpHR3.0 or eYFP mice. Right: rotational bias. C. Inset: postmortem histology showing eNpHR3.0-eYFP positive striatal neurons. Right, rotational bias. A,C scale bar equals 20 μ m. Data is displayed as average \pm SEM. See also Figure S4.



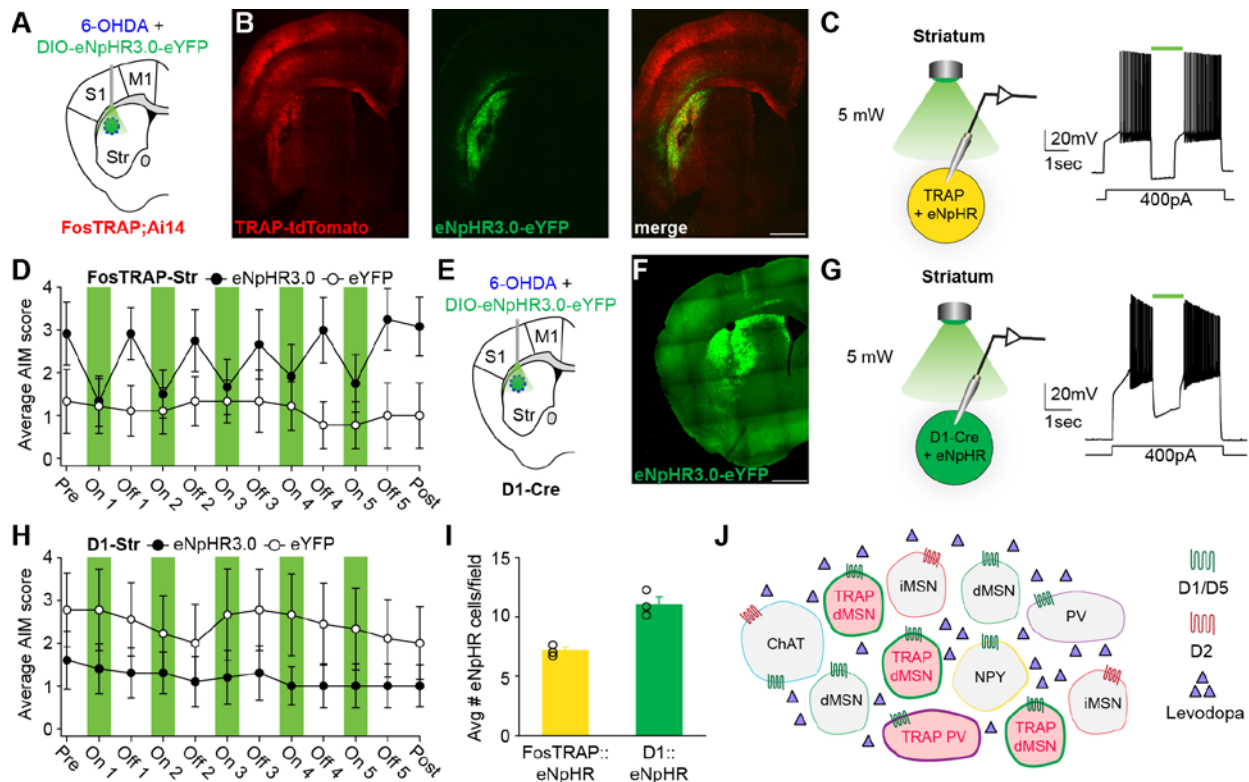
Supplemental Figure 1. Related to Figure 1. Levodopa-induced dyskinesia is associated with c-Fos expression. A-J. Wild-type mice were separated into four experimental groups based on a combination of intracerebral injection (saline or 6-OHDA) and subsequent chronic drug treatment (saline or levodopa). A. Experimental timeline. B. Coronal schematic showing sites of 6-OHDA or saline injection in the dorsolateral striatum. C. Average abnormal involuntary movement (AIM) score measured after intraperitoneal (IP) injection of levodopa or saline in 6-OHDA-treated or control groups. D. Average composite AIM score over 3 weeks of treatment. E. Contralateral rotations after IP injection of levodopa or saline over 3 weeks of treatment. F-I. Representative coronal histological images of striatal tissue stained with anti-c-Fos (left panels) and anti-TH (right panels) in mice from each of the four experimental groups. I. Inset: 20x image showing c-Fos positive nuclei in the dorsolateral striatum. J. Average number of c-Fos-positive nuclei per striatal section in all four experimental groups. K-L. FosTRAP mice were separated into four experimental groups, same as above. K. Representative sagittal section showing TRAPed cells in the striatum (Str), primary somatosensory cortex (S1), and primary motor cortex (M1) in a 6-OHDA/levodopa treated mouse. i, ii, iii, 40x confocal images of TRAP-tdTomato cells in the striatum, S1, and M1, respectively. L. Average number of TRAP-tdTomato positive cells per section in the striatum, S1, and M1 of animals from each group. M-P. FosTRAP mice were administered levodopa 2 hours prior to perfusion. TRAPed cells reflect those activated during a levodopa session approximately 2 weeks prior, while Δ FosB or Erg-1 positive neurons reflect cells activated during the terminal levodopa session. M. Confocal images showing colocalization of TRAP-tdtomato (left), Δ FosB (middle), and merged image (right). N. Percent colocalization of Δ FosB with TRAP-tdTomato (left) and TRAP with Δ FosB (right). O. Confocal images showing colocalization of TRAP-tdtomato (left), Erg-1 (middle), and merged image (right). P. Percent colocalization of Erg-1 with TRAP-tdTomato (left) and TRAP with Erg-1 (right). Q. Schematic representing the striatal neurons reproducibly activated during each levodopa administration. F-I, K (left) scale bar equals 1 mm. K (right), M, O, scale bar equals 20 μ m. Arrowhead shows colocalization. Data is displayed as average \pm SEM.



Supplemental Figure 2. Related to Figure 2. c-Fos activated neurons are primarily direct pathway cells. A-B. Drd1a-tdTomato mice were rendered parkinsonian with intrastriatal 6-OHDA, then treated with daily levodopa. After the last levodopa injection, mice were time-perfused for assessment of c-Fos expression. A. Experimental timeline. B. Sagittal schematic showing 6-OHDA injection sites. C. Average AIM scores after IP injection of levodopa. D. Average composite AIM score over 3 weeks of levodopa treatment. E. Contralateral rotations over 3 weeks of treatment. F. Percent of c-Fos positive cells that colocalize with Drd1a-tdTomato or D2-GFP. G. Representative 40X images from the striatum of a Drd1a-tdTomato mouse immunostained for c-Fos. Left: c-Fos, middle: Drd1-tdTomato, right: merged. H. Representative 40X images from the striatum of a D2-GFP mouse immunostained for c-Fos. Left: c-Fos, middle: D2-GFP, right: merged. White arrowheads denote colocalization. G-H, scale bar equals 20 μ m. Data is displayed as average \pm SEM.



Supplemental Figure 3. Related to Figure 3. Optogenetic reactivation of TRAPed striatal neurons, but not TRAPed S1 or M1 cortical neurons, causes dyskinesia in the absence of levodopa. A. FosTRAP mice were injected with 6-OHDA in the striatum. B. Correlation between the average number of TRAPed cells per section vs total AIM score. C. Left: Coronal schematic of optrode recording configuration. Right: Average peak firing rate (in one second bins) achieved by optogenetically labeled TRAPed striatal neurons during 30 second blue light pulses at various light intensities. D, H, L. Schematic diagrams showing sites of AAV and 6-OHDA injection in the DLS, S1, and M1 of FosTRAP mice. E, I, M. Representative coronal sections showing colocalization of TRAP-tdTomato (left), ChR2-eYFP (middle), and merged (right) in DLS, S1, and M1. In E, note optical fiber track in DLS. F, J, N. Schematic of whole-cell recording configuration for slice validation of ChR2 (top). Light-evoked spiking of a TRAPed neuron in the striatum (F), S1 (J), or M1 (M) during illumination with 473 nm light (bottom). G. Average AIM scores during light on and off epochs for striatal reactivation experiments. K. Average AIM scores during continuous light on/off epochs and 10Hz light on/off epochs for S1 reactivation experiments. O. Average AIM scores during continuous light on/off epochs and 10Hz light on/off epochs for M1 reactivation experiments. E, I, M scale bar equals 1 mm. Data is displayed as average \pm SEM.



Supplemental Figure 4. Related to Figure 4. Optogenetic inhibition of TRAPed striatal neurons, but not a random subset of direct pathway striatal neurons, ameliorates dyskinesia. FosTRAP (A-D) or Drd1-Cre mice (E-H) were treated with intrastriatal 6-OHDA and daily levodopa. The striatum was injected with DIO-eYFP or DIO-eNpHR3.0. A, E. Schematic diagram showing sites of AAV and 6-OHDA injection in the DLS of FosTRAP and D1-Cre mice, respectively. B. Representative coronal section showing colocalization of TRAP-tdTomato (left), eNpHR3.0-eYFP (middle), and merged (right) in the striatum. Optical fiber track can be seen in the area of eYFP signal. C, G. Schematic of whole-cell recording configurations for slice validation of eNpHR3.0 (left). Optical inhibition of a striatal neuron with 562 nm light (5mW, right) during a 400 pA current injection to evoke spiking. D, H. Average AIM scores during light on and off epochs for striatal inhibition experiments. F. Representative coronal section showing expression of eNpHR3.0-eYFP in D1-Cre mouse. I. Average number of eNpHR3.0-positive cells per field (adjacent to optical fiber track) in FosTRAP-eNpHR3.0 and D1-eNpHR3.0 animals. J. TRAPed cells are proposed as a specific subset of striatal neurons, composed primarily of dMSNs, that are necessary for the development of levodopa-induced dyskinesia. B, F, scale bar equals 1 mm. Data is displayed as average \pm SEM.

3.9 References

- Alam, M., Rumpel, R., Jin, X., von Wrangel, C., Tschirner, S.K., Krauss, J.K., Grothe, C., Ratzka, A., and Schwabe, K. (2017). Altered somatosensory cortex neuronal activity in a rat model of Parkinson's disease and levodopa-induced dyskinesias. *Exp Neurol* 294, 19-31.
- Alberico, S.L., Kim, Y.C., Lence, T., and Narayanan, N.S. (2017). Axial levodopa-induced dyskinesias and neuronal activity in the dorsal striatum. *Neuroscience* 343, 240-249.
- Alcacer, C., Andreoli, L., Sebastianutto, I., Jakobsson, J., Fieblinger, T., and Cenci, M.A. (2017). Chemogenetic stimulation of striatal projection neurons modulates responses to Parkinson's disease therapy. *J Clin Invest* 127, 720-734.
- Andersson, M., Hilbertson, A., and Cenci, M.A. (1999). Striatal fosB expression is causally linked with L-DOPA-induced abnormal involuntary movements and the associated upregulation of striatal prodynorphin mRNA in a rat model of Parkinson's disease. *Neurobiol Dis* 6, 461-474.
- Bagetta, V., Sgobio, C., Pendolino, V., Del Papa, G., Tozzi, A., Ghiglieri, V., Giampa, C., Zianni, E., Gardoni, F., Calabresi, P., *et al.* (2012). Rebalance of striatal NMDA/AMPA receptor ratio underlies the reduced emergence of dyskinesia during D2-like dopamine agonist treatment in experimental Parkinson's disease. *J Neurosci* 32, 17921-17931.
- Bergson, C., Mrzljak, L., Smiley, J.F., Pappy, M., Levenson, R., and Goldman-Rakic, P.S. (1995). Regional, cellular, and subcellular variations in the distribution of D1 and D5 dopamine receptors in primate brain. *J Neurosci* 15, 7821-7836.
- Berke, J.D., Okatan, M., Skurski, J., and Eichenbaum, H.B. (2004). Oscillatory entrainment of striatal neurons in freely moving rats. *Neuron* 43, 883-896.
- Berton, O., Guigoni, C., Li, Q., Bioulac, B.H., Aubert, I., Gross, C.E., Dileone, R.J., Nestler, E.J., and Bezard, E. (2009). Striatal overexpression of DeltaJunD resets L-DOPA-induced dyskinesia in a primate model of Parkinson disease. *Biol Psychiatry* 66, 554-561.
- Boraud, T., Bezard, E., Bioulac, B., and Gross, C.E. (2001). Dopamine agonist-induced dyskinesias are correlated to both firing pattern and frequency alterations of pallidal neurones in the MPTP-treated monkey. *Brain* 124, 546-557.
- Borgkvist, A., Avegno, E.M., Wong, M.Y., Kheirbek, M.A., Sonders, M.S., Hen, R., and Sulzer, D. (2015). Loss of Striatonigral GABAergic Presynaptic Inhibition Enables Motor Sensitization in Parkinsonian Mice. *Neuron* 87, 976-988.
- Buck, K., Voehringer, P., and Ferger, B. (2010). Site-specific action of L-3,4-dihydroxyphenylalanine in the striatum but not globus pallidus and substantia nigra pars

reticulata evokes dyskinetic movements in chronic L-3,4-dihydroxyphenylalanine-treated 6-hydroxydopamine-lesioned rats. *Neuroscience* 166, 355-358.

Cao, X., Yasuda, T., Uthayathas, S., Watts, R.L., Mouradian, M.M., Mochizuki, H., and Papa, S.M. (2010). Striatal overexpression of DeltaFosB reproduces chronic levodopa-induced involuntary movements. *J Neurosci* 30, 7335-7343.

Cenci, M.A., and Lundblad, M. (2007). Ratings of L-DOPA-induced dyskinesia in the unilateral 6-OHDA lesion model of Parkinson's disease in rats and mice. *Current protocols in neuroscience / editorial board, Jacqueline N Crawley [et al] Chapter 9, Unit 9 25.*

Engeln, M., Bastide, M.F., Toulme, E., Dehay, B., Bourdenx, M., Doudnikoff, E., Li, Q., Gross, C.E., Boue-Grabot, E., Pisani, A., *et al.* (2014). Selective Inactivation of Striatal FosB/DeltaFosB-Expressing Neurons Alleviates L-Dopa-Induced Dyskinesia. *Biol Psychiatry*.

Fieblinger, T., Graves, S.M., Sebel, L.E., Alcacer, C., Plotkin, J.L., Gertler, T.S., Chan, C.S., Heiman, M., Greengard, P., Cenci, M.A., *et al.* (2014). Cell type-specific plasticity of striatal projection neurons in parkinsonism and L-DOPA-induced dyskinesia. *Nat Commun* 5, 5316.

Filion, M., Tremblay, L., and Bedard, P.J. (1991). Effects of dopamine agonists on the spontaneous activity of globus pallidus neurons in monkeys with MPTP-induced parkinsonism. *Brain Res* 547, 152-161.

Gage, G.J., Stoetzner, C.R., Wiltschko, A.B., and Berke, J.D. (2010). Selective activation of striatal fast-spiking interneurons during choice execution. *Neuron* 67, 466-479.

Gerfen, C.R., Engber, T.M., Mahan, L.C., Susel, Z., Chase, T.N., Monsma, F.J., Jr., and Sibley, D.R. (1990). D1 and D2 dopamine receptor-regulated gene expression of striatonigral and striatopallidal neurons. *Science* 250, 1429-1432.

Gernert, M., Hamann, M., Bennay, M., Loscher, W., and Richter, A. (2000). Deficit of striatal parvalbumin-reactive GABAergic interneurons and decreased basal ganglia output in a genetic rodent model of idiopathic paroxysmal dystonia. *J Neurosci* 20, 7052-7058.

Gittis, A.H., Hang, G.B., LaDow, E.S., Shoenfeld, L.R., Atallah, B.V., Finkbeiner, S., and Kreitzer, A.C. (2011a). Rapid target-specific remodeling of fast-spiking inhibitory circuits after loss of dopamine. *Neuron* 71, 858-868.

Gittis, A.H., Leventhal, D.K., Fensterheim, B.A., Pettibone, J.R., Berke, J.D., and Kreitzer, A.C. (2011b). Selective inhibition of striatal fast-spiking interneurons causes dyskinesias. *J Neurosci* 31, 15727-15731.

Gong, S., Zheng, C., Doughty, M.L., Losos, K., Didkovsky, N., Schambra, U.B., Nowak, N.J., Joyner, A., Leblanc, G., Hatten, M.E., *et al.* (2003). A gene expression atlas of the central nervous system based on bacterial artificial chromosomes. *Nature* *425*, 917-925.

Guenther, C.J., Miyamichi, K., Yang, H.H., Heller, H.C., and Luo, L. (2013). Permanent genetic access to transiently active neurons via TRAP: targeted recombination in active populations. *Neuron* *78*, 773-784.

Halje, P., Tamte, M., Richter, U., Mohammed, M., Cenci, M.A., and Petersson, P. (2012). Levodopa-induced dyskinesia is strongly associated with resonant cortical oscillations. *J Neurosci* *32*, 16541-16551.

Harris, K.D., Henze, D.A., Csicsvari, J., Hirase, H., and Buzsaki, G. (2000). Accuracy of tetrode spike separation as determined by simultaneous intracellular and extracellular measurements. *J Neurophysiol* *84*, 401-414.

Heiman, M., Heilbut, A., Francardo, V., Kulicke, R., Fenster, R.J., Kolaczyk, E.D., Mesirov, J.P., Surmeier, D.J., Cenci, M.A., and Greengard, P. (2014). Molecular adaptations of striatal spiny projection neurons during levodopa-induced dyskinesia. *Proc Natl Acad Sci U S A* *111*, 4578-4583.

Hernandez, L.F., Castela, I., Ruiz-DeDiego, I., Obeso, J.A., and Moratalla, R. (2017). Striatal activation by optogenetics induces dyskinesias in the 6-hydroxydopamine rat model of Parkinson disease. *Mov Disord*.

Jenner, P. (2008). Molecular mechanisms of L-DOPA-induced dyskinesia. *Nat Rev Neurosci* *9*, 665-677.

Kravitz, A.V., Owen, S.F., and Kreitzer, A.C. (2013). Optogenetic identification of striatal projection neuron subtypes during in vivo recordings. *Brain Res* *1511*, 21-32.

Levy, R., Dostrovsky, J.O., Lang, A.E., Sime, E., Hutchison, W.D., and Lozano, A.M. (2001). Effects of apomorphine on subthalamic nucleus and globus pallidus internus neurons in patients with Parkinson's disease. *Journal of Neurophysiology* *86*, 249-260.

Liang, L., DeLong, M.R., and Papa, S.M. (2008). Inversion of dopamine responses in striatal medium spiny neurons and involuntary movements. *J Neurosci* *28*, 7537-7547.

Lindenbach, D., and Bishop, C. (2013). Critical involvement of the motor cortex in the pathophysiology and treatment of Parkinson's disease. *Neurosci Biobehav Rev* *37*, 2737-2750.

Lozano, A.M., Lang, A.E., Levy, R., Hutchison, W., and Dostrovsky, J. (2000). Neuronal recordings in Parkinson's disease patients with dyskinesias induced by apomorphine. *Ann Neurol* *47*, S141-146.

- Papa, S.M., Desimone, R., Fiorani, M., and Oldfield, E.H. (1999). Internal globus pallidus discharge is nearly suppressed during levodopa-induced dyskinesias. *Annals of Neurology* 46, 732-738.
- Pavon, N., Martin, A.B., Mendiola, A., and Moratalla, R. (2006). ERK phosphorylation and FosB expression are associated with L-DOPA-induced dyskinesia in hemiparkinsonian mice. *Biol Psychiatry* 59, 64-74.
- Perez, X.A., Zhang, D., Bordia, T., and Quik, M. (2017). Striatal D1 medium spiny neuron activation induces dyskinesias in parkinsonian mice. *Mov Disord*.
- Picconi, B., Centonze, D., Hakansson, K., Bernardi, G., Greengard, P., Fisone, G., Cenci, M.A., and Calabresi, P. (2003). Loss of bidirectional striatal synaptic plasticity in L-DOPA-induced dyskinesia. *Nat Neurosci* 6, 501-506.
- Rothwell, P.E., Hayton, S.J., Sun, G.L., Fuccillo, M.V., Lim, B.K., and Malenka, R.C. (2015). Input- and Output-Specific Regulation of Serial Order Performance by Corticostriatal Circuits. *Neuron* 88, 345-356.
- Shen, W., Plotkin, J.L., Francardo, V., Ko, W.K., Xie, Z., Li, Q., Fieblinger, T., Wess, J., Neubig, R.R., Lindsley, C.W., *et al.* (2015). M4 Muscarinic Receptor Signaling Ameliorates Striatal Plasticity Deficits in Models of L-DOPA-Induced Dyskinesia. *Neuron* 88, 762-773.
- Shuen, J.A., Chen, M., Gloss, B., and Calakos, N. (2008). *Drd1a-tdTomato* BAC transgenic mice for simultaneous visualization of medium spiny neurons in the direct and indirect pathways of the basal ganglia. *J Neurosci* 28, 2681-2685.
- Singh, A., Liang, L., Kaneoke, Y., Cao, X., and Papa, S.M. (2015). Dopamine regulates distinctively the activity patterns of striatal output neurons in advanced parkinsonian primates. *J Neurophysiol* 113, 1533-1544.
- Surmeier, D.J., Carrillo-Reid, L., and Bargas, J. (2011). Dopaminergic modulation of striatal neurons, circuits, and assemblies. *Neuroscience* 198, 3-18.
- Swann, N.C., de Hemptinne, C., Miciunovic, S., Qasim, S., Wang, S.S., Ziman, N., Ostrem, J.L., Luciano, M.S., Galifianakis, N.B., and Starr, P.A. (2016). Gamma Oscillations in the Hyperkinetic State Detected with Chronic Human Brain Recordings in Parkinson's Disease. *Journal of Neuroscience* 36, 6445-6458.
- Westin, J.E., Andersson, M., Lundblad, M., and Cenci, M.A. (2001). Persistent changes in striatal gene expression induced by long-term L-DOPA treatment in a rat model of Parkinson's disease. *Eur J Neurosci* 14, 1171-1176.
- Zhang, Y., Meredith, G.E., Mendoza-Elias, N., Rademacher, D.J., Tseng, K.Y., and Steece-Collier, K. (2013). Aberrant restoration of spines and their synapses in L-DOPA-

induced dyskinesia: involvement of corticostriatal but not thalamostriatal synapses. *J Neurosci* 33, 11655-11667.

CHAPTER 4

Altered synaptic connectivity onto a distinct subset of striatal neurons in levodopa-induced dyskinesia

4.1 Abstract

Action selection requires coordinated function of the striatal direct and indirect pathways. In Parkinson's disease, loss of dopaminergic inputs alters this balance, leading to motor deficits. While dopamine replacement therapy with levodopa alleviates parkinsonian symptoms, treatment is limited by the development of drug-induced abnormal involuntary movements, termed levodopa-induced dyskinesia. Recently, a unique subpopulation of predominantly direct pathway striatal neurons, captured using an activity-dependent mouse line (FosTRAP), was found to causally produce dyskinesia. Here we find that during levodopa treatment, the firing of these FosTRAP neurons is elevated, compared to other direct pathway neurons, and correlated with dyskinesia severity on a fine timescale. We used optogenetically identified single-unit recordings, retrograde synaptic tracing, and slice electrophysiology to identify the unique cellular and circuit properties of this novel subpopulation from striatal direct pathway neurons. Using these techniques, we found FosTRAP neurons receive increased excitatory input, with little alteration in the anatomical distribution of synaptic input, compared to direct pathway neurons. This increase appears to be mediated by changes in presynaptic function. These results highlight the need for cell-type specific strategies for treating LID, and point the way to new therapeutic targets.

4.2 Introduction

Goal-directed actions require the coordinated and precise output of many brain circuits, including those within the basal ganglia. The input nucleus of the basal ganglia, the striatum, plays a key role in this process by controlling action selection, habit formation, and movement (Graybiel, 2008; Redgrave et al., 2010). This control is mediated largely by two populations of intermixed striatal GABAergic output neurons, termed medium spiny neurons (MSNs), that bidirectionally modulate basal ganglia output and downstream motor nuclei. Direct pathway medium spiny neurons (dMSNs) express D1-like dopamine receptors (Gerfen et al., 1990) and project directly to and inhibit basal ganglia output, the internal segment of the globus pallidus and substantia nigra pars reticulata. Indirect pathway medium spiny neurons (iMSNs), conversely, express D2-like dopamine receptors (Gerfen et al., 1990) and project via multiple nuclei to influence basal ganglia output. It is hypothesized that the coordinated output of these two pathways is required for contextually appropriate behavior, habits, and movements to arise (Redgrave et al., 2010).

Dopamine is believed to regulate direct and indirect pathway neurons in an opposing fashion. According to the classical model of basal ganglia function, dopamine excites dMSNs and inhibits iMSNs, leading to action selection and movement (Albin et al., 1989; DeLong, 1990). In Parkinson's disease, however, the degeneration of nigrostriatal dopamine neurons is thought to disrupt this balance, leading to motor dysfunction. Dopamine replacement therapy with the dopamine precursor levodopa improves many aspects of motor performance. The efficacy of long-term levodopa therapy can be limited, however, by the development of abnormal drug-induced

involuntary movements, termed levodopa-induced dyskinesia (LID). While the cellular underpinnings of LID are unknown, biochemical (Jenner, 2008) and electrophysiological studies (Papa et al., 1999; Ryan et al., 2018) suggest the striatal direct pathway is a key driver. Indeed, optogenetic and chemogenetic studies have shown that direct pathway stimulation in the sensorimotor (dorsolateral) striatum can evoke dyskinesia (Alcacer et al., 2017; Perez et al., 2017; Ryan et al., 2018). However, increasing evidence suggests striatal direct pathway neurons are not a homogenous population. Several studies in both healthy and disease models have found heterogeneity at the level of gene expression (Gokce et al., 2016; Heiman et al., 2014), neural activity in awake behaving animals (Liang et al., 2008; Ryan et al., 2018; Singh et al., 2015) and causal relationship to dyskinesia (Girasole et al., 2018). This heterogeneity was highlighted in a recent study in parkinsonian mice, using *in vivo* single-unit electrophysiology, which identified a subpopulation of striatal dMSNs (approximately 20% of all striatal units) with high levodopa-evoked firing rates which correlated with dyskinesia severity (Ryan et al., 2018). In addition, heterogeneity has been seen within other basal ganglia nuclei, including the external segment of the globus pallidus (Hernandez et al., 2015; Mastro et al., 2014) and parafaciscular thalamus (Mandelbaum et al., 2019). In a condition like LID, such heterogeneity might contribute to the therapeutic versus pathological effects of levodopa, and understanding this heterogeneity might ultimately lead to improved treatments.

With this issue in mind, we recently identified a subpopulation of sensorimotor striatal neurons, predominantly from the direct pathway, whose activity is both necessary and sufficient in producing LID (Girasole et al., 2018). We converged upon this population using Targeted Recombination in Active Populations (TRAP), an activity-dependent

mouse line that captures neurons activated during a defined time period (Guenther et al., 2013), and determined that this LID-associated population represents approximately 20% of all striatal cells. Further, this subpopulation is stably activated across multiple episodes of dyskinesia (Girasole et al., 2018). It is unclear, however, if this subpopulation of “TRAPed” neurons exhibit the exceptionally high levodopa-evoked firing rates and correlation to dyskinesia previously described (Ryan et al., 2018). In addition, determining precisely how the synaptic connections onto TRAPed neurons differ, both anatomically and functionally, from their dMSN neighbors might inform our understanding of how LID develops, with the hopes of designing better therapeutics. We hypothesized that TRAPed neurons might differentially express some of the forms of plasticity previously described in the striatum of parkinsonian animals, such as reorganization and/or strengthening of excitatory or inhibitory synaptic inputs (Bagetta et al., 2012; Picconi et al., 2003; Shen et al., 2015; Taverna et al., 2008) changes in intrinsic excitability (Fieblinger et al., 2014), or sensitivity to dopamine itself (Jenner, 2008). Here, using TRAP in conjunction with optogenetically labeled single-unit recordings, monosynaptic rabies tracing, and slice electrophysiology, we sought to identify the unique features of TRAPed neurons. We found that optogenetically labeled TRAPed neurons show high levodopa-evoked firing rates, which in turn correlated with dyskinesia severity. We also found that excitatory transmission is preferentially increased onto TRAPed neurons. These findings confirm physiological and functional heterogeneity within the striatal direct pathway in the context levodopa-induced dyskinesia, and identify a potential cellular mechanism.

4.3 Results

TRAPed neurons exhibit high firing rates correlated to dyskinetic behavior.

Converging evidence suggests that striatal direct pathway neurons are a heterogeneous population of neurons. While it has previously been demonstrated that a subpopulation of direct pathway striatal neurons contributes causally to dyskinesia (Girasole et al., 2018), it is unclear whether the firing of these neurons shows distinct correlations to levodopa-evoked behaviors, as have been found within direct pathway neurons previously (Ryan et al., 2018). To investigate this question, we turned to optogenetically labeled single-unit recordings in freely moving parkinsonian and levodopa treated mice (Fig 1). Using methods similar to those in Girasole et al., FosTRAP (*Fos^{CreER/+} R26^{Ai14/+}*) animals were rendered parkinsonian by injection of the neurotoxin 6-hydroxydopamine (6-OHDA) in the left medial forebrain bundle (Figure 1A). This caused near-complete depletion of ipsilateral dopaminergic projections, resulting in reduced movement velocity and predominantly ipsilateral rotations in parkinsonian mice (data not shown). Cre-dependent Channelrhodopsin (AAV-DIO-ChR2-eYFP) was also injected in the dorsolateral striatum (DLS). Three weeks later, parkinsonian FosTRAP mice began daily levodopa injections. Mice developed both contralateral rotations and abnormal involuntary movements (AIMs). After one week of levodopa treatment, we used FosTRAP to capture neurons activated during LID by administering the short-acting tamoxifen metabolite 4-hydroxytamoxifen (4-OHT) together with levodopa. As demonstrated previously, pairing 4-OHT with a behavioral state that activates c-Fos, such as dyskinesia, drives Cre-dependent recombination and expression of tdTomato and/or ChR2-eYFP in TRAPed neurons (Girasole et al., 2018; Guenther et al., 2013) (Figure

1C). TRAP-TdTomato positive neurons were seen brain-wide, but were most numerous in the striatum. The DLS was subsequently implanted with a 32-channel optrode array for single-unit recordings (Figure 1B-C). Striatal activity was recorded during each session before and after levodopa administration. At the end of each recording session, a series of blue light pulses was delivered to determine whether the recorded cell expressed ChR2 (Cohen et al., 2012; Kravitz et al., 2013; Lima et al., 2009). Units with short-latency responses to blue light pulses were classified as optogenetically identified TRAPed neurons (see Methods; Figure 1D). We went on to characterize units as putative dMSNs, iMSNs or interneurons, based on their waveforms and response to levodopa administration (Figure 1E) (Ryan et al., 2018). Seven of nine (78%) optogenetically labeled TRAPed neurons were MSNs, based on waveform; 94% of all recorded units were MSNs. As predicted based on postmortem histological analysis in Girasole et al., 2018, optogenetically labeled TRAPed MSNs were enriched for putative direct pathway neurons (6/7, or 86%), compared to the total proportion of putative dMSNs (113/247, or 46%; Figure 1E). These results confirm that while striatal neurons show variable responses to levodopa across the whole population, physiological measures suggest TRAP captures mostly direct pathway neurons.

Within the striatal direct pathway, it is known that individual neurons show variable responses to levodopa, as evidenced by changes in pattern and firing rate (Liang et al., 2008; Singh et al., 2015) as well as correlations to motor behavior (Ryan et al., 2018). To test whether TRAPed direct pathway neurons are aberrantly activated by levodopa, we performed two additional analyses. First, we compared the firing rates of TRAPed dMSNs to those of putative dMSNs, in both the parkinsonian state and following levodopa, using

the firing of optogenetically identified striatal dMSNs in healthy controls as a control (Figure 1F). While both optically labeled TRAPed dMSNs and unlabeled dMSNs showed significantly lower firing rates in the parkinsonian state, as compared to dMSNs in healthy control mice, labeled TRAPed dMSNs achieved higher levodopa-evoked firing rates than unlabeled dMSNs (Figure 1F). In fact, TRAPed dMSNs reached rates of approximately double that of neighboring dMSNs. Second, given that TRAPed dMSNs achieved higher levodopa-evoked firing rates than other dMSNs, which was previously reported in a subset of dMSNs whose firing correlated with dyskinesia severity (Ryan et al., 2018), we next tested whether the firing rates of TRAPed neurons correlated on a moment to moment basis with motor behavior. We measured locomotor behavior with video tracking and scored dyskinesia before and after an intraperitoneal injection (IP) of levodopa. As expected, dyskinesia developed within about 5 minutes after injection, and reached a peak around 30-60 minutes, eventually returning to baseline levels after 90 minutes (Figure 1G). Across all striatal units, we observed a small subset of dMSNs whose firing correlated with dyskinesia severity on a fine timescale (31/113, or 27%; Figure J) and units that did not correlate with dyskinesia (Figure 1I). However, we observed an enrichment of dyskinesia-correlated cells in labeled TRAPed dMSNs (3/6, or 50%; Figure 1H, J). Taken together, these results suggest that optogenetically labeled TRAPed dMSNs achieve higher levodopa-evoked firing rates and more often correlated to dyskinesia than putative dMSNs, consistent with the hypothesis that they play a causal role in dyskinetic movements.

Retrograde tracing reveals similar distribution of synaptic input onto striatal TRAPed neurons and direct pathway neurons

While optogenetically labeled TRAPed neurons showed aberrant responses to levodopa *in vivo*, it is unclear what drives these responses. Indeed, LID is associated with changes in both excitatory and inhibitory inputs (Bagetta et al., 2012; Borgkvist et al., 2015; Picconi et al., 2003; Shen et al., 2015), intrinsic excitability (Fieblinger et al., 2014), sensitivity to neuromodulators (Heiman et al., 2014), and intracellular signaling (Jenner, 2008). As many prior studies were performed in unidentified neurons, and none in TRAPed neurons, we sought to test whether differential expression of these changes in TRAPed, compared to unTRAPed, dMSNs could explain their distinct firing *in vivo*. One potential explanation for the aberrant firing and correlation to dyskinesia of TRAPed dMSNs would be differences in the pattern of inputs onto TRAPed neurons. We examined this possibility using a retrograde tracing strategy. While several studies have used retrograde tracing to map inputs onto direct and indirect pathway neurons in healthy animals (Guo et al., 2015; Wall et al., 2013), it is unclear how the distribution of inputs changes in the face of chronic dopamine depletion or dopamine replacement therapy with levodopa. Using monosynaptic Cre-dependent rabies tracing in the DLS of FosTRAP, D1-Cre, and A2a-Cre mice, we assessed changes in the anatomical distribution of synaptic inputs onto TRAPed neurons, dMSNs and iMSNs, respectively (Figure 2).

We first compared the distribution of inputs onto dMSNs and iMSNs between healthy (Control) and disease (LID) states. A Cre-dependent helper virus (AAV-DIO-sTpEpB-GFP) was first injected into the DLS to express the EnvA receptor, TVA, and rabies glycoprotein necessary for rabies infection and replication, in a cell-type specific manner. Following

viral expression of helper proteins, a modified rabies virus (EnvA-G-deleted-rabies-mCherry) was injected into the DLS, using the same coordinates. Using this approach, functional rabies virus travels one synapse retrogradely from a Cre-expressing starter population of striatal neurons (Figure 2A). Ten days later, animals were sacrificed to assess expression of the helper virus (green) and presynaptic partners (red) (Figure 2A-B). Brains were then imaged, mapped onto the Allen Brain Atlas to identify specific brain regions, and then analyzed using a Gaussian cell-detection algorithm (Eastwood et al., 2018). To minimize the contribution of extra striatal start cells, the total proportion of brain-wide starter cells outside of the striatum could not exceed 15% (Figure 2C). This approach allowed us to compare monosynaptic inputs to TRAPed, direct, and indirect striatal neurons in healthy and levodopa-treated parkinsonian mice.

To look at the effects of chronic parkinsonism and its treatment, we first compared the distribution of monosynaptic inputs onto D1- and A2a-expressing DLS neurons in healthy and dopamine depleted and levodopa-treated mice. We found that dMSNs and iMSNs received a similar distribution of inputs in healthy animals (Figure 3; D1-Cre: N= 4, A2a-Cre: N = 3), with the greatest source of excitatory inputs coming from cortical areas, as has been observed in multiple previous studies (Guo et al., 2015; Wall et al., 2013). Following dopamine depletion and levodopa treatment, however, there were extensive changes in monosynaptic inputs onto direct and indirect pathway neurons (Figure 4; D1-Cre/LID: N=4, A2a-Cre/LID: N=4). To date, few if any studies have systematically examined changes in the synaptic inputs to direct and indirect pathway neurons in levodopa-treated parkinsonian animals (Fieblinger et al., 2014), but prior studies in parkinsonian (untreated) animals have shown an overall decrease in striatal

dendritic spines (Azdad et al., 2009; Day et al., 2006; Ingham et al., 1989; Smith and Villalba, 2008; Villalba et al., 2009; Zaja-Milatovic et al., 2005) suggesting there might be a decrease in corticostriatal input overall. We thus predicted that not only would parkinsonism and its treatment alter the distribution of synaptic inputs, but that this would differ between the direct and indirect pathway. Indeed, we found fewer retrogradely labeled cortical and thalamic cells in D1-Cre animals, while we found an increase in such cells in A2a-Cre animals. Interestingly, we found changes in the opposite direction in the striatum, where intrastriatal, likely inhibitory, connections onto direct pathway neurons were markedly increased in parkinsonian/levodopa-treated animals, and decreased onto indirect pathway neurons (Figure 3). As we know that striatal direct and indirect pathway neurons show an increase in and suppression of activity, respectively, during levodopa treatment (Ryan et al., 2018), most of these results may be consistent with homeostatic changes within the circuit in an effort to re-balance direct and indirect pathway activity.

We next returned to our primary question: whether differences in the anatomical distribution of inputs onto TRAPed striatal neurons, versus those of direct pathway neurons more generally, might explain the differential activity of these neurons *in vivo*, and their role in LID. We compared monosynaptic inputs onto direct, indirect, and TRAPed neurons in parkinsonian/levodopa-treated mice. In particular, given their enhanced response to levodopa *in vivo*, we wondered if we would find an increase in particular excitatory inputs in TRAPed neurons, at an anatomical level. Based on a small initial group of animals (N = 4 FosTRAP), however, it appears that TRAPed neurons and dMSNs receive similar distribution of inputs across both cortical and subcortical regions (Figure 4). One exception is the number of labeled presynaptic neurons in the external

segment of the globus pallidus (GPe), which were slightly more numerous in Fos-TRAP than in D1-Cre or A2a-Cre mice (Figure 5A-F). Immunohistochemical characterization of these cells showed that they are parvalbumin (PV) negative and Npas1 positive (Figure 5), consistent with previous research suggesting Npas1 positive neurons project to DLS (Hernandez et al., 2015). As this is an inhibitory projection, it seemed unlikely that these inputs could drive aberrant activity in TRAPed neurons *in vivo*; further functional investigation will be needed. Additionally, to rule out any bias generated by labeling a large number of intrastriatal inputs, we investigated whether there was a change within cortical inputs in all experimental conditions by looking at the percentage of presynaptically labeled cells for a given cortical area as a fraction of all labeled cortical inputs (Figure 6). Consistent with our previous findings, there was no change in the pattern of cortical projections onto TRAPed cells compared to dMSNs or iMSNs. Though there are caveats and biases to retrograde tracing using the rabies approach, based on these results, it appears that TRAPed neurons do not have a substantially different *anatomical* distribution of inputs compared to dMSNs in dopamine depleted and levodopa-treated animals.

Excitatory transmission is preferentially increased onto TRAPed neurons in dopamine depleted and levodopa treated mice

Another explanation for the aberrant activity seen in TRAPed neurons *in vivo* is *functional* changes in synaptic inputs onto TRAPed neurons compared to their neighbors, as the lack of differential input assessed with the retrograde tracing approach does not preclude changes in functional connectivity. As MSNs depend on excitatory input for

much of their activity *in vivo*, an increase in excitatory connectivity onto TRAPed neurons might explain their high levodopa-evoked activity and/or the fact that this firing correlates with dyskinesia severity. To assess whether synaptic inputs onto TRAPed dMSNs differed from their unTRAPed dMSN and iMSN neighbors, we crossed our FosTRAP;Ai14 mouse to a D2-GFP indirect pathway reporter line. In slices from these animals, we were able to record from TRAPed dMSNs, unTRAPed dMSNs, and unTRAPed iMSNs in a single preparation (Figure 7A-B). We performed whole-cell voltage clamp experiments in FosTRAP;Ai14;D2-GFP mice rendered parkinsonian and treated chronically with levodopa, as described previously. To increase our confidence in the recorded cell type, we included biocytin in the pipette for post hoc confirmation of the presence of TdTomato (TRAP), D2-GFP, or no fluorescent marker (Figure 7B). To broadly assess for changes in the number, strength, or release probability of excitatory inputs, we first measured miniature excitatory postsynaptic currents (mEPSC; in TTX and picrotoxin), recording from TRAPed dMSNs, unTRAPed dMSNs, and unTRAPed iMSNs in sequential recordings from the same region of DLS (Figure 7C). To our surprise, there was an increased frequency of mEPSCs onto TRAPed neurons compared to other MSNs (Figure 7D, $n=20, 20, 22$ cells; $N= 8, 6, 8$ animals for TRAPed dMSNs, unTRAPed dMSNs, and unTRAPed iMSNs, respectively, $p < 0.01$). The amplitude of mEPSCs onto TRAPed dMSNs, however, was not significantly higher than in unTRAPed dMSNs. We saw higher amplitude mEPSCs in direct pathway neurons (both TRAP and unTRAPed dMSNs) compared to unTRAPed iMSNs (Figure 7E, $n=20, 20, 22$ cells; $N= 8, 6, 8$ animals for TRAPed dMSNs, unTRAPed dMSNs, and unTRAPed iMSNs, respectively, $p < 0.05$). These results suggest that excitatory inputs onto TRAPed dMSNs are altered compared

to unTRAPed dMSNs in parkinsonian/levodopa-treated animals, likely mediated by changes in presynaptic function, such as an increased probability of release.

To further investigate changes in presynaptic function on TRAPed dMSNs, we recorded evoked EPSCs, using a similar approach. We electrically evoked EPSCs by placing a glass stimulating electrode 100-200 μm away from the recorded neuron, and delivering a series of current pulses. We stimulated with two pulses at varying interstimulus intervals (ISIs; 25, 50, 75, 100, 250, and 500 ms) in order to assess the paired-pulse ratio (PPR), a measure that can reflect presynaptic parameters such as probability of release. Consistent with our mEPSC recordings, we saw a marked decrease in the PPR in TRAPed dMSNs compared to other MSNs (Figure 7F, $n= 11, 7, 5$ cells; $N= 4, 3, 3$ animals for TRAPed dMSNs, unTRAPed dMSNs, and unTRAPed iMSNs, respectively). This decrease in PPR was different at every ISI less than 500 ms. While this data is preliminary, these results are consistent with two possibilities: (1) increased release probability at some or all excitatory synapses (which appears most likely, as retrograde tracing did not reveal significant changes in the distribution of synapses anatomically) or (2) a redistribution of inputs from high-PPR synapses, such as those from the cortex (Ding et al., 2008) to low-PPR synapses, such as those from the thalamus (Ding et al., 2008).

Though our mEPSC recordings did not show a significant increase in mEPSC amplitude, we also used the evoked EPSC measurements to assess for changes in postsynaptic function. We measured the AMPA to NMDA ratio in evoked EPSCs onto TRAPed and unTRAPed dMSN, and unTRAPed iMSNs from parkinsonian/levodopa-treated mice (Figure 7G). An increase in the AMPA/NMDA ratio for a given input is often

interpreted to indicate strengthening of synapses via postsynaptic mechanisms (Mameli et al., 2011; Ungless et al., 2001). This interpretation is based on the observation that in many forms of long-term potentiation (LTP), AMPA receptors are inserted in the membrane, yielding a higher AMPA-mediated current (Luscher and Malenka, 2012). To test this possibility, we measured the amplitude of evoked EPSCs at two different holding potentials, -70 mV and +40 mV, to distinguish AMPA and NMDA receptor-mediated currents. Our preliminary results indicate the AMPA/NMDA ratio is increased in TRAPed dMSNs compared to other MSNs (Figure 7G, n= 12, 7, 5 cells; N= 4, 3, 3 animals for TRAPed dMSNs, unTRAPed dMSNs, and unTRAPed iMSNs, respectively). However, given the variability in this physiological measure, more data are needed to draw a final conclusion. Together, these results suggest that both a presynaptic and postsynaptic mechanism may contribute to the aberrant activity of TRAPed neurons *in vivo*.

Another potential cellular mechanism contributing to the aberrant activation of TRAPed neurons *in vivo* is intrinsic excitability or its regulation by dopamine. This mechanism is a particularly attractive candidate, as dopamine is known to increase the excitability of direct pathway neurons in slices from healthy rodents (Hernandez-Lopez et al., 1997; Planert et al., 2013), and the primary changes we saw in the firing of TRAPed neurons were in response to levodopa. We first explored whether the basic intrinsic properties of TRAPed dMSNs differed from those of unTRAPed dMSNs and iMSNs, using whole-cell current-clamp recordings, again in parkinsonian/levodopa-treated FosTRAP;Ai14;D2-GFP mice (Figure 8A-B). We included biocytin in the pipette for post hoc confirmation of the presence of TdTomato (TRAP) or D2-GFP (Figure 8B). In the absence of acute dopaminergic treatment, the passive and active properties (resting

membrane potential, input resistance, rheobase -- minimum current injection needed for an action potential to be generated, action potential threshold, afterhyperpolarization amplitude, or action potential half width) of TRAPed dMSNs and unTRAPed dMSNs and iMSNs were not different from one another (Figure 8C, E-G, Table 1, n=5, 5, 6 cells; N=3, 3, 3 animals for TRAPed dMSNs, unTRAPed dMSNs, and unTRAPed iMSNs, respectively). These results suggest that intrinsic excitability alone (in the absence of dopamine) does not explain the differential activity in TRAPed dMSNs *in vivo*.

As the firing of TRAPed dMSNs did not differ from overall dMSNs in the parkinsonian state *in vivo*, and that we did not find any changes in their baseline intrinsic excitability, we next tested whether TRAPed neurons showed enhanced excitability in the presence of the dopamine agonist, SKF 81297, compared to unTRAPed dMSNs and iMSNs (Figure 8D-G). Previous findings have shown a modest increase in the number of spikes elicited in the presence of dopamine or dopamine D1 agonists by short current pulses just above the rheobase (Hernandez-Lopez et al., 1997; Planert et al., 2013). Therefore, we hypothesized that similar increases in excitability might be seen in dMSNs in parkinsonian mice, but might be differentially expressed in TRAPed and unTRAPed dMSNs. After cells were patched and achieved a stable baseline, a series of current injections was provided to assess the input current-output firing frequency (IF) relationship within each cell type (Figure 8C-D). Next, 5 μ M SKF was washed onto the slice and the IF was reassessed (Figure 8D). By and large the passive and active properties of TRAPed and unTRAPed MSNs were unchanged by SKF application (Table 1), but as predicted, we observed a modest increase in the number of spikes elicited at rheobase in dMSNs, which was more pronounced in TRAPed versus unTRAPed dMSNs

and iMSNs (Figure 8H, n= 5, 5, 6 cells; N= 3, 3, 3 animals for TRAPed dMSNs, unTRAPed dMSNs, and unTRAPed iMSNs, respectively). However, we did not see significant changes in the maximum firing rates achieved between TRAPed, unTRAPed dMSNs, and unTRAPed iMSNs (data not shown). These results suggest that a change in sensitivity to dopamine may be enhanced in TRAPed neurons, however, more data is needed to reach statistical power to truly make this comparison.

4.4 Discussion

Here, we used *in vivo* and *in vitro* electrophysiology, monosynaptic rabies tracing, and TRAP to investigate the cellular and synaptic mechanisms of levodopa-induced dyskinesia. In single-unit recordings, we found that levodopa evoked higher firing rates in TRAPed neurons than in putative dMSNs overall, and further that the firing of TRAPed neurons often correlated with dyskinesia severity on a moment-to-moment basis. In addition, we found a preferential enhancement of excitatory inputs onto TRAPed dMSNs compared to other nearby dMSNs and iMSNs, suggesting presynaptic plasticity may develop during chronic parkinsonism or its treatment, and explain the aberrant *in vivo* firing seen in LID.

It is generally accepted that the striatum can be divided into anatomical or functional channels, composed of multiple cortico-striatal-thalamic circuits (Alexander and Crutcher, 1990; Redgrave et al., 2010) and further subdivided into the striatal direct and indirect pathways, which are generally viewed as homogeneous pathways projecting to various downstream nuclei (Albin et al., 1989; DeLong, 1990). However, whether there is heterogeneity within each channel/pathway, in healthy animals or in animal models of disease, is less clear (Liljeholm and O'Doherty, 2012). Our underlying hypothesis was that within the direct pathway neurons in the sensorimotor “channel”, there is heterogeneity amongst neurons in synaptic connectivity, excitability, and/or in dopamine-related neural plasticity. Further, we hypothesized that this heterogeneity is one of the reasons that levodopa evokes both therapeutic and dyskinetic responses in parkinsonian animals. In keeping with this hypothesis, we found that a subset of striatal neurons (TRAPed cells) showed aberrant levodopa-evoked firing rates in parkinsonian animals,

and that these same neurons receive increased excitatory input. These findings were predicted by heterogeneity in striatal single-unit responses to levodopa and to behavior in parkinsonian primates (Liang et al., 2008). However, our study allowed us to link a subpopulation of neurons that causally contribute to dyskinesia (TRAPed striatal neurons, Girasole et al., 2018) with single-unit physiological characteristics and anatomical connections *in vivo* and cellular and synaptic changes in *ex vivo* preparations.

What are the cellular or synaptic features that distinguish TRAPed dMSNs from other dMSNs? Answering this question would not only inform our understanding of the heterogeneity found in healthy and parkinsonian mice, but could lead to more targeted therapeutics for Parkinson's disease. One hypothesis is that these neurons differ in the distribution or strength of synaptic inputs. The sensorimotor striatum receives excitatory synaptic input from all over the brain (Berendse and Groenewegen, 1990; Gerfen, 1992; Gerfen and Bolam, 2010; Hunnicutt et al., 2016; Smith et al., 2011), but these inputs might be re-weighted by chronic dopamine depletion and/or dopamine replacement therapy (Azdad et al., 2009; Fieblinger and Cenci, 2015; Fieblinger et al., 2014; Nishijima et al., 2014; Suarez et al., 2014; Zhang et al., 2013) and this type of anatomical plasticity could be differentially expressed in TRAPed vs unTRAPed dMSNs. However, using monosynaptic rabies tracing, we saw no evidence of differences in inputs between TRAPed neurons and dMSNs more generally. We found a relatively symmetrical distribution of excitatory inputs onto dMSNs and iMSNs in healthy animals, as previously demonstrated (Guo et al., 2015; Wall et al., 2013). Not unexpectedly, this distribution shifted in chronically dopamine-depleted/levodopa-treated animals. Overall, we saw changes that suggested homeostatic readjustment to the altered firing patterns of MSNs

in such animals: we found an increase in excitatory inputs to iMSNs compared to dMSNs, which could help compensate for the suppressed activity of iMSNs and higher activity of dMSNs seen in levodopa-treated mice (Parker et al., 2018; Ryan et al., 2018). We hope to address whether these differences track the loss and replacement of dopamine with the addition of a cohort of chronically parkinsonian (6OHDA) but untreated (levodopa-naïve) mice, along with larger sample sizes in all groups. Whether these differences in inputs in LID are indeed homeostatic, as suggested previously by a study of dendritic spines in dMSNs and iMSNs in LID (Fieblinger et al., 2014), is yet to be determined. Interestingly, we observed changes in the opposite direction for intrastriatal (likely inhibitory) connections onto dMSNs and iMSNs, which might also be homeostatic in nature. Again, there was no difference in the distribution of inputs onto TRAPed neurons versus overall dMSNs, suggesting changes in the distribution of inputs onto dMSNs do not explain the aberrant firing of TRAPed neurons during dyskinesia, nor perhaps do they explain the development of dyskinetic movements. Finally, the lack of obvious differences in the sources of input, as assessed with rabies tracing, does not exclude the possibility of changes in synaptic function, which we found using *ex vivo* electrophysiology. However, whether those functional changes arise in some inputs and not others is still unclear.

A longstanding hypothesis in the field suggests that the chronic loss of dopamine, or dopamine replacement, leads to impaired synaptic plasticity; evidence for this hypothesis has been found in *ex vivo* recording studies (Bageetta et al., 2012; Fieblinger et al., 2014; Jenner, 2008; Picconi et al., 2003; Shen et al., 2015). In animals with LID, investigators have observed changes in long term potentiation (LTP), specifically in the

inability to depotentiate previously strengthened excitatory inputs in unidentified and direct pathway neurons (Picconi et al., 2003; Shen et al., 2015). One group found this plasticity was dependent on cholinergic signaling via large cholinergic interneurons within the striatum and the muscarinic type 4 (M4) receptor (Shen et al., 2015). Such aberrant plasticity may lead to changes in synaptic properties--another group showed that parkinsonian/levodopa-treated animals had alterations in AMPA/NMDA ratio (Bagetta et al., 2012). Indeed, an attractive hypothesis is that synaptic function may be differentially altered in TRAPed dMSNs compared to neighboring dMSNs. We found an increase in mEPSC frequency and a decrease in PPR in evoked EPSCs, suggestive of a change in presynaptic function in TRAPed dMSNs. These findings might reflect a change in function of a similar group of presynaptic release sites, or might reflect a shift from lower probability of release (Pr) sites to higher Pr sites. Interestingly, we qualitatively observed that the PPR from TRAPed neurons in LID is very similar to that of thalamic inputs onto MSNs in healthy mice (Ding et al., 2008). While we did not observe any anatomical changes in thalamic inputs to TRAPed animals from rabies tracings, other studies have noted functional changes in thalamic inputs in Parkinson's disease (Parker et al., 2016; Tanimura et al., 2019). Thus, testing if thalamic inputs could be driving these presynaptic changes is an exciting prospect moving forward. Finally, in pilot experiments, we also found an increase in the AMPA/NMDA ratio in evoked EPSCs in TRAPed neurons. This finding suggests a possible postsynaptic component, as well, which would be in line with several previously reported findings in dMSNs or unidentified MSNs. Unfortunately, direct comparison of prior studies is difficult, as they were performed under different conditions

(duration of parkinsonism/treatment; recording configuration), typically in unidentified cell types.

Dissociating the mechanisms by which TRAPed and unTRAPed neurons respond to levodopa might inform development of new treatments to prevent or reduce LID. With such information, pharmacological blockers of TRAPed neurons, given in conjunction with levodopa, might reduce dyskinesia while preserving the therapeutic aspects of levodopa. Pharmacological activators of unTRAPed dMSNs might promote therapeutic responses without evoking dyskinesia. Future studies using single-cell sequencing could help further explain differences in TRAPed dMSNs at the molecular level, which in turn might focus future physiological or pharmacological studies.

4.5 Experimental Procedures

Animals:

We used 3-9 month old C57Bl/6 mice of either sex. Hemizygous FosTRAP mice (Liquin Luo, Stanford) were bred to either wild-type C57Bl/6 mice (WT, Jackson Labs) or homozygous Ai14 mice (Jackson Labs) to yield FosTRAP or FosTRAP;Ai14 mice. Hemizygous D2-GFP mice (Gong et al., 2003) were bred against WT mice to produce D2-GFP animals. For slice electrophysiology experiments, hemizygous FosTRAP;Ai14 mice were bred to hemizygous D2-GFP mice to yield FosTRAP;Ai14;D2-GFP mice. Animals were housed 1-5 per cage on a 12-hour light/dark cycle with *ad libitum* access to rodent chow and water. All behavioral manipulations were performed during the light phase. We complied with local and national ethical and legal regulations regarding the use of mice in research. All experimental protocols were approved by the UC San Francisco Institutional Animal Care and Use Committee.

Surgical Procedures:

All surgical procedures were performed at 3-6 months of age. Anesthesia was induced with intraperitoneal (IP) injection ketamine/xylazine and maintained with 0.5%-1.0% inhaled isoflurane. Mice were placed in a stereotaxic frame and a mounted drill was used to create holes over the left medial forebrain bundle (MFB) and/or the left dorsolateral striatum (DLS). To render mice parkinsonian, the left MFB (-1.0 AP, +1.0 ML, -4.9 mm DV) was injected using a 33-gauge needle with 1-1.5 μ L per site of 6-Hydroxydopamine (6-OHDA)-bromide. In some experiments, AAV5-DIO-ChR2-eYFP (UPenn Vector Core, 1-1.5 μ L) was also injected in the left DLS (+0.8 AP, + 2.3 ML, - 2.5 mm DV). 6-OHDA and virus were injected at a rate of 0.15 μ L/min, after which the injection

cannula was left in place for 10-15 minutes prior to being withdrawn and the scalp being sutured. For Cre-dependent rabies tracing experiments, 300 nL helper virus, rAAV1/synp-DIO-sTbEpB-GFP (UNC Vector Core, lot AV6118CD) was injected into two left DLS sites (+/- 0.8 AP, -2.4 ML, -2.5 DV) at a rate of 100 nL/min. Two weeks after helper virus injection, 300nL modified EnvA G-deleted Rabies-mcherry (Salk Viral Vector Core) virus was also injected in the two left DLS sites at 100 nL/min.

In preparation for *in vivo* single-unit recordings, FosTRAP;Ai14 mice were injected with 6-OHDA and ChR2, as described above, and optrode arrays were implanted in a second surgical procedure. After the scalp was reopened, a large craniectomy (1.5 x 1 mm) was created over the left DLS, and two small holes were drilled in the right frontal and right posterior parietal areas for placement of a skull screw (Fine Scientific Tools, FST) and ground wire, respectively. A fixed multichannel electrode array (32 Tungsten microwires, Innovative Neurophysiology) coupled to a 200 μ m optical fiber (Thorlabs) was slowly lowered through the craniectomy into the DLS. The final location of the electrode tips was targeted 100-200 μ m above the previous ChR2 injection (-2.3-2.4 mm DV). The array was covered and secured into place with dental cement (Metabond) and acrylic (Ortho-Jet).

All animals were given buprenorphine (IP, 0.05 mg/kg) and ketoprofen (subcutaneous injection, 5 mg/kg) for postoperative analgesia. Parkinsonian animals were monitored closely for 1 week following surgery: mouse cages were kept on a heating pad, animals received daily saline injections and were fed nutritional supplements (Diet-Gel Recovery Packs and forage/trail mix).

Behavior:

Postoperatively, parkinsonian mice were monitored in the open field 1-2 times per week for 10 minutes per session. All mice were habituated to the open field (clear acrylic cylinders, 25 cm diameter) for 30 minutes 1-2 days prior to behavioral sessions. The mice were monitored via two cameras, one directly above (to capture overall movement) and one in front of the chamber (to capture fine motor behaviors). Video-tracking software (Noldus Ethovision) was used to quantify locomotor activity, including rotations (90° contralateral or ipsilateral turns), distance traveled, and velocity. After a three-week baseline period, daily injections of levodopa commenced. Levodopa-induced dyskinesia (LID) was scored during weekly sessions in which mice were injected, then placed in a clean, clear cage for visualization. For regular weekly dyskinesia scoring, 1-2 blinded experimenters rated AIMs (for details see Statistical Procedures below).

Pharmacology:

6-OHDA (Sigma Aldrich) for MFB dopamine depletions was prepared at 5 µg/µL in normal saline solution. Levodopa (Sigma Aldrich) was administered with benserazide (Sigma Aldrich) and prepared in normal saline solution. Levodopa (5-10 mg/kg) was given via IP injection 5-7 days per week over the course of the experiment. Initially, on the 7th day of levodopa treatment for FosTRAPxWT, FosTRAP;Ai14, and FosTRAP;Ai14;D2-GFP mice, animals were given 4-hydroxytamoxifen (4-OHT, 50 mg/kg in Chen oil, IP) exactly one hour post-levodopa injection, to capture dyskinesia-associated neurons (Figure 1B). 4-OHT was prepared as previously described (Guenther et al., 2013). Briefly, to prepare a 20 mg/mL stock in ethanol of 4-OHT, 4-OHT was added to 200 proof ethanol, vortexed, and placed on a horizontal shaker at 37° C for 30 minutes or until the

4-OHT dissolved. The stock solution was kept covered in foil to minimize light exposure. Next, to prepare a 10 mg/mL working solution in oil, the 4-OHT/ethanol mixture was combined with Chen Oil (a mixture of 4 parts sunflower seed oil and 1 part castor oil) and placed into 1.5 mL Eppendorf tubes. The tubes were vigorously mixed, wrapped in foil, and left on a nutator for 45 min at room temperature, vortexed and shaken periodically. The tubes were then placed in a speed-vac for 2-3 hours to evaporate the ethanol. If necessary, the final volume was adjusted with Chen Oil to 1 mL to reach a final concentration of 10 mg/mL. Both levodopa and 4-OHT were injected in a quiet, familiar environment, and animals were returned to their home cages, to minimize additional stimuli. Daily levodopa injections continued for 2-6 weeks to allow expression of Cre-dependent constructs. For *in vitro* experiments, picrotoxin (Sigma) was dissolved in warm water to prepare a 5 mM stock solution, which was subsequently diluted in ACSF for a final concentration of 50 μ M. Tetrodotoxin (TTX, Abcam) was dissolved in water at a stock concentration of 1 mM and added to ACSF for a final concentration of 1 μ M. SKF 81298 was dissolved in water at a concentration of 1mM and added to ACSF for a final concentration of 5 μ M. For all *in vitro* experiments, biocytin (1-2.5 mg/mL) was included in the internal solution for post-hoc confirmation of the presence or absence of Ai14 and D2-GFP.

***In Vivo* Electrophysiology:**

Two weeks after optrode array implantation, mice were habituated to tethering and the recording chamber for 1-2 days. After habituation, experimental sessions occurred 3-5 times per week for 2-6 weeks. During each session, electrical signals (single-unit and LFP data from each of 32 channels) were collected using a multiplexed 32 channel

headstage (Triangle Biosystems), an electrical commutator equipped with a fluid bore (Dragonfly), filtered, amplified, and recorded on a MAP system, using RASPUTIN 2.4 HLK3 acquisition software (Plexon). Spike waveforms were filtered at 154–8800 Hz and digitized at 40 kHz. The experimenter manually set a gain and threshold for storage of electrical events.

During recording sessions, after a baseline period of 30 minutes in the parkinsonian state, levodopa (5-10 mg/kg) was injected IP. After a period of 2-3 hours of recording spontaneous activity in the open field, an optogenetic cell identification protocol was applied (Kravitz et al., 2013), consisting of 100 msec blue light pulses, given at 1 Hz. At each of 4 light powers (0.5, 1, 2, and 4 mW), 1000 light pulses were delivered via a lightweight patch cable (Doric Lenses) connected to a blue laser (Shanghai Laser and Optics Century), via an optical commutator (Doric Lenses), and controlled by TTL pulses from a behavioral monitoring system (Noldus Ethovision).

Single-units were identified offline by manual sorting using Offline Sorter 3.3.5 (Plexon) and principle components analysis (PCA). Clusters were considered to represent a single unit if (1) the unit's waveforms were statistically different from multiunit activity and any other single-units on the same wire, in 3D PCA space, (2) no interspike interval <1 msec was observed. Single-units were then classified as putative medium spiny neurons (MSNs) as previously described (Berke et al., 2004; Gage et al., 2010; Harris et al., 2000) using features of the spike waveform (peak to valley and peak width), as well as inter-spike interval distribution.

After single-units had been selected for further study, their firing activity was analyzed using NeuroExplorer 4.133 (Nex Technologies). To determine if a unit was

optogenetically identified, a peristimulus time histogram was constructed around the onset of laser pulses. To be considered optogenetically identified, a unit had to fulfill 3 criteria: (1) the unit had to increase firing rate above the 99% confidence interval of the baseline within 15 msec of laser onset; (2) the unit's firing was above this threshold for at least 15 msec; (3) the unit's laser-activated waveforms were not statistically distinguishable from spontaneous waveforms.

***In Vitro* Electrophysiology:**

Prior to terminal anesthesia and preparation of brain slices, animals (3-9 months) were coinjected with levodopa and benserazide (5-10 mg/kg and 2.5-5 mg/kg, respectively) to induce LID. After 30-45 minutes in the dyskinetic state, mice were deeply anesthetized with an IP ketamine-xylazine injection, transcardially perfused with ice-cold glycerol-based slicing solution, decapitated, and the brain was removed. Glycerol-based slicing solution contained (in mM): 250 glycerol, 2.5 KCl, 1.2 NaH₂PO₄, 10 HEPES, 21 NaHCO₃, 5 glucose, 2 MgCl₂, 2 CaCl₂. The brain was mounted on a submerged chuck, and sequential 300 µm coronal slices were cut on a vibrating microtome (Leica), transferred to a chamber of warm (34° C) carbogenated ACSF containing (in mM) 125 NaCl, 26 NaHCO₃, 2.5 KCl, 1 MgCl₂, 2 CaCl₂, 1.25 NaH₂PO₄, 12.5 glucose for 30-60 minutes, then stored in carbogenated ACSF at room temperature. Each slice was then submerged in a chamber superfused with carbogenated ACSF at 31-33°C for recordings.

Striatal neurons were targeted for recordings using differential interference contrast (DIC) optics in FosTRAP;Ai14 or FosTRAP;Ai14;D2GFP mice on a Olympus BX 51 WIF microscope. In FosTRAP;Ai14 and FosTRAP;Ai14;D2GFP mice, TRAPed neurons were identified by their td-Tomato positive somata and D2 positive neurons were

identified by GFP fluorescence. Fluorescence-negative neurons with GABAergic interneuron physiological properties (membrane tau decay <1 ms for both fast-spiking and persistent low-threshold spiking subtypes; input resistance >500 M Ω in persistent low-threshold spiking subtype) were excluded from the analysis.

Neurons were patched in whole-cell voltage-clamp configurations using borosilicate glass electrodes (3-5 M Ω) filled with cesium-based (voltage-clamp) or potassium methanesulfonate-based internal solution. Cesium based solution containing (in mM) respectively: 120 CsMeSO₃, 15 CsCl, 8 NaCl, 0.5 EGTA, 10 HEPES, 2 MgATP, 0.3 NaGTP, 5 QX-314, pH 7.3. Potassium based solution containing (in mM): 130 KMeSO₃, 10 NaCl, 2 MgCl₂, 0.16 CaCl₂, 0.5 EGTA, 10 HEPES, 2 MgATP, 0.3 NaGTP, pH 7.3. Picrotoxin (50 μ M) was added to the external solution to block synaptic currents mediated by GABA_A receptors. Drugs were prepared as stock solutions and added to the ACSF to yield the final concentration.

Whole-cell voltage-clamp recordings were made using a MultiClamp 700B amplifier (Molecular Devices) and ITC-18 A/D board (HEKA). Data was acquired using Igor Pro 6.0 software (Wavemetrics) and custom acquisition routines (mafPC, courtesy of M. A. Xu-Friedman). Voltage-clamp recordings were filtered at 2 kHz and digitized at 10 kHz. All recorded neurons exhibited electrophysiological characteristics of medium spiny neurons. Synaptic currents were monitored at a holding potential of -70 mV. Series resistance and leak currents were monitored continuously. Miniature EPSCs were recorded at -70 mV in 1 μ M TTX and 50 μ M picrotoxin. Only cells with at least 500 events were included in the analysis. Cumulative probability plots were generated from 500 randomly selected mEPSC events. Evoked EPSCs onto medium spiny neurons were

elicited in the presence of picrotoxin (50 μ M) with a stimulus isolator (IsoFlex, AMPI) and a glass electrode placed dorsolateral to the recorded neuron, typically 100-200 μ m away. Stimulus intensity was adjusted to yield EPSC amplitudes of approximately 400 pA. Stimulus duration was 300 μ s. For evaluation of the paired pulse ratio, two stimuli were given at variable interstimulus intervals (ISIs; 25, 50, 100, 200, 500 ms) with a 20 sec intertrial interval. Paired-pulse ratio is defined as EPSC₂/EPSC₁. Five-eight repetitions at each ISI were averaged to yield the PPR for that ISI. For monitoring of EPSC amplitude over time, two pulses delivered with 50 ms interstimulus interval were given every 20 seconds. For AMPA/NMDA ratio experiments, one stimulus at -70 mV or +40 mV was given every 20 seconds, at 15-20 repetitions per holding potential. AMPA/NMDA ratios were calculated as the ratio of the magnitude of the EPSC at +40 mV at 50 ms following stimulation (NMDA) to the peak of the EPSC at -70 mV (AMPA).

Monosynaptic Rabies Tracing:

D1-Cre and A2a-Cre mice were used to perform monosynaptic retrograde tracing onto direct and indirect pathway neurons, respectively. Groups of healthy (non-depleted) and parkinsonian, levodopa-treated mice were used within each genotype. Mice were rendered parkinsonian as described above. Four weeks after dopamine depletion, animals received daily injections of levodopa. Parkinsonian mice (one week into daily levodopa injections) or untreated, healthy mice, were then anesthetized and a Cre-dependent helper virus (AAV-DIO- sTpEpB-GFP) was stereotaxically injected into the left DLS (ipsilateral to the depletion in parkinsonian mice). The helper virus expresses the EnvA receptor, TVA, and rabies glycoprotein necessary for rabies infection and replication in a cell-type specific manner, termed “starter cells,” which are labeled with the

green fluorophore GFP. Animals are allowed to recover for two weeks, at which point they are anesthetized and a replication-incompetent form of the rabies virus (EnvA-G-deleted-rabies-mCherry) is stereotaxically injected into the DLS using the same coordinates. The rabies virus will then infect a subset of starter cells and travel retrogradely one synapse, expressing the red fluorophore mCherry in infected cells. Once the rabies virus infects a presynaptic neuron, uninfected with the helper virus, it will no longer be capable of replication and/or retrograde synaptic infection. Rabies injections were performed in an approved Biosafety Level 2 (BSL-2) surgical suite. Animals were then allowed to recover for ten days, at which point they were terminally anesthetized with ketamine/xylazine (200/40 mg/kg I.P.), transcardially perfused with 4% paraformaldehyde (PFA), and the brain dissected from the skull. The brain was post-fixed overnight in 4% PFA and then placed in 30% sucrose at 4°C.

Parkinsonian, levodopa-treated FosTRAP mice were prepared in a similar fashion as D1-Cre and A2a-Cre mice, with some alterations made to the experimental timeline to accommodate helper virus expression using the conditional Cre (CreER) in the FosTRAP line. In FosTRAP mice, helper virus was injected in the left DLS at the same time as the initial dopamine depletion. Three weeks after dopamine depletion, FosTRAP mice began daily levodopa injections. After one week of daily levodopa injections, as above, FosTRAP mice were injected with levodopa followed by an injection of 4-OHT, allowing for recombination and expression of the helper virus. Two weeks later, FosTRAP mice were anesthetized and the modified rabies virus was injected using the same procedures described above. The remainder of the experimental timeline was similar to that for D1-Cre and A2a-Cre mice as described above.

Fixed brains, stored in sucrose, were then sent to Charles Gerfen at the NIMH for sectioning, mounting, imaging, and analysis using published methods (Eastwood et al., 2018). Briefly, brains were sectioned coronally at 50 μm using a freezing microtome. Slices are then imaged using a Zeiss microscope equipped with a z axis drive, imaging each fluorophore

Histology & Microscopy:

After rabies tracing or behavioral experiments, mice were deeply anesthetized with IP ketamine-xylazine and transcardially perfused with 4% paraformaldehyde in PBS. Following *in vivo* electrophysiology experiments, prior to perfusion, electrode array location was marked by electrolytic lesioning. After deep anesthesia, the implant was connected to a solid state, direct current (DC) Lesion Maker (Ugo Basile). A current of 100 μA was passed through each microwire for 5 seconds. After perfusion, the brain was dissected from the skull and post-fixed overnight in 4% paraformaldehyde, then placed in 30% sucrose at 4°C for cryoprotection. The brain was then cut into 35 μm coronal or sagittal sections on a freezing microtome (Leica) and then mounted in Vectashield Mounting Medium onto glass slides for imaging. For immunohistochemistry, the tissue was blocked with 3% normal donkey serum (NDS) and permeabilized with 0.1% Triton X-100 for 2 hours at room temperature on a shaker. Primary antibodies were added to 3% NDS and incubated overnight at 4° C on a shaker. Primary antibodies used: Rabbit anti-TH (Pel-Freez, 1:1000), Chicken anti-TH (Sigma, 1:1000), and Chicken anti-GFP (1:500). Slices were then incubated in secondary antibodies (donkey anti-rabbit or chicken Alexafluor 488, 593, or 647, 1:500, JacksonImmuno Research) for 2-4 hours at 4°C on a

shaker, washed, and mounted onto slides for imaging. 4 or 10x images were acquired on a Nikon 6D conventional widefield microscope.

For slice electrophysiology experiments in which the internal solution contained biocytin, slices were subsectioned at 50 μ m and washed in PBS. Slices were blocked for 2 hours at room temperature on a shaker in a 5% NDS and 0.3% Tween-20 PBS-based solution. Primary antibodies were the same as described above. Slices were then incubated in secondary antibodies (donkey anti-rabbit or chicken Alexafluor 488, 593, or 647, 1:500, JacksonImmuno Research and Streptavidin Alexa 350, 3:500, Sigma) for 6-12 hours at 4°C on a shaker, washed, and mounted onto slides for imaging. Images were acquired on a Nikon 6D conventional widefield or Nikon Spinning Disk confocal microscope with a 40x objective microscope. Exposure times were matched between images of the same type

Quantification and Statistical Analysis

Behavior:

Dyskinesia was quantified using a standard scoring method (Cenci and Lundblad, 2007), which takes into account abnormal involuntary movements (AIMs) in axial, limb, and orofacial (ALO) body segments. Briefly, dyskinesia was quantified every 20 minutes, over a two-hour period, using a scale of 0-4. A score of 0 indicates no abnormal movement, and a score of 4 describes continuous and uninterrupted dyskinetic movements; 12 (4 x 3 body segments) is the maximum score possible for a given time point.

***In Vitro* Electrophysiology:**

Comparisons of mEPSC frequency and amplitude from TRAPed dMSNs, unTRAPed dMSNs, and unTRAPed iMSNs were made with a One-Way ANOVA with Tukey post hoc test after reaching a predetermined n of 20 cells per group.

***In Vivo* Electrophysiology:**

For the majority of analyses of single-unit firing rate and behavior, firing rate was averaged in 1 minute bins. Modulation of firing rate by levodopa was determined by comparing single-unit firing rates before and after drug administration, during the peak behavioral effects. The 30-minute baseline period was compared to a 30-minute period following drug injection (10-40 minutes post-injection). Following levodopa administration, unlabeled single-units were categorized into three broad groups as follows, based on significant changes in firing rate ($p < 0.01$, Wilcoxon rank-sum test (denoted Mann-Whitney)) following levodopa treatment: putative dMSNs (On MSNs, increase in firing rate), putative iMSNs (Off MSNs, decrease in firing rate), or no change units (NC, nonsignificant change in firing rate) (Figure 1E). For levodopa sessions, putative dMSNs were further divided using rate-based and behavior-based methods.

For the rate-based method, we compared single-unit firing rates of putative dMSNs from parkinsonian mice after levodopa injection to the firing rates of healthy mice. We calculated the 99% confidence interval of firing rate for all single-units recorded in healthy mice and used the upper bound of this interval as our threshold. A putative dMSN was classified as High FR if the post-levodopa firing rate (10-40 minutes post-injection of levodopa) exceeded the 99% confidence interval of MSNs from healthy mice in any single bin. For the behavior-based method, AIM scores were also averaged in 1 minute bins and

correlated with firing rate using linear regression. Labeled TRAPed neurons or putative dMSNs with a significant correlation ($R^2 > 0.35$) to AIM score were labeled dyskinesia (DYSK) units and those with no significant correlation ($R^2 < 0.35$) to AIMs were classified as on-unclassified (ON) units (Figures 1H-J).

Firing rates recorded in the ipsilesional striatum of parkinsonian mice before (Park) or after (LID) levodopa were compared to recordings from healthy mice (Ctrl, Figures 1F) using Mann-Whitney tests. Firing rates of parkinsonian mice before (Park) and after drug administration (levodopa (LID), Figure 1F) were compared using Wilcoxon signed-rank test (denoted Wilcoxon). Comparisons of firing rates between labeled TRAPed neurons, putative dMSN subtypes (ON and DYSK), and MSNs in healthy controls were made using a One-Way ANOVA with Tukey post hoc test (Figure 1F).

4.6 Author Contributions and Acknowledgments

Author Contributions

AEG, MBR, and ABN designed all experiments. AEG, MBR, and ABN performed all *in vivo* experiments. AEG, MBR, CJBM, XT, and RRB performed surgical experiments. AEG, MBR, MMM, and ABN performed slice physiology experiments. CRG processed, analyzed, and consulted on all monosynaptic rabies injected brains. RRB assisted with immunohistochemistry. AEG and ABN wrote the manuscript with contributions from all authors.

Acknowledgments

We thank Match McGregor, Jonathan Schor, Guy Bouvier, Rea Brakaj, Kevin Bender, Anatol Kreitzer, and Philip Starr for valuable discussion. This work was supported by the Parkinson's Foundation (PDF-JFA-1688) (ABN), NINDS 1R01NS101354 (ABN), National Science Foundation Graduate Research Fellowship (AEG), UCSF Discovery Fellows Program (AEG), F31 NS106827 (MBR). ABN is the Richard and Shirley Cahill Endowed Chair in Parkinson's Disease Research.

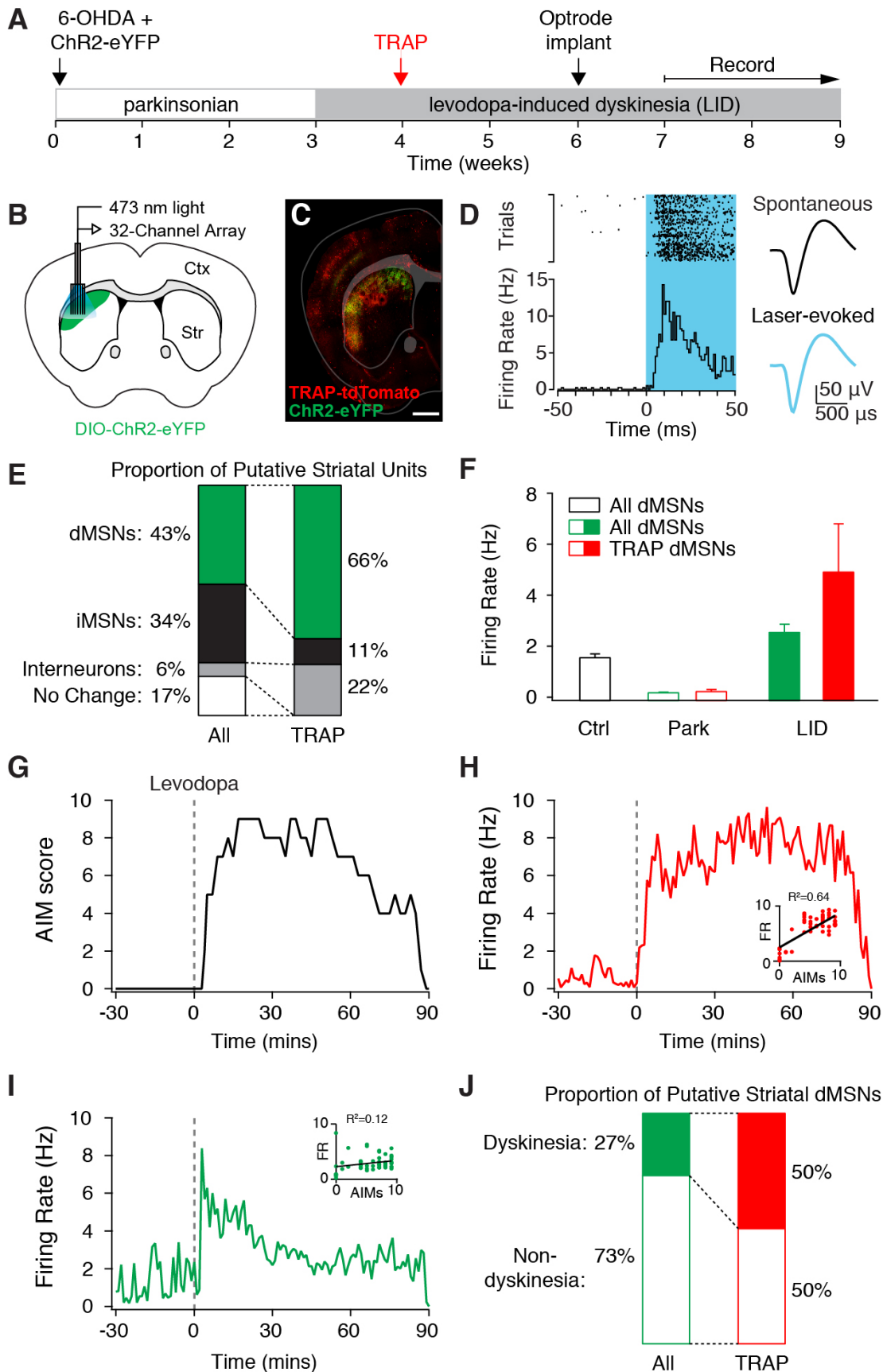


Figure 1: Levodopa evokes high firing rates in TRAPed neurons, which correlate with dyskinesia severity. A. Experimental timeline for *in vivo* single unit recordings in parkinsonian FosTRAP mice. B. Coronal schematic of optrode recording configuration (left) and representative histological section from a parkinsonian FosTRAP mouse injected with DIO-ChR2-eYFP (right). All recordings are ipsilateral to the injection of 6-OHDA. D. Representative optogenetically-identified unit, showing short-latency response to blue light pulses. Top: rasterized firing over 1,000 trials at 4 mW. Bottom: peristimulus time histogram showing average short-latency response across 4,000 trials. E. Proportions of putative striatal units found in all cells recorded compared to optogenetically labeled TRAPed neurons. Note: increased proportion of putative direct pathway neurons found in TRAPed cells. F. Average firing rate of putative direct pathway neurons in healthy mice (Ctrl) and parkinsonian mice before (Park) and after (LID) levodopa injection, comparing all putative direct pathway neurons to optogenetically labeled TRAPed cells. G. Example AIM score from a session in which a TRAPed neuron was optogenetically identified. Levodopa was administered at time zero (dotted line). H. Example firing rate of an optogenetically labeled TRAPed neuron in response to an intraperitoneal (IP) injection of levodopa. Inset: correlation of firing rate to AIMs, $R^2 = 0.64$. I. Example firing rate of a putative direct pathway neuron in response to an IP injection of levodopa. Inset: correlation of firing rate to AIMs, $R^2 = 0.12$. J. Proportion of putative direct pathways neurons that correlate to dyskinesia in all cells recorded compared to optogenetically labeled TRAPed cells. Dyskinesia-correlated units are enriched in labeled TRAPed cells. n = cells, N = animals. Scale bar in C = 1mm. All data presented as mean +/- SEM.

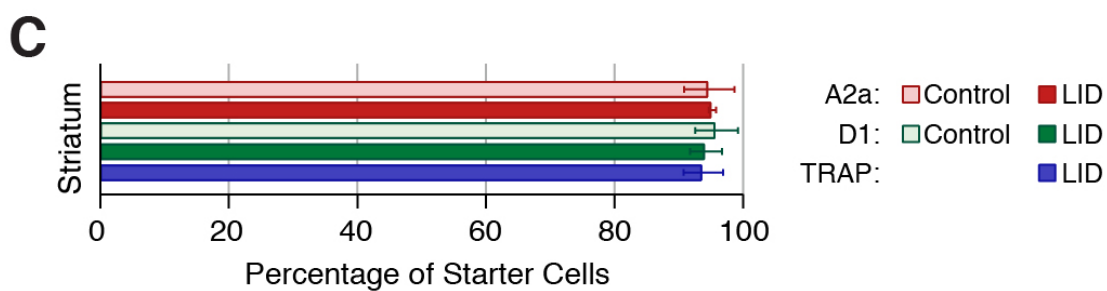
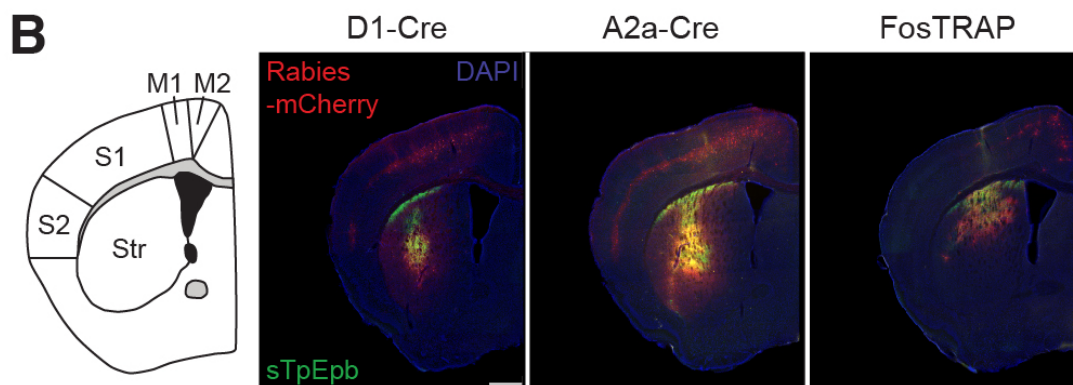
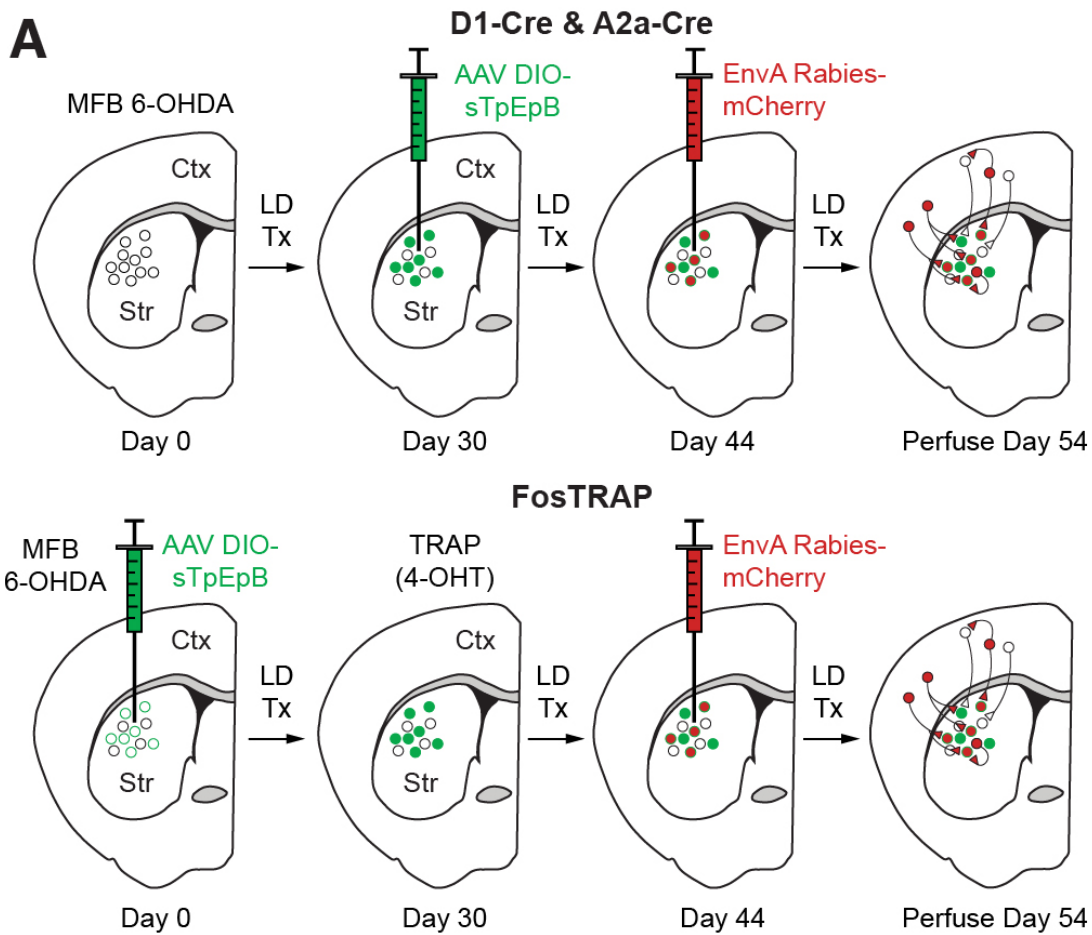


Figure 2. Experimental design for monosynaptic rabies tracing studies. A. Schematic of Cre-dependent rabies tracing workflow. (Top) Adult D1-Cre and A2a-Cre mice were treated with saline or rendered parkinsonian (injection of 6-OHDA) and injected with AAV1-DIO- sTpEpB in the dorsolateral striatum (DLS). (Bottom) FosTRAP mice were rendered parkinsonian and injected with AAV1-DIO- sTpEpB as above. After treating 6-OHDA treated animals with levodopa and administration of 4-hydroxytamoxifen (4-OHT) for Cre-dependent recombination (TRAP) in FosTRAP animals, all mice were injected in the DLS with modified monosynaptic EnvA Rabies-mCherry virus. Animals were perfused 10 days after rabies injection to visualize presynaptic inputs onto direct (D1-expressing) and indirect (A2a-expressing) pathway and FosTRAP neurons. B. Left: coronal schematic illustrating anatomical areas of interest in the ipsilateral hemisphere. Right: representative histological sections from representative dopamine-depleted and levodopa treated D1-Cre, A2a-Cre, and FosTRAP mice injected with DIO-sTpEpB and EnvA Rabies-mCherry. C. Percentage of starter cells found within the striatum for D1-Cre, A2a-Cre, and FosTRAP animals. Healthy mice: N = 4 D1-Cre, 3 A2a-Cre, Parkinsonian mice treated with levodopa (LID): 4 D1-Cre, 4 A2a-Cre, 4 FosTRAP. Abbreviations: Str (striatum), M1 (primary motor cortex), M2 (secondary motor cortex), S1 (primary somatosensory cortex), S2 (secondary somatosensory cortex). Scale bar in C = 1 mm. All data presented as mean +/- SEM.

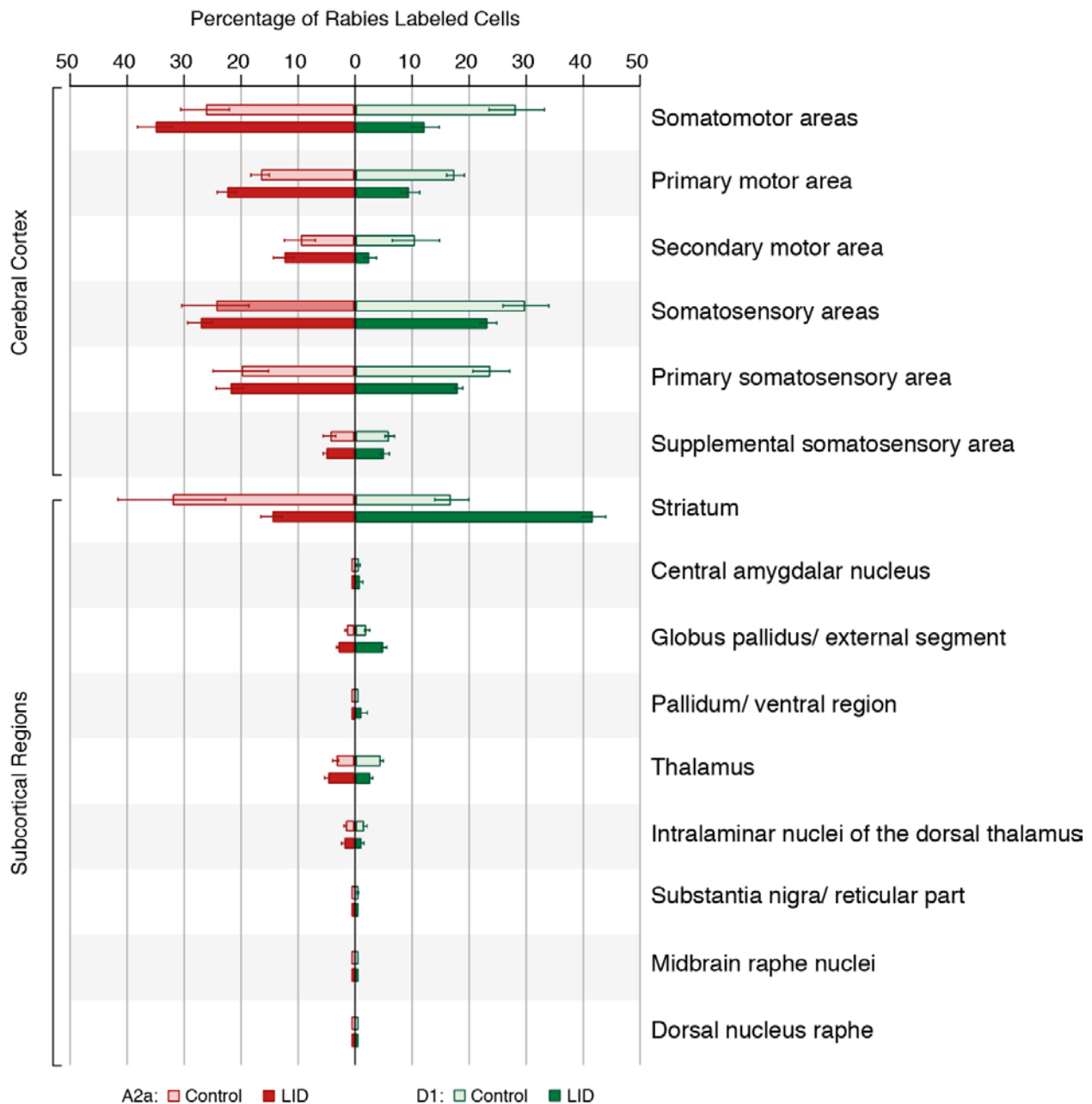


Figure 3: Summary of monosynaptic inputs onto direct and indirect pathway neurons in healthy and 6-OHDA/levodopa treated mice. Monosynaptic inputs onto direct pathway neurons are summarized in green (healthy mice = light green and parkinsonian mice treated with levodopa (LID) = dark green) and inputs onto indirect pathway neurons are summarized in red (healthy mice = pink and parkinsonian mice treated with levodopa (LID) = red). Healthy mice: N = 4 D1-Cre, 3 A2a-Cre, Parkinsonian mice treated with levodopa: N=4 D1-Cre, 4 A2a-Cre. All data presented as mean +/- SEM.

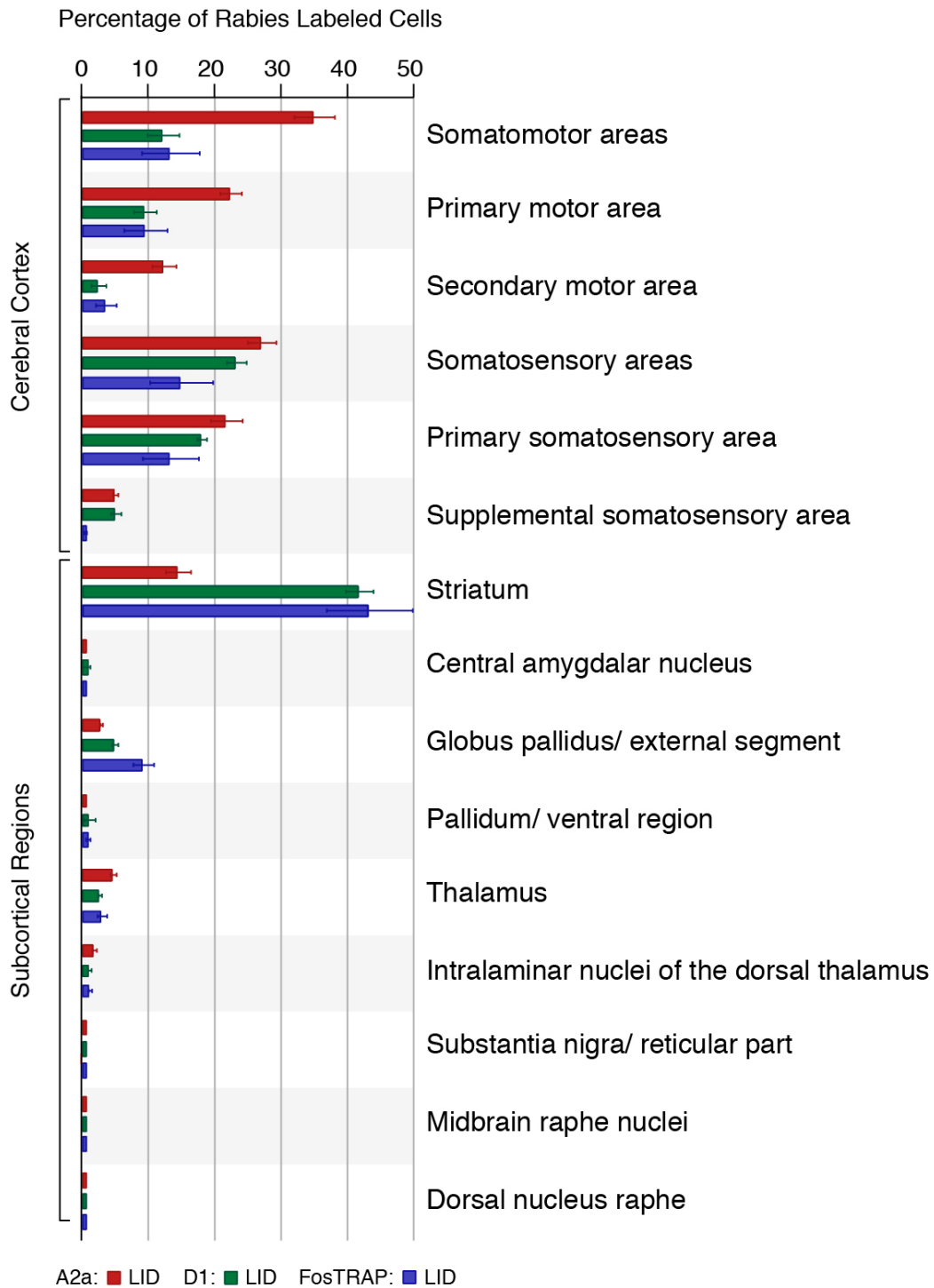


Figure 4: Comparison of monosynaptic inputs onto striatal direct, indirect, and TRAPed neurons in parkinsonian mice treated with levodopa. Monosynaptic inputs onto direct and indirect pathway neurons are summarized in green and red, respectively, while those onto FosTRAP neurons are summarized in blue. N = 3 D1-Cre, 3 A2a-Cre, and 3 FosTRAP mice. All data presented as mean +/- SEM.

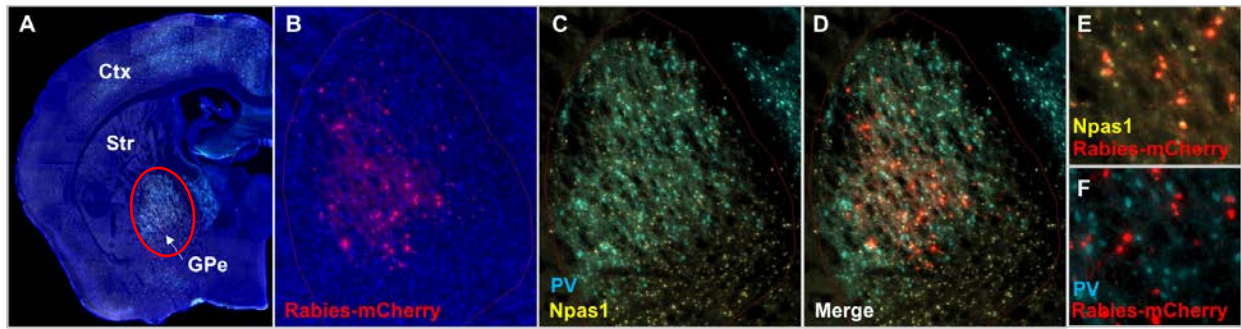


Figure 5: TRAPed neurons show increased presynaptic input from Npas1+ GPe neurons.
 A. Representative 4x coronal histological section showing rabies labeled presynaptic inputs to TRAPed striatal neurons. B. 10x magnification image showing rabies labeled neurons in A from GPe. C. 10x magnification image of PV and Npas1 positive interneurons in the GPe. D. Merge of B and C. E. High magnification image showing colocalization of Npas1 positive and rabies-mCherry labeled cells in the GPe. F. High magnification image showing no overlap between PV positive and rabies-mCherry labeled cells in the GPe.

Percentage of Cortical Rabies Labeled Cells

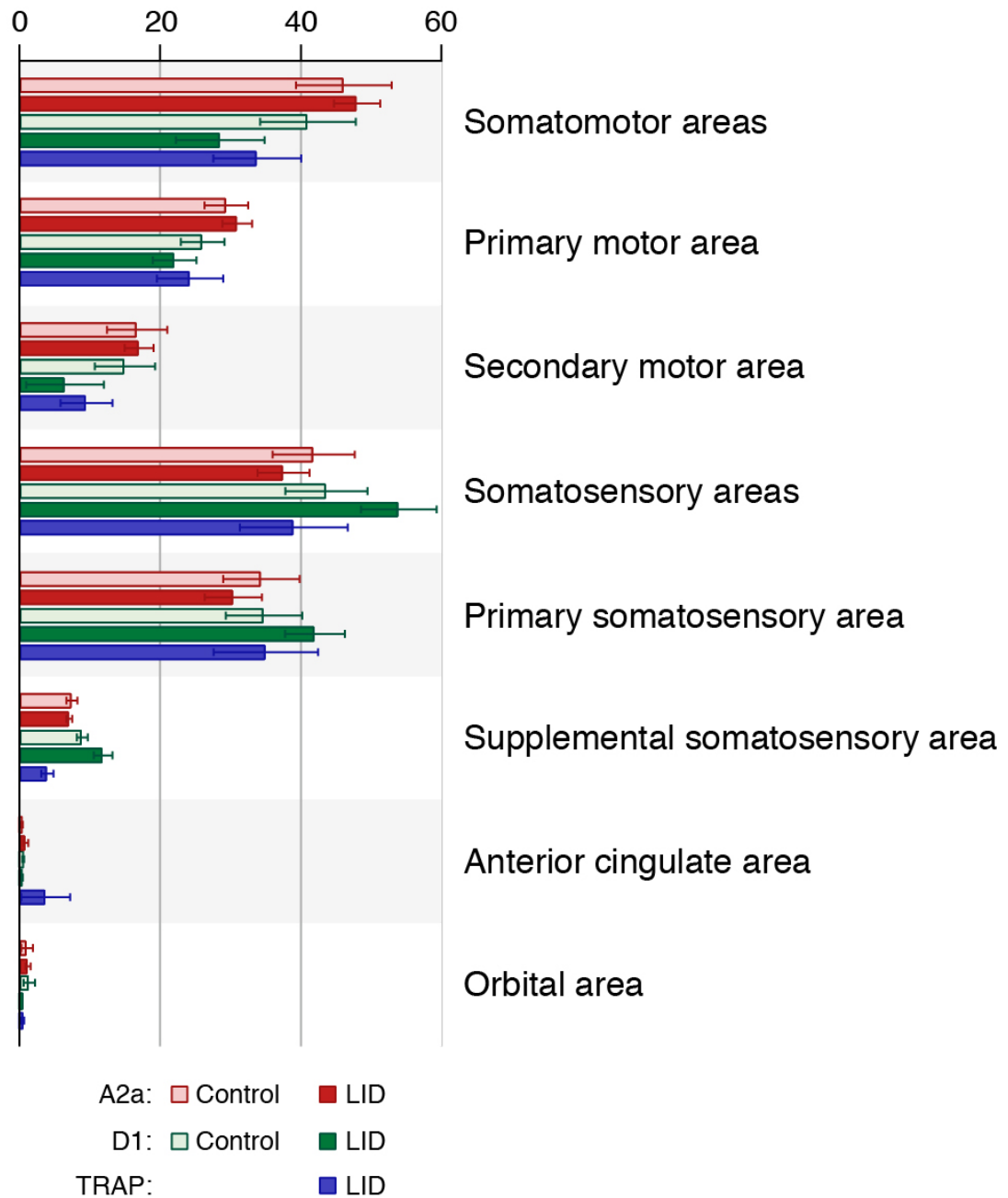


Figure 6: Summary of cortical inputs onto direct pathway and indirect pathway, and FosTRAP neurons in healthy and 6-OHDA and levodopa treated mice. Direct pathway neurons are labeled in green (healthy mice = light green and 6-OHDA/levodopa treated mice = dark green), indirect pathway neurons are labeled in red (healthy mice = pink and 6-OHDA/levodopa treated mice = red), and FosTRAP mice are labeled in blue. N = 4 D1-Cre healthy, 3 A2a-Cre healthy, 4 D1-Cre 6-OHDA/levodopa, 4 A2a-Cre 6-OHDA/levodopa, and 4 FosTRAP 6-OHDA/levodopa treated mice. All data presented as mean +/- SEM.

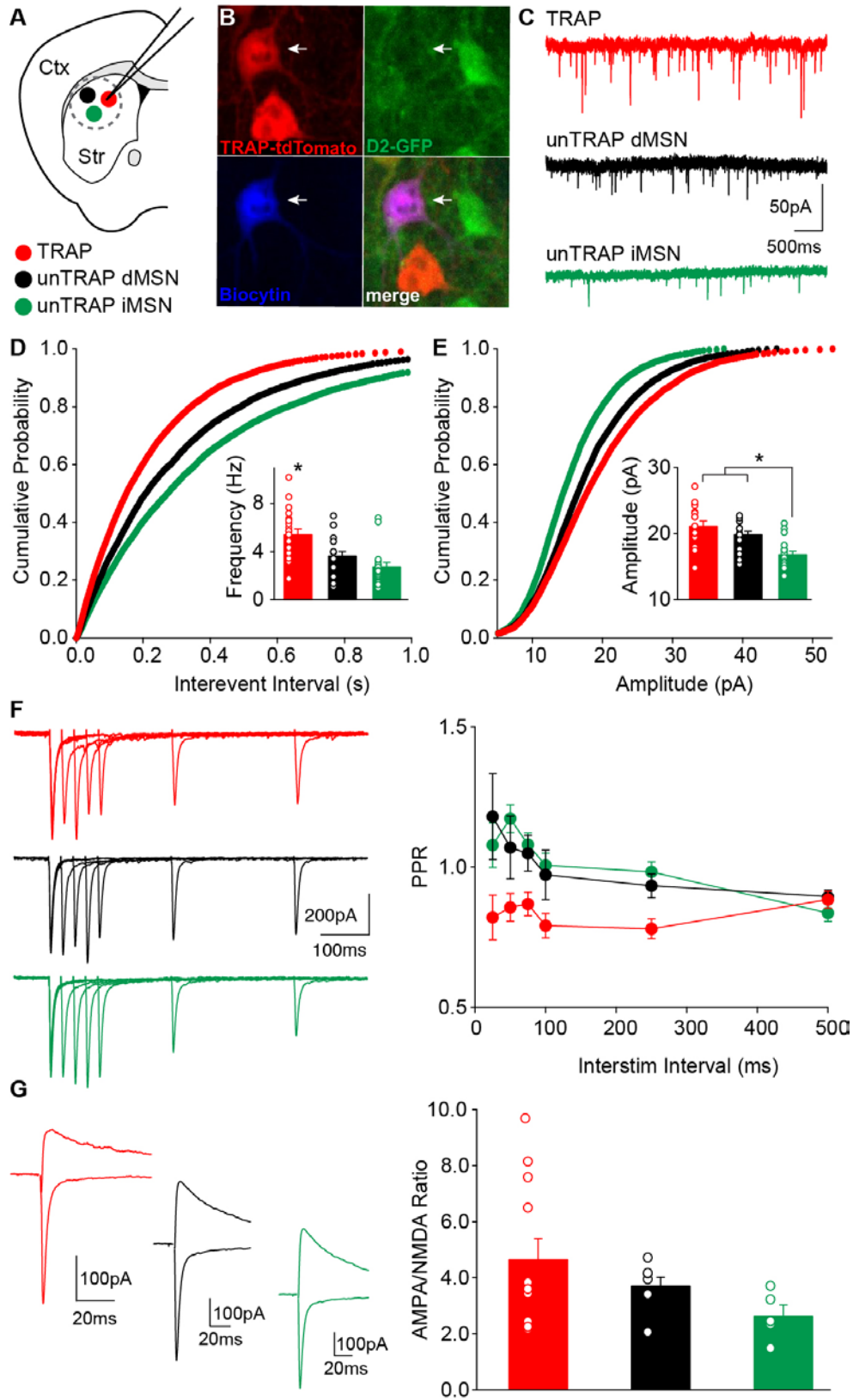


Figure 7. Excitatory transmission is preferentially increased onto TRAPed neurons in 6-OHDA/levodopa treated mice. A. Coronal schematic from a FosTRAP;Ai14;D2-GFP mouse illustrating slice electrophysiology configuration. This configuration allows the ability to record TRAPed dMSNs, unTRAPed dMSNs, and D2-GFP positive unTRAPed iMSNs in one preparation. B. Confocal image showing a biocytin filled (blue) TRAPed neuron (red) that is negative for D2-GFP. C. Representative traces of miniature excitatory postsynaptic currents (mEPSCs) from TRAPed dMSNs (red), unTRAPed dMSNs (black), and unTRAPed iMSNs (green). D. mEPSC frequency cumulative histogram. Inset: Average mEPSC frequencies from TRAPed dMSNs, unTRAPed dMSNs, and unTRAPed iMSNs. Note: increased mEPSC frequency onto TRAPed neurons. E. mEPSC amplitude cumulative histogram. Inset: Average mEPSC amplitude from TRAPed dMSNs, unTRAPed dMSNs, and unTRAPed iMSNs. Note: increased mEPSCs amplitude onto TRAPed and unTRAPed dMSNs. F-G. Electrically evoked EPSCs in slices from FosTRAP;Ai14;D2-GFP mice. F. Left: Representative EPSCs with 25, 50, 75, 100, 150, and 500 ms interstim interval (ISI). Right: Average paired pulse ratio (PPR) of evoked EPSCs onto TRAPed and unTRAPed dMSNs and unTRAPed iMSNs. G. Left: Representative EPSC traces recorded at -70 mV and +40 mV in TRAPed and unTRAPed dMSNs and unTRAPed iMSNs. Right: Average ratio of the AMPA-receptor EPSC (peak at -70 mV) to the NMDA-receptor EPSC (measured at 50 ms after stimulus at +40 mV) for TRAPed dMSNs, unTRAPed dMSNs, and unTRAPed iMSNs. All values are displayed as average \pm SEM.

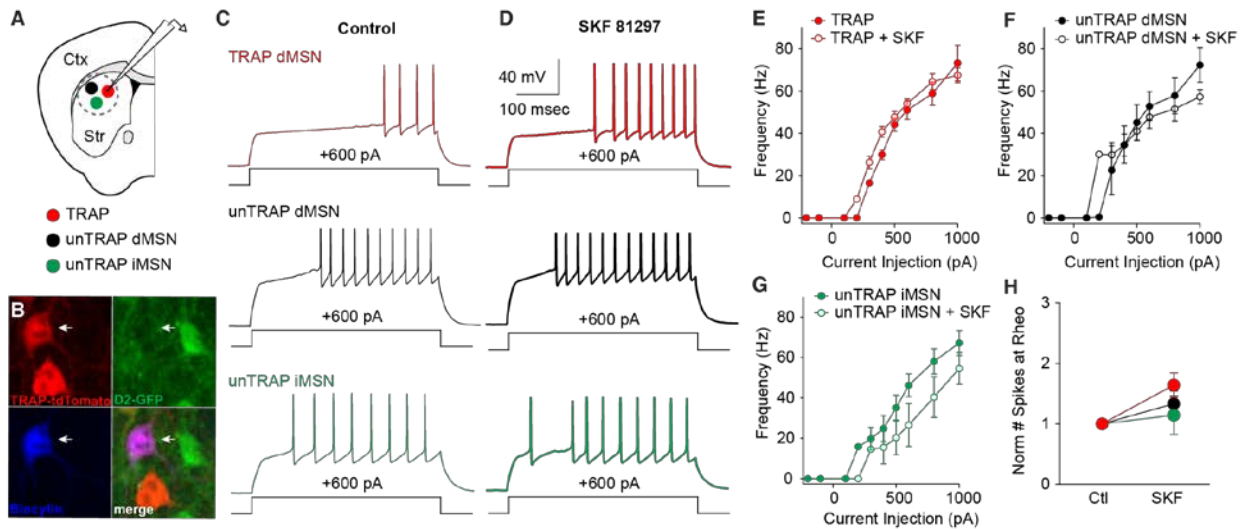


Figure 8: Intrinsic excitability is not altered in striatal medium spiny neurons in the presence of dopamine agonists in LID mice. A. Coronal schematic from a FosTRAP;Ai14;D2-GFP mouse illustrating slice electrophysiology configuration. This configuration allows the ability to record TRAPed dMSNs, unTRAPed dMSNs, and D2-GFP positive iMSNs in one preparation. B. Confocal image showing a biocytin filled (blue) TRAPed neuron (red) that is negative for D2-GFP. C-D. Current clamp recordings from TRAPed dMSNs, unTRAPed dMSNs, and unTRAPed iMSNs before and after 5 μ M SKF 81297. C. Representative control TRAP dMSNs, unTRAP dMSNs, and unTRAP iMSNs displaying responses to a +600 pA current injection. D. Representative TRAP dMSNs, unTRAP dMSNs, and unTRAP iMSNs displaying responses to a +600 pA current injection after 5 μ M SKF 81297. E. Summary of firing frequency in response to injected current before and after SKF 81297 in TRAPed dMSNs. F. Summary of firing frequency in response to injected current before and after SKF 81297 in unTRAPed dMSNs. G. Summary of firing frequency in response to injected current before and after SKF 81297 in unTRAPed iMSNs. H. Normalized # of action potentials seen at rheobase in control and after SKF 81297. All values are displayed as average \pm SEM.

Parameters	TRAP	TRAP + SKF	unTRAP dMSN	unTRAP dMSN + SKF	unTRAP iMSN	unTRAP iMSN + SKF
Rin (MOhms)	88 +/- 31	87 +/- 8	70 +/- 10	111 +/- 40	61 +/- 6	74 +/- 10
Vm (mV)	-91 +/- 1.8	-89 +/- 3.0	-92 +/- 1.0	-88 +/- 2	-88 +/- 2.0	-84 +/- 3.0
Rheobase (pA)	380 +/- 40	320 +/- 20	330 +/- 45	300 +/- 32	450 +/- 80	483 +/- 70
AP threshold (mV)	-35 +/- 1.6	-34 +/- 3.1	-41 +/- 2.0	-37 +/- 1.8	-43 +/- 3.4	-39 +/- 7.0
AHP amplitude (mV)	15 +/- 0.4	15 +/- 0.9	15 +/- 1.7	14 +/- 1.5	16 +/- 1.1	19 +/- 3.8
Half width (ms)	1.5 +/- 0.10	1.5 +/- 0.16	1.2 +/- 0.09	1.2 +/- 0.14	1.1 +/- 0.17	1.0 +/- 0.30

Table 1: *Ex vivo* excitability parameters for TRAPed dMSNs, unTRAPed dMSNs, and unTRAPed iMSNs before and after SKF 81297. Intrinsic excitability measurements recorded in TRAPed cells, unTRAPed dMSNs, and unTRAPed iMSNs before and after application of 5 μ M SKF81927. Rin = input resistance, Vm = resting membrane potential, AP threshold = action potential threshold, AHP amplitude = amplitude of the action potential afterhyperpolarization. Rheobase is the minimum amplitude current step (of 450 msec duration) that evoked spiking. Half width is the width of the action potential at half-maximal spike amplitude. All values are displayed as average \pm SEM.

4.9 References

- Albin, R.L., Young, A.B., and Penney, J.B. (1989). The functional anatomy of basal ganglia disorders. *Trends Neurosci* 12, 366-375.
- Alcacer, C., Andreoli, L., Sebastianutto, I., Jakobsson, J., Fieblinger, T., and Cenci, M.A. (2017). Chemogenetic stimulation of striatal projection neurons modulates responses to Parkinson's disease therapy. *J Clin Invest* 127, 720-734.
- Alexander, G.E., and Crutcher, M.D. (1990). Functional architecture of basal ganglia circuits: neural substrates of parallel processing. *Trends Neurosci* 13, 266-271.
- Azdad, K., Chavez, M., Don Bishop, P., Wetzelaer, P., Marescau, B., De Deyn, P.P., Gall, D., and Schiffmann, S.N. (2009). Homeostatic plasticity of striatal neurons intrinsic excitability following dopamine depletion. *PLoS One* 4, e6908.
- Bagetta, V., Sgobio, C., Pendolino, V., Del Papa, G., Tozzi, A., Ghiglieri, V., Giampa, C., Zianni, E., Gardoni, F., Calabresi, P., *et al.* (2012). Rebalance of striatal NMDA/AMPA receptor ratio underlies the reduced emergence of dyskinesia during D2-like dopamine agonist treatment in experimental Parkinson's disease. *J Neurosci* 32, 17921-17931.
- Berendse, H.W., and Groenewegen, H.J. (1990). Organization of the thalamostriatal projections in the rat, with special emphasis on the ventral striatum. *J Comp Neurol* 299, 187-228.
- Berke, J.D., Okatan, M., Skurski, J., and Eichenbaum, H.B. (2004). Oscillatory entrainment of striatal neurons in freely moving rats. *Neuron* 43, 883-896.
- Borgkvist, A., Avegno, E.M., Wong, M.Y., Kheirbek, M.A., Sonders, M.S., Hen, R., and Sulzer, D. (2015). Loss of Striatonigral GABAergic Presynaptic Inhibition Enables Motor Sensitization in Parkinsonian Mice. *Neuron* 87, 976-988.
- Cenci, M.A., and Lundblad, M. (2007). Ratings of L-DOPA-induced dyskinesia in the unilateral 6-OHDA lesion model of Parkinson's disease in rats and mice. *Curr Protoc Neurosci Chapter 9, Unit 9 25*.
- Cohen, J.Y., Haesler, S., Vong, L., Lowell, B.B., and Uchida, N. (2012). Neuron-type-specific signals for reward and punishment in the ventral tegmental area. *Nature* 482, 85-88.
- Day, M., Wang, Z., Ding, J., An, X., Ingham, C.A., Shering, A.F., Wokosin, D., Ilijic, E., Sun, Z., Sampson, A.R., *et al.* (2006). Selective elimination of glutamatergic synapses on striatopallidal neurons in Parkinson disease models. *Nat Neurosci* 9, 251-259.
- DeLong, M.R. (1990). Primate models of movement disorders of basal ganglia origin. *Trends Neurosci* 13, 281-285.

Ding, J., Peterson, J.D., and Surmeier, D.J. (2008). Corticostriatal and thalamostriatal synapses have distinctive properties. *J Neurosci* 28, 6483-6492.

Eastwood, B.S., Hooks, B.M., Paletzki, R.F., O'Connor, N.J., Glaser, J.R., and Gerfen, C.R. (2018). Whole mouse brain reconstruction and registration to a reference atlas with standard histochemical processing of coronal sections. *J Comp Neurol*.

Fieblinger, T., and Cenci, M.A. (2015). Zooming in on the small: the plasticity of striatal dendritic spines in L-DOPA-induced dyskinesia. *Mov Disord* 30, 484-493.

Fieblinger, T., Graves, S.M., Sebel, L.E., Alcacer, C., Plotkin, J.L., Gertler, T.S., Chan, C.S., Heiman, M., Greengard, P., Cenci, M.A., *et al.* (2014). Cell type-specific plasticity of striatal projection neurons in parkinsonism and L-DOPA-induced dyskinesia. *Nat Commun* 5, 5316.

Gage, G.J., Stoetzner, C.R., Wiltschko, A.B., and Berke, J.D. (2010). Selective activation of striatal fast-spiking interneurons during choice execution. *Neuron* 67, 466-479.

Gerfen, C.R. (1992). The Neostriatal Mosaic - Multiple Levels of Compartmental Organization in the Basal Ganglia. *Annual Review of Neuroscience* 15, 285-320.

Gerfen, C.R., and Bolam, J.P. (2010). The Neuroanatomical Organization of the Basal Ganglia. *Hbk Behav Neurosci* 20, 3-28.

Gerfen, C.R., Engber, T.M., Mahan, L.C., Susel, Z., Chase, T.N., Monsma, F.J., Jr., and Sibley, D.R. (1990). D1 and D2 dopamine receptor-regulated gene expression of striatonigral and striatopallidal neurons. *Science* 250, 1429-1432.

Girasole, A.E., Lum, M.Y., Nathaniel, D., Bair-Marshall, C.J., Guenther, C.J., Luo, L., Kreitzer, A.C., and Nelson, A.B. (2018). A Subpopulation of Striatal Neurons Mediates Levodopa-Induced Dyskinesia. *Neuron* 97, 787-795 e786.

Gokce, O., Stanley, G.M., Treutlein, B., Neff, N.F., Camp, J.G., Malenka, R.C., Rothwell, P.E., Fuccillo, M.V., Sudhof, T.C., and Quake, S.R. (2016). Cellular Taxonomy of the Mouse Striatum as Revealed by Single-Cell RNA-Seq. *Cell Rep* 16, 1126-1137.

Gong, S., Zheng, C., Doughty, M.L., Losos, K., Didkovsky, N., Schambra, U.B., Nowak, N.J., Joyner, A., Leblanc, G., Hatten, M.E., *et al.* (2003). A gene expression atlas of the central nervous system based on bacterial artificial chromosomes. *Nature* 425, 917-925.

Graybiel, A.M. (2008). Habits, rituals, and the evaluative brain. *Annu Rev Neurosci* 31, 359-387.

Guenther, C.J., Miyamichi, K., Yang, H.H., Heller, H.C., and Luo, L. (2013). Permanent genetic access to transiently active neurons via TRAP: targeted recombination in active populations. *Neuron* 78, 773-784.

- Guo, Q., Wang, D., He, X., Feng, Q., Lin, R., Xu, F., Fu, L., and Luo, M. (2015). Whole-brain mapping of inputs to projection neurons and cholinergic interneurons in the dorsal striatum. *PLoS One* *10*, e0123381.
- Harris, K.D., Henze, D.A., Csicsvari, J., Hirase, H., and Buzsaki, G. (2000). Accuracy of tetrode spike separation as determined by simultaneous intracellular and extracellular measurements. *Journal of Neurophysiology* *84*, 401-414.
- Heiman, M., Heilbut, A., Francardo, V., Kulicke, R., Fenster, R.J., Kolaczyk, E.D., Mesirov, J.P., Surmeier, D.J., Cenci, M.A., and Greengard, P. (2014). Molecular adaptations of striatal spiny projection neurons during levodopa-induced dyskinesia. *Proc Natl Acad Sci U S A* *111*, 4578-4583.
- Hernandez-Lopez, S., Bargas, J., Surmeier, D.J., Reyes, A., and Galarraga, E. (1997). D1 receptor activation enhances evoked discharge in neostriatal medium spiny neurons by modulating an L-type Ca²⁺ conductance. *J Neurosci* *17*, 3334-3342.
- Hernandez, V.M., Hegeman, D.J., Cui, Q., Kever, D.A., Fiske, M.P., Glajch, K.E., Pitt, J.E., Huang, T.Y., Justice, N.J., and Chan, C.S. (2015). Parvalbumin+ Neurons and Npas1+ Neurons Are Distinct Neuron Classes in the Mouse External Globus Pallidus. *J Neurosci* *35*, 11830-11847.
- Hunnicutt, B.J., Jongbloets, B.C., Birdsong, W.T., Gertz, K.J., Zhong, H., and Mao, T. (2016). A comprehensive excitatory input map of the striatum reveals novel functional organization. *Elife* *5*.
- Ingham, C.A., Hood, S.H., and Arbuthnott, G.W. (1989). Spine density on neostriatal neurones changes with 6-hydroxydopamine lesions and with age. *Brain Res* *503*, 334-338.
- Jenner, P. (2008). Molecular mechanisms of L-DOPA-induced dyskinesia. *Nat Rev Neurosci* *9*, 665-677.
- Kravitz, A.V., Owen, S.F., and Kreitzer, A.C. (2013). Optogenetic identification of striatal projection neuron subtypes during in vivo recordings. *Brain Res* *1511*, 21-32.
- Liang, L., DeLong, M.R., and Papa, S.M. (2008). Inversion of dopamine responses in striatal medium spiny neurons and involuntary movements. *J Neurosci* *28*, 7537-7547.
- Liljeholm, M., and O'Doherty, J.P. (2012). Contributions of the striatum to learning, motivation, and performance: an associative account. *Trends Cogn Sci* *16*, 467-475.
- Lima, S.Q., Hromadka, T., Znamenskiy, P., and Zador, A.M. (2009). PINP: a new method of tagging neuronal populations for identification during in vivo electrophysiological recording. *PLoS One* *4*, e6099.

- Luscher, C., and Malenka, R.C. (2012). NMDA receptor-dependent long-term potentiation and long-term depression (LTP/LTD). *Cold Spring Harb Perspect Biol* 4.
- Mameli, M., Bellone, C., Brown, M.T., and Luscher, C. (2011). Cocaine inverts rules for synaptic plasticity of glutamate transmission in the ventral tegmental area. *Nat Neurosci* 14, 414-416.
- Mandelbaum, G., Taranda, J., Haynes, T.M., Hochbaum, D.R., Huang, K.W., Hyun, M., Venkataraju, K.U., Straub, C., Wang, W., Roberson, K., *et al.* (2019). Distinct Cortical-Thalamic-Striatal Circuits through the Parafascicular Nucleus. *Neuron*.
- Mastro, K.J., Bouchard, R.S., Holt, H.A., and Gittis, A.H. (2014). Transgenic mouse lines subdivide external segment of the globus pallidus (GPe) neurons and reveal distinct GPe output pathways. *J Neurosci* 34, 2087-2099.
- Nishijima, H., Suzuki, S., Kon, T., Funamizu, Y., Ueno, T., Haga, R., Suzuki, C., Arai, A., Kimura, T., Suzuki, C., *et al.* (2014). Morphologic changes of dendritic spines of striatal neurons in the levodopa-induced dyskinesia model. *Mov Disord* 29, 336-343.
- Papa, S.M., Desimone, R., Fiorani, M., and Oldfield, E.H. (1999). Internal globus pallidus discharge is nearly suppressed during levodopa-induced dyskinesias. *Ann Neurol* 46, 732-738.
- Parker, J.G., Marshall, J.D., Ahanonu, B., Wu, Y.W., Kim, T.H., Grewe, B.F., Zhang, Y., Li, J.Z., Ding, J.B., Ehlers, M.D., *et al.* (2018). Diametric neural ensemble dynamics in parkinsonian and dyskinesic states. *Nature* 557, 177-182.
- Parker, P.R., Lalive, A.L., and Kreitzer, A.C. (2016). Pathway-Specific Remodeling of Thalamostriatal Synapses in Parkinsonian Mice. *Neuron* 89, 734-740.
- Perez, X.A., Zhang, D., Bordia, T., and Quirk, M. (2017). Striatal D1 medium spiny neuron activation induces dyskinesias in parkinsonian mice. *Mov Disord* 32, 538-548.
- Picconi, B., Centonze, D., Hakansson, K., Bernardi, G., Greengard, P., Fisone, G., Cenci, M.A., and Calabresi, P. (2003). Loss of bidirectional striatal synaptic plasticity in L-DOPA-induced dyskinesia. *Nat Neurosci* 6, 501-506.
- Planert, H., Berger, T.K., and Silberberg, G. (2013). Membrane Properties of Striatal Direct and Indirect Pathway Neurons in Mouse and Rat Slices and Their Modulation by Dopamine. *Plos One* 8.
- Redgrave, P., Rodriguez, M., Smith, Y., Rodriguez-Oroz, M.C., Lehericy, S., Bergman, H., Agid, Y., DeLong, M.R., and Obeso, J.A. (2010). Goal-directed and habitual control in the basal ganglia: implications for Parkinson's disease. *Nat Rev Neurosci* 11, 760-772.

Ryan, M.B., Bair-Marshall, C., and Nelson, A.B. (2018). Aberrant Striatal Activity in Parkinsonism and Levodopa-Induced Dyskinesia. *Cell Rep* 23, 3438-3446 e3435.

Shen, W., Plotkin, J.L., Francardo, V., Ko, W.K., Xie, Z., Li, Q., Fieblinger, T., Wess, J., Neubig, R.R., Lindsley, C.W., *et al.* (2015). M4 Muscarinic Receptor Signaling Ameliorates Striatal Plasticity Deficits in Models of L-DOPA-Induced Dyskinesia. *Neuron* 88, 762-773.

Singh, A., Liang, L., Kaneoke, Y., Cao, X., and Papa, S.M. (2015). Dopamine regulates distinctively the activity patterns of striatal output neurons in advanced parkinsonian primates. *J Neurophysiol* 113, 1533-1544.

Smith, Y., Surmeier, D.J., Redgrave, P., and Kimura, M. (2011). Thalamic Contributions to Basal Ganglia-Related Behavioral Switching and Reinforcement. *Journal of Neuroscience* 31, 16102-16106.

Smith, Y., and Villalba, R. (2008). Striatal and extrastriatal dopamine in the basal ganglia: an overview of its anatomical organization in normal and Parkinsonian brains. *Mov Disord* 23 Suppl 3, S534-547.

Suarez, L.M., Solis, O., Carames, J.M., Taravini, I.R., Solis, J.M., Murer, M.G., and Moratalla, R. (2014). L-DOPA treatment selectively restores spine density in dopamine receptor D2-expressing projection neurons in dyskinetic mice. *Biol Psychiatry* 75, 711-722.

Tanimura, A., Du, Y., Kondapalli, J., Wokosin, D.L., and Surmeier, D.J. (2019). Cholinergic Interneurons Amplify Thalamostriatal Excitation of Striatal Indirect Pathway Neurons in Parkinson's Disease Models. *Neuron* 101, 444-458 e446.

Taverna, S., Ilijic, E., and Surmeier, D.J. (2008). Recurrent collateral connections of striatal medium spiny neurons are disrupted in models of Parkinson's disease. *J Neurosci* 28, 5504-5512.

Ungless, M.A., Whistler, J.L., Malenka, R.C., and Bonci, A. (2001). Single cocaine exposure in vivo induces long-term potentiation in dopamine neurons. *Nature* 411, 583-587.

Villalba, R.M., Lee, H., and Smith, Y. (2009). Dopaminergic denervation and spine loss in the striatum of MPTP-treated monkeys. *Exp Neurol* 215, 220-227.

Wall, N.R., De La Parra, M., Callaway, E.M., and Kreitzer, A.C. (2013). Differential innervation of direct- and indirect-pathway striatal projection neurons. *Neuron* 79, 347-360.

Zaja-Milatovic, S., Milatovic, D., Schantz, A.M., Zhang, J., Montine, K.S., Samii, A., Deutch, A.Y., and Montine, T.J. (2005). Dendritic degeneration in neostriatal medium spiny neurons in Parkinson disease. *Neurology* 64, 545-547.

Zhang, Y., Meredith, G.E., Mendoza-Elias, N., Rademacher, D.J., Tseng, K.Y., and Steece-Collier, K. (2013). Aberrant restoration of spines and their synapses in L-DOPA-induced dyskinesia: involvement of corticostriatal but not thalamostriatal synapses. *J Neurosci* 33, 11655-11667.

CHAPTER 5

Conclusion

The work presented in this dissertation provides new insights into striatal dysfunction in hyperkinetic movement disorders. We have demonstrated that alterations in striatal activity are critical for generating dyskinesia in two etiologically distinct mouse models (Chapter 2 and 3), and that changes in presynaptic striatal excitatory plasticity may be a common underlying mechanism (Chapter 2 and 4).

Perhaps the most exciting finding in this dissertation is in the discovery that two forms of dyskinesia, LID and PNKD, are characterized by profound dysfunction in different basal ganglia pathways, but may share both upstream causes (aberrant synaptic plasticity) and downstream changes in circuit function (an imbalance in the direct and indirect pathways). In PNKD we found profound reductions in striatal indirect pathway activity underlying dyskinesia, whereas in LID abnormally high firing rates in striatal direct pathway neurons seem to drive dyskinetic behavior. If propagated to downstream basal ganglia as predicted by the classical model, these changes in striatal firing could converge at the level of basal ganglia output (strongly inhibiting SNr/GPi firing) and disinhibit motor patterns.

Though this simple model is attractive, our work in Chapters 3 and 4 identified functional heterogeneity within the direct pathway. Given the diversity of functions associated with the striatum, from regulation of motivation and mood to contextually appropriate decision-making, to fine calibration of movement, it is not surprising that there would be interconnected physiological and functional diversity within the canonical direct

pathway. However, this prediction had not been evaluated in the context of disease, and furthermore, our data suggest reprogramming of normal synaptic connectivity to subserve novel (disease-related) functions may be a more general mechanism in basal ganglia disease. Given LID-associated or TRAPed neurons were only 20% of the striatum, yet were reliably activated from levodopa session to levodopa session, we are hopeful that targeting these neurons, with either pharmacological or DBS approaches, could be a fruitful avenue for new Parkinson's disease treatments. Discovering the mechanisms that distinguish these neurons from other direct pathway cells could be critical for treating basal ganglia disorders. Further genetic profiling will be needed to explore what makes these neurons unique. Beyond dissecting the underlying causes of dyskinesias, understanding the heterogeneity that exists within the basal ganglia will allow for more complete and complex models of the diverse functions of these ancient, interconnected nuclei.

Publishing Agreement

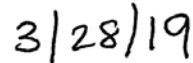
It is the policy of the University to encourage the distribution of all theses, dissertations, and manuscripts. Copies of all UCSF theses, dissertations, and manuscripts will be routed to the library via the Graduate Division. The library will make all theses, dissertations, and manuscripts accessible to the public and will preserve these to the best of their abilities, in perpetuity.

Please sign the following statement:

I hereby grant permission to the Graduate Division of the University of California, San Francisco to release copies of my thesis, dissertation, or manuscript to the Campus Library to provide access and preservation, in whole or in part, in perpetuity.



Author Signature



Date